Cellular and circuit mechanisms of network responses in auditory cortex

By

Bryan M. Krause

A dissertation submitted in partial fulfillment of

the requirements for the degree of

Doctor of Philosophy

Neuroscience

at the

UNIVERSITY OF WISCONSIN-MADISON

2015

Date of final oral examination: 7/10/2015

The dissertation is approved by the following members of the Final Oral Committee:

Matthew I. Banks, Associate Professor, Anesthesiology
Mathew V. Jones, Associate Professor, Neuroscience
Peter Lipton, Professor, Neuroscience
Philip H. Smith, Professor, Neuroscience
Daniel J. Uhlrich, Professor, Neuroscience

Dedication

This work is dedicated to Al, Gladys, Kenneth, and Caroline.

Acknowledgements

This dissertation would not have been possible without the constant support of my advisor, Matt, who has always been available to me whether providing prompt feedback or participating in a philosophical argument, who has put up with my incessant indecision and wavering over the finest of details, and who has always felt as much a colleague as a boss. If future graduate students read this looking for how to mollify the demands of one Dr. Banks, I have two pieces of advice: first, if he criticizes your work, he probably likes it; second, if he is your advisor, you already won the game: you can answer all his questions before, instead of during, your committee meetings and defenses.

For everyone who flowed through the lab during my time here, as undergraduates, graduate students, post-docs, and visitors, I am grateful to you all. Though some of your scientific contributions are noted in the chapters that follow, your roles as comrades in the lab and friends outside goes unmentioned except here. Thank you for putting up with me.

For my parents, your support in everything I do is all I ever needed from you, but you have generously given me so much more. The way you taught me to think about the world is what made me a scientist – and I have come a long way since feeding the backyard ducks.

And finally, for my wife Irene Ann, my grad school buddy and partner in everything – next to you, these pages are nothing but a radiator full of penguins.

Table of Contents

Abstract

Modern study of sensory processing at the cellular and circuit level has shifted focus from the tuning and coding properties of individual cells to their operation within complex networks. The ways in which cortical network activity shapes responses to sensory stimuli is crucial to understanding aberrant cortical processing, as occurs in autism, schizophrenia, tinnitus, and delirium, as well as understanding the mechanisms of loss of consciousness in sleep and anesthesia. In this thesis, I investigate the circuitry underlying network responses to afferent input in auditory cortex.

In the first section of the thesis, I focus on epidural recordings of cortical responses to sensory stimuli and challenge the idea that "evoked" activity driven by sensory stimulation is fundamentally separate from "induced" activity generated intrinsically or from phase reset of ongoing oscillations. Instead, variable network responses can explain changes in all three measures.

Second, I study the engagement of different auditory cortical layers in response to input from thalamus in auditory thalamocortical brain slices. Laminar patterns of activity are crucial to understanding cortical information flow, because different cortical layers receive inputs from and send outputs to different structures both within and outside cortex. I show that there is a discordance between anatomical patterns of thalamocortical/interlaminar connectivity and the actual sequence in which cortical layers are activated by thalamocortical input. These results support a model of cortical processing in which spiking in the entire column depends on recurrent "UP state" activity triggered by the infragranular layers, and that activity in the supragranular layers that project to higher order cortex only occurs in certain circumstances.

Finally, I study the contribution of specific populations of inhibitory interneurons to cortical network activity. I show that parvalbumin-positive cells affect the onset of network activity in infragranular layers and inhibit the spread of activity to supragranular layers, while somatostatin-positive cells contribute to terminating network activity. The latter effect may be a specialization of auditory cortex, where network events are brief compared to other cortical areas.

These results emphasize the importance of intrinsic cortical activity in determining signal flow during sensory processing. The response properties of cortical networks may be poorly predicted from the features of individual synapses and cells, and emergent network properties may dominate the encoding of sensory features and integration of intrinsic and extrinsic information sources. Future experiments will elucidate the details of these population coding strategies and integrative processes, and their regulation by cortical inhibition and exogenous pharmaceutical agents.

Chapter 1

Traditional studies of cortical response properties and receptive fields have depended on single-cell recordings over dozens or hundreds of consecutive trials. This averaging methodology produces a representation that differs from the representation that is actually accessible by the brain, in which information must be extracted in a single pass and in which individual neurons fire in a context defined by the recent past and present activity of many other cells. More recently, experimental techniques that allow for simultaneous recordings of many cells have suggested that sparse "modes" of simultaneously active cells encode stimulus categories (Bathellier et al., 2012). Activity in these "modes" of organization may be structured temporally as "packets" of activity that occur occasionally during sleep and anesthesia but at a near continuous rate in the active, desynchronized state (Luczak et al., 2013). Under these schemes, the tuning properties of individual cells arise out of their tendency to be activated along with other cells as part of these modes/packets (Bathellier et al., 2012; Luczak et al., 2013).

Cortical processing via "modes" or "packets" may complicate existing theories about serial interlaminar cortical processing (Brumberg et al., 1999; Atencio et al., 2009; Atencio and Schreiner, 2010). It may be impossible or misguided to separate activity driven directly by a stimulus from activity produced locally in cortex. Almost all synapses onto cortical neurons are from other, local cortical cells, and recurrent excitation is a characteristic feature of cortical networks (Douglas et al., 1995). Bursts of population activity are a natural consequence of recurrent connectivity and the temporal dynamics of synaptic transmission in cortex (Tsodyks et al., 2000), such that feed-forward processing is accompanied by recurrent activity within milliseconds (Panzeri et al., 2001).

Chapter 2 of this thesis involves the detection in epidural recordings of "evoked" activity driven directly by sensory stimuli, versus "induced" activity or "phase reset" caused by modulation of ongoing

activity in amplitude or phase, respectively. In Chapters 3 and 4, the thesis turns toward the involvement in responses to thalamocortical input of cells located in particular cortical layers or of particular types. In those chapters, the emphasis is on spiking activity occurring during "UP states," periods of shared depolarization that occur *in vivo* and *in vitro* (Steriade et al., 1993; Sanchez-Vives and McCormick, 2000; Rigas and Castro-Alamancos, 2007; Sakata and Harris, 2009) that are likely related to the "packets" referenced in the previous paragraphs as well as the network activity measured in Chapter 2. Before discussing these results more completely, in this chapter I review existing knowledge of circuitry and processing in sensory neocortex to provide background to understanding the later chapters.

Laminar and columnar structure of neocortex

Cells in a strip of neocortex perpendicular to the surface tend to have similar tuning properties which differ from neighboring regions, often in a continuous or systematic manner. This "columnar" organization is a unifying feature of primary visual (Hubel and Wiesel, 1977; Obermayer and Blasdel, 1993; Hubener et al., 1997), somatosensory (Sretavan and Dykes, 1983; Sur et al., 1984), and auditory (Abeles and Goldstein, 1970; Brugge and Merzenich, 1973; Merzenich et al., 1975; Middlebrooks et al., 1980; Kelly and Sally, 1988; Sally and Kelly, 1988; Clarey et al., 1994; Sugimoto et al., 1997; Shen et al., 1999) cortex, and likely extends to all other neocortical areas as well (Mountcastle, 1997).

Within each column, neocortex is principally a six-layered sheet, with each layer containing a population of cell types with distinct afferent and efferent connectivity. Cells in the cortical column are highly interconnected within and between layers (Thomson and Bannister, 2003; Atencio and Schreiner, 2010), and these local connections dominate the total synaptic input to a cell. Extrinsic inputs from thalamus (Ahmed et al., 1994) and other cortical columns (Shepherd and Svoboda, 2005) make up less than half of total input to a column. Each layer of cortex in the column has a specific role in receiving input and/or directing output to other layers and to external structures such that the column as a whole

is required to integrate inputs and reach all target areas. This laminar structure has been most closely studied in primary sensory areas, especially primary visual cortex (V1), and (for better or worse) other cortical areas are typically described based on their variations from V1. Cortical layers can be grouped into a superficial (or 'supragranular') subdivision consisting of layers 2 and 3 and deep (or 'infragranular') subdivision consisting of layers 5 and 6. Together these layers are the primary output layers of cortex, containing pyramidal cells with a variety of cortical and subcortical targets. Additionally, some cortical areas (particularly sensory areas) have a granular layer 4, which is less defined or absent in higher-order association cortex, motor cortex, and entorhinal cortex. When present, layer 4 is often considered to be the primary recipient layer for information arriving from thalamus (Miller et al., 2001) because the "specific" or "core" thalamic sensory nuclei (for example, the lateral geniculate nucleus for visual cortex and the medial geniculate for auditory cortex) terminate with the greatest density in layer 4 (LeVay and Gilbert, 1976; Romanski and LeDoux, 1993; Kimura et al., 2003; Smith et al., 2012). Where layer 4 is absent, cells in layer 3 may take on this "recipient" role despite the absence of granular cytoarchitecture (Yamawaki et al., 2015).

Finally, layer 1 is the "crowning mystery" of neocortex (Hubel, 1982), a mostly acellular layer containing neuropil and a few GABAergic interneurons (Douglas and Martin, 2004). Layer 1 is distinct from the other layers in that it lacks any glutamatergic cells, but does contain small numbers of various inhibitory interneuron populations. However, layer 1 contains dendrites of pyramidal cells from every layer except layer 6, as well as axons from numerous sources, including parts of thalamus, higher-order cortical areas, some local axon collaterals, Martinotti interneurons, and various neuromodulatory systems (Vogt, 1991; Cauller, 1995; Cauller et al., 1998; Mechawar et al., 2000; Mitchell and Cauller, 2001; Karube et al., 2004; Rubio-Garrido et al., 2009). Glutamatergic inputs to layer 1 that synapse on pyramidal cells evoke EPSPs that are propagated actively to the soma despite long electrotonic distances, and can have non-linear effects on action potential generation (Larkum et al., 1999, 2001;

Larkum et al., 2004). Therefore, both excitation and inhibition in layer 1 can have strong effects on activity throughout the column.

External projections from neocortex

Excitatory cells in layer 4 are typically thought to project locally, supporting their purported role as an input layer that relays excitation within the column (Lübke et al., 2000; Staiger et al., 2004). However, layer 4 cells can also be callosally projecting or project to nearby columns (Vercelli et al., 1992; Staiger et al., 2004). The functional significance of the non-local projections of layer 4 cells is unclear.

Pyramidal cells in layers 2/3 project horizontally to layers 2/3 of the same cortical area, as well as in a bottom-up fashion to higher-order cortex, terminating in the middle layers of those areas (Rockland and Pandya, 1979). Layers 2 and 3 have often been grouped together for functional studies, although recently some differences between the layers have been highlighted in auditory cortex (Oviedo et al., 2010). At this point it is unclear whether differences between layers 2 and 3 are generalized to other cortical regions or a specialization of auditory cortex. Given the limited study of layers 2 and 3 as separate entities it is difficult to know whether functions generally attributed to layer 2/3 are in fact general or specific to either individual layer.

Layer 5 pyramidal cells have diverse projection targets that define different subpopulations. Smaller layer 5 cells have thin apical dendrites and fire in a regular-spiking pattern, whereas large layer 5 cells have thick apical dendrites that branch extensively in layer 1 and fire in a burst-spiking pattern (Chagnac-Amitai et al., 1990). Thin layer 5 cells project to distant cortical targets, including the contralateral hemisphere (Mitani and Shimokouchi, 1985; Games and Winer, 1988; Hubener and Bolz, 1988; Larsen et al., 2007; Le Be et al., 2007). Nearly all thick-tufted cells project to subcortical structures including superior and inferior colliculus and pontine nuclei, with targets depending on cortical area (Games and Winer, 1988; Kasper et al., 1994; Winer and Prieto, 2001). The thick-tufted descending

projection neurons also send axon collaterals to thalamus, specifically to regions of thalamus that in turn project to higher order areas of cortex (Deschênes et al., 1994; Ojima, 1994; Llano and Sherman, 2008). These projections, therefore, form the possibility for cortico-thalamo-cortical loops (Sherman and Guillery, 1998; Theyel et al., 2010) that form a parallel, if not predominant, bottom-up pathway alongside the supragranular projections.

Many layer 6 pyramidal cells also project to thalamus. Some, like layer 5 corticofugal cells, target higher order regions in thalamus (Thomson, 2010). Others send a feedback projection to the region of thalamus that sends driving inputs to the more superficial layers (Diamond et al., 1969) and both excites directly and inhibits indirectly thalamic relay neurons (with indirect inhibition through excitation of cells in the reticular nucleus) (Ojima, 1994; Lam and Sherman, 2009). Although this projection is mostly reciprocal to the thalamic nuclei that project to a given cortical column, sometimes other similar thalamic regions are targeted by these "feedback" projections (Deschênes et al., 1998; Lam and Sherman, 2009). Although the significance of these offset projections is not clear, they seem to follow the pattern of pre-thalamic sensory inputs and therefore may be an alternative pathway for propagation of intrinsically rather than extrinsically generated stimuli (Deschênes et al., 1998). Other cells in layer 6 that do not project to thalamus instead send long horizontal axons to the infragranular layers of cortex. Interestingly, the cortico-cortical projection cells of both layers 5 and 6 are separate from those that send descending projections to the thalamus, midbrain, or brainstem, indicating that intracortical and extrinsic output streams are somewhat segregated (Petrof et al., 2011) (although cells projecting to subcortical structures do have local axon collaterals).

Thalamocortical projections to neocortex

Thalamocortical afferents to sensory cortex can be divided into two categories: specific and non-specific (Jones, 1998; Jones, 2001; Hu, 2003). Specific thalamic afferents arise from "core" regions of

thalamus, carry precise sensory input to cortex, and are most clearly responsible for the tuning properties of their target column (Jones, 1998; Miller et al., 2002). Non-specific afferents from "matrix" thalamic cells serve a modulatory role and may coordinate activity over large regions of cortex (Jones, 2001; Hu, 2003; Hawkins and Blakeslee, 2005).

For primary auditory cortex, the specific thalamic afferents originate in the ventral division of the medial geniculate nucleus (MGv) (Romanski and LeDoux, 1993; Smith et al., 2012). The specific thalamic inputs terminate primarily in layer 4 and are thought to preferentially drive layer 4 cells, though they may also contact apical dendrites of cells located in layers 5 and 6 and the basal dendrites of cells in layers 2 & 3 (Thomson and Bannister, 2003). The notion that layer 4 cells serve as the primary thalamorecipient cells is somewhat dubious in that only about 5-6% of the synapses on a given spiny stellate cell in V1 arrive from the lateral geniculate nucleus (Ahmed et al., 1994) and only about 40% of the dendritic length in layer 4 originates from spiny stellate cells (Binzegger et al., 2004), positioning many other cell types to receive thalamocortical input in layer 4 (White and Hersch, 1982; Mitani and Shimokouchi, 1985; Agmon and Connors, 1992; Gil and Amitai, 1996).

Non-specific inputs arrive in auditory cortex from a variety of matrix thalamic nuclei, including the medial division of the medial geniculate (MGm), suprageniculate, and posterior intralaminar nuclei; these inputs terminate diffusely but especially in layers 1, 5 and 6 (Ryugo and Killackey, 1974; Herkenham, 1980; Huang and Winer, 2000; Linke and Schwegler, 2000; Kimura et al., 2003; Smith et al., 2010). Matrix thalamic nuclei receive their inputs from diverse areas including somatosensory thalamus, limbic cortex, the superior colliculus, the (external and dorsal cortex of the) inferior colliculus, and brainstem auditory nuclei (Wepsic, 1966; Benevento and Fallon, 1975; Hicks et al., 1986; Winer, 1992; Linke, 1999; Malmierca et al., 2002).

Interlaminar connectivity and the canonical microcircuit

A crude understanding of cortical processing based only on external inputs and outputs is possible, but understanding how cortex internally processes information necessitates knowledge about local interlaminar connectivity. What is the functional circuit within a cortical column? Early studies of local cortical circuitry focused primarily on visual cortex in anesthetized animals, particularly cats. These early works focused on the anatomy of thalamocortical and local intracortical projections. In primary visual cortex, spiny stellate cells in layer 4 (thought of as the thalamo-recipient layer) project preferentially to layer 2/3, where pyramidal cells project preferentially to layer 5, where pyramidal cells project preferentially to layer 6 (Gilbert and Wiesel, 1983). This feed-forward network is referred to as the "canonical microcircuit" (Douglas and Martin, 2004). The anatomical "canonical microcircuit" also fits with the receptive field properties in different layers of visual cortex, with "simple" cells in layers 4 and 6 exhibiting response properties most similar to core thalamic cells, and "complex" cells in layers 2/3 and 5 exhibiting more complicated responses derived from local computations (Hubel and Wiesel, 1962; Dow, 1974; Gilbert, 1977; Alonso and Martinez, 1998). In addition to the anatomical and receptive field support for this model, glutamate uncaging experiments and paired recordings in slices confirm the relative strength of connections underlying the canonical microcircuit model (Callaway, 2002; Thomson and Bannister, 2003; Thomson and Lamy, 2007; Hooks et al., 2011). These methods have also revealed more nuance to the microcircuit, as targets even within a given layer are non-uniform. For example, layer 3 cell projections to layer 5 are specifically targeted to the intrinsically-bursting large tufted pyramidal cells and not the smaller RS cells (Thomson and Bannister, 1998).

Despite what seems to be overwhelming evidence in favor of the canonical microcircuit model, recent work has questioned whether thalamocortical input activates cortical circuitry in the layer 4 to layer 2/3 to layer 5 pattern, including work covered in Chapter 3 of this thesis (Krause et al., 2014). In somatosensory cortex, monosynaptic thalamocortical EPSPs are observed in layer 5 as early or earlier

than in layer 4, and inactivation of layer 4 does not affect these direct inputs to layer 5 (Agmon and Connors, 1992; Constantinople and Bruno, 2013). Similarly, *in vivo*, in multiple cortical areas, layer 5 cells fire at shorter latencies than cells in layers 2/3 and/or layer 4 (Maunsell and Gibson, 1992; Sugimoto et al., 1997; Shen et al., 1999; de Kock et al., 2007; Sakata and Harris, 2009; Christianson et al., 2011; Constantinople and Bruno, 2013).

How is it possible to resolve these discrepancies? Measuring the probability and efficacy of connections between pairs of cells does not account for laminar differences in firing rate, spike threshold, or response latency. The emphasis on the serial feed-forward model deemphasizes intralaminar connectivity as well as secondary interlaminar connections that are only slightly weaker than the strongest interlaminar connections. A better model for intralaminar connectivity must consider not only the strength of individual connections (i.e., synaptic weights) but also the level of activity in the presynaptic population. For example, although the canonical microcircuit presumes that activation flows from supragranular layers 2/3 to infragranular layer 5 due to stronger average connections from layer 2/3 to layer 5, layer 2/3 pyramidal cells fire sparsely and at long latencies (de Kock et al., 2007; Kerr et al., 2007; Sakata and Harris, 2009; Barth and Poulet, 2012), whereas layer 5 pyramidal cells fire robustly at low thresholds and short latencies (de Kock et al., 2007; de Kock and Sakmann, 2009; Sakata and Harris, 2009; Constantinople and Bruno, 2013). Therefore, activity could actually flow predominantly in the layer 5 to layer 2/3 direction despite stronger pairwise connectivity in the opposite direction (Beltramo et al., 2013).

Distinguishing characteristics of auditory cortex

The following chapters of this thesis will focus on primary auditory cortex, which is similar but not identical to other primary sensory areas in structure and connectivity (Winer et al., 2005). The differences between auditory cortex and other areas might relate to the physical properties of auditory

stimuli. Behaviorally relevant auditory stimuli have rapid dynamic content unmatched by the other sensory modalities (Wang, 2007). Spatial reconstruction of the auditory scene is more complicated than for visual or somatosensory stimuli and does not relate directly to topography at the receptor level, unlike retinotopic or somatotopic maps (Schnupp et al., 2001; Linden and Schreiner, 2003). Perhaps for these physical reasons, there is extensive pre-thalamic processing of auditory stimuli in the brainstem and inferior colliculus that has no functional analogy in visual or somatosensory systems (Smith and Populin, 2001; Winer et al., 2005).

The complexity of potential representations of auditory stimuli has complicated efforts to understand the organizing principles of cortical columns in auditory cortex. Unlike visual and somatosensory cortex, the transformations that occur during intracolumnar processing in auditory cortex are a mystery (Linden and Schreiner, 2003). The laminar receptive-field hierarchy present in visual cortex is less definitive in auditory cortex (Atencio et al., 2009; Atencio and Schreiner, 2010; Winkowski and Kanold, 2013), and it is not clear which features might define specialization between layers (Linden and Schreiner, 2003).

In primary visual and primary somatosensory cortex, layer 4 excitatory cells are mostly spiny stellate interneurons that have small dendritic arbors and mostly local axonal projections (Yabuta and Callaway, 1998; Feldmeyer and Sakmann, 2000; Lübke et al., 2000; Staiger et al., 2004; Egger et al., 2008). Spiny stellate cells are the traditional recipients of strong, direct inputs from the thalamus (LeVay and Gilbert, 1976; White, 1978; White and Rock, 1979). By contrast, layer 4 of primary auditory cortex (A1) contains primarily pyramidal cells which seem to take on the role of spiny stellate cells but have dendrites that ascend to layer 1 (Smith and Populin, 2001; Barbour and Callaway, 2008). Auditory cortex also sends more extensive callosal projections to contralateral auditory cortex, arising from multiple layers (Code and Winer, 1985, 1986).

Inhibitory interneuron subtypes

In the previous sections I have reviewed the excitatory connectivity with and within neocortex, but inhibition within cortex is critically important and may even dominate responses to sensory stimuli (Haider et al., 2013). Inhibitory interneurons are diverse, varying in dendritic and axonal morphology, post-synaptic targets, intrinsic membrane properties, spiking patterns, and expression of a variety of peptides and proteins (Markram et al., 2004; Kubota, 2014).

Of these various peptides and proteins, a few are expressed in mostly non-overlapping populations of inhibitory interneurons, and can therefore be used to define particular classes (Kawaguchi and Kondo, 2002; Xu et al., 2010; Kubota et al., 2011; Rudy et al., 2011). Of these, parvalbumin (PV)- and somatostatin (Sst)-expressing cells appear to be definitively separate populations, and together make up well over half of all inhibitory interneurons in neocortex. Most of the remainder express vasoactive intestinal peptide (VIP), cholecystokinin (CCK), calretinin (CR), or a combination (Kubota et al., 2011). Other expression patterns can more completely cover the population of GABAergic cells, but overlap with the others to the extent that they are less helpful in classification without dual-labeling.

PV+ cells are the most homogeneous of the expression-defined interneuron classes. They almost completely overlap with the fast-spiking (FS) cells, such that PV+ and FS cells can be considered interchangeable designations. PV+ cells include soma-targeting basket cells and axon-targeting chandelier cells (Kubota, 2014). Both morphologies have local dendritic and axonal arbors and both receive inputs and send output to the layer in which their soma resides. Though PV+ basket cells are distinctive for their tendency to target the somata of pyramidal cells, they actually make more synapses on proximal dendrites and spine heads (Kubota, 2014). PV+ cells provide strong inhibitory control of post-synaptic pyramidal cells, but also inhibit other PV+ cells (Pfeffer et al., 2013).

Sst+ cells differ from PV+ cells in that they mostly target dendrites, particularly the apical dendritic tufts of pyramidal cells (Kubota, 2014). The most common and also most distinctive morphology of Sst+ cells is the Martinotti cell. Martinotti cells can be located in layers 2/3 or 5, but are characterized by their axons which ascend to and arborize in layer 1 to target dendritic tufts (Kawaguchi and Kubota, 1996). Sst+ cells receive facilitating glutamatergic inputs from pyramidal cells and mediate disynaptic inhibition in the infragranular layers that is especially strong during periods of high activity (Silberberg and Markram, 2007). Sst+ cells can also cause disinhibition by their targeting of other interneuron subtypes such as PV+ cells, though they do not target other Sst+ cells (Pfeffer et al., 2013; Xu et al., 2013).

Of the remaining interneuron types, the most functionally studied are the disinhibitory VIP+ cells. Although Sst+ cells have also been implicated in disinhibitory circuits (Xu et al., 2013), VIP+ cells are functionally distinct from PV+ and Sst+ cells in that they primarily target other interneurons (Lee et al., 2013; Pi et al., 2013). VIP+ cells send mostly descending axons that target deeper layers than the soma (Kawaguchi and Kubota, 1996; Kubota, 2014).

The role of inhibitory interneurons in processing sensory information versus controlling network activity more generally is somewhat unclear. On one hand, inhibitory cells tend to have fairly non-specific connectivity to neighboring cells (Fino and Yuste, 2011; Packer and Yuste, 2011) and lack tuning to certain stimulus features (Sohya et al., 2007; Kerlin et al., 2010), suggesting that they cannot be involved in elaborate computational schemes. On the other hand, some inhibitory cells are sharply tuned (Runyan et al., 2010; Moore and Wehr, 2013) and both sharp and broad tuning of interneurons can shape the tuning of pyramidal cells (Wang et al., 2000; Oswald et al., 2006; Isaacson and Scanziani, 2011). Even non-specific connectivity from interneurons to pyramidal cells could sharpen tuning if spiking to non-optimal stimuli is reduced. It is likely that the specific contributions of interneurons to

tuning in single cells and population activity more broadly depends on the diversity of interneuron subtypes.

Synchronized vs. desynchronized cortical states

Cortex is always spontaneously active under normal circumstances, although the organization of this spontaneous activity depends on brain state. Often, these brain states are presented as a dichotomy between "synchronized" and "desynchronized" cortical activity, defined by the amplitude of low-frequency oscillations in the surface EEG or local field potential. I will first discuss the common themes of this dichotomy; later, I will complicate the synchronized/desynchronized dichotomy and suggest that the desynchronized state may consist of elements more readily observed in the synchronized state.

The desynchronized state is most associated with active behavior and consists of long-lasting depolarization and tonic population firing (Poulet and Petersen, 2008; Niell and Stryker, 2010; Harris and Thiele, 2011; Poulet et al., 2012). It is important to note that the idea of the 'desynchronized state' as an active state is based specifically on desynchronization at low frequencies around 1 Hz, although there may be increases in synchrony at higher frequencies (Steriade et al., 1996)). The synchronized state is most associated with sleep, anesthesia, and quiet wakefulness and consists of an alternation between UP and DOWN states, as described by (Steriade et al., 1993) during sleep. As suggested in a recent review (Harris and Thiele, 2011), the terminology of UP and DOWN "states" may be misleading because these terms truly refer to relatively brief "phases" that occur within a long-lasting synchronized state maintained for minutes or more. I will continue to use the more common "states" terminology here, but note the potential for confusion.

During the synchronized state, cortical neurons are depolarized and fire action potentials at a relatively high rate within UP states, much like the desynchronized state (Steriade et al., 2001; Destexhe et al., 2007; Constantinople and Bruno, 2011); during DOWN states, most neurons are hyperpolarized

and fire sparsely or not at all. The synchronized depolarization/hyperpolarization across the network directly produces the slow oscillation in the EEG. UP states are triggered by recurrent activity in layer 5 (Chauvette et al., 2010; Wester and Contreras, 2012; Beltramo et al., 2013; Stroh et al., 2013), although recurrent activity in other layers, particularly layers 2/3, can modulate their intensity and propagation (Wester and Contreras, 2012). UP states can be produced by cortex without outside input, but the presence of thalamo-cortical input can increase their frequency in slices (Rigas and Castro-Alamancos, 2007). It is not clear whether UP states can indeed begin in thalamus, or whether the thalamo-cortical inputs simply raise the level of activity in cortex and therefore UP state threshold is reached more quickly. Some controversy has been raised regarding the presence of UP states in auditory cortex, with one group insisting that UP states do not occur in auditory cortex and are instead replaced by brief "bumps" (DeWeese and Zador, 2006; Hromadka et al., 2013). However, these "bumps" share nearly all of the same properties as UP states, except for their duration, and other authors freely refer to these brief events using the terminology of UP states (Sakata and Harris, 2009). Because awake auditory cortex also shows activity periods that are briefer than other cortical regions (Sakata and Harris, 2009; Hromadka et al., 2013), related circuit mechanisms may underlie UP states/bumps in both waking and anesthetized states.

Synchronous silences in active cortex

Nearby neurons in sensory cortices often share tuning properties, leading to correlated firing rates in response to sensory stimuli. In addition to these stimulus correlations, which can be observed by averaging responses over many stimulus presentations, neurons can also share trial-by-trial variation, referred to as noise correlations. Simultaneous paired recordings have shown that cortical neurons have substantial noise correlation (Zohary et al., 1994; Bair et al., 2001; Cohen and Kohn, 2011). Some level of noise correlation persists even in cells with dissimilar tuning properties (Kohn and Smith, 2005),

suggesting that the pairwise correlations are not only a function of shared bottom-up input. Also, thalamocortical neurons show less variability than cortical neurons (Schölvinck et al., 2015), suggesting that the shared variability (i.e., noise correlations) in cortical neurons is generated in cortex. Noise correlations are often thought of as detrimental to coding efficiency (Zohary et al., 1994), but this is not always the case (Abbott and Dayan, 1999). However, for an external observer to obtain ideal predictions from a correlated population, it is necessary to know the underlying correlation structure (Averbeck et al., 2006).

Recent evidence suggests that a large fraction of the pairwise noise correlations can be accounted for by global population correlations shared among all simultaneously recorded cells (Ecker et al., 2014; Mochol et al., 2015; Schölvinck et al., 2015). These global correlations depend highly on brief periods of silence, even in the desynchronized state (Mochol et al., 2015). The presence of these silences challenges the view of the desynchronized state as a period of steady or stochastic depolarization, and suggests instead that there is a continuum between synchronized and desynchronized defined by the ratio of UP states to DOWN states.

These findings suggest a new interpretation for the result that attention and sensory stimuli can cause neuronal decorrelation (Vinje and Gallant, 2000; Cohen and Maunsell, 2009; Mitchell et al., 2009; Churchland et al., 2010; Ecker et al., 2010): cortical variability is decreased by reducing the probability of silences/DOWN states (Harris and Thiele, 2011). Whether or not this decorrelation is helpful to a downstream decoder would depend on the structure of the correlations and how much information the decoder has about the correlation structure and average population activity. However, correlations that are shared within a large population are computationally easy to account for with a simple inhibitory circuit that subtracts an average of the population activity.

UP states and cortical processing

There are two views of the connection between UP states and cortical processing. One view is that UP states are merely a part of the synchronized state and therefore represent an inactive or non-processing cortical state. This view suggests that one should focus on awake, preferably behaving, animals to understand cortical processing and that results from anesthetized animals or brain slices are misleading or incomplete. While there are certainly advantages to studying behaving animals, reduced preparations also have advantages and certain experiments may only be feasible in those preparations. A second view is that UP states are brief periods of active-like activity flanked by inactive DOWN states (Destexhe et al., 2007; Constantinople and Bruno, 2011; Contreras et al., 2013). This second view suggests that important properties of the cortical circuit are maintained in the synchronized state, and that UP states provide brief windows in which to understand active cortical processing, whether in anesthetized animals, brain slices, or cultures. Although the validity of these two viewpoints is not resolved, the evidence that UP states in the synchronized state are detrimental to processing is weak, whereas the evidence that UP states are useful to processing and related to the desynchronized state is strengthening (Destexhe et al., 2007; Reig and Sanchez-Vives, 2007; Sakata and Harris, 2009; Constantinople and Bruno, 2011; Hirata and Castro-Alamancos, 2011; Luczak et al., 2013; Reig et al., 2015).

Compared to DOWN states *in vivo* or quiescence in slices, UP states and the awake state are periods of high conductance (Destexhe et al., 2003). Whether the high conductance during UP states limits or enhances the effectiveness of external inputs has been controversial, and may depend on how that efficacy is defined. For example, one study claimed that spontaneous UP states in slices limit the efficacy of thalamocortical input (Watson et al., 2008). However, this study included evoked UP states that occurred in response to thalamocortical input during the DOWN as part of the "thalamocortical efficacy." It should not be surprising that the effect of thalamic stimulation during the DOWN state,

which includes subsequent UP state activity, does not sum linearly with the ongoing UP state, as noted elsewhere (Rigas and Castro-Alamancos, 2009). Similar conclusions drawn *in vivo* also seem to depend on the failure of stimuli to evoke UP states when an UP state is already ongoing (Petersen et al., 2003; Sachdev et al., 2004). In contrast, when using measures that do not include the evoked UP state as part of the sensory response, responses during UP states are more consistent and reliable (Reig and Sanchez-Vives, 2007; Hirata and Castro-Alamancos, 2011) and detection of weaker stimuli is improved (Reig et al., 2015).

However, these measures are dependent on membrane depolarizations and not suprathreshold activity. Given that UP state activity at times seems to dominate spiking responses to sensory stimuli, how can stimulus information be encoded? One observation that hints at a potential mechanism is that changes in UP state probability during stimulus presentation follow the tuning properties of the participating cells (Anderson et al., 2000). Even when evoked UP states appear to be similar in population activity, the participation of individual cells can vary according to their tuning properties (Luczak et al., 2013). This scheme is reminiscent of the "modes" of coactivation mentioned at the beginning of this chapter (Bathellier et al., 2012). UP states could reflect the ongoing noise necessary for an attractor network to function (Cossart et al., 2003) or the timescale on which cell assemblies operate (Harris, 2005).

Evoked and induced cortical activity and phase reset of ongoing oscillations

Particularly in the context of EEG recordings, distinctions have been made between "evoked" and "induced" responses to sensory stimuli or changes in state (e.g., attention, sleep) (Bullock and Achimowicz, 1994; Tallon-Baudry et al., 1996; Klimesch et al., 1998; Tallon-Baudry and Bertrand, 1999). "Evoked" responses are those that are phase-locked to some event, such as a stimulus onset, and are therefore seen when averaging over trials in the time domain (often referred to as the "event-related

potential," ERP). "Induced" activity refers to changes in the amplitude of ongoing oscillations. Although these changes may also occur at a particular point of time, they are not observed when averaging in the time domain because the phase of the underlying oscillations is random and therefore the time domain average will always approach zero (assuming there is no entrainment of the ongoing activity due to predictability of the stimuli or other experimental causes (Lakatos et al., 2008)). Induced activity can be either synchronizing or desynchronizing by increasing or reducing the amplitude of ongoing oscillations, respectively, though these effects do not necessarily correspond to the spectrum of synchronized versus desynchronized cortical state, given that low frequency desynchronization can be associated with higher frequency synchronization (Steriade et al., 1996).

Evoked and induced components have been attributed to different network mechanisms (Klimesch et al., 1998; Pfurtscheller and Lopes da Silva, 1999; Klimesch et al., 2000; David et al., 2006). Evoked components arise from strong feed-forward and initial feed-back volleys initiated in ascending afferents to thalamus (Pfurtscheller and Lopes da Silva, 1999). Induced components arise from structural changes in the network such as intrinsic membrane properties (Pfurtscheller and Lopes da Silva, 1999; David et al., 2006). These mechanistic differences evoke comparisons to the functionally distinct driver and modulator synapses in thalamus ((Sherman and Guillery, 1998), as noted by (David et al., 2006)) or to core versus matrix thalamocortical projections (Jones, 1998; Guillery and Sherman, 2002; Sherman and Guillery, 2002). Driver synapses with high efficacy are likely to evoke time-locked responses, whereas modulator synapses induce structural changes in their targets that influence their response to subsequent inputs or ongoing activity.

A third, distinct, contributor to oscillatory responses has been proposed in addition to evoked and induced responses: the phase reset (Makeig et al., 2002). Phase reset refers to a coherent shift in phase of ongoing activity such that phases are no longer randomly distributed, but no energy has been added to the signal on a given trial. Because phase reset will appear in the time-domain average, and

because evoked responses also create non-uniform phase distributions, it is difficult to isolate phase reset from the evoked response (Yeung et al., 2004; David et al., 2006; Martinez-Montes et al., 2008; Krieg et al., 2011). The difference between phase reset and an evoked event is only evident when considering the phase of ongoing activity on single trials compared to the phase of the response in the time-domain average (Martinez-Montes et al., 2008). In the case of an evoked response, the single-trial waveform will have an increased amplitude relative to pre-stimulus baseline on in-phase trials, and a decreased amplitude relative to pre-stimulus baseline on out-of-phase trials. However, in the case of phase reset, the single-trial waveform will always have the same amplitude as the pre-stimulus baseline. These comparisons are trivial when considering sinusoidal signals of constant amplitude, but EEG signals consist of dynamic oscillations at many frequencies, which makes single-trial comparisons not trivial at all. As a result, many mentions of phase reset in the literature are actually from evoked events because the measure of "phase reset" they use only considers the non-uniformity of phase after a stimulus (Tallon-Baudry et al., 1996; Makeig et al., 2002). Phase synchrony is an attractive solution to the binding activity across distant processing areas (Varela, 1994; Singer and Gray, 1995; Kopell et al., 2000; Varela et al., 2001). However, support for stimulus-related phase synchronization should only be emphasized in rare cases when evoked and phase-reset effects are clearly separate (Lakatos et al., 2007).

Preface to Chapters 2-5

The three chapters to follow all involve network responses of auditory cortex to sensory or thalamocortical input. In Chapter 2, I look at time-frequency analysis of evoked, induced, and phase-reset contributions to epidural responses to auditory stimuli. Although the proposed mechanisms behind changes in oscillatory activity described in the previous section create a nice story and suggest that identifying these mechanisms in various experimental paradigms will provide insight into underlying processing, induced and phase-reset effects can also be explained by variability in evoked response

components (David et al., 2006; Hu et al., 2009), as shown in Chapter 2 (Krause and Banks, 2013). Given the background presented on evoked and spontaneous UP states, a plausible explanation for the variability in evoked responses seen in Chapter 2 is that those evoked responses are not simply the result of feed-forward driver inputs to auditory cortex, but instead reflect evoked network events (UP states) as seen in Chapter 3 (Krause et al., 2014). The regulation of these events by inhibitory PV+ and Sst+ interneurons is the subject of Chapter 4. Finally, in Chapter 5 of this thesis I will re-summarize the prior chapters and suggest future lines of work.

References

Abbott LF, Dayan P (1999) The effect of correlated variability on the accuracy of a population code. Neural Comput 11:91-101.

Abeles M, Goldstein MH, Jr. (1970) Functional architecture in cat primary auditory cortex: columnar organization and organization according to depth. J Neurophysiol 33:172-187.

Agmon A, Connors BW (1992) Correlation between intrinsic firing patterns and thalamocortical synaptic responses of neurons in mouse barrel cortex. Journal of Neuroscience 12:319-329.

Ahmed B, Anderson JC, Douglas RJ, Martin KA, Nelson JC (1994) Polyneuronal innervation of spiny stellate neurons in cat visual cortex. JComp Neurol 341:39-49.

Alonso J-M, Martinez LM (1998) Functional connectivity between simple cells and complex cells in cat striate cortex. Nature neuroscience 1:395-403.

Anderson J, Lampl I, Reichova I, Carandini M, Ferster D (2000) Stimulus dependence of two-state fluctuations of membrane potential in cat visual cortex. Nature Neuroscience 3:617-621.

Atencio CA, Schreiner CE (2010) Columnar connectivity and laminar processing in cat primary auditory cortex. PLoS One 5:e9521.

Atencio CA, Sharpee TO, Schreiner CE (2009) Hierarchical computation in the canonical auditory cortical circuit. Proceedings of the National Academy of Sciences 106:21894-21899.

Averbeck BB, Latham PE, Pouget A (2006) Neural correlations, population coding and computation. Nature Reviews Neuroscience 7:358-366.

Bair W, Zohary E, Newsome WT (2001) Correlated firing in macaque visual area MT: time scales and relationship to behavior. JNeurosci 21:1676-1697.

Barbour DL, Callaway EM (2008) Excitatory Local Connections of Superficial Neurons in Rat Auditory Cortex. Journal of Neuroscience 28:11174-11185.

Barth AL, Poulet JF (2012) Experimental evidence for sparse firing in the neocortex. Trends Neurosci 35:345-355.

Bathellier B, Ushakova L, Rumpel S (2012) Discrete neocortical dynamics predict behavioral categorization of sounds. Neuron 76:435-449.

Beltramo R, D'Urso G, Dal Maschio M, Farisello P, Bovetti S, Clovis Y, Lassi G, Tucci V, Tonelli DDP, Fellin T (2013) Layer-specific excitatory circuits differentially control recurrent network dynamics in the neocortex. Nature Neuroscience 16:227-234.

Benevento L, Fallon JH (1975) The ascending projections of the superior colliculus in the rhesus monkey (Macaca mulatta). Journal of Comparative Neurology 160:339-361.

Binzegger T, Douglas RJ, Martin KA (2004) A quantitative map of the circuit of cat primary visual cortex. JNeurosci 24:8441-8453.

Brugge JF, Merzenich MM (1973) Responses of neurons in auditory cortex of the macaque monkey to monaural and binaural stimulation. JNeurophysiol 36:1138-1158.

Brumberg JC, Pinto DJ, Simons DJ (1999) Cortical columnar processing in the rat whisker-to-barrel system. Journal of Neurophysiology 82:1808-1817.

Bullock TH, Achimowicz JZ (1994) A comparative survey of oscillatory brain activity, especially gamma-band rhythms. Oscillatory event related brain dynamics:11-26.

Callaway E (2002) Cell type specificity of local cortical connections. Journal of Neurocytology 31:231-237.

Cauller L (1995) Layer I of primary sensory neocortex: where top-down converges upon bottom-up. Behavioural Brain Research 71:163-170.

Cauller LJ, Clancy B, Connors BW (1998) Backward cortical projections to primary somatosensory cortex in rats extend long horizontal axons in layer I. Journal of Comparative Neurology 390:297-310.

Chagnac-Amitai Y, Luhmann HJ, Prince DA (1990) Burst generating and regular spiking layer 5 pyramidal neurons of rat neocortex have different morphological features. Journal of Comparative Neurology 296:598-613.

Chauvette S, Volgushev M, Timofeev I (2010) Origin of active states in local neocortical networks during slow sleep oscillation. Cerebral Cortex 20:2660-2674.

Christianson GB, Sahani M, Linden JF (2011) Depth-dependent temporal response properties in core auditory cortex. JNeurosci 31:12837-12848.

Churchland MM et al. (2010) Stimulus onset quenches neural variability: a widespread cortical phenomenon. Nat Neurosci 13:369-378.

Clarey JC, Barone P, Imig TJ (1994) Functional organization of sound direction and sound pressure level in primary auditory cortex of the cat. JNeurophysiol 72:2383-2405.

Code RA, Winer JA (1985) Commissural neurons in layer III of cat primary auditory cortex (AI): pyramidal and non-pyramidal cell input. J Comp Neurol 242:485-510.

Code RA, Winer JA (1986) Columnar organization and reciprocity of commissural connections in cat primary auditory cortex (AI). HearRes 23:205-222.

Cohen MR, Maunsell JH (2009) Attention improves performance primarily by reducing interneuronal correlations. Nature neuroscience 12:1594-1600.

Cohen MR, Kohn A (2011) Measuring and interpreting neuronal correlations. Nature neuroscience 14:811-819.

Constantinople CM, Bruno RM (2011) Effects and mechanisms of wakefulness on local cortical networks. Neuron 69:1061-1068.

Constantinople CM, Bruno RM (2013) Deep cortical layers are activated directly by thalamus. Science 340:1591-1594.

Contreras EJB, Schjetnan AGP, Muhammad A, Bartho P, McNaughton BL, Kolb B, Gruber AJ, Luczak A (2013) Formation and reverberation of sequential neural activity patterns evoked by sensory stimulation are enhanced during cortical desynchronization. Neuron 79:555-566.

Cossart R, Aronov D, Yuste R (2003) Attractor dynamics of network UP states in the neocortex. Nature 423:283-288.

David O, Kilner JM, Friston KJ (2006) Mechanisms of evoked and induced responses in MEG/EEG. Neuroimage 31:1580-1591.

de Kock CP, Sakmann B (2009) Spiking in primary somatosensory cortex during natural whisking in awake head-restrained rats is cell-type specific. ProcNatlAcadSciUSA 106:16446-16450.

de Kock CP, Bruno RM, Spors H, Sakmann B (2007) Layer- and cell-type-specific suprathreshold stimulus representation in rat primary somatosensory cortex. JPhysiol 581:139-154.

Deschênes M, Bourassa J, Pinault D (1994) Corticothalamic projections from layer V cells in rat are collaterals of long-range corticofugal axons. Brain research 664:215-219.

Deschênes M, Veinante P, Zhang Z-W (1998) The organization of corticothalamic projections: reciprocity versus parity. Brain research reviews 28:286-308.

Destexhe A, Rudolph M, Pare D (2003) The high-conductance state of neocortical neurons in vivo. Nature Reviews Neuroscience 4:739-751.

Destexhe A, Hughes SW, Rudolph M, Crunelli V (2007) Are corticothalamic 'up' states fragments of wakefulness? Trends in Neurosciences 30:334-342.

DeWeese MR, Zador AM (2006) Non-Gaussian Membrane Potential Dynamics Imply Sparse, Synchronous Activity in Auditory Cortex. Journal of Neuroscience 26:12206-12218.

Diamond I, Jones E, Powell T (1969) The projection of the auditory cortex upon the diencephalon and brain stem in the cat. Brain research 15:305-340.

Douglas RJ, Martin KA (2004) Neuronal circuits of the neocortex. AnnuRevNeurosci 27:419-451.

Douglas RJ, Koch C, Mahowald M, Martin KA, Suarez HH (1995) Recurrent excitation in neocortical circuits. Science 269:981-985.

Dow BM (1974) Functional classes of cells and their laminar distribution in monkey visual cortex. J Neurophysiol 37:927-946.

Ecker AS, Berens P, Keliris GA, Bethge M, Logothetis NK, Tolias AS (2010) Decorrelated neuronal firing in cortical microcircuits. Science 327:584-587.

Ecker AS, Berens P, Cotton RJ, Subramaniyan M, Denfield GH, Cadwell CR, Smirnakis SM, Bethge M, Tolias AS (2014) State dependence of noise correlations in macaque primary visual cortex. Neuron 82:235-248.

Egger V, Nevian T, Bruno RM (2008) Subcolumnar Dendritic and Axonal Organization of Spiny Stellate and Star Pyramid Neurons within a Barrel in Rat Somatosensory Cortex. Cerebral Cortex 18:876-889.

Feldmeyer D, Sakmann B (2000) Synaptic efficacy and reliability of excitatory connections between the principal neurones of the input (layer 4) and output layer (layer 5) of the neocortex. Journal of Physiology 525 Pt 1:31-39.

Fino E, Yuste R (2011) Dense inhibitory connectivity in neocortex. Neuron 69:1188-1203.

Games KD, Winer JA (1988) Layer V in rat auditory cortex: projections to the inferior colliculus and contralateral cortex. Hearing Research 34:1-25.

Gil Z, Amitai Y (1996) Properties of convergent thalamocortical and intracortical synaptic potentials in single neurons of neocortex. Journal of Neuroscience 16:6567-6578.

Gilbert CD (1977) Laminar differences in receptive field properties of cells in cat primary visual cortex. The Journal of physiology 268:391-421.

Gilbert CD, Wiesel TN (1983) Functional organization of the visual cortex. ProgBrain Res 58:209-218.

Guillery RW, Sherman SM (2002) Thalamic Relay Functions and Their Role in Corticocortical Communication: Generalizations from the Visual System. Neuron 33:163-175.

Haider B, Häusser M, Carandini M (2013) Inhibition dominates sensory responses in the awake cortex. Nature 493:97-100.

Harris KD (2005) Neural signatures of cell assembly organization. Nature Reviews Neuroscience 6:399-407.

Harris KD, Thiele A (2011) Cortical state and attention. NatRevNeurosci 12:509-523.

Hawkins J, Blakeslee S (2005) On Intelligence. New York: Henry Holt & Co.

Herkenham M (1980) Laminar organization of thalamic projections to the rat neocortex. Science 207:532-535.

Hicks T, Stark C, Fletcher W (1986) Origins of afferents to visual suprageniculate nucleus of the cat. Journal of Comparative Neurology 246:544-554.

Hirata A, Castro-Alamancos MA (2011) Effects of cortical activation on sensory responses in barrel cortex.

Hooks B, Andrew Hires S, Zhang Y-X, Huber D, Petreanu L, Svoboda K, Shepherd GM (2011) Laminar analysis of excitatory local circuits in vibrissal motor and sensory cortical areas. PLoS-Biology 9:80.

Hromadka T, Zador AM, DeWeese MR (2013) Up states are rare in awake auditory cortex. JNeurophysiol 109:1989-1995.

Hu B (2003) Functional organization of lemniscal and nonlemniscal auditory thalamus. Experimental Brain Research 153:543-549.

Hu L, Boutros NN, Jansen BH (2009) Evoked potential variability. JNeurosciMethods 178:228-236.

Huang CL, Winer JA (2000) Auditory thalamocortical projections in the cat: laminar and areal patterns of input. J Comp Neurol 427:302-331.

Hubel DH (1982) Cortical neurobiology: a slanted historical perspective. Annual review of neuroscience 5:363-370.

Hubel DH, Wiesel TN (1962) Receptive fields, binocular interaction and functional architecture in the cat's visual cortex. J Physiol 160:106-154.

Hubel DH, Wiesel TN (1977) Ferrier lecture. Functional architecture of macaque monkey visual cortex. ProcRSocLond B BiolSci 198:1-59.

Hubener M, Bolz J (1988) Morphology of identified projection neurons in layer 5 of rat visual cortex. Neurosci Lett 94:76-81.

Hubener M, Shoham D, Grinvald A, Bonhoeffer T (1997) Spatial relationships among three columnar systems in cat area 17. J Neurosci 17:9270-9284.

Isaacson Jeffry S, Scanziani M (2011) How Inhibition Shapes Cortical Activity. Neuron 72:231-243.

Jones EG (1998) Viewpoint: the core and matrix of thalamic organization. Neuroscience 85:331-345.

Jones EG (2001) The thalamic matrix and thalamocortical synchrony. Trends in neurosciences 24:595-601.

Karube F, Kubota Y, Kawaguchi Y (2004) Axon branching and synaptic bouton phenotypes in GABAergic nonpyramidal cell subtypes. The Journal of neuroscience 24:2853-2865.

Kasper EM, Larkman AU, Lubke J, Blakemore C (1994) Pyramidal neurons in layer 5 of the rat visual cortex. I. Correlation among cell morphology, intrinsic electrophysiological properties, and axon targets. Journal of Comparative Neurology 339:459-474.

Kawaguchi Y, Kubota Y (1996) Physiological and morphological identification of somatostatin- or vasoactive intestinal polypeptide-containing cells among GABAergic cell subtypes in rat frontal cortex. The Journal of Neuroscience 16:2701-2715.

Kawaguchi Y, Kondo S (2002) Parvalbumin, somatostatin and cholecystokinin as chemical markers for specific GABAergic interneuron types in the rat frontal cortex. Journal of Neurocytology 31:277-287.

Kelly JB, Sally SL (1988) Organization of auditory cortex in the albino rat: binaural response properties. J Neurophysiol 59:1756-1769.

Kerlin AM, Andermann ML, Berezovskii VK, Reid RC (2010) Broadly tuned response properties of diverse inhibitory neuron subtypes in mouse visual cortex. Neuron 67:858-871.

Kerr JND, de Kock CPJ, Greenberg DS, Bruno RM, Sakmann B, Helmchen F (2007) Spatial Organization of Neuronal Population Responses in Layer 2/3 of Rat Barrel Cortex. Journal of Neuroscience 27:13316-13328.

Kimura A, Donishi T, Sakoda T, Hazama M, Tamai Y (2003) Auditory thalamic nuclei projections to the temporal cortex in the rat. Neuroscience 117:1003-1016.

Klimesch W, Russegger H, Doppelmayr M, Pachinger T (1998) A method for the calculation of induced band power: implications for the significance of brain oscillations. ElectroencephalogrClinNeurophysiol 108:123-130.

Klimesch W, Doppelmayr M, Roehm D, Poellhuber D, Stadler W (2000) Simultaneous desynchronization and synchronization of different alpha responses in the human electroencephalograph: a neglected paradox? Neuroscience letters 284:97-100.

Kohn A, Smith MA (2005) Stimulus dependence of neuronal correlation in primary visual cortex of the macaque. JNeurosci 25:3661-3673.

Kopell N, Ermentrout GB, Whittington MA, Traub RD (2000) Gamma rhythms and beta rhythms have different synchronization properties. Proceedings of the National Academy of Sciences of the United States of America 97:1867-1872.

Krause BM, Banks MI (2013) Analysis of stimulus-related activity in rat auditory cortex using complex spectral coefficients. J Neurophysiol 110:621-639.

Krause BM, Raz A, Uhlrich DJ, Smith PH, Banks MI (2014) Spiking in auditory cortex following thalamic stimulation is dominated by cortical network activity. Frontiers in Systems Neuroscience 8:170.

Krieg J, Trebuchon-Da FA, Martinez-Montes E, Marquis P, Liegeois-Chauvel C, Benar CG (2011) A comparison of methods for assessing alpha phase resetting in electrophysiology, with application to intracerebral EEG in visual areas. Neuroimage 55:67-86.

Kubota Y (2014) Untangling GABAergic wiring in the cortical microcircuit. Current opinion in neurobiology 26:7-14.

Kubota Y, Shigematsu N, Karube F, Sekigawa A, Kato S, Yamaguchi N, Hirai Y, Morishima M, Kawaguchi Y (2011) Selective Coexpression of Multiple Chemical Markers Defines Discrete Populations of Neocortical GABAergic Neurons. Cerebral Cortex 21:1803-1817.

Lakatos P, Chen CM, O'Connell MN, Mills A, Schroeder CE (2007) Neuronal oscillations and multisensory interaction in primary auditory cortex. Neuron 53:279-292.

Lakatos P, Karmos G, Mehta AD, Ulbert I, Schroeder CE (2008) Entrainment of neuronal oscillations as a mechanism of attentional selection. Science 320:110-113.

Lam Y-W, Sherman SM (2009) Functional organization of the somatosensory cortical layer 6 feedback to the thalamus. Cerebral Cortex:bhp077.

Larkum ME, Zhu JJ, Sakmann B (1999) A new cellular mechanism for coupling inputs arriving at different cortical layers. Nature 398:338-341.

Larkum ME, Zhu JJ, Sakmann B (2001) Dendritic mechanisms underlying the coupling of the dendritic with the axonal action potential initiation zone of adult rat layer 5 pyramidal neurons. JPhysiol 533:447-466.

Larkum ME, Senn W, Luscher HR (2004) Top-down Dendritic Input Increases the Gain of Layer 5 Pyramidal Neurons. Cerebral Cortex 14:1059-1070.

Larsen DD, Wickersham IR, Callaway EM (2007) Retrograde Tracing with Recombinant Rabies Virus Reveals Correlations Between Projection Targets and Dendritic Architecture in Layer 5 of Mouse Barrel Cortex. Frontiers in Neural Circuits 1:5.

Le Be JV, Silberberg G, Wang Y, Markram H (2007) Morphological, electrophysiological, and synaptic properties of corticocallosal pyramidal cells in the neonatal rat neocortex. CerebCortex 17:2204-2213.

Lee S, Kruglikov I, Huang ZJ, Fishell G, Rudy B (2013) A disinhibitory circuit mediates motor integration in the somatosensory cortex. Nat Neurosci 16:1662-1670.

LeVay S, Gilbert CD (1976) Laminar patterns of geniculocortical projection in the cat. Brain research 113:1-19.

Linden JF, Schreiner CE (2003) Columnar transformations in auditory cortex? A comparison to visual and somatosensory cortices. Cerebral Cortex 13:83-89.

Linke R (1999) Differential projection patterns of superior and inferior collicular neurons onto posterior paralaminar nuclei of the thalamus surrounding the medial geniculate body in the rat. European Journal of Neuroscience 11:187-203.

Linke R, Schwegler H (2000) Convergent and complementary projections of the caudal paralaminar thalamic nuclei to rat temporal and insular cortex. CerebCortex 10:753-771.

Llano DA, Sherman SM (2008) Evidence for nonreciprocal organization of the mouse auditory thalamocortical-corticothalamic projection systems. J Comp Neurol 507:1209-1227.

Lübke J, Egger V, Sakmann B, Feldmeyer D (2000) Columnar organization of dendrites and axons of single and synaptically coupled excitatory spiny neurons in layer 4 of the rat barrel cortex. The Journal of Neuroscience 20:5300-5311.

Luczak A, Bartho P, Harris KD (2013) Gating of sensory input by spontaneous cortical activity. JNeurosci 33:1684-1695.

Makeig S, Westerfield M, Jung TP, Enghoff S, Townsend J, Courchesne E, Sejnowski TJ (2002) Dynamic brain sources of visual evoked responses. Science 295:690-694.

Malmierca MS, Merchán MA, Henkel CK, Oliver DL (2002) Direct projections from cochlear nuclear complex to auditory thalamus in the rat. The Journal of neuroscience 22:10891-10897.

Markram H, Toledo-Rodriguez M, Wang Y, Gupta A, Silberberg G, Wu CZ (2004) Interneurons of the neocortical inhibitory system. Nature Reviews Neuroscience 5:793-807.

Martinez-Montes E, Cuspineda-Bravo ER, El-Deredy W, Sanchez-Bornot JM, Lage-Castellanos A, Valdes-Sosa PA (2008) Exploring event-related brain dynamics with tests on complex valued time-frequency representations. StatMed 27:2922-2947.

Maunsell JH, Gibson JR (1992) Visual response latencies in striate cortex of the macaque monkey. JNeurophysiol 68:1332-1344.

Mechawar N, Cozzari C, Descarries L (2000) Cholinergic innervation in adult rat cerebral cortex: a quantitative immunocytochemical description. J Comp Neurol 428:305-318.

Merzenich MM, Knight PL, Roth GL (1975) Representation of cochlea within primary auditory cortex in the cat. JNeurophysiol 38:231-249.

Middlebrooks JC, Dykes RW, Merzenich MM (1980) Binaural response-specific bands in primary auditory cortex (AI) of the cat: topographical organization orthogonal to isofrequency contours. Brain Res 181:31-48.

Miller KD, Pinto DJ, Simons DJ (2001) Processing in layer 4 of the neocortical circuit: new insights from visual and somatosensory cortex. CurrOpinNeurobiol 11:488-497.

Miller LM, Escabi MA, Read HL, Schreiner CE (2002) Spectrotemporal receptive fields in the lemniscal auditory thalamus and cortex. JNeurophysiol 87:516-527.

Mitani A, Shimokouchi M (1985) Neuronal connections in the primary auditory cortex: an electrophysiological study in the cat. JComp Neurol 235:417-429.

Mitchell BD, Cauller LJ (2001) Corticocortical and thalamocortical projections to layer I of the frontal neocortex in rats. Brain Research 921:68-77.

Mitchell JF, Sundberg KA, Reynolds JH (2009) Spatial attention decorrelates intrinsic activity fluctuations in macaque area V4. Neuron 63:879-888.

Mochol G, Hermoso-Mendizabal A, Sakata S, Harris KD, de la Rocha J (2015) Stochastic transitions into silence cause noise correlations in cortical circuits. Proceedings of the National Academy of Sciences 112:3529-3534.

Moore AK, Wehr M (2013) Parvalbumin-expressing inhibitory interneurons in auditory cortex are well-tuned for frequency. The Journal of Neuroscience 33:13713-13723.

Mountcastle VB (1997) The columnar organization of the neocortex. Brain 120 (Pt 4):701-722.

Niell CM, Stryker MP (2010) Modulation of visual responses by behavioral state in mouse visual cortex. Neuron 65:472-479.

Obermayer K, Blasdel GG (1993) Geometry of orientation and ocular dominance columns in monkey striate cortex. J Neurosci 13:4114-4129.

Ojima H (1994) Terminal morphology and distribution of corticothalamic fibers originating from layers 5 and 6 of cat primary auditory cortex. CerebCortex 4:646-663.

Oswald AM, Schiff ML, Reyes AD (2006) Synaptic mechanisms underlying auditory processing. Current Opinion in Neurobiology 16:371-376.

Oviedo HV, Bureau I, Svoboda K, Zador AM (2010) The functional asymmetry of auditory cortex is reflected in the organization of local cortical circuits. NatNeurosci 13:1413-1420.

Packer AM, Yuste R (2011) Dense, unspecific connectivity of neocortical parvalbumin-positive interneurons: a canonical microcircuit for inhibition? The Journal of Neuroscience 31:13260-13271.

Panzeri S, Rolls ET, Battaglia F, Lavis R (2001) Speed of feedforward and recurrent processing in multilayer networks of integrate-and-fire neurons. Network: Computation in Neural Systems 12:423-440.

Petersen CCH, Hahn TTG, Mehta M, Grinvald A, Sakmann B (2003) Interaction of sensory responses with spontaneous depolarization in layer 2/3 barrel cortex. Proceedings of the National Academy of Sciences of the United States of America 100:13638-13643.

Petrof I, Viaene AN, Sherman SM (2011) Two populations of corticothalamic and interareal corticocortical cells in the subgranular layers of the mouse primary sensory cortices. JComp Neurol.

Pfeffer CK, Xue M, He M, Huang ZJ, Scanziani M (2013) Inhibition of inhibition in visual cortex: the logic of connections between molecularly distinct interneurons. Nature Neuroscience 16:1068-1076.

Pfurtscheller G, Lopes da Silva FH (1999) Event-related EEG/MEG synchronization and desynchronization: basic principles. ClinNeurophysiol 110:1842-1857.

Pi HJ, Hangya B, Kvitsiani D, Sanders JI, Huang ZJ, Kepecs A (2013) Cortical interneurons that specialize in disinhibitory control. Nature 503:521-524.

Poulet JF, Petersen CC (2008) Internal brain state regulates membrane potential synchrony in barrel cortex of behaving mice. Nature 454:881-885.

Poulet JF, Fernandez LM, Crochet S, Petersen CC (2012) Thalamic control of cortical states. Nat Neurosci 15:370-372.

Reig R, Sanchez-Vives MV (2007) Synaptic transmission and plasticity in an active cortical network. PLoS One 2:e670-e670.

Reig R, Zerlaut Y, Vergara R, Destexhe A, Sanchez-Vives MV (2015) Gain modulation of synaptic inputs by network state in auditory cortex in vivo. The Journal of Neuroscience 35:2689-2702.

Rigas P, Castro-Alamancos MA (2007) Thalamocortical Up states: differential effects of intrinsic and extrinsic cortical inputs on persistent activity. The Journal of Neuroscience 27:4261-4272.

Rigas P, Castro-Alamancos MA (2009) Impact of persistent cortical activity (up states) on intracortical and thalamocortical synaptic inputs. Journal of Neurophysiology 102:119-131.

Rockland KS, Pandya DN (1979) Laminar origins and terminations of cortical connections of the occipital lobe in the rhesus monkey. Brain Res 179:3-20.

Romanski LM, LeDoux JE (1993) Organization of rodent auditory cortex: anterograde transport of PHA-L from MGv to temporal neocortex. CerebCortex 3:499-514.

Rubio-Garrido P, Pérez-de-Manzo F, Porrero C, Galazo MJ, Clascá F (2009) Thalamic input to distal apical dendrites in neocortical layer 1 is massive and highly convergent. Cerebral Cortex 19:2380-2395.

Rudy B, Fishell G, Lee S, Hjerling-Leffler J (2011) Three groups of interneurons account for nearly 100% of neocortical GABAergic neurons. Developmental neurobiology 71:45-61.

Runyan CA, Schummers J, Van Wart A, Kuhlman SJ, Wilson NR, Huang ZJ, Sur M (2010) Response Features of Parvalbumin-Expressing Interneurons Suggest Precise Roles for Subtypes of Inhibition in Visual Cortex. Neuron 67:847-857.

Ryugo DK, Killackey HP (1974) Differential telencephalic projections of the medial and ventral divisions of the medial geniculate body of the rat. Brain Research 82:173-177.

Sachdev RN, Ebner FF, Wilson CJ (2004) Effect of subthreshold up and down states on the whisker-evoked response in somatosensory cortex. Journal of neurophysiology 92:3511-3521.

Sakata S, Harris KD (2009) Laminar structure of spontaneous and sensory-evoked population activity in auditory cortex. Neuron 64:404-418.

Sally SL, Kelly JB (1988) Organization of auditory cortex in the albino rat: sound frequency. J Neurophysiol 59:1627-1638.

Sanchez-Vives MV, McCormick DA (2000) Cellular and network mechanisms of rhythmic recurrent activity in neocortex. NatNeurosci 3:1027-1034.

Schnupp JW, Mrsic-Flogel TD, King AJ (2001) Linear processing of spatial cues in primary auditory cortex. Nature 414:200-204.

Schölvinck ML, Saleem AB, Benucci A, Harris KD, Carandini M (2015) Cortical State Determines Global Variability and Correlations in Visual Cortex. The Journal of Neuroscience 35:170-178.

Shen JX, Xu ZM, Yao YD (1999) Evidence for columnar organization in the auditory cortex of the mouse. Hearing Research 137:174-177.

Shepherd GMG, Svoboda K (2005) Laminar and Columnar Organization of Ascending Excitatory Projections to Layer 2/3 Pyramidal Neurons in Rat Barrel Cortex. Journal of Neuroscience 25:5670-5679.

Sherman SM, Guillery RW (1998) On the actions that one nerve cell can have on another: distinguishing "drivers" from "modulators". Proceedings of the National Academy of Sciences 95:7121-7126.

Sherman SM, Guillery R (2002) The role of the thalamus in the flow of information to the cortex. Philosophical Transactions of the Royal Society B: Biological Sciences 357:1695-1708.

Silberberg G, Markram H (2007) Disynaptic inhibition between neocortical pyramidal cells mediated by Martinotti cells. Neuron 53:735-746.

Singer W, Gray CM (1995) Visual feature integration and the temporal correlation hypothesis. Annual Review of Neuroscience 18:555-586.

Smith PH, Populin LC (2001) Fundamental differences between the thalamocortical recipient layers of the cat auditory and visual cortices. JComp Neurol 436:508-519.

Smith PH, Manning KA, Uhlrich DJ (2010) Evaluation of inputs to rat primary auditory cortex from the suprageniculate nucleus and extrastriate visual cortex. JComp Neurol 518:3679-3700.

Smith PH, Uhlrich DJ, Manning KA, Banks MI (2012) Thalamocortical projections to rat auditory cortex from the ventral and dorsal divisions of the medial geniculate nucleus. JComp Neurol 520:34-51.

Sohya K, Kameyama K, Yanagawa Y, Obata K, Tsumoto T (2007) GABAergic neurons are less selective to stimulus orientation than excitatory neurons in layer II/III of visual cortex, as revealed by in vivo functional Ca2+ imaging in transgenic mice. The Journal of neuroscience 27:2145-2149.

Sretavan D, Dykes RW (1983) The organization of two cutaneous submodalities in the forearm region of area 3b of cat somatosensory cortex. Journal of Comparative Neurology 213:381-398.

Staiger JF, Flagmeyer I, Schubert D, Zilles K, Kötter R, Luhmann HJ (2004) Functional Diversity of Layer IV Spiny Neurons in Rat Somatosensory Cortex: Quantitative Morphology of Electrophysiologically Characterized and Biocytin Labeled Cells. Cerebral Cortex 14:690-701.

Steriade M, Nunez A, Amzica F (1993) A Novel Slow (Less-Than-1 Hz) Oscillation of Neocortical Neurons In-Vivo - Depolarizing and Hyperpolarizing Components. Journal of Neuroscience 13:3252-3265.

Steriade M, Amzica F, Contreras D (1996) Synchronization of fast (30-40 Hz) spontaneous cortical rhythms during brain activation. Journal of Neuroscience 16:392-417.

Steriade M, Timofeev I, Grenier F (2001) Natural waking and sleep states: A view from inside neocortical neurons. Journal of Neurophysiology 85:1969-1985.

Stroh A, Adelsberger H, Groh A, Ruhlmann C, Fischer S, Schierloh A, Deisseroth K, Konnerth A (2013) Making waves: initiation and propagation of corticothalamic Ca2+ waves in vivo. Neuron 77:1136-1150.

Sugimoto S, Sakurada M, Horikawa J, Taniguchi I (1997) The columnar and layer-specific response properties of neurons in the primary auditory cortex of Mongolian gerbils. Hearing Research 112:175-185.

Sur M, Wall JT, Kaas J (1984) Modular distribution of neurons with slowly adapting and rapidly adapting responses in area 3b of somatosensory cortex in monkeys. Journal of neurophysiology 51:724-744.

Tallon-Baudry C, Bertrand O (1999) Oscillatory gamma activity in humans and its role in object representation. Trends Cogn Sci 3:151-162.

Tallon-Baudry C, Bertrand O, Delpuech C, Pernier J (1996) Stimulus specificity of phase-locked and non-phase-locked 40 Hz visual responses in human. JNeurosci 16:4240-4249.

Theyel BB, Llano DA, Sherman SM (2010) The corticothalamocortical circuit drives higher-order cortex in the mouse. Nat Neurosci 13:84-88.

Thomson A, Bannister A (1998) Postsynaptic pyramidal target selection by descending layer III pyramidal axons: dual intracellular recordings and biocytin filling in slices of rat neocortex. Neuroscience 84:669-683.

Thomson AM (2010) Neocortical Layer 6, A Review. Frontiers in Neuroanatomy 4:13.

Thomson AM, Bannister AP (2003) Interlaminar connections in the neocortex. CerebCortex 13:5-14.

Thomson AM, Lamy C (2007) Functional maps of neocortical local circuitry. Front Neurosci 1:19-42.

Tsodyks M, Uziel A, Markram H (2000) Synchrony generation in recurrent networks with frequency-dependent synapses. JNeurosci 20:RC50.

Varela F, Lachaux JP, Rodriguez E, Martinerie J (2001) The brainweb: phase synchronization and large-scale integration. NatRevNeurosci 2:229-239.

Varela FJ (1994) Resonant cell assemblies: a new approach to cognitive functions and neuronal synchrony. Biological research 28:81-95.

Vercelli A, Assal F, Innocenti GM (1992) Emergence of callosally projecting neurons with stellate morphology in the visual cortex of the kitten. Exp Brain Res 90:346-358.

Vinje WE, Gallant JL (2000) Sparse coding and decorrelation in primary visual cortex during natural vision. Science 287:1273-1276.

Vogt BA (1991) The role of layer I in cortical function. In: Cerebral Cortex (Peters A, Jones EG, eds), pp 49-79. New York: Plenum Press.

Wang J, Caspary D, Salvi RJ (2000) GABA-A antagonist causes dramatic expansion of tuning in primary auditory cortex. Neuroreport 11:1137-1140.

Wang X (2007) Neural coding strategies in auditory cortex. Hearing Research 229:81-93.

Watson BO, MacLean JN, Yuste R (2008) UP states protect ongoing cortical activity from thalamic inputs. PLoSOne 3:e3971.

Wepsic JG (1966) Multimodal sensory activation of cells in the magnocellular medial geniculate nucleus. Experimental neurology 15:299-318.

Wester JC, Contreras D (2012) Columnar interactions determine horizontal propagation of recurrent network activity in neocortex. JNeurosci 32:5454-5471.

White EL (1978) Identified neurons in mouse Sml cortex which are postsynaptic to thalamocortical axon terminals: a combined Golgi-electron microscopic and degeneration study. Journal of Comparative Neurology 181:627-661.

White EL, Rock MP (1979) Distribution of thalamic input to different dendrites of a spiny stellate cell in mouse sensorimotor cortex. NeurosciLett 15:115-119.

White EL, Hersch SM (1982) A quantitative study of thalamocortical and other synapses involving the apical dendrites of corticothalamic projection cells in mouse SmI cortex. J Neurocytol 11:137-157.

Winer JA (1992) The functional architecture of the medial geniculate body and the primary auditory cortex. In: The mammalian auditory pathway: Neuroanatomy, pp 222-409: Springer.

Winer JA, Prieto JJ (2001) Layer V in cat primary auditory cortex (AI): cellular architecture and identification of projection neurons. JComp Neurol 434:379-412.

Winer JA, Miller LM, Lee CC, Schreiner CE (2005) Auditory thalamocortical transformation: structure and function. Trends Neurosci 28:255-263.

Winkowski DE, Kanold PO (2013) Laminar transformation of frequency organization in auditory cortex. The Journal of Neuroscience 33:1498-1508.

Xu H, Jeong HY, Tremblay R, Rudy B (2013) Neocortical Somatostatin-Expressing GABAergic Interneurons Disinhibit the Thalamorecipient Layer 4. Neuron 77:155-167.

Xu X, Roby KD, Callaway EM (2010) Immunochemical characterization of inhibitory mouse cortical neurons: three chemically distinct classes of inhibitory cells. Journal of Comparative Neurology 518:389-404.

Yabuta NH, Callaway EM (1998) Functional streams and local connections of layer 4C neurons in primary visual cortex of the macaque monkey. The Journal of neuroscience 18:9489-9499.

Yamawaki N, Borges K, Suter BA, Harris KD, Shepherd GMG (2015) A genuine layer 4 in motor cortex with prototypical synaptic circuit connectivity.

Yeung N, Bogacz R, Holroyd CB, Cohen JD (2004) Detection of synchronized oscillations in the electroencephalogram: an evaluation of methods. Psychophysiology 41:822-832.

Zohary E, Shadlen MN, Newsome WT (1994) Correlated neuronal discharge rate and its implications for psychophysical performance. Nature 370:140-143.

Chapter 2

This Chapter was published previously as:

Krause BM, Banks MI (2013) Analysis of stimulus-related activity in rat auditory cortex using complex spectral coefficients. J Neurophysiol 110:621-639.

Analysis of stimulus-related activity in rat auditory cortex using complex spectral coefficients

Bryan M. Krause[†], B.S. and Matthew I. Banks, Ph.D.[*]

Department of Anesthesiology, University of Wisconsin, Madison, WI 53706

[*]Associate Professor of Anesthesiology

[†]Research Assistant, Neuroscience Training Program

Financial support: *Supported by National Institutes of Health (Bethesda, MD) DC006013 (to M. I. Banks) and T32-GM007507 (to B.M. Krause), the American Hearing Research Foundation, and the Department of Anesthesiology, University of Wisconsin, Madison, WI.*

Acknowledgements: *The authors thank Jane Sekulski (Senior Programmer, Department of Anesthesiology, University of Wisconsin, Madison, WI), Sneha Shrestha, Rita S. Burlingame, Abigail Schuh, Michael R. Rummel and Bryan Baxter (Lab Assistants, Department of Anesthesiology, University of Wisconsin, Madison, WI) for technical support, and Harald Hentschke (Department of Anesthesiology, Eberhard Karls Universität Tübingen, Tübingen, Germany) for comments on the manuscript.*

Abstract

The neural mechanisms of sensory responses recorded from the scalp or cortical surface remain controversial. Evoked versus induced response components (i.e. changes in mean versus variance) are associated with bottom-up versus top-down processing, but trial-by-trial response variability can confound this interpretation. Phase reset of ongoing oscillations has also been postulated to contribute to sensory responses. Here, we present evidence that responses under passive listening conditions are dominated by variable evoked response components. We measured the mean, variance and phase of complex time-frequency coefficients of epidurally-recorded responses to acoustic stimuli in rats. During the stimulus, changes in mean, variance and phase tended to co-occur. After the stimulus, there was a small, low frequency offset response in the mean, and modest, prolonged desynchronization in the alpha band. Simulations showed that trial-by-trial variability in the mean can account for most of the variance and phase changes observed during the stimulus. This variability was state-dependent, with smallest variability during periods of greatest arousal. Our data suggest that cortical responses to auditory stimuli reflect variable inputs to the cortical network. These analyses suggest that caution should be exercised when interpreting variance and phase changes in terms of top-down cortical processing.

Introduction

Neural responses recorded from sensory cortex as stimulus-related surface potentials (SRSPs, e.g. from the scalp or dura) are frequently used to investigate drug effects on perception and cognition and circuit manifestations of neuropathologies (Kane et al 2000; Banoub et al 2003; Roach and Mathalon 2008). A critical issue when interpreting SRSPs is the source of the response itself. SRSPs may consist of a rearrangement of ongoing activity and/or an entirely new, additive component. Because ongoing

activity in cortex is large compared to perturbations associated with sensory stimuli, under experimental and diagnostic conditions the stimulus typically is repeated and SRSPs averaged over many trials to capture the 'evoked' response, which reflects additive components precisely time-locked to stimulus onset. However, a substantial amount of information is discarded when considering only the evoked response, as cortical responses are quite variable and this trial-by-trial variability may contain information about the circuit components responding to the stimulus and about their recent activity. Some of the latter information is captured in the ‘induced’ response, which reflects poorly phase-locked additive components and rearrangements of ongoing activity that contribute to the variance but not the mean of the response (Tallon-Baudry et al 1996; Klimesch et al 1998).

The distinction between evoked and induced responses is of interest because of the postulated mechanisms generating these components. Evoked activity is thought to arise from feed-forward propagation of sensory information through the cortical network, and is typically associated with the response of a static network to input from the periphery. Under this model, the evoked response results from a linear combination of an invariant additive component with variable background activity. By contrast, the induced response is thought to arise from stimulus-related modulation of network parameters (e.g. connection strength, membrane properties) and/or activation of cortico-cortical or cortico-thalamo-cortical feedback loops (Pfurtscheller and Lopes da Silva 1999; David et al 2006). By far the most common method for extracting the 'induced' component is to obtain the residual after subtracting the averaged evoked component from the single trial responses and estimate its power (Kalcher and Pfurtscheller 1995; Klimesch et al 1998). To the extent that this theoretical dichotomy holds, it is useful for assigning neural mechanisms to different response components. In reality, however, evoked and induced responses can become entangled in several ways, complicating their interpretation in terms of bottom-up versus top-down and static versus dynamic network properties. Nonlinear interactions between stimulus and ongoing activity can result in non-stationary background

activity, and the evoked response itself can vary from trial to trial. Thus, the residual is a combination of both components due to processes commonly ascribed to induced components, e.g. reorganization of ongoing activity and indirect triggering of oscillatory responses, as well as contributions due to trial-by-trial variability in amplitude and timing of the evoked response (Truccolo et al 2002; David et al 2006; Hu et al 2009). Top-down processes that are reliably elicited by sensory stimuli will also appear in the evoked response (Picton 1992).

A third contributor to SRSPs is a phase reset of ongoing oscillatory activity. Phase synchrony has been proposed as a useful mechanism for facilitating integration between local neural assemblies (Varela et al 2001). A phase reset produces an average time-domain response in the absence of an additive component. However, commonly used measures of phase reset such as inter-trial coherence (ITC) (Tallon-Baudry et al 1996; Makeig et al 2002; Lakatos et al 2007) are particularly susceptible to confounds due to additive components (Yeung et al 2004; Martinez-Montes et al 2008; Krieg et al 2011), and other methods are susceptible to this confound as well (e.g. Jansen et al 2003; for a more complete discussion, see Krieg et al 2011).Thus, as for evoked versus induced components, phase reset and additive components can become entangled, complicating their interpretation, and the contribution of phase reset to auditory SRSPs remains controversial (Sayers et al 1974; Jervis et al 1983; Makeig et al 2002; Makinen et al 2005; Hanslmayr et al 2007; Sauseng et al 2007; Krieg et al 2011). Here, we present and discuss methods to separate these components that would be useful for simplifying their interpretation.

In particular, we show that trial-by-trial variability in an additive component can be manifested as changes in variance and phase, and thus open to misinterpretation. The primary means by which we show this is via simulations based on our recorded data. The purpose of analyzing simulated responses was twofold: first, these analyses provide a proof of principle that apparent induced and phase reset responses can be produced solely by trial-by-trial variability in the amplitude or latency of evoked

components. Second, a crucial benefit of having a generative or forward model of trial-by- trial variability is that we can address key questions about the relationship between the variability of evoked responses and background activity. We estimate the amplitude and latency variability of evoked responses by fitting the simulation model to empirical data features, then show that this variability is state dependent and correlates with electrophysiological measures of cortical arousal. This would not be possible without a generative model with which we could estimate the amplitude and latency variations.

Ongoing activity and SRSPs are broadband, and distinct frequency components have been associated with specific behavioral states, cortical loci and circuit mechanisms (Buzsaki 2006). Thus, substantial information about underlying cortical processes may be gained via spectral decomposition, most typically via time-frequency analysis (Jordan et al 1997), which yields spectrograms that portray the evolution of frequency-specific activity over time relative to stimulus onset. The utility of analyzing complex spectral coefficients for disentangling evoked, induced and phase reset response components has been highlighted recently (Martinez-Montes et al 2008; Krieg et al 2011). In this analysis, the set of coefficients at each time-frequency point recorded over many trials and plotted in the complex plane was shown to exhibit specific stimulus-related behaviors depending on the components contributing to the response. We have adapted this analysis to assist in disentangling changes in mean, variance and phase of spectral coefficients, and we discuss several ways in which this analysis can still be confounded due to trial-by-trial variability in the additive component.

Materials and Methods

All experimental protocols conformed to American Physiological Society/National Institutes of Health guidelines and were approved by the University of Wisconsin Research Animal Resources Committee.

Electrode preparation

Epidural electrode arrays were used for all electrophysiological recordings. The arrays consisted of 16 formvar-insulated stainless steel microwires (100 μm diameter; stainless steel 304; California Fine Wire, Grover Beach, CA) separated by 660 μm and arranged in three rows separated by 1000 μm and embedded in a 4.0 mm diameter, 2 mm thick epoxy disc. Wires were cut flush with the surface of the epoxy disc and the disc ground with a curved burr bit to form a concavity that complemented the surface of the brain. The microwires were attached to an electrode interface board (EIB-16, Neuralynx Inc., Bozeman, MT) which provided contact with a small profile connector (0.025 dual row 18 pin connector, Omnetics Connector Corporation, Minneapolis, MN) for the amplifier head stage. The impedance of the electrodes at 1 kHz was typically 50 – 200 kΩ.

Electrode implantation

Sixteen female rats 8 – 12 weeks old were surgically implanted with electrode arrays over the left (n = 10) or right (n = 6) auditory cortex. Results from recordings from the right versus left hemispheres were indistinguishable and were pooled for analysis. The surgical procedures were as follows. Anesthesia was induced using isoflurane. Following induction, animals were medicated with midazolam (3 mg/kg, IP, to reduce the anesthetic requirement during surgery), the non-steroidal anti-inflammatory agent ketoprofen (5 mg/kg, SQ, for postoperative swelling and pain), the opiate analgesic buprenorphine (0.05 mg/kg, SQ, for postoperative pain), the local anesthetic bupivicaine (1 mg/kg, SQ, applied to the injection site and into the left or right temporalis muscle, depending on the implant site, for perioperative pain). Animals were then placed in a stereotaxic head holder (Model 1900, David Kopf Instruments, **Tujunga**, CA). Anesthesia was maintained with isoflurane at 1.2 – 1.6% mixed with 50% O_2 and 50% room air applied through a small rodent anesthesia mask, with the exact dosage adjusted to maintain an adequate surgical level as determined by immobility and lack of response to toe pinch.

Animals were hydrated via subcutaneous injections of ~2 ml 0.9% saline, and ophthalmic ointment was applied to prevent dehydration of the cornea. The animal's body temperature was monitored using a rectal probe thermometer, and was maintained at ~37°C throughout the surgery by wrapping the animal in a warm water blanket.

The fur over the dorsal skull was removed with a clipper and the skin disinfected with iodine solution and alcohol. An incision was made in the scalp overlying the dorsal surface of the skull along the midline, the skin retracted to expose the skull, and subcutaneous tissue and periosteum retracted laterally. Membranous tissue was removed from the skull using a scraper. Self-tapping stainless steel bone screws (1.17 mm diameter; Fine Science Tools, Foster City, CA) were placed in the skull in the ipsilateral frontal, contralateral parietal and ipsilateral occipital bones to assist in anchoring the electrode and interface board. A silver wire was attached to the screw in the parietal bone and served as a reference electrode. The ipsilateral temporalis muscle was dissected away from the skull and retracted laterally and ventrally using a three-pronged retractor to expose the skull ridge. Care was taken to minimize damage to the temporalis muscle to facilitate recovery after the surgery. A hole 4 mm in diameter was made in the temporal bone centered over the auditory cortex using a trephine (#18004-50, Fine Science Tools, Foster City, CA) while leaving the dura intact. Published stereotaxic coordinates of auditory cortex in the rat were used to determine the center of the craniotomy (Doron et al 2002). The multielectrode recording array was lowered onto the dura and covered in dental acrylic, and the electrode interface board cemented onto the top of the skull using dental acrylic to form a head cap. Buprenorphine (0.05 mg/kg, SQ, every 12 hours) and ketoprofen (5 mg/kg, SQ, every 24 hours) were administered for three days postoperatively for pain.

Electrophysiological recordings

Animals were allowed to recover one week before their first recording session. Animals were placed in a home-made acrylic enclosure (length x width x height = 24 x 18 x 12cm) inside a sound attenuation chamber (Industrial Acoustics Company, Inc., Bronx, NY). A small speaker (TDT- ES1, Tucker Davis Technologies, Alachua, FL) was mounted on the top ('ceiling') of the enclosure, oriented towards the animal. The speaker was calibrated using a microphone (#4016, ACO Pacific, Inc., Belmont, CA) placed approximately 4 cm from the speaker, and stimuli presented at approximately 75 dB SPL assuming the animal's head was this distance from the speaker. Speaker output varied by ±3 dB SPL over the range 10 – 20 kHz. A sixteen channel preamplifier on a flexible tether (HS16, Neuralynx Inc., Bozeman, MT) entered the enclosure and was attached to the animal's head. The animal was able to move freely in the enclosure. Since the animal was unrestrained, actual stimulus levels on each trial varied slightly.

Free-field stimuli were applied using software (RPVDX, Tucker-Davis Technologies, Alachua, FL) triggered by the electrophysiological recording software (pClamp v8.2, Molecular Devices, Sunnyvale, CA). Stimuli consisted of 250 ms FM sweeps (10 – 20 kHz), presented every 8 seconds for a period of one hour. We note that this intertrial interval is long relative to most studies in which shorter, nonrandom inter-trial intervals result in more predictable stimulus times and possibly minimize endogenous sources of response variability. We observed considerable variability of responses during the initial portion of the recording session as the animals became acclimated to the environment, and the data presented here represent the final 100 trials from each recording session. Sporadic remote video observations during this period indicated that the animals typically were awake but immobile during this time period, but we did not verify the animal's behavioral state on a trial-by-trial basis. Data were pooled across multiple recording sessions (n = 2 – 7 recording sessions for each animal, one session per day).

Responses were bandpass-filtered at 0.1-3000 Hz, amplified 2500X (Lynx 8, Neuralynx, Tucson, AZ) and digitized at 6.25 kHz (Digidata 1322A, Molecular Devices, Sunnyvale, CA). Each trial consisted of a single stimulus presentation presented at time $t = 0$. For each trial, data were collected for 3200 ms, beginning 658 ms before the stimulus.

Analysis of electrophysiological data

Recorded auditory responses were averaged, and the channel with the shortest latency and largest amplitude response (i.e. largest root-mean-square power computed during the time window 0 < t <300 ms) was assumed to be over primary auditory cortex and was chosen for analysis. We will refer to the single trial responses as $y_{i,k}$, $i = 1..L$, $k = 1..N_{Samples}$, where L is the number of trials and $N_{Samples}$ is the number of sampled data points in a trial. Two criteria were used to reject trials contaminated by electrical or mechanical artifacts. The first criterion eliminated trials during which the headstage amplifier saturated following mechanical impact, e.g. with the walls of the recording chamber: $\mu_i > \mu_{Crit}$, where $\mu_i = \sum_{k=1}^{N_{Samples}} y_{i,k} \Big/ N_{Samples}$ and μ_{Crit} was set to 1 mV. The second criterion eliminated trials that had large spurious electrical and mechanical artifacts: $\sigma_i > \sigma_{Crit}$, where $\sigma_i = \sqrt{\sum_{k=1}^{N_{Samples}} (y_{i,k} - \mu_i)^2} \Big/ (N_\sigma - 1)$, computed over the portion of the trial excluding the window $0 < t < 1000$ ms (so as not to exclude trials due to unusually large responses), N_σ is the number of sample points in the computation, and σ_{Crit} was set to 0.25 mV. In all experiments, ≤5% of the trials were rejected under these criteria.

Time-frequency analysis

We used time-frequency analysis to gain a detailed view of how specific frequency components contributed to the stimulus-related response, and how the stimulus-related changes in these

components related to ongoing activity. Time-frequency analysis of neural activity recorded over auditory cortex was performed using short-term Fourier transforms (STFT) for five frequencies from 3 to 16 Hz and continuous complex Morlet wavelet transforms (5 cycles) for frequencies from 16 to 300 Hz. STFTs were implemented by first down-sampling the data by a factor of 4 (sample interval = 0.64 msec), then tapering the data with a Hamming window and computing sliding Fourier transforms with window width of 512 points and window overlap of 496 points. This choice of window width was a compromise between time and frequency resolution, and determined the minimum analysis frequency of 3 Hz. For the analysis of Figure 11 in which we explored the state-dependence of variability in the additive component of the response, we also calculated the coefficients at ~1.5 Hz by doubling the size of this window to 1024 points. Pre-stimulus delta power for this analysis was then calculated by averaging the power at f = 1.5 Hz and f = 3 Hz. Wavelet transforms were implemented as in (Jordan et al 1997), with 35 frequencies spaced exponentially to ensure 90% overlap in the pass band of adjacent Morlet filters. Transforms were computed for each trial for the initial 16384 data samples (2621 ms). The frequency boundary (16 Hz) at which we transitioned from STFT to wavelet analysis was chosen based on the time resolution of the method, which was 164 msec for the STFT analysis and ≤164 msec (and improving with increasing frequency) for the wavelet analysis.

Statistical analysis of wavelet and STFT data was performed using a recently described method that performs tests on the complex coefficients computed on each trial for each frequency component (Martinez-Montes et al 2008). Briefly, the time-frequency analysis yields a complex valued coefficient $z_i(t,f)$ on the i^{th} trial at each time point and for each frequency. At any time point, these coefficients can be visualized as points or vectors in the complex plane, specified by their magnitude and phase. In the pre-stimulus period, ongoing activity is characterized by coefficients whose magnitudes and phases are randomly distributed and over many trials will form a cloud centered at the origin with zero mean and a uniform distribution of phases. The radius of the cloud, which is related to its variance, represents the

amplitude of ongoing activity for that frequency component at that time point. A sensory stimulus may alter this ongoing activity, and thus this cloud of coefficients, in three ways. First, evoked activity describes new ('added') activity at a particular frequency that is time-locked to the stimulus onset. Evoked activity is represented in the complex plane as a shift of the complex coefficients in the direction of a vector representing the additive component's amplitude and phase (i.e. its angle with the horizontal axis). Second, an increase or decrease in the magnitude of the frequency component that is not time-locked to the stimulus (i.e. a change in variance) corresponds to induced synchronization or desynchronization of activity. Induced activity will change the variance of the cloud, but will not shift its center away from origin. Note that the terms 'synchronization' and 'desynchronization' suggest a simple reorganization of extant neuronal activity, but could also involve an increase or decrease in activity levels (i.e. more or fewer neurons participating) as long as those changes are not time-locked to the stimulus. Finally, if the stimulus does not evoke additional activity but instead reorganizes the ongoing activity in the cortical network, i.e. triggers a phase reset, the coefficients will have nonrandom phase, but the magnitude of the distance from the origin to each point will be unchanged from the pre-stimulus condition. The stimulus may trigger evoked, induced and/or phase reset responses simultaneously.

Among the several ways we will measure the average properties of these complex coefficients, there are two that are distinct but easily confused. The complex mean *('mean')* is the mean of all the points in the cloud, taking into account their directions from the origin. Stimulus-related changes in the *mean* are usually associated with additive response components, but the *mean* can also be changed by phase reset. Synchronization and desynchronization (i.e. increases and decreases in the *variance* of complex coefficients) refer to amplitude changes that are phase-invariant and have no effect on the *mean*. By contrast, the power of the coefficients is their magnitude squared, regardless of their phase, and is represented by the average of single-trial power spectrograms. The power is equal to the *variance* plus the square of the magnitude of the *mean*. Thus, both additive and synchronizing/desynchronizing

effects will appear as changes in the power spectrum, as in both cases the magnitude of the complex coefficients will change, whereas phase resets will not affect power (as any increases in the magnitude of the *mean* are offset by decreases in the *variance*). The analysis utilized here is intended to better distinguish between the three mechanisms that could mediate changes in the *mean* and the power spectrum. It should be noted that while the three mechanisms proposed are independent, their measures (as discussed in the following paragraphs) are not. In the Results section, "*Disentangling effects on mean, variance and phase*", we estimate the contribution of this interdependence to the observed measures.

The three measures of interest, i.e. *mean*, *variance* and $phase_{STM}$, are defined (Martinez-Montes et al 2008) as

$$mean(t, f) = \frac{1}{L}\sum_{i=1}^{L} z_i(t, f) \qquad variance(t, f) = \frac{1}{L-1}\sum_{i=1}^{L} \left| z_i(t, f) - \bar{z}(t, f) \right|^2$$

$$phase_{STM}(t, f) = \left| \frac{1}{L}\sum_{i=1}^{L} \left(\frac{z_i(t, f) - \bar{z}(t, f)}{\left| z_i(t, f) - \bar{z}(t, f) \right|} \right)^2 \right|$$

where L is the number of trials, and $\bar{z}$ is the *mean* of the coefficients across trials. The *mean* and *variance* measures are standard forms; when plotting data, it was often more convenient to plot the square root of the *variance* (i.e. standard deviation), to which we will refer as $var^{1/2}$. The $phase_{STM}$ measure merits some additional comments. This measure, the second trigonometric moment or STM (Krieg et al 2011), tries to capture any phase concentrations that may occur as the result of a stimulus and attempts to correct for the possibility that phase concentration is due to an additive shift in the complex coefficients by first subtracting the *mean* and then measuring the uniformity of phase values

such that a bimodal distribution results in high values of the measure and a uniform distribution results in low values.

To determine the effects of the stimulus on the *mean*, *variance* and $phase_{STM}$ measures, we followed the procedure of Martinez-Montes et al (Martinez-Montes et al 2008) and computed 't-like' statistics that compare the value of these measures at any particular point in the time-frequency plane with the pre-stimulus distribution in a comparison window (t = -550 to -125 milliseconds) as follows:

$$T\text{-}mean(t,f) = \sqrt{N-1}\left(\frac{mean(t,f) - \mu_{mean}(f)\big|_{comparison}}{\sigma_{mean}(f)\big|_{comparison}}\right)$$

where $\mu_{mean}(f)$ and $\sigma_{mean}(f)$ are the mean and standard deviation of *mean(t,f)* computed across trials over the time window spanning the comparison region and *N* is the number of points in the comparison region. The t-*variance* and t-$phase_{STM}$ statistics are computed in an analogous manner. These statistics are called 't-like' because they do not follow the t-distribution, even though they are computed similarly. Because the distribution of these statistics is not known a priori, we tested the significance of these effects by comparing the computed t-statistics with a null distribution computed using data from the pre-stimulus period. The major problem with testing the significance of effects on coefficients in the time-frequency plane is correcting for multiple comparisons - there are many hundreds or thousands depending on the time and frequency resolution. We used a procedure similar to Martinez-Montes et al (Martinez-Montes et al 2008) and computed the local false discovery rate (*fdr*; Efron 2004), i.e. the ratio of the expected distribution (the null distribution normalized to the number of observations) to the data distribution, with a threshold criterion of $q < 0.1$, i.e. bins in the data distribution in which there are >10 times as many points as there are in the expected distribution were assumed to be significant. The value of 0.1 is the upper limit on the false positive rate yielded by the analysis over all bins. In practice, this

rate is much lower, and is obtained by dividing the tail area of the expected distribution by the tail area of the data distribution, with the tail defined as all bins ≥ smallest significant bin on the right side ≤ largest significant bin on the left side. Here, these rates varied from 0.0034 to 0.030, with a median of 0.011. Note that wavelet and STFT coefficients were analyzed separately, as their time resolution was different. (For an alternative approach to statistical analysis of time-frequency data, see Kilner et al 2005).

To obtain the null distribution, we computed the t-like statistics on the pre-stimulus data, smoothed this distribution using a Gaussian filter with $\sigma = 2$ bins, and computed the expected distribution by scaling this estimate of the null to match the area of the similarly smoothed data distribution (i.e. the t-like statistics obtained from the post-stimulus data; the portion of the data used for scaling were the bins corresponding to the central 98% of the null distribution). We note that our implementation of the local *fdr* analysis diverges from that of Efron and Martinez-Montes et al in our choice of the null distribution. In the original description of this technique, the null distribution was obtained by fitting the middle part of the data distribution, (i.e. the distribution not including the tails) under the assumption that the 'uninteresting' data points are normally distributed and that the 'interesting' data points are only located in the tails. This method is highly dependent on the assumed distribution (e.g., an assumption of normality) and the range of data used to fit the chosen distribution. Fitting to a narrow range of data is likely to result in poor estimates of the null distribution, particularly if the null diverges from the assumed distribution, and fits to a large range of data may inadvertently incorporate 'interesting' data points into the null. By contrast, we know *a priori* that the pre-stimulus baseline period of our data consists entirely of 'uninteresting' points, and thus provides an excellent estimate for the null distribution under the relatively benign assumption that the statistical properties of the null distribution do not change over the ~2 second recording window. Our method also does not require assumptions about the shape of the null distribution, which is unknown for the t-like statistics.

We note, however, that this choice is nonstandard and has not been rigorously tested. We also note that different, independent methods for determining statistically significant response components across our dataset (see below) gave very similar results (Figure 6), indicating that the method is sound at least in this context.

To pool data across animals, we compared two methods. In the first, we calculated for each animal the significance at each time-frequency point of changes in the *mean*, *variance* and $phase_{STM}$ according to the local *fdr* method described above, then calculated the fraction of animals exhibiting significant changes at each time frequency point (for *variance* and $phase_{STM}$, we accounted for the sign of the change by coding in each animal at each time frequency point a significant decrease as -1 and a significant increase as +1, adding up these values across animals and then dividing by the number of animals). In the second method, we computed the *mean*, *variance* and $phase_{STM}$ measures across trials as described above, then tested for significant changes from baseline using the Mann-Whitney U test. Before significance testing, *mean* and *variance* measures were normalized at each frequency to $var^{1/2}$ of the ongoing activity at that frequency. We used two correction methods for multiple comparisons: the local *fdr* method described above, and the unweighted Bonferroni correction (i.e. the significance level is adjusted by dividing by the number of simultaneous tests, here the number of points in the time-frequency plane). The two methods yielded very similar results, differing qualitatively only for the $phase_{STM}$ measure. Because the Bonferroni method strictly minimizes type I errors (i.e. false positives) at the expense of statistical power, it is considered to be an extremely conservative correction (Shaffer 1995). By contrast, false discovery rate methods are designed to maximize statistical power while setting less stringent control on type I errors (Efron 2004). Thus, it is likely that these two methods provide an upper and lower bound on the occurrence of significant stimulus-related changes in the measures of interest.

All electrophysiological data were analyzed using software written in Matlab v7.11 (Mathworks, Inc., Natick, MA).

Simulations

We used simulations to determine the extent to which trial-by-trial variability in the amplitude and latency of an additive component could account for the observed changes in *variance*. Simulations were specific to each experiment, using ongoing activity and the evoked response from that experiment. For each experiment, we first estimated the spectrum of the ongoing activity just prior to the stimulus by averaging the wavelet transform and STFT data over the time period -0.5<t<-0.1 sec, where the stimulus onset occurred at t = 0. Next, for each trial, we simulated ongoing activity by adding sinusoidal components (frequency resolution = 1Hz, $1<f<f_{Nyquist}$) with phases uniformly distributed over $(0, 2\pi)$ and amplitudes normally distributed over ($\mu = 1$, $\sigma^2 = 0.5$) across frequencies and trials. The spectrum of this simulated ongoing activity was matched to the recorded ongoing activity by multiplying each frequency component by the corresponding magnitude in the ongoing spectrum. For the additive component, we took the average time-domain response from that experiment from -0.1 < t < 0.5 sec and windowed it by a tapered cosine (Tukey) window with $\alpha = 0.05$. This additive component was then scaled by a normally distributed amplitude factor ($\mu_{amp} = 1$, $0<\sigma_{amp}< 2.4$) added at variable latency ($\mu_{lat} = 0$, $0 <\sigma_{lat}<$ 3.0 ms) to the ongoing activity on each trial. As expected, the simulated *mean* measure matched well the recorded *mean* measure. The *variance* measure was a function of σ_{amp} and σ_{lat}. We compared the simulation results with the recorded data by finding the values for σ_{amp} and σ_{lat} that minimized the mean squared error between the normalized $var^{1/2}$ for the simulated and recorded data. To simplify this calculation, we evaluated the $var^{1/2}$ measure at one time point for each frequency, corresponding to the

maximum of the *mean* measure during the peri-stimulus time window. Because the frequency components were logarithmically spaced, the error function was weighted by $1/f^{0.5}$.

Phase resets will appear as increases in the *mean* measure and will also affect the *variance* measure. We used simulations to evaluate the magnitude of this effect, essentially asking whether the changes in *mean* and *variance* could be due to a phase reset whose magnitude equaled the observed phase concentration (Fig. 10). We simulated ongoing activity as complex coefficients having real and imaginary parts that are jointly normally distributed with common variance. To simulate a pure phase reset, the magnitudes of these coefficients were maintained but their phases concentrated to adhere to a von Mises distribution with variable standard deviation. We then computed the complex mean and variance of the phase-concentrated simulated data, and created lookup tables to relate these mean and variance values to the $phase_{STM}$ measure (Fig. 10A). Finally, we took the median $phase_{STM}$ across animals and, using the lookup tables, computed the expected changes in the normalized *mean* and $var^{1/2}$ measures that would occur if they were entirely due to a phase reset producing these $phase_{STM}$ values (Fig. 10B).

Results

Ongoing and stimulus-related activity in the time and time-frequency domain

Time-domain responses to acoustic stimuli averaged across trials were similar to epidurally-recorded auditory responses reported previously in rats (Fig. 1A) (e.g.Ruusuvirta et al 1998; Lazar and Metherate 2003; Nakamura et al 2011), with a short latency component that peaked between 10 and 20 ms after stimulus onset, followed by a series of peaks and troughs lasting for several hundred milliseconds. As previously described for cortical sensory responses, we observed a large amount of trial-by-trial variability; in many cases, single trial responses were only as large as or were even dwarfed

by ongoing activity (Fig. 1A). As we describe below, this variability has implications for interpreting responses in terms of evoked and induced components. We used time-frequency analysis to investigate ongoing and stimulus-related activity in more detail.

Time-frequency spectra of single trial responses (Fig. 1B) also exhibited considerable trial-by-trial variability. Mean spectrograms averaged across trials (Fig. 1C) illustrate that power in the pre-stimulus period falls off rapidly with frequency, as expected, and suggest that sensory stimuli evoke a strong, broad-band, transient response that terminates with stimulus offset (Fig. 1C). To help visualize these features, we averaged these spectrograms across specific time windows before and after stimulus onset to yield the average spectral content of ongoing and stimulus-related cortical signals (Fig. 2)**.** Mean pre-stimulus spectra were similar in shape across animals, but spanned an order of magnitude in overall power. Spectra from individual animals and spectra averaged across animals showed that ongoing activity rarely exhibited distinct peaks that would correspond to strong oscillations; instead, the power of ongoing activity fell off as $\sim 1/f^2$ (Fig 2Ai, *dashed line*).

Power spectra averaged across trials and across several time windows during and following the stimulus (20 msec-wide windows centered at t = 25, 125, 250 and 500 ms, where stimulus onset is at t = 0 ms and offset is at t = 250 ms) are illustrated in Figure 2Aii-v; the power spectrum of ongoing activity averaged across animals is replotted in each panel for comparison (*dotted line*). The relative increase in power due to the stimulus was computed by taking the ratio of the mean spectrum in each time window to the mean ongoing spectrum (Fig. 2B). Relative to ongoing activity, auditory stimuli triggered a rapid increase in power that grew in magnitude with frequency, and was particularly pronounced at ~20 and ~200 Hz (Fig. 2Aii; Fig. 2B, *thick solid line*). Midway through and at the end of the stimulus, there was a relative increase in low frequency components, while the high frequency components had largely returned to baseline (Fig. 2Aiii,iv; Fig. 2B, *dashed and dotted lines*). A small relative decrease in power was observed following stimulus offset at ~10 Hz (Fig 2B, *dot-dashed line*). In general, however, analysis

of relative increases in these power spectra cannot resolve the contribution of evoked versus induced response components. Below, we will dissect these contributions using a more sensitive analysis method of complex spectral coefficients.

Complex coefficients in the time-frequency domain

As illustrated in Figure 1, there was marked trial-by-trial variability in ongoing activity and the responses to acoustic stimuli. This variability can be visualized by plotting the magnitude and phase of each frequency component on successive trials in the complex plane. In Figure 3, we show the values of complex coefficients of four frequency components (*rows*, from *top* to *bottom*: f = 100, 30, 10 and 3 Hz) measured at a single time point (t = -0.25 sec; *left column*) during the pre-stimulus period and at specific times following stimulus onset (*2nd, 3rd* and *4th columns*: t = 0.025, 0.2 and 0.75 sec) for all 664 trials from this animal (pooled across 7 recording sessions). In these plots, each point is the coefficient from one trial and one instant in time plotted in the complex plane. The magnitude of the frequency component is the distance of this point from the origin; the angle this vector forms with the positive real axis is the phase of the frequency component at that instant in time. The *mean* of the coefficients across trials is indicated by the line emanating from the origin. During the pre-stimulus period (left column), the coefficients have approximately zero mean (i.e. the clouds are centered at the origin). Changes in the *mean* of the coefficients correspond to an additive component at constant phase at that frequency, i.e. an evoked response. The *variance* of the coefficients across trials is indicated by the radius of the circle, which is centered at the *mean*. Changes in the *variance* correspond to an increase or decrease in the magnitude of that frequency component at random phase, i.e. so-called induced response components. Transient changes in the *mean* and *variance* of the coefficients are evident following the stimulus, as indicated by shifts in the centers of the circles (i.e. changes in the *mean*) and changes in the radii of the circles (i.e. changes in *variance*). For example, at 10 Hz, there is a large shift in the *mean* following

stimulus onset, with a small associated change in the *variance* (Fig. 3, 3rd row, 2nd column), while after stimulus offset a small decrease in *variance* (i.e. desynchronization) is apparent (Fig. 3, 3rd row, 4th column). Stimulus-triggered phase concentrations would appear as deviations from circularity of the data cloud at particular angles relative to the positive real axis. One example is the first post-stimulus time point for the 10 Hz component (Fig. 3, 3rd row, 2nd column). It is evident from these plots that (1) both the *mean* and *variance* of the data cloud can be affected by the stimulus, but (2) that they also can be affected independently and (3) that strong phase concentrations, i.e. non-circularity of the data clouds, occur only occasionally and transiently. These three points are illustrated more clearly in Figure 4, which plots the magnitude of the *mean*, $var^{1/2}$ and $phase_{STM}$ measures averaged across trials for these four frequency components as a function of time relative to stimulus onset. In this example, changes in *mean* and *variance* are tightly linked during the stimulus (0<t<0.25 sec), though for the 3 Hz component the later changes in *mean* occur without concomitant changes in *variance* (Fig. 4D). Note also that changes in the $phase_{STM}$ measure tended to occur near peak changes in the *mean*.

Statistical analysis of complex coefficients

To quantify changes in the distribution of complex coefficients and determine the time course of these changes relative to baseline, we compared the *mean*, *variance* and $phase_{STM}$ values with those recorded in the pre-stimulus period by calculating 't-like' statistics as described in Methods. Because we do not know the distributions of these statistics *a priori*, we tested the significance of these changes by comparing the calculated distributions with a null distribution of t-values computed during the pre-stimulus period (Fig. 5A) using the local *fdr* measure (Efron 2004; Martinez-Montes et al 2008). Histograms of t-*mean* (Fig. 5A, *left*), t-*variance* (Fig. 5A, *center*) and t-$phase_{STM}$ (Fig. 5A, *right*) values from the null region are smoothed to create null distributions (*dashed lines*). We used these empirically

derived null distributions to determine significance. The corresponding raw (*bars*) and smoothed (*solid lines*) histograms of t-values for the post-stimulus data at one specific frequency (9 Hz) are shown in Figure 5B, in which we also plot the expected distributions (*dashed lines*; see Methods). The underlying assumption of the local *fdr* technique is that the interesting (i.e. significant) data points are those with t-values that are in the tails of the data distribution, i.e. t-values that are rarely observed in the null distribution. These 'interesting' points are illustrated in Figure 5B (*black bars*) and their t-values are indicated via color-code in the time-frequency contour plots of Figure 5C. In this experiment, the auditory stimulus triggered a broad-band increase in the *mean* that for low frequencies lasted well beyond the stimulus offset (Fig. 5C, *left*). A broadband increase in *variance* (synchronization) during the stimulus was also observed, which at lower frequencies was followed by an extended period of desynchronization (Fig. 5C, *center*). Significant changes in $phase_{STM}$ were observed at lower frequencies during the stimulus (Fig. 5C, *right*). Note that the increases in *variance* and $phase_{STM}$ during the stimulus tended to co-occur with increases in the *mean*. Below, we show evidence that these correlated (i.e. co-occurring and of the same sign) changes in *mean*, *variance* and $phase_{STM}$ during the stimulus are likely the result of trial-by-trial variability in the additive (i.e. evoked) component, rather than reflecting independent modulation of ongoing activity or true phase resets, as they are often interpreted.

Summary across animals

The method illustrated in Figure 5 for determining significance of stimulus-related effects on *mean*, *variance* and $phase_{STM}$ is effective for a single experiment, but leaves open the issue of summarizing data across experiments and subjects. Epidural signals can vary widely across subjects in terms of raw power (Fig. 2), potentially complicating statistical comparisons. We compared two approaches to summarizing data across subjects, illustrated in Figure 6. In the first approach, we

computed 'significance maps' averaged across animals (Figure 6A; see Methods), representing the fraction of animals showing significant stimulus-related effects at each point in the time-frequency plane. [Note that for the *variance* map, negative values indicate the fraction of animals showing a decrease in *variance*.] Key features of the stimulus-related activity are (1) a broadband increase in the *mean* and an offset response that persists for up to 500 msec at the lowest frequencies analyzed (Fig. 6A, *left column*), (2) a broadband synchronization that is always shorter than the duration of the stimulus (Fig. 6A, *center column*), (3) a late desynchronization for frequencies <30 Hz that lasts for several hundred milliseconds after stimulus offset (Fig. 6A, *center column*), and (4) a phase concentration that is significant in a minority of animals and that is broadband and brief at high frequencies but progressively longer at frequencies<30 Hz (Fig. 6, *right column*). Note that using this analysis technique (and unlike our observations using the power spectra of Figure 2), we are able to detect substantial effects on spectral coefficients after stimulus offset.

Presentation of data as in Figure 6A demonstrates the location of significant changes in the time-frequency plane but is not sufficient for describing the magnitude of these effects, and it is not easy to compare the relative effects across frequencies or between measures using these plots. Therefore, in Figure 6B we summarize the measures themselves across animals by plotting the grand median for all points in the time-frequency plane, and in Figure 6C-E we present these measures after thresholding for significance across animals as tested using a Mann-Whitney U test at each time-frequency point and corrected for multiple comparisons using local *fdr* (Fig. 6C, E) or the much more conservative Bonferroni correction (Fig, 6D). Values at each frequency are normalized to the mean of $var^{1/2}$ at that frequency during the pre-stimulus period for each experiment, and then the grand median at each time-frequency point was computed across animals. For the *mean* measure (Fig. 6B-E, *left*), a value of 1 indicates an additive component equal in power to the pre-stimulus ongoing activity. Peaks in the *mean* measure occurred at ~155 Hz (latency ~10 msec), 50.1 Hz (~25 msec), 19.2 Hz (~35 msec) and 9.19 Hz (~65 msec).

The persistent post-stimulus *mean* component detected in this analysis was less prominent that in the analysis of Figure 6A, and appeared only at <30 Hz and had a duration <150 msec. In the center column of Figure 6B-E, we plot the $var^{1/2}$ measure normalized as for the *mean* measure, and thus a value of 1 represents no change compared to the pre-stimulus ongoing activity. Changes in the *variance* during the stimulus were highly correlated with changes in the *mean* (best seen in the expanded view of Fig. 6E; for example compare the high frequency peak >100Hz, as well as the secondary peaks in the gamma and beta range). As in Figure 6A, after stimulus offset there is a late and long-lasting desynchronization in the alpha frequency band (~10 Hz; Fig. 6C&D, *center*) that is not associated with any changes in the *mean*. The $phase_{STM}$ measure (Fig. 6B-E, *right*) can take on values ranging from zero to one (and thus needs no normalization), where one represents perfect phase alignment and zero represents uniform phase distribution. On average, we observed values of the $phase_{STM}$ measure that were at most ~0.15 (Fig. 6B, *right*) but were consistent enough across animals to be statistically significant using the local *fdr* correction (Fig. 6C, E, *right*) but not the Bonferroni correction. As with the *variance* measure, these changes in the $phase_{STM}$ measure were highly correlated with changes in the *mean* component. Below, we examine the origin and interpretation of the observed peri-stimulus changes in the *variance* and $phase_{STM}$ measures.

Disentangling effects on mean, variance and phase

Origin of stimulus-related changes in variance.

When interpreting the data of Figure 6, it is important to explore the potential confounds that may be introduced by the entanglement of the *mean*, *variance* and $phase_{STM}$ measures. For example, two aspects of our data raise the possibility that the observed changes in *variance* may be due to variability in the timing or amplitude of the additive component, rather than a modulation of ongoing

activity expected of an 'induced' response. These aspects relate to the nature of *variance* changes that would be expected if these changes were due to timing and amplitude variability in the additive component, and are illustrated in Figure 7A. The result of such variability would be a distortion of the data clouds of spectral coefficients at each time-frequency point across trials in two different ways. Variability in the amplitude of an additive component will result in increased *variance*, i.e. a bulge in the cloud, in the direction of the *mean* component vector. This effect is easily understood if one considers the extreme case in which on half the trials the additive component is zero and on half its amplitude is constant and nonzero (Figure 7A, *top row*). In this case, the data cloud would split into two sub-clouds, and the *variance* across the whole cloud would be increased. Importantly, this *variance* would be correlated with the amplitude of the additive component (Figure 7A, *top row*). (Note also that such variability would also lead to a phase concentration, and thus a change in the $phase_{STM}$ measure. This issue will be discussed in more detail below.) Variability in timing of an additive component would result in increased *variance* in the orthogonal dimension. Again, this effect is easily illustrated by considering the extreme case in which on half the trials one latency (i.e. phase) is observed and on the other half a second phase is observed, splitting the data into two subclouds at right angles to the direction of the additive component (Figure 7A, *bottom row*). Less extreme cases of amplitude and latency variability will lead to smaller effects on *variance* (not shown), and it should be noted that simultaneous variability in latency and amplitude will have additive effects on the *variance*, but will mitigate apparent phase concentrations (due to a less distorted data cloud). We will return to this point below.

Previous work (David et al 2006) has shown, based on theoretical considerations, that amplitude and latency variability will have different effects on the *mean* and *variance* measures. Introducing trial-by-trial variability in the amplitude of the additive component without changing its average value will result in correlated increases in the *variance* measure without decreases in stimulus-related changes in the *mean* measure. By contrast, varying the latency of the additive component on each trial will change

its average value, thus decreasing the changes in the *mean* measure. However, this effect will be frequency dependent, with larger effects at higher frequencies (Figure 7A, *bottom row*): if the latency variability is frequency-independent (e.g. σ = 3 msec), then frequencies with periods comparable to this latency variability will be smeared out and their *mean* reduced and *variance* increased, while frequencies with periods much greater will be relatively unaffected. In this case, high frequency components of the *mean* measure will be transferred to the corresponding frequencies in the *variance* measure. Our data suggest that both sources of variability contributed to stimulus related changes in *variance*.

When considering the observed changes in *mean* and *variance* illustrated in Figure 6B, we note that these changes were quite similar in their duration and frequency range, as would be expected if the stimulus-related *variance* changes were secondary to trial-by-trial variability in the amplitude of an additive component. Figure 7B summarizes the co-occurrence of *mean* and *variance* changes as measured by the two-dimensional (i.e. time and frequency) cross correlation of changes in *mean* and *variance* over the peri-stimulus time window. For both STFT (f<16 Hz) and wavelet coefficients (i.e. f > 16 Hz), we observed a significant correlation in all animals (median correlation coefficients = 0.68 & 0.59, respectively).

Although stimulus-related changes in *mean* and *variance* tended to co-occur, leading to the correlation illustrated in Figure 7B, the magnitude of changes in *variance* relative to simultaneous changes in *mean* was greater for high versus low frequency components, as would be expected if the underlying mechanism was variability in the latency of additive components (David et al 2006). We quantified this effect by measuring $var^{1/2}$ at one time point for each frequency, corresponding to the time of the peak of the change in the mean measure. The median normalized $var^{1/2}$ σacross our dataset is much larger for frequencies above about 100 Hz (Figure 7C), an observation that is consistent with

trial-by-trial variability in latency of the additive component contributing to the observed stimulus-related changes in *variance* (David et al 2006).

To determine whether these two types of variability could account for the observed peri-stimulus changes in *variance*, we simulated the occurrence of only an additive component, which varied from trial to trial in amplitude and latency, and looked for the effects on the *variance* and $phase_{STM}$ measures. Simulations based on data from one experiment are illustrated in Figure 8. The top row (Fig. 8A) shows the mean spectrogram (*left column*), normalized *mean* and $var^{1/2}$ measures (*middle columns*) and $phase_{STM}$ measure (*right column*). The raw recorded data from this experiment (Fig. 8A) are typical, i.e. the changes in *variance* and *mean* are highly correlated during the stimulus (2-D correlation coefficient for the window $0<t<0.25$ sec is 0.73 for $3<f<16$ Hz and 0.52 for $16<f<300$ Hz), but the change in *variance* at high frequencies is much larger, relative to the *mean*, compared to lower frequencies. As expected, when we simulate the ongoing activity with an invariant additive component (Fig. 8B), the mean spectrogram and normalized *mean* measure (*left two columns*) exhibit an excellent fit to the recorded data, and with no variability included in the model there are no observed changes in *variance* and $phase_{STM}$ (*right two columns*). We varied σ_{amp} and σ_{lat} systematically over a wide range of values and found the best fit of the model to the data by finding the parameter values that minimized the difference between the observed and simulated changes in normalized $var^{1/2}$ measure (see Methods). With $\sigma_{lat} = 0$, the best fit of the model occurred for $\sigma_{amp} = 1.0$ (i.e. equal to the mean amplitude; Fig. 8C). This amplitude variability successfully captured key features of the recorded *variance* changes, i.e. the simulated changes in *variance* measure were highly correlated with the changes in *mean*, especially for $f<100$ Hz. At higher frequencies, the magnitude of changes in the recorded *variance* measure was far greater than could be accounted for by amplitude variability alone. In addition, the amplitude variability caused an apparent phase concentration, as expected due to the elongation of the data cloud along the direction of the additive vector, and this phase concentration was somewhat larger than observed in the

recorded data. When we varied both σ_{amp} (0.8) and σ_{lat} (1.8 ms), we could capture some of the 'extra' *variance* at high frequencies (Fig. 8D), though the observed *variance* still exceeded that of the model, and because the latency variability caused an elongation in the data cloud in the orthogonal direction, the apparent phase concentration was reduced.

We determined the optimal model parameters by minimizing the difference between the recorded data and the model output over the normalized $var^{1/2}$ as a function of frequency. The resulting functions for the experiment of Fig. 8A-D are shown in Fig. 8E. We repeated this analysis for each animal and found that the median across animals of the optimal variability was 0.9 (1^{st}, 3^{rd} quartiles = 0.7, 1.8) for σ_{amp} and 1.8 msec (1^{st}, 3^{rd} quartiles = 0.7, 2.0 msec) for σ_{lat}. Using these best fits, we computed the median of the normalized $var^{1/2}$ as a function of frequency across animals (Figure 8F). In both the single animal example in Figure 8E and the summary across animals in Figure 8F, we note that the model produced excellent fits for f<100 Hz with σ_{lat} = 0, and improved fits for f>100 Hz when σ_{lat} was also varied. The divergence of the fits for f>100 Hz reflects a limitation of the model, which is based solely on the observed additive component. Introducing amplitude variability is straightforward; such variability will not affect the mean of the additive component. However, introducing latency variability is more complicated, as varying the latency of the additive component will alter its mean in a frequency-dependent manner (i.e. the additive component becomes smeared, and the smearing is worse for frequency components on the order of the inverse of the latency variability). Therefore, with this modeling approach, we are likely to underestimate the contribution of an additive component with variable latency to the observed *variance* at those high frequencies. In spite of this limitation, the modeling results strongly suggest that broadband changes in *variance* that co-occur with changes in the *mean*, as well as high frequency changes in *variance* that can occur even in the absence of changes in the *mean*, are all likely to reflect variability in amplitude and latency, respectively, of an additive

component, rather than induced responses secondary to reorganization of ongoing activity or top-down modulation of network connectivity parameters.

To summarize these simulations across animals, we computed the median stimulus-related changes in normalized $var^{1/2}$ and $phase_{STM}$, as in Figure 6B, from the best fits of the model for each experiment. This analysis is illustrated in Figure 9, where we have also plotted the recorded data for comparison (Fig. 9A&B; *first column*). Over the dataset, the model with only amplitude variability was able to capture much of the changes in *variance* that were correlated with changes in the *mean* (Fig. 9A, *second column*), but in this case the changes in $phase_{STM}$ were far stronger than those in the recorded data (Fig. 9B, *second column*). A modest improvement in model fit for *variance* and a substantial improvement in $phase_{STM}$ was observed with both amplitude and latency variability (Fig. 9A&B, *third column*). Although the $phase_{STM}$ values still exceeded those in the recorded data, subtracting the model fit from the data revealed that those differences were modest (Fig. 9B, *fourth column*). By subtracting the *variance* measure obtained from simulations from the recorded data (Fig. 9A, *fourth column*), we observe that nearly all the early *variance* changes <30 Hz, and most of these early changes up to 100 Hz, could be accounted for by the model with both amplitude and latency variability.

Effect of phase reset on stimulus-related changes in mean.

As stated above, additive components can appear as phase concentrations, and the $phase_{STM}$ measure employed here was specifically designed to address this confound (at least in the case of invariant amplitude). However, the complementary problem is not addressed: phase resets can still appear as changes in the *mean* (this problem is why phase resets can contribute to the time domain mean response and have thus been postulated to underlie evoked responses Sayers et al 1974; Makeig et al 2002). The conflation of phase reset and amplitude variability has also been observed in the

context of relating amplitude variations and dynamic correlations in human MEG data (Friston et al 1997). This effect is easily illustrated when considering the coefficients in the complex plane. Beginning with a cloud of coefficients scattered about the origin (i.e. with zero mean), as in Figure 3 (*left column*), changing the phases of those points so that they are all restricted to one quadrant will produce a data cloud with nonzero *mean* and altered *variance* (see Martinez-Montes et al 2008 for illustrative figures). Thus, it is possible in the data of Figure 6 that some portion of the stimulus-related change in *mean* (Fig. 6, *left column*) may actually be due to a stimulus-related phase concentration (Fig. 6, *right column*). Ideally, one would estimate the contribution of phase reset to the *mean* effect using the $phase_{STM}$ measure, i.e. by calculating how much of a change in the *mean* is expected from the observed phase concentration. However, because of the way the $phase_{STM}$ measure is defined, its values cannot be analytically translated into relative effects on the *mean*. Instead, we used simulations to estimate the changes in normalized *mean* and $var^{1/2}$ expected if they were entirely due to phase resets whose magnitude is given by changes in the $phase_{STM}$ measure (see Methods; Fig. 10A&B). From these simulations, it is clear that phase resets can have non-trivial effects on the *mean* and *variance* of coefficients (Fig. 10B). However, when we compare these phase effects with the observed changes in *mean* and *variance* (Fig. 10C), we note two major discrepancies. First, the magnitude of predicted changes in the *mean* are far smaller than those observed (Fig. 10B&C, *left column*), and second, the simulated phase reset is associated with a *decrease* in *variance*, not the large increase that we observe (Fig. 10B&C, *center column*). Thus, although we cannot rule out the possibility that the observed $phase_{STM}$ values represent true phase resets and contribute to the changes in *mean* and *variance* observed, these effects cannot account for all of the observed changes in the *mean*, and would require a large compensatory increase in *variance*. As we illustrated above, a far more parsimonious explanation for the observed changes in *mean*, *variance* and $phase_{STM}$ derives from variability in the additive component.

State-dependence of response variability

Previous reports have shown that cortical response variability is state-dependent (Kisley and Gerstein 1999; Curto et al 2009; Pasley et al 2009; White et al 2012), and in humans discriminability of acoustic stimuli depends upon the level of ongoing activity in auditory cortex (Sadaghiani et al 2009). Delta power is an indicator of level of arousal (Santamaria and Chiappa 1987; Jung et al 1997), and sensory responses have been shown to depend on delta power and delta phase previously (Lakatos et al 2005; Curto et al 2009; Luo et al 2010). We investigated whether the variability of the additive component depended on the state of the cortical network by comparing this variability for each animal with the ratio of gamma to delta power in the pre-stimulus period. Low values of this ratio are associated with lower levels of arousal (Curto et al 2009). Amplitude and latency variability for each animal was measured using the parameters σ_{amp} and σ_{lat}, respectively, of the best model fit to the data. We found that SD_{amp} declined exponentially with gamma/delta ratio over the sixteen recorded animals, and a linear fit to σ_{amp} versus the log of this ratio yielded a significant negative correlation (Fig. 11A; slope = -0.78; $r^2 = 0.38$; $p = 0.01$). No significant correlation was evident for σ_{lat} (not shown; $m = 0.50$ $r^2 = 0.17$; $p = 0.11$).

The data of Figure 11A indicate that animals exhibiting higher levels of cortical arousal had less variable additive components in their stimulus-related responses. Because the data were collected over a period of ~0.5 – 1.5 hours spread across multiple days, it is likely that cortical state varied over the recording period and even on a trial-by-trial basis. To obtain a single trial measure of response variability, we calculated the Euclidean distance between single trial responses and the mean response (over the first 125 msec of the response), and compared that distance measure to the gamma to delta power ratio on that trial. Large values of the distance measure indicate responses that are very different from the typical response, and thus more variable. An example from one animal is shown in Figure 11B, which exhibited a small but significant negative correlation between distance and gamma/delta ratio,

indicating (as in Fig. 11A) that variability tended to be smallest on trials in which the animal was most aroused. Similar results were obtained in 14 of 16 animals (Fig. 11C).

Unlike the data of Figure 11A, the Euclidean distance measure of Figures 11B&C cannot distinguish between variability in the response due to ongoing activity summing with an invariant additive component and variability in the additive component itself. Thus it is possible that some of the effect observed in Figure 11B is due to variability introduced directly by ongoing delta oscillations on trials in which gamma/delta ratio was low. By contrast, it is also possible that the delta component of the evoked response is correlated with the ongoing delta power and that this evoked delta component contributes to the state-dependent variability. We repeated the analysis of Figures 11B&C on data that had been high pass filtered above 4Hz, and thus lacked significant delta power (the gamma/delta ratio was still computed on the unfiltered data). Although we cannot differentiate between these two possible contributions of the delta component using this method, this filtering would eliminate both of the effects discussed above. High pass filtering reduced the dependence of the distance measure on gamma/delta ratio (Fig. 11D), but 8 of 16 animals still exhibited significant negative correlations. Since this filtering is potentially removing components of the response that are relevant to the variability in the additive component, the true dependence likely lies somewhere in between the analysis of Figure 11C (which may include effects of ongoing delta power) and the analysis of Figure 11D (which may lack state-dependent effects on the variability of the delta component of the response).

Discussion

Summary and Conclusions

By analyzing the mean, variance and phase of complex spectral coefficients of cortical neural activity in rats, we demonstrate that auditory stimuli lead to broadband changes in all three measures

that are onset-dominated and tend to co-occur. In the peri-stimulus response window, the high correlation in these measures in the time-frequency plane is consistent with a simple model in which an evoked response component is elicited on each trial with variable amplitude and latency. Simulations of trial-by-trial variability using this model account for most of the observed changes in *variance* and $phase_{STM}$ without engaging any nonlinear, 'top-down' changes in ongoing activity typically associated with induced responses or true phase resets. The only unequivocal induced response component we detected in our dataset was a long-latency, long-lasting desynchronization in the alpha band that was modest but consistent across animals. Using simulations and single trial measures of variability in our recorded data, we show that this variability was most pronounced when ongoing cortical activity indicated the lowest levels of cortical arousal. These observations are consistent with auditory cortical responses in these passive listening conditions being dominated by a variable, state-dependent, 'bottom-up' information stream, with only modest, long-lasting changes in cortical network activity.

Variability in amplitude and latency of additive components

The contribution of amplitude and latency variability to apparent induced responses has been noted previously (David et al 2006). The classical model of evoked response generation consists of an additive component with fixed latency and amplitude that linearly combines with variable ongoing activity to produce single trial responses. According to this model, averaging can reliably recover the invariant additive component, and subtraction of this mean evoked response from single trials will reveal interactions between the evoked response and ongoing activity that comprise the induced response. However, it is now well-established that this model can result in a poor estimate of the evoked response, whose amplitude and latency can vary considerably from trial to trial (Mocks et al 1987; Lange et al 1997; Truccolo et al 2002; D'Avanzo et al 2011). Nevertheless, the most common

method for computing the induced response component continues to be subtraction of the time-domain evoked response from single trial responses (e.g. Crone et al 2001; Trautner et al 2006; Steinschneider et al 2008). Our data shows that caution must be used when interpreting induced responses, particularly when they co-occur with evoked responses, and that trial-by-trial variability in latency and amplitude can account for a significant portion of observed increases in variance of spectral coefficients.

Contribution of phase reset to stimulus-related activity

The contribution to evoked responses of phase reset versus additive components continues to be hotly debated, and previous studies in humans investigating the origin of the evoked response and the contribution of phase reset have reached contradictory conclusions (Sayers et al 1974; Jervis et al 1983; Makeig et al 2002; Makinen et al 2005; Hanslmayr et al 2007; Sauseng et al 2007; Krieg et al 2011). Detailed analyses and simulations have shown that it is often difficult to conclude unequivocally that observed phase concentrations are due to phase resets per se rather than an additive component (Sauseng et al 2007; Krieg et al 2011). The $phase_{STM}$ measure employed here, in which the *mean* is subtracted before calculating the phase concentration (Martinez-Montes et al 2008), was developed specifically to address this confound, and performs well in the case of an invariant additive component (Krieg et al 2011). However, our simulations show that variability in the amplitude of the additive component will also lead to a phase concentration, as this variability elongates the cloud of spectral coefficients in the complex plane along the axis of the *mean* component, and thus would be detected as a phase concentration even after subtracting the averaged *mean* component. Indeed, such an effect can be pronounced (e.g. Fig. 9B, *second column*). Adding to the model variability in the latency of the additive component reduces this effect, especially at high frequencies (Fig. 9B, *third column*), by widening the data cloud in the orthogonal direction and thereby reducing the apparent phase

concentration. Importantly, these simulations illustrate that a phase concentration exceeding that observed in our recorded data (Fig. 9) can be produced solely through variability in the amplitude and latency of an additive component. Because there is strong evidence that such variability is occurring in the animals recorded here in response to acoustic stimuli, it is not necessary to invoke a true phase reset of ongoing activity to account for the observed phase concentration.

A few studies that pay careful attention to these confounds have presented some evidence for the contribution of phase reset to cortical sensory responses (Krieg et al 2011), but in auditory cortex such responses appear to be limited to integration with stimuli from other modalities (Lakatos et al 2007; Luo et al 2010). This is consistent with our results that phase reset contributes little to auditory cortical responses under passive listening conditions in the frequency range examined (3 – 300 Hz). However, in our recordings, we also observed very little structure in the frequency content of ongoing activity (Fig. 2), and it is possible that phase reset of ongoing components may contribute more to the evoked response when there is more structure to the ongoing activity (Sauseng et al 2007), or during dynamic naturalistic stimuli (Ng et al 2013). Finally, it should be noted that although phase concentration due to an additive component is not the same as a phase reset of ongoing of activity, and implies primarily bottom-up influences rather than modulation of ongoing activity, the end result of both mechanisms is an alignment or phase synchronization that could equivalently facilitate integration within the cortical network.

We note here that the opposite confound can also occur, i.e. a phase reset can also cause apparent changes in the *mean* and *variance* (Fig. 10), as has been reported previously (Sauseng et al 2007; Krieg et al 2011), and an intuitive understanding of this effect can also be gained by considering the cloud of spectral coefficients in the complex plane. However, we have used simulations of phase reset to show that resulting changes in the *mean* and *variance* are smaller than (in the case of the *mean*)

or are in the opposite direction of (in the case of the *variance*) the changes observed in our recordings, and thus a phase reset is unlikely to contribute to the changes in *mean* and *variance* reported here.

Spectral content of ongoing activity

In our recordings, we observed little evidence for peaks in power spectra derived from ongoing activity (Fig. 2). In one previous study on auditory cortex in monkeys, peaks in the delta, theta and gamma bands were suggestive of consistent oscillations in these frequency ranges, and stimulus-triggered phase resets of these oscillations are reported to contribute to the response (Lakatos et al 2005). Other studies did not find such peaks in ongoing activity (Brosch et al 2002), indicating that such structure could be state-dependent. It is unclear, however, what bearing such peaks have on the relationship between ongoing activity and stimulus-related responses. For example, a dominant peak in the power spectrum may not be necessary for phase reset at that frequency to occur (Sauseng et al 2007). The presence of induced response components may similarly be unconnected to such peaks. For example, we observed evidence for stimulus-related alpha band desynchronization (Fig. 6) even in the absence of a prominent alpha peak in the spectrum of ongoing activity (Fig. 2), and induced oscillatory activity in the gamma band has been observed in the absence of detectable gamma peaks in the ongoing spectrum (Brosch et al 2002). Thus the presence or absence of 'peaks' in the ongoing spectrum may not be indicative of the network's capacity for stimulus-induced reorganization of oscillatory activity, perhaps because of the local nature of these rhythms or modulation of specific dynamic components of the network in a stimulus-specific manner.

Alpha band desynchronization

We observed desynchronization centered in the alpha band around 10 Hz (Fig. 6A-D, *center column*). Cortical alpha band desynchronization is well known in human studies of visual, somatosensory and auditory sensory processing to reflect arousal and attentional mechanisms (for recent reviews, see Palva and Palva 2007; Weisz et al 2011; Foxe and Snyder 2011). The desynchronization we observed in the alpha band is similar to what has been observed in human auditory cortex (Lehtela et al 1997; Crone et al 2001; Palva and Palva 2007), though other studies report increases in alpha power in response to acoustic stimulation (Krause et al 1996; Karrasch et al 1998) (Steinschneider et al 2008). Interestingly, there have been few reports of alpha desynchronization in auditory cortex of animals, though this response has been observed in other sensory cortices (Wiest and Nicolelis 2003; Sobolewski et al 2011). It is possible that the modest reduction in *variance* that we observed here is common and may have remained undetected in some studies. In human subjects, alpha desynchronization coincides with increased excitation in the cortical circuit during information processing (Klimesch et al 2007; Weisz et al 2011), i.e. alpha power is positively correlated with local inhibitory tone, and is postulated to reflect 'behavioral idling' that is suppressed during enhanced information flow through the thalamo-cortical network (Sobolewski et al 2011). Thus, according to this model, the long-lasting desynchronization reflects a long-lasting rebound excitation (Recanzone et al 2000; Qin et al 2007), in parallel with a similar rebound or persistent excitation indicated by the post-stimulus change in *mean*. If the desynchronization does indeed reflect changes in inhibitory network activity, the observation that these changes are not time-locked to the stimulus may mean that changes in inhibitory tone are governed by intracortical connections, e.g. top-down inputs (Klimesch et al 2007).

Gamma response components

In sensory cortex, changes in gamma band (30 – 120 Hz) power and in gamma frequency synchronization across cortical regions have been linked to feature binding, object representation, perception and memory of meaningful stimuli in humans (Tallon-Baudry et al 1996; Pulvermuller et al 1996). In auditory cortex, gamma band activity evoked by acoustic stimuli typically has a short latency, evoked (i.e. phase-locked) component (Galambos et al 1981; Pantev et al 1991), as well as both short latency and prolonged induced components that are poorly phase-locked and can outlast the stimulus duration by hundreds of milliseconds (MacDonald and Barth 1995; Tallon-Baudry and Bertrand 1999; Crone et al 2001; Brosch et al 2002; Steinschneider et al 2008; Jeschke et al 2008; Lenz et al 2008). In our recordings, we observed stimulus related activity throughout the gamma range, but our data and simulations indicate that these responses were dominated by evoked response components. This result is in contrast to results obtained during discrimination tasks in humans and rodents (Crone et al 2001; Lenz et al 2008; Jeschke et al 2008), in which 'induced' gamma band responses were observed and whose power could correlate with memory and sensory processes. The differences between these results and those reported here could be ascribed to the passive listening conditions under which we recorded our data, though high gamma induced responses have also been reported for passive listening conditions in monkeys (Steinschneider et al 2008). It should be noted that in these studies no attempt was made to distinguish between changes in *variance* associated with amplitude and latency variability in an additive component, versus changes in *variance* due to reorganization of ongoing activity or top-down modulation of cortical network connectivity. Indeed, although the latency of the induced high gamma activity in the latter study (~50 msec) was longer than in our recordings, it was striking that these effects were concentrated in the highest frequency components, consistent with these 'induced' components being due to latency variability in the evoked component.

State-dependence of variability and functional implications

It is widely recognized that cortical responses exhibit substantial trial-by-trial variability (Whitsel et al 1977; Shadlen and Newsome 1998; de Kock et al 2007; Luczak et al 2013). However, the origin of this variability is still under debate, with some reports arguing that cortical responses can be modeled as a constant additive component combined with variable ongoing activity (Dawson 1954; Arieli et al 1996; Shah et al 2004; Risner et al 2009), while others demonstrate that models including variable response components provide superior fits to the data (Truccolo et al 2002). The difference between these models depends on the relative importance of *local* variable ongoing activity in the cortical network itself, as opposed to variability in *ascending input* to the network. Our data are consistent with these latter models, and provide strong evidence that under passive listening conditions, stimulus related responses in auditory cortex of rats are dominated by an evoked component with variable amplitude and latency, consistent with variability in the ascending input to auditory cortex. This trial-by-trial variability is not surprising given the probabilistic nature of neuronal responses throughout the ascending sensory pathway. Although responses of cortical cells tend to be more variable than their thalamic inputs, the latter still exhibit substantial trial-by-trial variability (de Kock et al 2007) and in the ascending auditory pathway information content, reflecting in part variability in responses, is comparable between thalamus and cortex (Chechik et al 2006). Understanding the source of this variability and how it changes with behavioral state will yield insight into the state-dependence of sensory processing and the neural basis of sensory awareness.

We present evidence that the variability of stimulus-related activity depends on the state of the cortical network (Fig. 11). Using two different measures, we find that the amplitude variability of the additive component is smallest when the ratio of gamma to delta power is high. Because the latter is commonly used as a metric of arousal, this result suggests that arousal is associated with reduced response variability. We note that since variability was highest when the animals were most quiescent, it

is unlikely to derive from trial-by-trial variability in positioning of the animals' heads relative to the speakers. The inter-trial interval employed here is far longer than is typical for electrophysiological studies of the auditory system, in which intervals of 1 second or less are not uncommon. These long intervals likely reduce the predictability of the stimulus time and thus may reveal more strongly endogenous sources of response variability. Previous reports have demonstrated such state-dependence of response variability. For example, the variability of cortical responses is reduced over the course of perceptual learning (Adab and Vogels 2011), and exhibits dose-dependence under general anesthesia (Kisley and Gerstein 1999). Attention also reduces variability and is associated with improved behavioral performance (Ledberg et al 2012). However, in some reports spontaneous cortical activity is reduced on average during slow wave sleep (Steriade et al 1978; Nir et al 2012), when delta power is high, and this would likely reduce response variability, contrary to our findings that variability is maximal when delta power is low. Analyses such as those presented here that can identify this variability and how it changes with learning or awareness will prove useful tools for understanding the underlying mechanisms of these state changes.

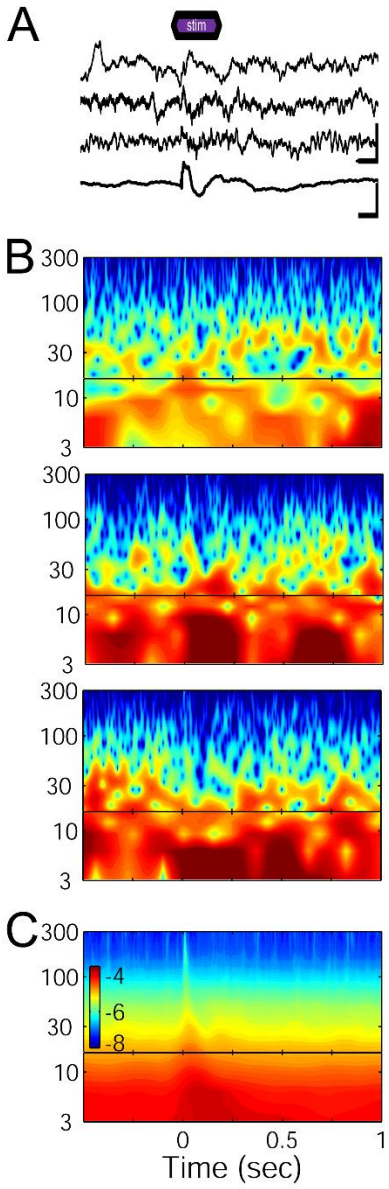

Figure 1. Ongoing and stimulus-related activity. Time domain (***A***) and time-frequency domain (***B-C***) representations of epidural field potentials recorded from auditory cortex of a rat. ***A.*** Three randomly selected trials (*top traces*) and the average of 664 trials (*bottom trace*). Scale bars for single trials: 100 ms, 0.1 mV. Scale bars for average: 100 ms, 0.05 mV. ***B.*** Corresponding power spectrograms for the three single trials in *A*. ***C.*** Average of 664 single trial spectrograms. Color scale in ***C*** represents $\log_{10}$ power and applies to *B* as well. *Horizontal lines* in *B & C* mark transition from STFT (low frequencies) to wavelet (high frequencies) transforms. Time scale in *C* applies to *A* and *B* as well.

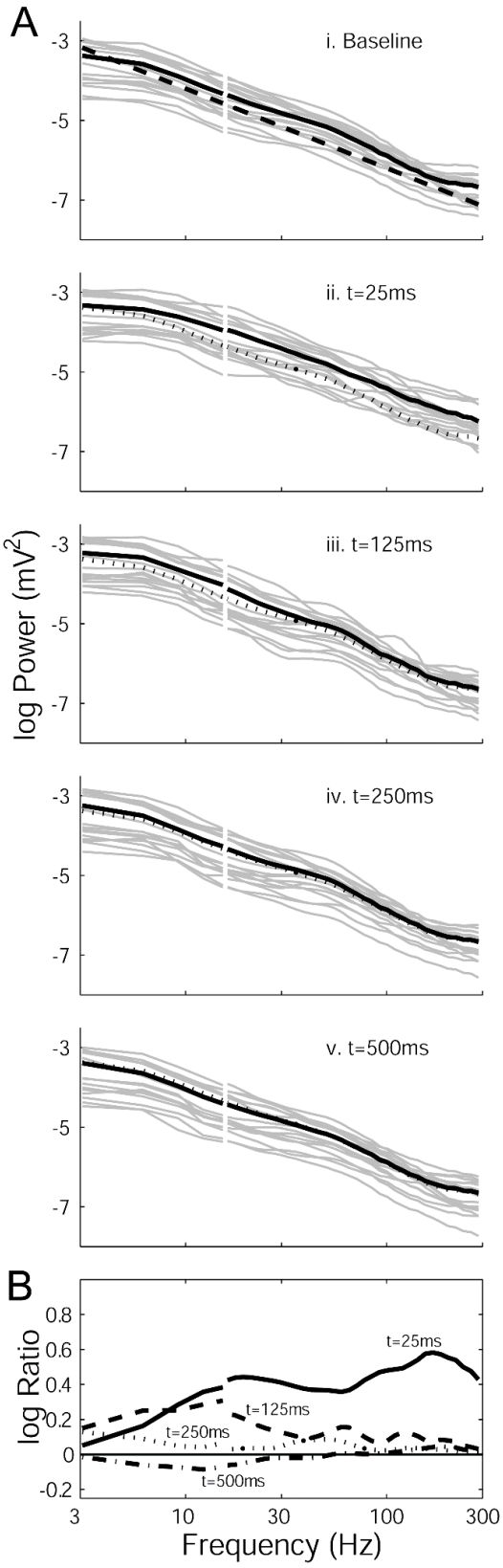

Figure 2. Analysis of mean spectra. ***A.*** Mean spectra averaged over the pre-stimulus period (***i;*** 'Baseline') and during four time windows relative to stimulus onset (***ii-v***; stimulus duration = 250 msec), then averaged across all trials for individual animals (*grey lines*), and finally averaged across animals (grand average; *solid black lines*). *Dashed line* in ***i*** is the line $y = k/f^2$, where k is an arbitrary constant and f is frequency. *Dotted lines* in ***ii-v*** are the grand average spectrum from the pre-stimulus period (***i***) replotted for comparison. ***B.*** The relative effect of the stimulus as a function of frequency during the time windows indicated in *A* is illustrated by plotting the ratios of the grand average spectra from ***ii-v*** to the ongoing spectrum in ***i***.

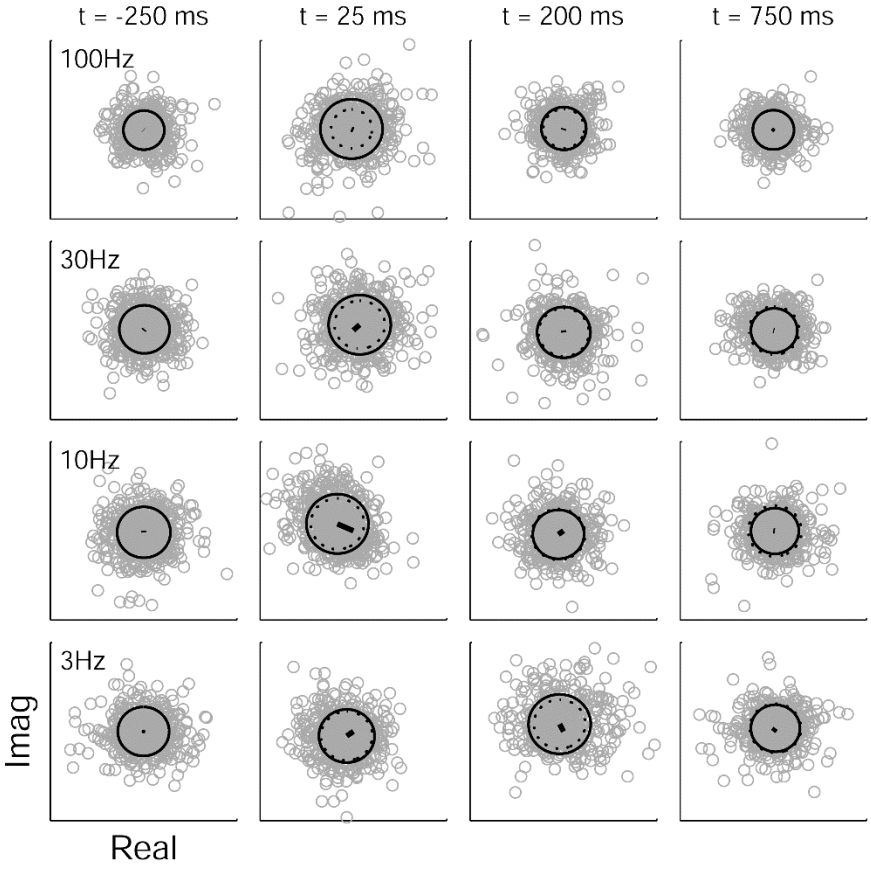

Figure 3. Spectral coefficients in the complex plane. Complex coefficients of the time-frequency transforms from the experiment in Figure 1 for the four indicated frequencies (rows) at the four indicated time points (columns). Each point represents the coefficient for a single trial at a single time and frequency. The *left column* represents baseline (i.e. pre-stimulus) activity. The *center two columns* represent peri-stimulus activity, and the *right column* represents post-stimulus activity. In each scatter plot, the *mean* of the coefficients across trials is indicated by a vector (*black line*), while the $var^{1/2}$ is indicated by the radius of the *circle*, whose origin is translated to the *mean*. The *dashed circles* in the right three columns are the $var^{1/2}$ from the ongoing activity replotted for comparison. In all panels, the real and imaginary axis limits are identical. The same axis limits apply throughout the row. The axis limits for each row are as follows: 3 Hz, ±0.055; 10 Hz, ±0.038; 30 Hz, ±0.0092; 100 Hz, ±0.0028.

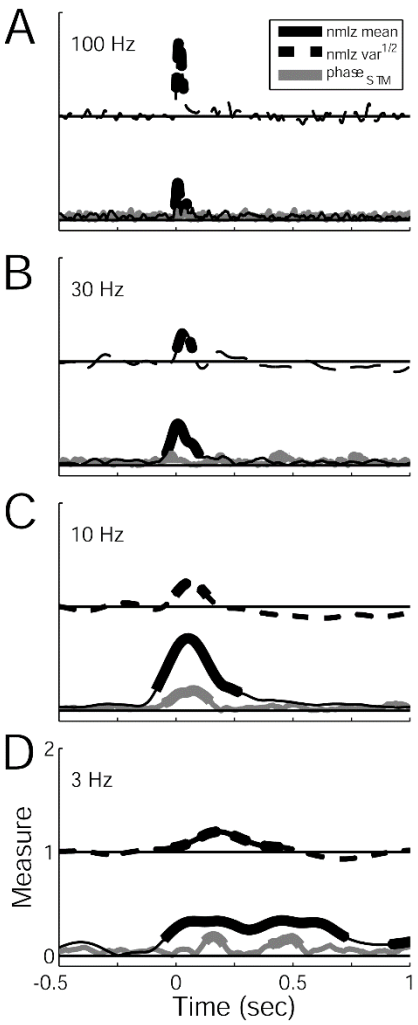

Figure 4. *Mean*, *variance* and *phase*$_{STM}$ measures. Same experiment as Figure 3. Shown are the *mean* (*solid black lines*), *var*$^{1/2}$ (*dashed black lines*) and *phase*$_{STM}$ (*grey lines*) as a function of time relative to stimulus onset at t=0 for the four indicated frequencies. The mean and *var*$^{1/2}$ measures have been normalized to the average of the *var*$^{1/2}$ during the pre-stimulus period. Note that the auditory stimulus causes a broadband increase in the *mean* of spectral coefficients whose time course differs for different frequencies. Note for the 3 Hz and 10 Hz components, the time resolution is ~150 msec, which is the window width of the STFT used for analysis of low frequency components, but for the 30 Hz and 100 Hz components the time resolution is an inverse function of frequency, as it is governed by the width of the wavelets used to analyze high frequency components. Thick lines identify epochs significantly different from baseline according to the local *fdr* method (see subsequent figure).

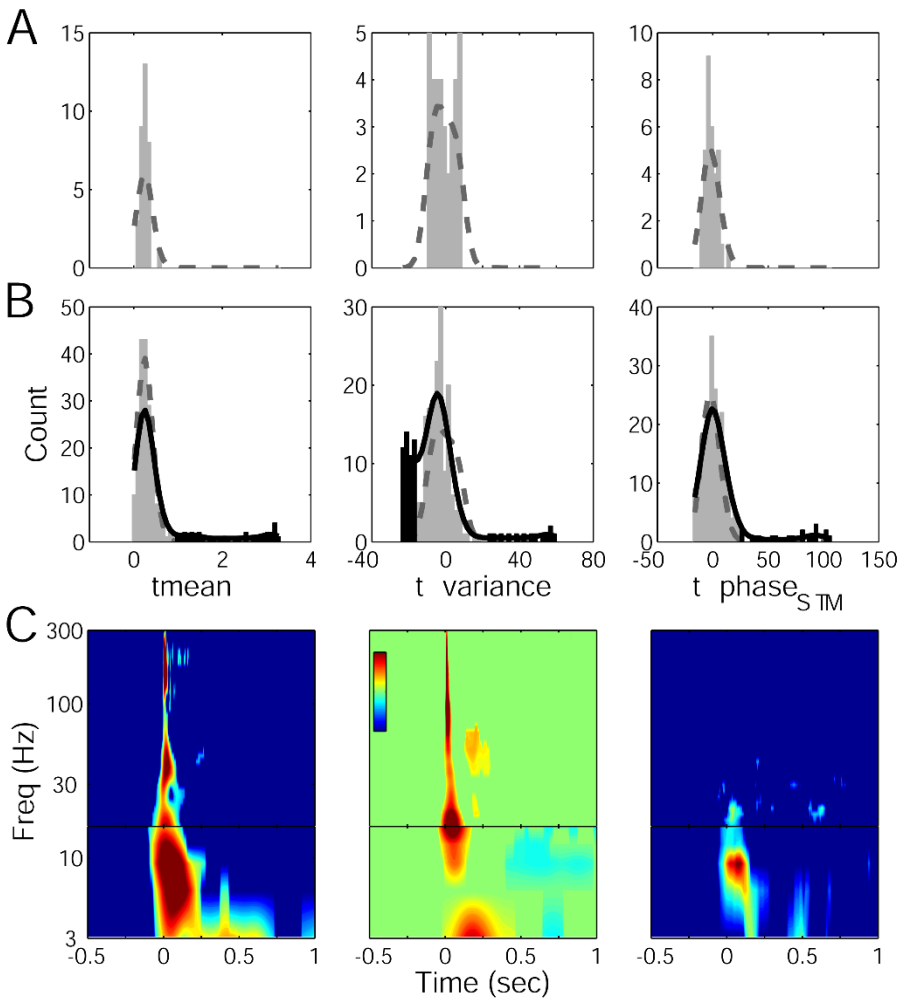

Figure 5. Complex t-statistics and local *fdr* analysis. *A., B.* The process of determining which t-values are "interesting" (i.e. significant) for one frequency component from this experiment (9 Hz) is shown. The *mean* (*left)*, *variance* (*middle*), and *phase*$_{STM}$ (*right*) at each point in the time-frequency plane were analyzed by computing complex t-statistics, calculated by comparing data in the test region to the comparison region prior to the stimulus (see Methods). Null distributions for each measure (*A*) were created by calculating t-values within the pre-stimulus comparison region and smoothing the resulting histograms (*A*, *dashed lines*). Scaling the null distribution to account for the number of data points in the post-stimulus region gives the expected distribution (*B, dashed lines*). The expected distribution is compared to the smoothed histogram of values from the test region (*B*, *solid lines*). By the local *fdr* method, bins where at least 10 times more observations were observed than expected were deemed

"interesting" (*B, black bars*), while the rest are "uninteresting" (*B, gray bars*). ***C.*** Time-frequency contour plots of t-values showing the results of the analysis applied to every time-frequency point. The plot is thresholded such that non-significant points are set to zero (*blue* in *left* and *right columns*, *green* in *center column*). Time and frequency scales in *left panel* apply to *center* and *right panels* as well. Note that unlike for the t-*mean* statistic , the t-*variance* and t-$phase_{STM}$ statistics can be either positive (*hot colors*) or negative (*cold colors*). Colorbar ranges for f>16 and f<16 Hz, respectively, are: t-*mean*: 0 - 10, 0 - 2.5; t-*variance*: -500 - 500, -100 - 100; t-*phase*STM: 0 - 400, 0 - 100.

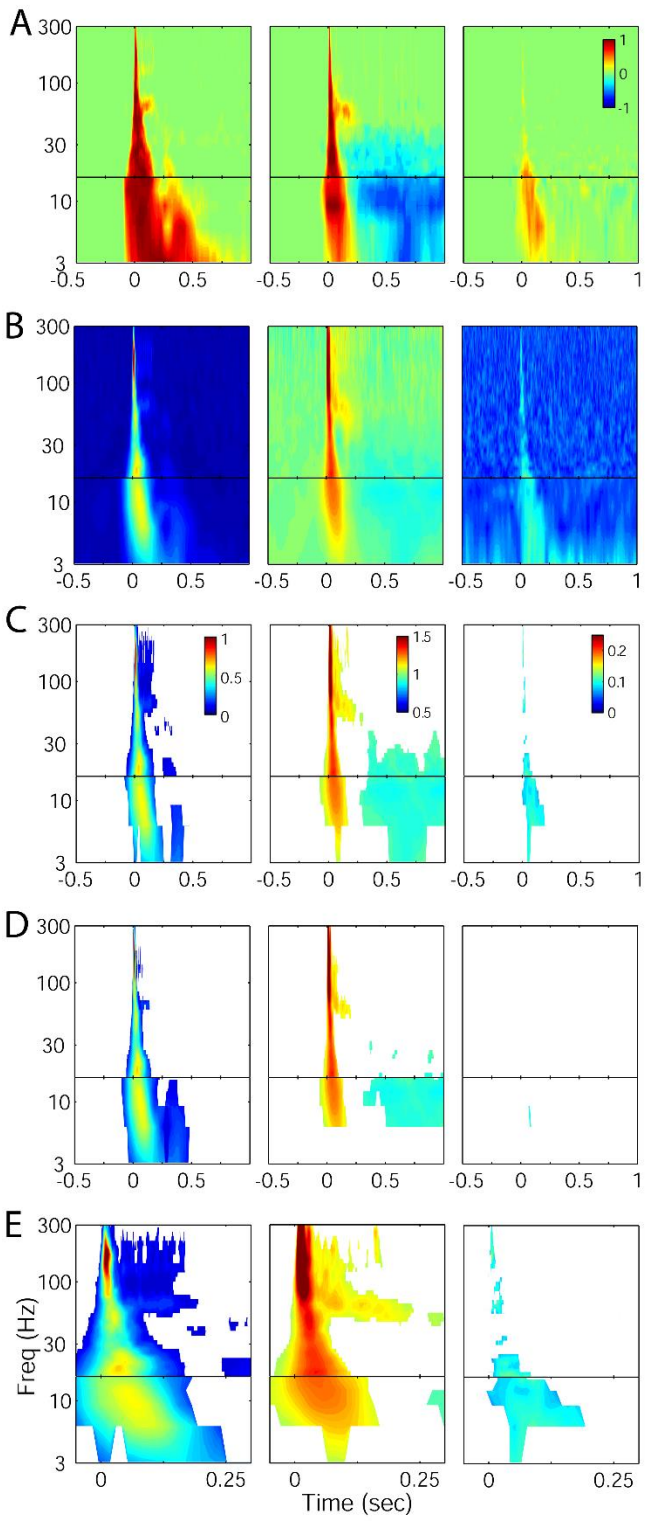

Figure 6. Summary across animals of stimulus-related effects on *mean*, *variance*, and *phase*$_{STM}$. *A*. For each animal, points in the time-frequency plane showing a significant increase in the *mean*, *variance* or *phase*$_{STM}$ measure were assigned a 1, and points showing a significant decrease were assigned a -1 (*variance* and *phase*$_{STM}$ only). These significance maps were then averaged across animals, giving a summary map that shows the fraction of animals exhibiting significant changes at each time-frequency point. ***B.*** Grand median of *mean* (*left column*), *var*$^{1/2}$ (*center column*) and *phase*$_{STM}$ (*right column*). *Mean* and *var*$^{1/2}$ measures were normalized for each animal to the *var*$^{1/2}$ averaged over the pre-stimulus period. ***C.*** The same as *B*, but thresholded for significance across animals as assessed using Mann-Whitney and corrected for multiple comparisons by local *fdr*. ***D.*** The same as *C*, but corrected for multiple comparisons using Bonferroni correction. ***E.*** Same data from *C* plotted on an expanded time scale. Note the high correlation, during the peri-stimulus period, of the *mean* and *var*$^{1/2}$ measures.

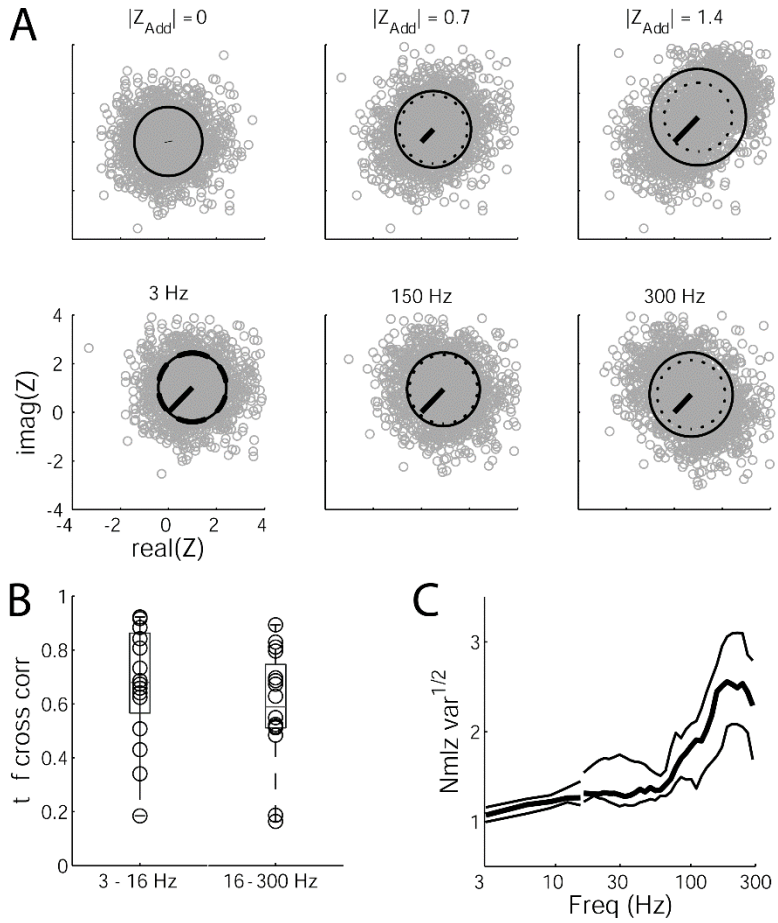

Figure 7. Evidence that *variance* changes are secondary to trial-by-trial variability in the mean. *A.* Illustration of effects of amplitude and latency variability on the *variance* of complex coefficients. Complex coefficients were simulated with real and imaginary components normally distributed with *mean* = 0 and *variance* = 1 (*top row, left panel*). In all panels, $var^{1/2}$ is indicated by the radius of the *circle*, and the *mean* is indicated by the *black line* connecting the origin to the center of the circle. The $var^{1/2}$ of the original data cloud (*top left panel*) is indicated by the *dashed circle*. *Top row* shows effect of amplitude variability on the $var^{1/2}$ measure, and that it is a monotonically increasing function of the magnitude of the additive component. For these data, half the points are unchanged, and half have a constant additive component with magnitude indicated in the panel title. *Bottom row* shows the effect of latency variability on the $var^{1/2}$ measure, and that it is a monotonically increasing function of the ratio of latency to 1/f. For these data, all points were summed with an additive component with constant amplitude, but for the two halves of the points the additive component had two different phase values, and the difference between the two phase values was set by the ratio of latency (3 ms) to 1/f multiplied by $\pi/4$. ***B.*** Two-dimensional (time-frequency) correlation coefficients between normalized *mean* and $var^{1/2}$ computed over the peri-stimulus time window for STFT coefficients (i.e. 3<f<16 Hz: *left*) and wavelet coefficients (i.e. 16<f<300

Hz; *right*). Data from individual animals appear as *open circles*. *Box plots* denote median (*horizontal line*) and first and third quartiles (*box*). Note the high correlation in most animals, as would be expected for variability in the amplitude of the additive component. ***C.*** Median (*thick line*) and first and third quartiles (*thin lines*) across animals of the normalized $var^{1/2}$, computed at each frequency at the time point corresponding to the peak in the normalized *mean* (see Methods). Note that the $var^{1/2}$ increases with frequency, as would be expected for variability in the latency of the additive component.

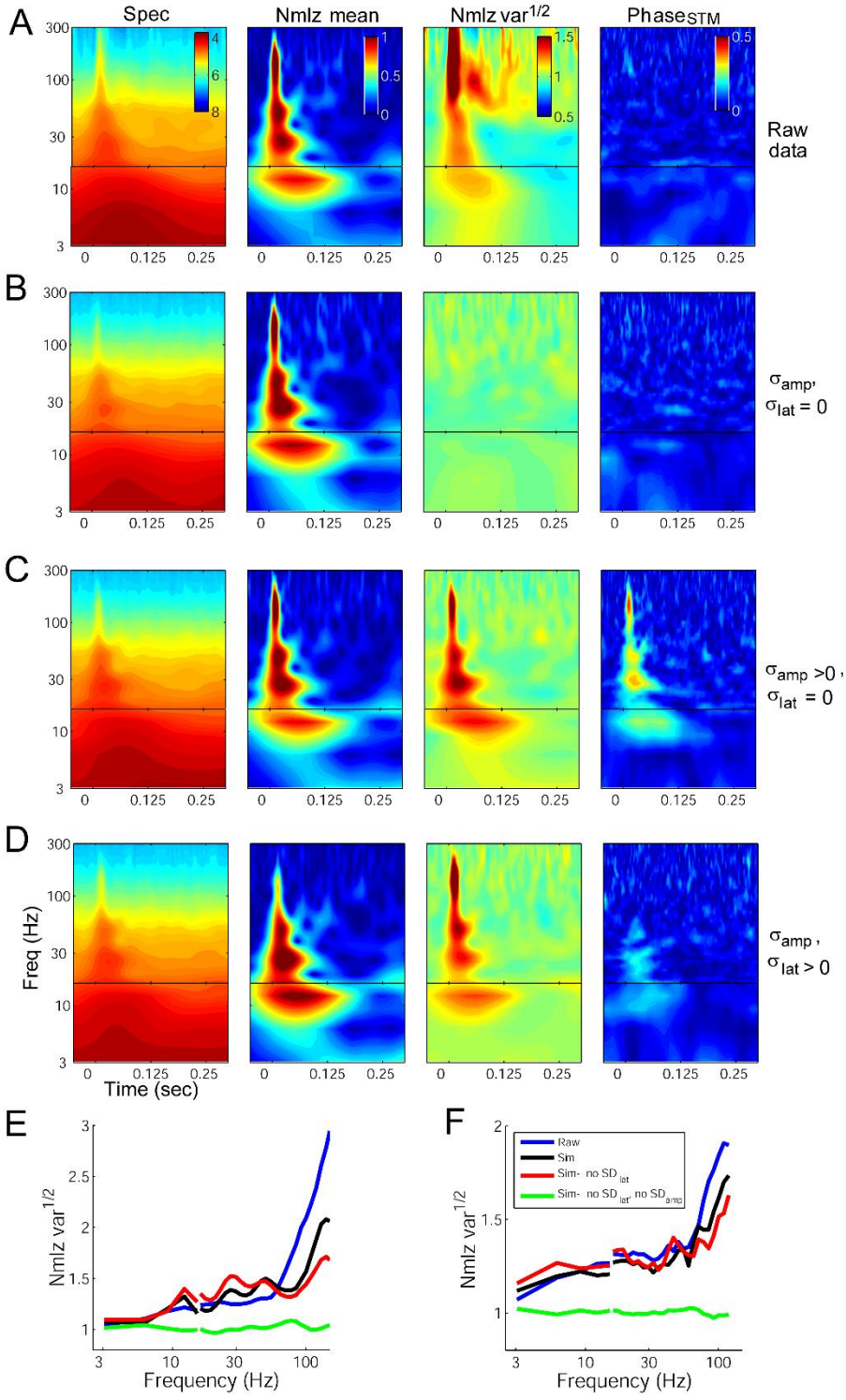

Figure 8. *Variance* changes in simulations incorporating trial-by-trial variability in amplitude and latency. *A – D.* Time-frequency spectra (*left column*), normalized *mean* (*second column*), normalized

var$^{1/2}$ (*third column*) and *phase*$_{STM}$ (*right column*) measures for data from a single animal (*A*) and simulations with zero trial-by-trial variability (*B*), variability only in the amplitude (*C*; σ_{amp} = 1.0) and variability in both amplitude and latency (*D*; σ_{amp} = 0.8, σ_{lat} = 1.8 msec). Note the absence of *variance* and *phase*$_{STM}$ changes in the absence of amplitude and latency variability (*B*), the presence of *variance* changes similar to the recorded data with such variability (*C, D*) and the improved fit of the *phase*$_{STM}$ measure to the recorded data with both amplitude and latency variability (*D*) compared to amplitude variability alone (*C*). ***E.*** Normalized *var*$^{1/2}$ (evaluated at each frequency at the peak of the normalized change in mean) from the experiment and simulations in *A*-*D* for the recorded data (*blue line*), simulated data with no trial-by-trial variability (*green line*), with only amplitude variability (σ_{amp} = 1.0; *red line*) and with both amplitude and latency variability (σ_{amp} = 0.8, σ_{lat} = 1.8 msec; *black line*). ***F.*** Same as *E*, but for the median data across animals. Simulations were the best fits to the data from each animal.

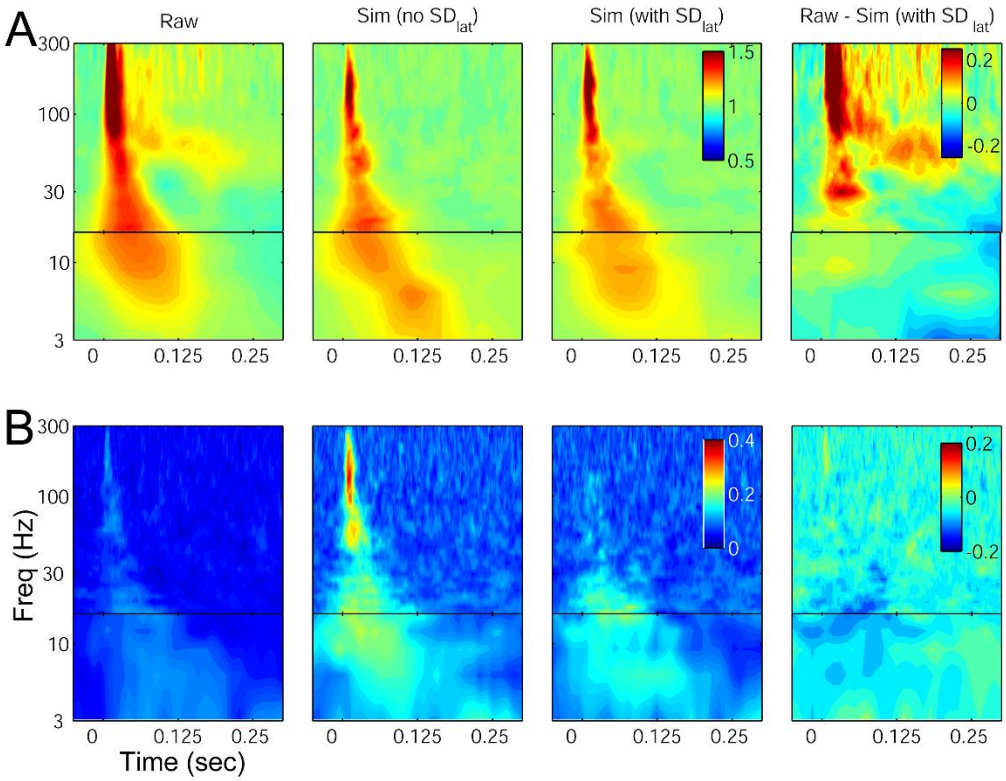

Figure 9. Summary of *variance* and *phase*$_{STM}$ changes observed with simulations. Plotted are the median recorded data (*left column*), and median best simulation results with only amplitude variability (*second column*), amplitude and latency variability (*third column*), and the difference between the recorded data and best simulation with both types of variability (*right column*) for the normalized $var^{1/2}$ (*A*) and *phase*$_{STM}$ (*B*) measures. Note that for f<100 Hz, the simulations are able to recreate most of the observed changes in *variance*, and that the *phase*$_{STM}$ measure is more similar to the recorded data when both types of variability are included in the model.

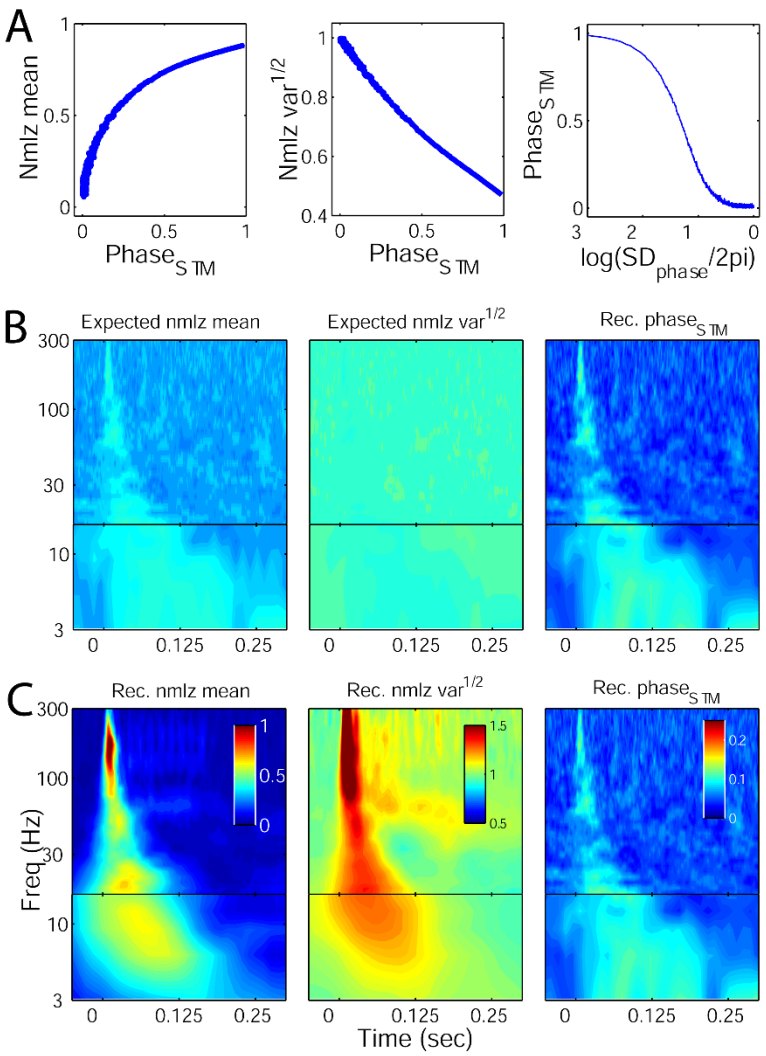

Figure 10. *Phase*$_{STM}$ measure simulations and predicted changes in *mean* and *variance* assuming the changes were entirely due to phase reset. Data were simulated by assuming that ongoing activity was described by complex coefficients having real and imaginary parts that are jointly normally distributed with common variance. The magnitudes of these coefficients were maintained but their phases concentrated to adhere to a von Mises distribution with the indicated standard deviation. ***A.*** *Right panel* shows the *phase*$_{STM}$ measure (STM) as function of phase dispersal. The expected changes in normalized *mean* and *var*$^{1/2}$ given a phase concentration yielding the indicated *phase*$_{STM}$ value are shown in the *left and center panels*, respectively. ***B.*** Corresponding *mean* and *var*$^{1/2}$ plots assuming that these were due entirely to a phase reset as measured by the *phase*$_{STM}$ in the *right panel*. ***C.*** The median raw data across animals, replotted from Figure 6.

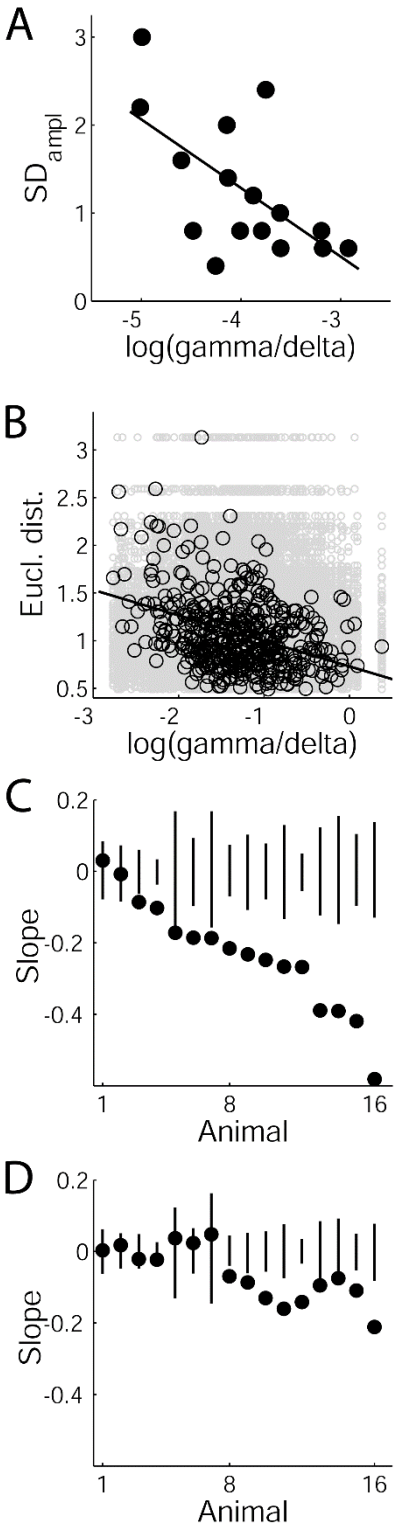

Figure 11. Cortical state-dependence of amplitude variability. *A*. Amplitude variability (σ_{amp}) from best fit of model to observed $var^{1/2}$ for each animal as a function of the log of the ratio of gamma to delta power in the pre-stimulus period averaged over all trials for that animal. *Solid line* is linear regression fit to data (slope = -0.78, r^2 = 0.38, p = 0.01). Note that amplitude variability was greatest in animals with small gamma/delta ratios. ***B.*** Single trial analysis for all trials recorded in one animal. For each trial, we calculated the Euclidean distance between that single trial response and the mean response for this animal. These single trial distance measures are plotted as a function of log gamma/delta ratio. *Straight line* is linear regression fit to the data (slope = -0.27, r^2 = 0.14, p = $1.1x10^{-16}$). *Grey circles* are the same data after shuffling trial number 100 times. ***C, D.*** Slopes (*black circles*) and 95% confidence intervals (*black lines*) obtained from linear regression fits as in *B* for all 16 animals without additional high pass filtering (*C*) and after filtering >4Hz (*D*). Note that before filtering 14 of 16 animals exhibit significant regression slopes, and that after filtering significant slopes are seen in 8 of 16 animals.

References

Adab HZ and Vogels R. Practicing coarse orientation discrimination improves orientation signals in macaque cortical area v4. *Curr Biol* 21: 1661-1666, 2011.

Arieli A, Sterkin A, Grinvald A and Aertsen A. Dynamics of ongoing activity: Explanation of the large variability in evoked cortical responses. *Science* 273: 1868-1871, 1996.

Banoub M, Tetzlaff JE and Schubert A. Pharmacologc and physiologic influences affecting sensory evoked potentials - Implications for perioperative monitoring. *Anesthesiology* 99: 716-737, 2003.

Brosch M, Budinger E and Scheich H. Stimulus-related gamma oscillations in primate auditory cortex. *J Neurophysiol* 87: 2715-2725, 2002.

Buzsaki G. *Rhythms of the Brain*. Oxford: Oxford University Press, 2006.

Chechik G, Anderson MJ, Bar-Yosef O, Young ED, Tishby N and Nelken I. Reduction of information redundancy in the ascending auditory pathway. *Neuron* 51: 359-368, 2006.

Crone NE, Boatman D, Gordon B and Hao L. Induced electrocorticographic gamma activity during auditory perception. *Clinical Neurophysiology* 112: 565-582, 2001.

Curto C, Sakata S, Marguet S, Itskov V and Harris KD. A simple model of cortical dynamics explains variability and state dependence of sensory responses in urethane-anesthetized auditory cortex. *J Neurosci* 29: 10600-10612, 2009.

D'Avanzo C, Schiff S, Amodio P and Sparacino G. A Bayesian method to estimate single-trial event-related potentials with application to the study of the P300 variability. *Journal of Neuroscience Methods* 198: 114-124, 2011.

David O, Kilner JM and Friston KJ. Mechanisms of evoked and induced responses in MEG/EEG. *Neuroimage* 31: 1580-1591, 2006.

Dawson GD. A summation technique for the detection of small evoked potentials. *Electroencephalogr Clin Neurophysiol* 6: 65-84, 1954.

de Kock CP, Bruno RM, Spors H and Sakmann B. Layer- and cell-type-specific suprathreshold stimulus representation in rat primary somatosensory cortex. *J Physiol* 581: 139-154, 2007.

Doron NN, LeDoux JE and Semple MN. Redefining the tonotopic core of rat auditory cortex: physiological evidence for a posterior field. *J Comp Neurol* 453: 345-360, 2002.

Efron B. Large-scale simultaneous hypothesis testing: The choice of a null hypothesis. *Journal of the American Statistical Association* 99: 96-104, 2004.

Foxe JJ and Snyder AC. The Role of Alpha-Band Brain Oscillations as a Sensory Suppression Mechanism during Selective Attention. *Front Psychol* 2: 154, 2011.

Friston KJ, Stephan KM and Frackowiak RS. Transient phase-locking and dynamic correlations: Are they the same thing? *Hum Brain Mapp* 5: 48-57, 1997.

Galambos R, Makeig S and Talmachoff PJ. A 40-Hz auditory potential recorded from the human scalp. *Proc Natl Acad Sci USA* 78: 2643-2647, 1981.

Hanslmayr S, Klimesch W, Sauseng P, Gruber W, Doppelmayr M, Freunberger R, Pecherstorfer T and Birbaumer N. Alpha phase reset contributes to the generation of ERPs. *Cereb Cortex* 17: 1-8, 2007.

Hu L, Boutros NN and Jansen BH. Evoked potential variability. *J Neurosci Methods* 178: 228-236, 2009.

Jansen BH, Agarwal G, Hegde A and Boutros NN. Phase synchronization of the ongoing EEG and auditory EP generation. *Clin Neurophysiol* 114: 79-85, 2003.

Jervis BW, Nichols MJ, Johnson TE, Allen E and Hudson NR. A fundamental investigation of the composition of auditory evoked potentials. *IEEE Trans Biomed Eng* 30: 43-50, 1983.

Jeschke M, Lenz D, Budinger E, Herrmann CS and Ohl FW. Gamma oscillations in gerbil auditory cortex during a target-discrimination task reflect matches with short-term memory. *Brain Research* In Press, Corrected Proof: 2008.

Jordan D, Miksad RW and Powers EJ. Implementation of the continuous wavelet transform for digital time series analysis. *Review of Scientific Instruments* 68: 1484-1494, 1997.

Jung TP, Makeig S, Stensmo M and Sejnowski TJ. Estimating alertness from the EEG power spectrum. *Biomedical Engineering, IEEE Transactions on* 44: 60-69, 1997.

Kalcher J and Pfurtscheller G. Discrimination between phase-locked and non-phase-locked event-related EEG activity. *Electroencephalogr Clin Neurophysiol* 94: 381-384, 1995.

Kane NM, Butler SR and Simpson T. Coma outcome prediction using event-related potentials: P(3) and mismatch negativity. *Audiology & Neuro-Otology* 5: 186-191, 2000.

Karrasch M, Krause CM, Laine M, Lang AH and Lehto M. Event-related desynchronization and synchronization during an auditory lexical matching task. *Electroencephalogr Clin Neurophysiol* 107: 112-121, 1998.

Kilner JM, Kiebel SJ and Friston KJ. Applications of random field theory to electrophysiology. *Neurosci Lett* 374: 174-178, 2005.

Kisley MA and Gerstein GL. Trial-to-trial variability and state-dependent modulation of auditory- evoked responses in cortex. *J Neurosci* 19: 10451-10460, 1999.

Klimesch W, Russegger H, Doppelmayr M and Pachinger T. A method for the calculation of induced band power: implications for the significance of brain oscillations. *Electroencephalogr Clin Neurophysiol* 108: 123-130, 1998.

Klimesch W, Sauseng P and Hanslmayr S. EEG alpha oscillations: the inhibition-timing hypothesis. *Brain Res Rev* 53: 63-88, 2007.

Krause CM, Lang AH, Laine M, Kuusisto M and Porn B. Event-related EEG desynchronization and synchronization during an auditory memory task. *Electroencephalogr Clin Neurophysiol* 98: 319-326, 1996.

Krieg J, Trebuchon-Da FA, Martinez-Montes E, Marquis P, Liegeois-Chauvel C and Benar CG. A comparison of methods for assessing alpha phase resetting in electrophysiology, with application to intracerebral EEG in visual areas. *Neuroimage* 55: 67-86, 2011.

Lakatos P, Chen CM, O'Connell MN, Mills A and Schroeder CE. Neuronal oscillations and multisensory interaction in primary auditory cortex. *Neuron* 53: 279-292, 2007.

Lakatos P, Shah AS, Knuth KH, Ulbert I, Karmos G and Schroeder CE. An Oscillatory Hierarchy Controlling Neuronal Excitability and Stimulus Processing in the Auditory Cortex. *J Neurophysiol* 94: 1904-1911, 2005.

Lange DH, Pratt H and Inbar GF. Modeling and estimation of single evoked brain potential components. *IEEE Trans Biomed Eng* 44: 791-799, 1997.

Lazar R and Metherate R. Spectral interactions, but no mismatch negativity, in auditory cortex of anesthetized rat. *Hear Res* 181: 51-56, 2003.

Ledberg A, Montagnini A, Coppola R and Bressler SL. Reduced variability of ongoing and evoked cortical activity leads to improved behavioral performance. *PLoS One* 7: e43166, 2012.

Lehtela L, Salmelin R and Hari R. Evidence for reactive magnetic 10-Hz rhythm in the human auditory cortex. *Neuroscience Letters* 222: 111-114, 1997.

Lenz D, Jeschke M, Schadow J, Naue N, Ohl FW and Herrmann CS. Human EEG very high frequency oscillations reflect the number of matches with a template in auditory short-term memory. *Brain Research* In Press, Corrected Proof: 2008.

Luczak A, Bartho P and Harris KD. Gating of sensory input by spontaneous cortical activity. *J Neurosci* 33: 1684-1695, 2013.

Luo H, Liu Z and Poeppel D. Auditory cortex tracks both auditory and visual stimulus dynamics using low-frequency neuronal phase modulation. *PLoS Biol* 8: e1000445, 2010.

MacDonald KD and Barth DS. High frequency (gamma-band) oscillating potentials in rat somatosensory and auditory cortex. *Brain Research* 694: 1-12, 1995.

Makeig S, Westerfield M, Jung TP, Enghoff S, Townsend J, Courchesne E and Sejnowski TJ. Dynamic brain sources of visual evoked responses. *Science* 295: 690-694, 2002.

Makinen V, Tiitinen H and May P. Auditory event-related responses are generated independently of ongoing brain activity. *Neuroimage* 24: 961-968, 2005.

Martinez-Montes E, Cuspineda-Bravo ER, El-Deredy W, Sanchez-Bornot JM, Lage-Castellanos A and Valdes-Sosa PA. Exploring event-related brain dynamics with tests on complex valued time-frequency representations. *Stat Med* 27: 2922-2947, 2008.

Mocks J, Gasser T, Pham DT and Kohler W. Trial-to-trial variability of single potentials: methodological concepts and results. *Int J Neurosci* 33: 25-32, 1987.

Nakamura T, Michie PT, Fulham WR, Todd J, Budd TW, Schall U, Hunter M and Hodgson DM. Epidural Auditory Event-Related Potentials in the Rat to Frequency and duration Deviants: Evidence of Mismatch Negativity? *Front Psychol* 2: 367, 2011.

Ng BS, Logothetis NK and Kayser C. EEG phase patterns reflect the selectivity of neural firing. *Cereb Cortex* 23: 389-398, 2013.

Nir, Y., Vyazovskiy, V. V., Cirelli, C., Banks, M. I., and Tononi, G. Auditory responses and stimulus-specific adaptation are largely preserved across NREM and REM sleep in rat primary auditory cortex. 902.16. 2012. Society for Neuroscience Abstracts.

Palva S and Palva JM. New vistas for alpha frequency band oscillations. *Trends in Neurosciences* 30: 150-158, 2007.

Pantev C, Makeig S, Hoke M, Galambos R, Hampson S and Gallen C. Human auditory evoked gamma-band magnetic fields. *Proc Natl Acad Sci USA* 88: 8996-9000, 1991.

Pasley BN, Allen EA and Freeman RD. State-dependent variability of neuronal responses to transcranial magnetic stimulation of the visual cortex. *Neuron* 62: 291-303, 2009.

Pfurtscheller G and Lopes da Silva FH. Event-related EEG/MEG synchronization and desynchronization: basic principles. *Clin Neurophysiol* 110: 1842-1857, 1999.

Picton TW. The P300 wave of the human event-related potential. *J Clin Neurophysiol* 9: 456-479, 1992.

Pulvermuller F, Eulitz C, Pantev C, Mohr B, Feige B, Lutzenberger W, Elbert T and Birbaumer N. High-frequency cortical responses reflect lexical processing: an MEG study. *Electroencephalography & Clinical Neurophysiology* 98: 76-85, 1996.

Qin L, Chimoto S, Sakai M, Wang J and Sato Y. Comparison between offset and onset responses of primary auditory cortex ON-OFF neurons in awake cats. *J Neurophysiol* 97: 3421-3431, 2007.

Recanzone GH, Guard DC and Phan ML. Frequency and intensity response properties of single neurons in the auditory cortex of the behaving macaque monkey. *J Neurophysiol* 83: 2315-2331, 2000.

Risner ML, Aura CJ, Black JE and Gawne TJ. The Visual Evoked Potential is independent of surface alpha rhythm phase. *Neuroimage* 45: 463-469, 2009.

Roach BJ and Mathalon DH. Event-related EEG time-frequency analysis: an overview of measures and an analysis of early gamma band phase locking in schizophrenia. *Schizophr Bull* 34: 907-926, 2008.

Ruusuvirta T, Penttonen M and Korhonen T. Auditory cortical event-related potentials to pitch deviances in rats. *Neurosci Lett* 248: 45-48, 1998.

Sadaghiani S, Hesselmann G and Kleinschmidt A. Distributed and antagonistic contributions of ongoing activity fluctuations to auditory stimulus detection. *J Neurosci* 29: 13410-13417, 2009.

Santamaria J and Chiappa KH. The EEG of drowsiness in normal adults. *J Clin Neurophysiol* 4: 327-382, 1987.

Sauseng P, Klimesch W, Gruber WR, Hanslmayr S, Freunberger R and Doppelmayr M. Are event-related potential components generated by phase resetting of brain oscillations? A critical discussion. *Neuroscience* 146: 1435-1444, 2007.

Sayers BM, Beagley HA and Henshall WR. The mechansim of auditory evoked EEG responses. *Nature* 247: 481-483, 1974.

Shadlen MN and Newsome WT. The variable discharge of cortical neurons: Implications for connectivity, computation, and information coding. *J Neurosci* 18: 3870-3896, 1998.

Shaffer JP. Multiple Hypothesis Testing. *Annu Rev Psychol* 46: 561-584, 1995.

Shah AS, Bressler SL, Knuth KH, Ding M, Mehta AD, Ulbert I and Schroeder CE. Neural Dynamics and the Fundamental Mechanisms of Event-related Brain Potentials. *Cerebral Cortex* 14: 476-483, 2004.

Sobolewski A, Swiejkowski DA, Wrobel A and Kublik E. The 5-12 Hz oscillations in the barrel cortex of awake rats--sustained attention during behavioral idling? *Clin Neurophysiol* 122: 483-489, 2011.

Steinschneider M, Fishman YI and Arezzo JC. Spectrotemporal Analysis of Evoked and Induced Electroencephalographic Responses in Primary Auditory Cortex (A1) of the Awake Monkey. *Cereb Cortex* 18: 610-625, 2008.

Steriade M, Oakson G and Kitsikis A. Firing rates and patterns of output and nonoutput cells in cortical areas 5 and 7 of cat during the sleep-waking cycle. *Exp Neurol* 60: 443-468, 1978.

Tallon-Baudry C and Bertrand O. Oscillatory gamma activity in humans and its role in object representation. *Trends Cogn Sci* 3: 151-162, 1999.

Tallon-Baudry C, Bertrand O, Delpuech C and Pernier J. Stimulus specificity of phase-locked and non-phase-locked 40 Hz visual responses in human. *J Neurosci* 16: 4240-4249, 1996.

Trautner P, Rosburg T, Dietl T, Fell J, Korzyukov OA, Kurthen M, Schaller C, Elger CE and Boutros NN. Sensory gating of auditory evoked and induced gamma band activity in intracranial recordings. *Neuroimage* 32: 790-798, 2006.

Truccolo WA, Ding M, Knuth KH, Nakamura R and Bressler SL. Trial-to-trial variability of cortical evoked responses: implications for the analysis of functional connectivity. *Clin Neurophysiol* 113: 206-226, 2002.

Varela F, Lachaux JP, Rodriguez E and Martinerie J. The brainweb: phase synchronization and large-scale integration. *Nat Rev Neurosci* 2: 229-239, 2001.

Weisz N, Hartmann T, Muller N, Lorenz I and Obleser J. Alpha rhythms in audition: cognitive and clinical perspectives. *Front Psychol* 2: 73, 2011.

White B, Abbott LF and Fiser J. Suppression of cortical neural variability is stimulus- and state-dependent. *J Neurophysiol* 108: 2383-2392, 2012.

Whitsel BL, Schreiner RC and Essick GK. An analysis of variability in somatosensory cortical neuron discharge. *J Neurophysiol* 40: 589-607, 1977.

Wiest MC and Nicolelis MA. Behavioral detection of tactile stimuli during 7-12 Hz cortical oscillations in awake rats. *Nat Neurosci* 6: 913-914, 2003.

Yeung N, Bogacz R, Holroyd CB and Cohen JD. Detection of synchronized oscillations in the electroencephalogram: an evaluation of methods. *Psychophysiology* 41: 822-832, 2004.

Chapter 3

This Chapter was published previously as:

Krause BM, Raz A, Uhlrich DJ, Smith PH, Banks MI (2014) Spiking in auditory cortex following thalamic stimulation is dominated by cortical network activity. Frontiers in Systems Neuroscience 8:170.

Spiking in auditory cortex following thalamic stimulation is dominated by cortical network activity

Bryan M. Krause[1], Aeyal Raz[2,3], Daniel J. Uhlrich[4], Philip H. Smith[4], Matthew I. Banks[2,4*]

[1]Neuroscience Training Program, University of Wisconsin, Madison, WI, USA

[2]Department of Anesthesiology, University of Wisconsin, Madison, WI, USA

[3]Department of Anesthesiology, Rabin Medical Center, Petah-Tikva, Israel, affiliated with Sackler School of Medicine, Tel Aviv University, Tel Aviv, Israel

[4]Department of Neuroscience, University of Wisconsin, Madison, WI, USA

*** Correspondence:** Matthew I. Banks, Department of Anesthesiology, University of Wisconsin, 1300 University Ave Room 4605, Madison, WI, 53706, USA.

mibanks@wisc.edu

Keywords: auditory cortex, thalamo-cortical (TC), UP states, canonical microcircuit, calcium imaging, multiunit activity, patch clamp.

Abstract

The state of the sensory cortical network can have a profound impact on neural responses and perception. In rodent auditory cortex, sensory responses are reported to occur in the context of network events, similar to brief UP states, that produce 'packets' of spikes and are associated with synchronized synaptic input (Bathellier et al., 2012;Hromadka et al., 2013;Luczak et al., 2013). However, traditional models based on data from visual and somatosensory cortex predict that ascending sensory thalamocortical (TC) pathways sequentially activate cells in layers 4 (L4), L2/3 and L5. The relationship between these two spatio-temporal activity patterns is unclear. Here, we used calcium imaging and electrophysiological recordings in murine auditory TC brain slices to investigate the laminar response pattern to stimulation of TC afferents. We show that although monosynaptically driven spiking in response to TC afferents occurs, the vast majority of spikes fired following TC stimulation occurs during brief UP states and outside the context of the L4>L2/3>L5 activation sequence. Specifically, monosynaptic subthreshold TC responses with similar latencies were observed throughout layers 2 - 6, presumably via synapses onto dendritic processes located in L3 & L4. However, monosynaptic spiking was rare, and occurred primarily in L4 and L5 non-pyramidal cells. By contrast, during brief, TC-induced UP states, spiking was dense and occurred primarily in pyramidal cells. These network events always involved infragranular layers, whereas involvement of supragranular layers was variable. During UP states, spike latencies were comparable between infragranular and supragranular cells. These data are consistent with a model in which activation of auditory cortex, especially supragranular layers, depends on internally generated network events that represent a nonlinear amplification process, are initiated by infragranular cells and tightly regulated by feed-forward inhibitory cells.

Introduction

For audition, somatosensation and vision, sensory information from the outside world is routed almost entirely through the thalamus, and is projected into neocortex via thalamo-cortical afferents. Classical experimental approaches to understanding how neocortex uses this information to construct perception relied on single cell recordings under passive (often unconscious) stimulation conditions, emphasizing bottom-up information streams and portraying neocortex as a passive receiver of sensory information (Mountcastle et al., 1957;Hubel and Wiesel, 1963;Gerstein and Kiang, 1964). These approaches provided enormous advances in understanding the hierarchical, columnar and topographic organization of neocortex (Creutzfeldt, 1977;Mountcastle, 1997;Kaas and Collins, 2001). In developing our current understanding of how the cortico-thalamic network constructs awareness, new emphasis is being placed on the pre-eminence of intracortical network activity that is perturbed periodically by volleys of ascending information (Bastos et al., 2012;Singer, 2013). This view is more consistent with the observations that perception depends heavily on internally-generated processes such as expectation, attention and arousal (Warren, 1970;Davis and Johnsrude, 2007;Fritz et al., 2007), that ascending afferents account for a small fraction of synaptic connections in neocortical circuits (Benshalom and White, 1986;Peters and Payne, 1993;Budd, 1998;Schoonover et al., 2014), and that cortical responses to sensory stimuli exhibit a high degree of trial-by-trial variability, due largely to variable cortical activity levels at the time of stimulation (Kisley and Gerstein, 1999;Lakatos et al., 2005;Curto et al., 2009;Pasley et al., 2009;White et al., 2012;Goris et al., 2014).

Nearly ubiquitous in classical descriptions of neocortical function, the 'canonical microcircuit model' sought to capture the sequential activation of cells in a neocortical column driven by bottom-up input following a sensory stimulus. As originally conceived, the model consisted of a supragranular network mediating horizontal and ascending cortical-cortical connections, and an infragranular network sending descending cortico-cortical and subcortical projections (Douglas et al., 1989;Douglas and

Martin, 1991). In later refinements of the model, based primarily on anatomical data in visual cortex of cat (Gilbert, 1983;Gilbert and Wiesel, 1983;Binzegger et al., 2004) and supported by data from paired recordings in cortical brain slices of rat and cat (Thomson and Bannister, 1998;Feldmeyer et al., 2002;Thomson et al., 2002;Lübke et al., 2003;Thomson and Bannister, 2003;Kampa et al., 2006;Thomson and Lamy, 2007), the model predicts a stereotyped pattern of information flow through cortex upon sensory stimulation: spiny stellate cells, excitatory interneurons in layer 4, are activated first by thalamic input, in turn driving ascending projection cells in supragranular layers, which drive descending projection cells in infragranular layers (Douglas and Martin, 2004;Hirsch and Martinez, 2006;Lubke and Feldmeyer, 2007).

In spite of its widespread acceptance, there is evidence that cortical spiking following sensory stimulation is governed by processes in addition to those described in this model. Although electrophysiological mapping studies have shown stronger synaptic strength and higher connection probability from L2/3 to L5 than the reverse (Thomson and Bannister, 1998), such data do not take into account the relative likelihood that cells will spike in response to sensory stimulation, i.e. the observation that L2/3 cells fire far more sparsely than cells in L5 (Sakata and Harris, 2009;Barth and Poulet, 2012), or that infragranular cells often fire with latencies as short or shorter than granular and supragranular cells (Maunsell and Gibson, 1992;Sugimoto et al., 1997;Shen et al., 1999;de Kock et al., 2007;Sakata and Harris, 2009;Christianson et al., 2011;Constantinople and Bruno, 2013;Sun et al., 2013). Indeed, most cortical cells have dendrites that traverse the thalamo-recipient layers, and thus may be activated monosynaptically (Bullier and Henry, 1979;Mitani and Shimokouchi, 1985;Douglas and Martin, 1991;Gil and Amitai, 1996;Verbny et al., 2006;Sun et al., 2013).

Other evidence suggests that features of the model may not apply to auditory cortex in particular. The canonical microcircuit was developed based on studies of visual cortex, where thalamic input contacts spiny stellate cells in layer 4 (Gilbert and Wiesel, 1983). However, spiny stellate cells are

rare in auditory cortex, their role likely being occupied by pyramidal cells (Smith and Populin, 2001;Barbour and Callaway, 2008;Sakata and Harris, 2009). Additionally, evidence for receptive field hierarchy from granular to supragranular to infragranular layers is weak compared to visual cortex and is not associated with longer latencies in the infragranular layers (Atencio et al., 2009).

In contrast to the orderly progression of mono-, di- and tri-synaptically-driven spiking activity in layers 4, 2/3 and 5, respectively, predicted by the canonical microcircuit model, spiking in neocortex during sensory stimulation also occurs in the context of synchronous network bursts termed 'UP states' (Petersen et al., 2003;Sakata and Harris, 2009) or 'bumps' (DeWeese and Zador, 2006). It should be noted that in auditory cortex *in vivo*, there is some debate as to whether these observed network events are true UP states, with some authors referring to them instead as 'bumps' (Hromadka et al., 2013) and others as 'UP states' (Sakata and Harris, 2009); for simplicity, we will refer to these events as UP states, but we note that there is some controversy regarding this terminology. Although most commonly observed during slow-wave sleep and certain types of anesthesia (Steriade et al., 1993), UP states may share some characteristics with the aroused state, including higher levels of ongoing activity (both excitatory and inhibitory) and depolarized membrane potentials (Steriade et al., 2001;Destexhe et al., 2003;Destexhe et al., 2007). Indeed, evidence suggests that cortical processing of sensory information occurs during similar, albeit briefer, events in the awake brain (Bathellier et al., 2012;Hromadka et al., 2013;Luczak et al., 2013;Tan et al., 2014). In this model, sensory stimuli trigger these network events with probability that depends on stimulus intensity and identity, in contrast to traditional views of sensory coding in which individual cells' response magnitudes are smoothly varying functions of stimulus properties. Although these events are regulated by subcortical inputs (Metherate et al., 1992;Goard and Dan, 2009;Constantinople and Bruno, 2011), similar activity has also been observed in auditory, visual and somatosensory brain slice preparations (Metherate and Cruikshank, 1999;Sanchez-Vives and McCormick, 2000;Cruikshank et al., 2002;MacLean et al., 2005;Watson et al., 2008;Rigas and Castro-

Alamancos, 2009), where it has been shown to be non-epileptiform in nature and represent an *in vitro* correlate of UP states that occur *in vivo* (Sanchez-Vives and McCormick, 2000;Shu et al., 2003;Cunningham et al., 2006;Rigas and Castro-Alamancos, 2007). UP states likely arise in layer 5 before spreading to other laminae (Chauvette et al., 2010;Wester and Contreras, 2012;Beltramo et al., 2013;Stroh et al., 2013), and may represent an intracortical filter that regulates incorporation of sensory signals into the cortical hierarchical processing stream (MacLean et al., 2005). Selective activation of infragranular layers by sensory input (Constantinople and Bruno, 2013) and failure of some UP states to propagate to supragranular layers (Sakata and Harris, 2009) suggests that full engagement of the cortical column may only occur in certain contexts. Here, we present data consistent with a model in which activation of sensory neocortex, especially cells in supragranular layers, depends on internally generated network events initiated by infragranular cells, a process likely tightly regulated by monosynaptic activation of feed-forward inhibitory cells.

Materials and methods

All experimental protocols conformed to American Physiological Society/National Institutes of Health guidelines and were approved by the University of Wisconsin Animal Care and Use Committee.

Slice preparation

Male B6CBAF1/J mice (first generation cross of C57BL/6J and CBA/J) were used in these studies to use genetically identical animals that lack recessive mutations known to affect sensory systems (Dräger and Hubel, 1978;Johnson et al., 1997). Mice (3 – 10 weeks, median 31 days old) were decapitated under isoflurane anesthesia, and their brains were extracted and immersed in cutting artificial CSF [cACSF; composed of (in mM) 111 NaCl, 35 $NaHCO_3$, 20 HEPES, 1.8 KCl, 1.05 $CaCl_2$, 2.8

$MgSO_4$, 1.2 KH_2PO_4, and 10 glucose] at 0-4°C. HEPES was included to improve slice health and prevent edema (MacGregor et al., 2001). Auditory TC brain slices (450 μm) were prepared from the right hemisphere as previously described (Cruikshank et al., 2002;Verbny et al., 2006). Slices were maintained in cACSF saturated with 95% O_2/5% CO_2 at 24°C for >1 h before transfer to the recording chamber, which was perfused at 3 - 6 ml/min with ACSF [composed of (in mM) 111 NaCl, 35 $NaHCO_3$, 20 HEPES, 1.8 KCl, 2.1 $CaCl_2$, 1.4 $MgSO_4$, 1.2 KH_2PO_4, and 10 glucose] at 30 - 34°C. Modified ACSF with elevated concentrations of divalent cations used in some calcium imaging experiments as described below was composed of 105 NaCl, 35 $NaHCO_3$, 20 HEPES, 3 KCl, 4 $CaCl_2$, 4.2 $MgCl_2$, and 10 glucose. Auditory cortex was identified based on its position relative to the hippocampus, strong granular layer responses to stimulation of thalamic afferents, and in preliminary experiments by the location of cells retrogradely labeled from the inferior colliculus, as in previous studies (Verbny et al., 2006;Banks et al., 2011). Cortical layers were identified by differences in cell density and based on distance from the pia in conjunction with previous studies (Banks et al., 2011). Afferents were activated using pairs of tungsten electrodes (0.1 MΩ, 75 μm diameter; FHC Inc., Bowdoin, ME). Stimuli (100 μs, 10-150 μA) were applied using constant current stimulus isolation units (A365, WPI Inc., Sarasota, FL; or STG4002, Multichannel Systems, Reutlingen, Germany) and consisted of either single pulses or brief trains (2 – 4 pulses, 40 Hz). Extracellular recordings in layer 4 taken at 200-300 μm intervals were used to locate the region of auditory cortex best activated by the stimulus and all further extra-/intra-cellular recording and calcium imaging was performed in this region. We followed the well-described procedure for preparing auditory thalamo-cortical slices, and based on the appearance of the slices and the published stereotaxic coordinates of auditory cortex we are confident that all recordings presented here are from auditory cortex. However, the slicing procedure was originally described for juvenile animals (Cruikshank et al., 2002) in which connections between MGv and core auditory cortex could be maintained. Developmental studies have shown that the circuit and membrane properties of neocortex are not fully

developed in juvenile animals (Metherate and Aramakis, 1999;Frick et al., 2007;Oswald and Reyes, 2008; 2011;Romand et al., 2011), consistent with observations *in vivo* showing developmental changes in tuning properties of auditory cortical neurons between 3 and 5 weeks of age (Chang and Merzenich, 2003;Chang et al., 2005). Thus, we confined our study to animals >3 weeks old, and in most cases >4 weeks old, in which the connections from MGv to core auditory cortex were not always intact. To activate auditory TC fibers in slices from older animals, we stimulated outside of MGv, just rostral to the nucleus or in the fiber bundle (the superior thalamic radiation) that runs from auditory thalamus to auditory cortex. We verified that stimulation of these fibers elicited current sinks in layer 4 in all experiments. However, we cannot exclude the possibility that some of our recordings were from areas outside of A1 that receive driving core auditory thalamic inputs, e.g. AuV or AuD in the Paxinos (Paxinos and Franklin, 2003) terminology. Indeed, given that the slices are 450 μm thick, even if we were to place stimulating electrodes in MGv and record responses in auditory cortex, it cannot be guaranteed that all the cells recorded are located in core auditory cortex and that we are only stimulating fibers arising in MGv.

Electrophysiological recordings

Electrophysiological recordings were obtained using patch pipettes fabricated from borosilicate glass (KG-33; 1.7 mm outer diameter; 1.1 mm inner diameter; Garner Glass, Claremont, CA) with a Flaming-Brown two-stage puller (P-87; Sutter Instruments, Novato, CA). For whole-cell current clamp recordings, pipettes had open tip resistances of 3-5 MΩ when filled with (in mM): 140 K-gluconate, 10 NaCl, 10 HEPES, 0.1 EGTA and 2 MgATP, 0.3% biocytin, pH 7.2. Cells were visualized using a video camera (Dage MTI VE-1000) connected to an upright microscope (Olympus BX51-WI) with a long working-distance water-immersion objective (Olympus 40X, 0.9 N.A.) and differential interference contrast optics. For extracellular field potentials, the tips of the pipettes were broken under visual

control to an outer tip diameter of 10 – 15 μm and had open-tip resistances of about 0.5 MΩ when filled with ACSF. Data were amplified (MultiClamp-700A; Molecular Devices, Union City, CA), low-pass filtered (4 kHz), digitized (40 kHz; DigiData 1322A; Molecular Devices), and recorded using pClamp version 9.2 (Molecular Devices). Current source density (CSD) and multiunit activity (MUA) was derived from extracellular recordings in which we recorded local field potentials simultaneously in all cortical layers using 16-channel silicon electrode arrays (A-series probes; 16 shanks spaced by 100μm, one recording site per shank; 1 MΩ impedance; NeuroNexus, Ann Arbor, MI) connected to a unity-gain headstage (HS-16; Neuralynx, Bozeman, MT), amplified 2000x (Lynx-8, Neuralynx), digitized at 20 kHz (Digidata 1440A; Molecular Devices, Sunnyvale, CA) and recorded using pClamp (Molecular Devices). The electrode array was inserted into the slice at an acute angle with the shanks oriented in parallel to the cortical laminae. Depending on the cortical thickness at the recording site, 11 to 13 of the electrode shanks were in cortex and used in calculating the CSD and MUA.

Calcium imaging

Calcium imaging using the acetoxymethyl ester form of Oregon Green BAPTA-1 (OGB-1 AM; Life Technologies, Grand Island, NY) was performed as described previously (Banks et al., 2011). Briefly, patch pipettes of ~2 μm outer tip diameter were filled with OGB-1 AM dissolved in DMSO containing 20% pluronic acid to a dye concentration of 5 mM and then gradually diluted using extracellular solution containing (in mM) 150 NaCl, 2.5 KCl, 10 HEPES, pH 7.4 to a final dye concentration of 0.165 mM. The tissue was loaded using pressure ejection (Picospitzer II, General Valve, Fairfield, NJ; 5 – 10 PSI, 1 – 10 sec pulses over 1 – 2min) at 5 – 7 locations over a period of ~45mins.The total area labeled in this way measured ~200 x ~800 μm. Data collection commenced ~60 minutes following the last injection. Data were collected using an upright microscope (BX51-WI, Olympus, Center Valley, PA), mercury arc lamp

light source (X-Cite exacte; Lumen Dynamics, Mississauga, Ontario, Canada) with an excitation filter 475-505 nm and emission filter 520-570 nm (U-N41026, Chroma, Bellows Falls, VT), and a 10X water immersion objective (UMPlanFL N, N.A.= 0.3, Olympus). Images were captured at 30 frames/sec with a cooled CCD camera (500 pixels x 500 pixels, corresponding to 800 x 800 μm, 16-bit; C9100-02, Hamamatsu Corp., Sewickley, PA) using SimplePCI software (v6.1, Hamamatsu). For calcium imaging experiments, the stimulus intensity was set high enough to trigger UP states under normal ACSF on consecutive trials using four pulses at 40 Hz and low enough that UP states were blocked using high divalent ACSF, typically 50-100 μA.

Data analysis

Electrophysiological recordings

EPSP latencies and amplitudes were obtained from averages of ten responses to single 100 μA pulses. EPSP latencies were measured as the time of rise to 10% of the peak. EPSP amplitude was measured as rest-to-peak and cells were omitted from amplitude measurement if they had a coincident IPSP revealed by depolarizing the cell. IPSPs were identified by stimulating while holding the cell at depolarized potentials using small current steps up to spike threshold. Step size varied with the input resistance, resting potential, and spike threshold of the cells as necessary to result in 5-10 steps between rest and threshold. Spike thresholds were measured as the membrane potential at the peak of the 2nd derivative of the voltage trace. Spike latencies were measured as time to peak. Monosynaptic spikes were those that occurred in response to a smooth, putative monosynaptic EPSP with short latency and low latency jitter (EPSP latency <5ms, SD <1ms; spike latency <10ms, SD <1ms) (Berry and Pentreath, 1976;Rose and Metherate, 2005). We note that the actual EPSP latency jitter preceding monosynaptic spikes was much more precise than this criterion (jitter mean±SD: 0.23±0.21 ms).

UP states were detected using the MUA signal obtained in extracellular recordings (using multichannel electrodes or glass field potential electrodes) from layer 5 using a method similar to that of Sakata and Harris (2009). We extracted the MUA signal by bandpass filtering the voltage signal between 0.5 and 3 kHz, taking the absolute value, and then smoothing with a lowpass filter (0.2 kHz cutoff) to yield the smoothed MUA signal, smMUA (t). A threshold was determined by computing the geometric mean $\bar{x}$ of smMUA (t) on data points greater than the mean of smMUA (t) during the pre-stimulus period. UP state onset was defined as the time at which smMUA (t) >$\bar{x}$ for 80% of the points in a 20ms window, and offset was defined as the subsequent time when smMUA (t) <$\bar{x}$ for 80% of the points in a following 20 ms window. For multichannel recordings, CSD (Freeman and Nicholson, 1975;Mitzdorf, 1985) was estimated using the spline CSD method (Pettersen et al., 2006). MUA in the form of single action potentials was extracted from these same multichannel recordings by bandpass filtering the extracellular signal between 0.5 and 3 kHz and detecting negative-going level crossings using a threshold of 5 times the standard deviation of the baseline period.

We sought to compare directly the observed pattern of spiking responses observed via calcium imaging to the pattern we observed in on-cell recordings, in which we measured the number of spikes fired for each cell over a series of 10 trials. To compare these spiking probabilities to the calcium imaging data, we converted the spiking probability to the likelihood to detect a cell according to our calcium imaging calibration data illustrated in Figure 3F (using linear interpolation when necessary) and averaged across cells in each layer.

All statistical analyses of electrophysiological data used native MATLAB (Mathworks, Natick, MA) functions. Non-parametric tests were used when data were distributed significantly different from the normal distribution (one-sample Kolmogorov-Smirnov test, $p<.05$). When multiple pairwise comparisons were performed, significance thresholds were adjusted using the Holm-Bonferroni method (nominal $\alpha=.05$); p-values were not adjusted.

Calcium imaging

Fluorescence traces (reported as ΔF/F, ***not*** *%ΔF/F*) were analyzed as described (Banks et al., 2011). Briefly, ΔF/F as a function of time was measured in single cells identified in averaged still images using custom software written in MATLAB. Traces were background-subtracted and peaks corresponding to action potential activity were detected. Cells were identified as "responsive" when the sustained peak increase in fluorescence (over a window of 4 data points or 133 ms) was greater than 3 times the standard deviation of a 1-second baseline before stimulation. In some experiments, we targeted responsive cells identified via calcium imaging for subsequent whole-cell patch clamp (see Results). Spikes were detected in all recordings of these cells, confirming that observed calcium transients were associated with action potentials. We computed the laminar spiking profile within a single experiment (e.g. Figure 7D) by dividing the cortical depth into 50 μm bins and counting the number of cells in each bin. When data were pooled across experiments (e.g. Fig. 10), bin size was expanded to 100 μm to make plots easier to read. All analyses presented here were insensitive to this change in bin size. To compare relative dye (OGB-1) levels across analysis windows, the average baseline fluorescence was integrated across space and normalized to the bin with the largest integrated baseline fluorescence from that experiment. By using an integral rather than a spatial average, this measure incorporates variability in background (labeling intensity) due to heterogeneous loading as well as depth bins that fell outside the square imaging window (particularly layers 1 and deep layer 6).
Statistical comparisons between layers and between bathing media (normal ACSF or ACSF modified with high divalent cations or APV) were made by fitting a Poisson, log-linked Generalized Estimating Equations (GEE) model to cell count measures normalized by layer thickness (Reed and Kaas, 2010). A standard ANOVA or general linear model (GLM) approach is less appropriate because the cell count data are not normally distributed, resulting in poor error estimates, especially when some counts are very low or zero. GEE models are suitable for repeated measures data (here, repeated across layers in each

experiment and within layers for each ACSF condition) in which population effects are of interest but within-subject prediction is not necessary. Because of the logarithmic link function, a linear combination of parameters results in a multiplicative effect on the outcome data, in this case cell count. When comparing level parameters, we computed the Wald test on the parameter estimates themselves, but then present the exponent of the parameter, e.g. as 'exp ($\beta_{Condition}$)', and its confidence interval because this exponent is an easily understood multiplicative factor to the cell counts. Significance thresholds were adjusted using the Holm-Bonferroni method as above.

The GEE model was fit using IBM SPSS Statistics 22. Post-hoc tests and all other analyses used native and custom MATLAB functions.

Histology

Slices containing biocytin-filled cells were carefully removed from the recording chamber and immediately fixed in freshly prepared 4% paraformaldehyde solution. After at least 24 hours in fixative, slices were sectioned and processed for biocytin staining using the cobalt/nickel intensification method (Adams, 1981). First, the slice was cryoprotected by passage through a series of glycerol–sucrose solutions. Labeled cells were often close to the slice surface so to assure that this tissue was not lost in the sectioning process the following method was used. The slice was placed on a glass slide and covered with a drop (s) of a 4% paraformaldehyde (1ml.)/egg albumin (10 ml.) solution. A second slide was gently laid over the slice to flatten it. After the albumin had solidified the slides were removed and the flattened albumin-embedded slice was mounted on a freezing microtome and 60 or 90 µm sections were cut and collected in 0.1 M phosphate buffer (pH 7.4). Sections were then washed in 0.01M phosphate buffered saline (PBS, pH 7.4), incubated in 0.5% H_2O_2 in PBS, and rinsed again in 0.01M PBS. Sections were then incubated overnight in the secondary antibody to the avidin-biotin-HRP complex

(ABC Kit, Vector Labs) in PBS with 0.3% Triton-X-100 and 2% BSA. On the second day, the sections were rinsed in 0.1M PBS and the HRP was reacted using 0.04% diaminobenzidine with DMSO and nickel/cobalt intensification. We then added 0.01% H_2O_2 in 0.1M PBS for 15 minutes followed by rinsing for forty minutes in PBS. The sections were then mounted on slides, allowed to air dry and the mounted sections were then stained with cresyl violet and coverslipped. Photomicrographs of labeled cells were taken at 5, 25, and 100X. For the image in Fig. 4E, the major processes of the labeled cell were found in two tissue sections. To overlay the images and produce a unified picture, the position of the superficial section relative to the deeper section was determined by aligning the 5X images with common structures. The Eyedropper tool in Adobe Photoshop was used to create a color mask to remove the background and Nissl-stained cells from the superficial section, leaving the darkly labeled processes, and this image was merged with the unaltered deep image section. The 'auto-contrast' function in Photoshop was used on both photomicrographs in Figure 4 to improve the differentiation between the Nissl-stained cell bodies in the background and the biocytin-labeled somata and processes of interest. All image processing steps were performed across the entire image and did not alter the information contained.

Results

Overview

The data presented here were obtained to answer a simple question: what is the pattern of spiking elicited in auditory cortex by stimulation of core thalamic afferents? In classical models of the cortical microcircuit, TC afferents terminating in layer 4 activate excitatory interneurons (spiny stellate cells) resident in that layer, and spiking activity in these cells triggers sequential activation of pyramidal cells and interneurons in supragranular and then in infragranular layers. In primary auditory cortex, where spiny stellate cells are rare or absent (Smith and Populin, 2001;Barbour and Callaway, 2008), it is

unclear whether this activation sequence is preserved. To address this issue, we recorded from 103 cells selected at random throughout layers 2 – 6 (L2/3=21, L4=19, L5=51, L6=12) using whole-cell patch clamp, and 104 cells selected at random throughout layers 2 – 6 (L2/3=27, L4=22, L5=47, L6=8) using on-cell recordings. We focus first on short latency, putatively monosynaptic responses, showing that spiking directly in response to these inputs is rare. We then show that spiking is common in the context of induced UP states and examine the laminar profile of this activity. We corroborate these findings from single cell recordings using two techniques that allow us to monitor spiking activity simultaneously across the cortical laminae: multichannel recordings of multiunit activity (n = 16 slices) and calcium imaging using bulk loading of neurons with OGB-1AM (n = 1588 cells in 17 slices).

Laminar profile of current sinks activated by TC stimulation

We first verified that stimulation of TC afferents resulted in the expected laminar profile of synaptic current flow using multichannel recordings (Fig. 1A). TC stimulation resulted in an early, large, fast sink ("early responses", LFP Fig. 1B; CSD Fig. 1C; time to 10% of peak= 2.0 ± 1.1 ms, n = 16 slices) located in layer 4 (mean depth=36 ± 5% of cortical depth) that sometimes extended into layer 3, as expected based on the laminar distribution of terminals in primary auditory cortex arising from MGv (Huang and Winer, 2000;Smith and Populin, 2001;Smith et al., 2012). There was usually an additional, weaker sink observed simultaneously in layer 6, which also receives direct MGv input. We typically observed modest depression of current sinks evoked by TC stimulation trains as seen previously with TC EPSPs (Rose and Metherate, 2005;Lee and Sherman, 2008).

Most of the data presented here were obtained in animals >4 weeks old, in which it is difficult or impossible to obtain slices with intact fiber bundles between MGv and auditory cortex. Thus, in most experiments stimulating electrodes were placed just rostral to the MGv, where the TC fibers coalesce, or in the superior thalamic radiation, just rostral and medial to hippocampus. In four experiments from 3 -

4 week old animals, we compared directly the current sinks obtained by stimulating in these locations with those obtained by stimulating in MGv. The results of one of these experiments are illustrated in Figure 1. In the same slice illustrated in Figure 1A-C, we moved the stimulating electrode to the fiber bundle just rostral to the hippocampus (Fig. 1D) and obtained similar LFP/CSD patterns (Fig. 1E&F) as those elicited by direct MGv stimulation (Fig. 1B&C). Similar results were obtained in all four experiments in which we compared directly stimulation in MGv, just rostral to MGv, and in the fiber bundle rostral to hippocampus. Note that larger current sinks could be obtained by stimulating in the superior thalamic radiation compared to MGv itself. These results suggest that stimulation in the fiber bundle in older animals elicited responses that are equivalent to stimulating in MGv itself.

We summarize the results of 16 such recordings in older animals in Figure 1G, which shows the laminar profiles of current sinks evoked by TC stimulation. To compare across slices with slightly varying cortical depths, we normalized the single experiment profiles by dividing by the distance from the pia to white matter. These recordings clearly show that the vast majority of synaptic current flow in response to TC stimulation occurs in layers 3 & 4, with a modest response component in layer 6. In none of these experiments were early current sinks observed in layers 1, 2 or 5, indicating that activation of 'matrix' (i.e. non-specific or extralemniscal) thalamic afferents in our stimulation protocol was minimal.

Brief UP states triggered by TC stimulation

In addition to early response components, TC stimulation typically triggered network events, seen in CSD profiles (Fig. 1C&F) as intense patterns of sources and sinks subsequent to the initial thalamocortical response. During these events, cells throughout the cortical region depolarized nearly simultaneously under a barrage of synaptic inputs (Fig. 2A), and occasionally fired action potentials. We also observed spontaneous UP states in 5/10 slices examined, but at low rates (0.2 to 2 per minute).

Between these occasional events, the slice was in a persistent DOWN state, as is typical of cortical brain slices (Sanchez-Vives and McCormick, 2000).

The UP state activity appeared in extracellular recordings in layer 5 as a low frequency negative or sometimes biphasic wave with associated high frequency (spiking) activity (Fig. 2B, *top*) that often spread to involve all cortical layers, as previously described *in vitro* and *in vivo* (Sanchez-Vives and McCormick, 2000;Luczak et al., 2007;Sakata and Harris, 2009;Chauvette et al., 2010;Wester and Contreras, 2012;Beltramo et al., 2013). Following the method of Sakata and colleagues (Sakata and Harris, 2009) for data recorded *in vivo*, we detected these events using the MUA signal derived from extracellular recordings in layer 5 (Fig. 2B, *bottom*; see Methods). Below, we show that although synaptic responses to TC afferents are widespread in auditory cortex, it is rare for cells to spike in direct response to these EPSPs. Rather, the vast majority of spiking in response to TC stimulation occurs instead in the context of these UP states.

Short latency responses to TC stimulation

Using whole-cell patch clamp recordings, we examined the intracellular responses to stimulation of TC afferents in 103 cells (n=21, 19, 51 and 12 cells randomly selected from layers 2/3, 4, 5, and 6, respectively; note that because layer 5 is roughly twice as thick as layers 2/3 and 4, this represents a roughly uniform sampling density for layers 2/3 through 5). Although the synaptic terminals of stimulated afferents target specific layers of cortex, we found that TC input triggered short latency EPSPs in cells of all layers (Fig.3A), most likely by synapsing on these cells' dendritic processes that span thalamo-recipient layers. Latencies were similar across the cortical laminae (Fig.3B; median latencies: L2/3, 3.0 ms; L4, 2.9ms; L5, 3.0ms; L6, 2.4 ms; no significant difference, Kruskal-Wallis H=2.79, 3 d.f., p=0.43). These short latencies are consistent with nearly all these responses being monosynaptic (Rose and Metherate, 2005;Verbny et al., 2006), except perhaps a few >5 msec in layers 5 & 6; likewise, the

similarity of latencies across laminae is inconsistent with EPSPs in layers 2/3 and 5 being di- and tri-synaptic responses driven by intracortical spiking activity. The amplitude distribution of the initial EPSPs was more heterogeneous (Fig.2C; Kruskal-Wallis H=14.79, 3 d.f., p=0.002): the largest EPSPs were observed in layer 4, but we observed large EPSPs (>5 mV) in layers 3-6 (median EPSP amplitudes: L2/3:2.9 mV; L4:8.1 mV; L5: 5.2 mV; L6:4.7 mV; L4 significantly greater than each of the other layers by Tukey HSD).

Although many cells throughout the cortical laminae received monosynaptic thalamocortical inputs, spiking in response to these short latency EPSPs was rare. In these 103 cells, spikes in response to putatively monosynaptic thalamic EPSPs triggered by the first TC stimulus were observed in only four cells, two in layer 4 and two in layer 5 (Fig. 3D). Both layer 4 cells (one example Fig. 4A-D) and one of the layer 5 cells were fast-spiking interneurons. The fast-spiking cells were smooth, non-pyramidal cells (Fig. 4A) and fit the classical characteristics of parvalbumin-positive interneurons (Kawaguchi and Kubota, 1997). The fourth monosynaptic-spiking cell was an intrinsically bursting pyramidal cell in layer 5 (Fig. 4E-H). We defined these four cells as "monosynaptic spiking" cells based on the EPSPs leading to spikes being short latency (like the EPSPs of Fig. 3A) and smooth, without evidence of additional di- or poly-synaptic activity prior to spike onset. We note that we are unable to ascertain without a doubt that these spikes were driven only by monosynaptic inputs, but given their latency and their occurrence prior to induced UP states, these are the only cells we observed that could potentially be driven monosynaptically. In both of the cells pictured, these monosynaptic spikes were followed by UP state activity such as in Fig. 2 which was associated with additional spikes driven by polysynaptic activity. In the remaining 99 whole-cell recordings, all cells that spiked following TC stimulation fired late, UP state-associated spikes.

Spiking responses are dominated by activity during UP states

The observed sparseness of monosynaptic spiking responses to thalamic stimulation is surprising, given the pre-eminence of thalamo-cortical pathways for carrying sensory information to cortex. Because the intracellular milieu is disturbed during whole-cell recordings, it is possible that spike thresholds and spiking probability were altered in the recordings presented above. In 33 cells, we obtained on-cell recordings prior to the whole-cell recordings from Figs. 3&4, including two of the previously described cells that fired monosynaptic spikes according to our definition. In on-cell recordings, both of these cells also fired short-latency (<10ms) spikes to TC stimulation with high temporal precision (standard deviation of spike times <1 ms) in the on-cell recordings. None of the other 31 cells fired spikes that met these criteria. We also recorded on-cell spiking responses to TC stimulation in 71 additional cells (for a total of 104 on-cell recordings). None of these cells fired spikes that met that <10ms latency and <1 ms standard deviation criterion. We acknowledge that we would be unable to confidently identify monosynaptic-spiking cells using the on-cell data alone, but emphasize that no cells in the 'on-cell only' dataset met even this less stringent criteria.

Despite the apparent paucity of monosynaptic spiking, TC stimulation consistently elicited robust spiking activity in the context of evoked UP states (Fig. 2). To investigate the laminar profile of this spiking activity and its latency distribution, we sequentially and systematically measured spike times during on-cell recordings from randomly targeted cells at different cortical depths in the same slice (n = 4 to 9 cells in each slice) while simultaneously recording extracellularly from layer 5 to monitor the occurrence of evoked UP states. The data from eight cells recorded in one such experiment are illustrated in Fig. 5. As was typical for these experiments, all spikes occurred during UP states (grey background) and at substantial delays relative to the first stimulus in the train. At low stimulus intensities (Fig. 5A), spikes were observed only in layer 5 cells. Increasing the stimulus intensity (Fig. 5B) decreased the latency of UP states and triggered spiking activity additionally in granular and

supragranular cells, but the density of spiking was greater for cells in layer 5, and the spike latency in these cells was often shorter than that of cells in layers 2-4. Electrophysiological responses to polarizing current pulses are shown in Fig. 5C; most of the cells in this experiment were regular spiking and likely pyramidal; the deepest layer 5 cell was intrinsically bursting.

We summarize data from all 104 cells in Figure 6A by showing the laminar profile of the spiking activity averaged across cells in each layer. Here we use a more inclusive definition of 'early' spikes that included all spikes that came before the onset of UP states and no later than 20 ms after the final stimulus pulse. It is clear from these data that thalamic stimuli are effective at triggering spiking in auditory cortex, but almost all of these spikes occurred during UP states. Almost all early spikes occurred in layers 4 and 5. Spike rates were highest in layer 5, but spikes were detected in all laminae examined. In Fig. 6B&C, we have plotted the cumulative distributions of latency relative to stimulus onset (Fig. 6B) or relative to UP state onset (Fig. 6C) for layers 2/3, 4 and 5. It is apparent that the earliest cells to spike are in layer 5 (Fig. 6B, *arrow*), and that majority of cells in layers 2/3 and layer 5 are activated at about the same latency (no significant difference between distributions, Kolmogorov-Smirnov test), both relative to stimulus onset and UP state onset. The high firing rate of layer 5 cells and the fact that early spikes were nearly nonexistent in layers 2/3 are more consistent with a model in which layer 5 is directly activated by thalamo-cortical input and subsequently by intralaminar activity, as opposed to being driven by layer 2/3 cells in a sequential layer 4 to layer 2/3 to layer 5 pattern as predicted by the canonical microcircuit.

The advantage of data obtained from patch clamp recordings such as those shown in Figures 5 and 6 is that we can identify spikes associated with individual cells, and we can identify the laminar position of the cell body and thus the position of the cell in the cortical microcircuit. However, it was necessary to obtain these recordings sequentially, which could potentially distort the laminar spiking profile by adding variability in latencies that could obscure the progression of latencies in different cell

types. To complement these single cell recordings, we also used multichannel MUA recordings to record from large numbers of cells simultaneously across the cortical laminae. To look at relative spiking latency between layers during UP states, we counted spikes in each layer in 5 ms bins after UP state onset, divided by the maximum spikes per bin for that layer for that experiment, and then averaged these normalized spike rates across experiments (Fig. 6D). The time of spiking onset, defined as the earliest bin with at least 10% as many spikes as the peak bin, was significantly different between layers [Friedman test, χ^2 (3)=28.84, p=.000002]; layer 5 was activated at the shortest latency (post-hoc Wilcoxon signed-rank test; z=-2.79, p=.0052; z=-2.36, p=.0181; z=-3.33, p=.0009 for comparison to layers 2/3, 4, and 6, respectively) and layer 2/3 at longest latency relative to the others (z=-4.14, p=.00003; z=-2.80, p=.0051 for comparison to layers 4 and 6, respectively); layers 4 and 6 were not significantly different from each other. These data are consistent with those obtained from single cell experiments.

In comparing the laminar EPSP amplitude profile (Fig. 3C) with the laminar spiking profile observed in electrophysiological recordings (Fig. 5&6), it is clear that this profile is not simply a function of the monosynaptic EPSP amplitude distribution. However, it is consistent with the laminar profile of resting potentials recorded in our whole-cell current clamp recordings (mean±SD: $E_{L2/3}$ = -78.1±5.5mV; E_{L4} = -70.1±7.9mV; E_{L5} = -65.2±5.4mV; E_{L6} = -72.3±4.3mV), which varied significantly by layer [one-way ANOVA, F(3,93)=24.96, p<.0000001]. Pairwise post-hoc tests (Tukey's HSD) showed that layer 5 cells had resting potentials that were significantly more depolarized than layer 2/3 cells ($E_{L2/3}$-E_{L5}=-13.0mV, 95% CI [-17.1 -8.9]), layer 4 cells (E_{L4}-E_{L5}=-4.9mV, 95% CI [-9.4 -0.44]), and layer 6 cells (E_{L6}-E_{L5}=-7.1 mV, 95% CI [-12.1 -2.2]), similar to previous studies (Huggenberger et al., 2009;Constantinople and Bruno, 2013). In addition, spike thresholds did not vary by layer [one-way ANOVA, F(3,93)=0.31, p=.82], such that depolarized cells were closer to threshold.

Together, the data from our intracellular, on-cell and multiunit recordings provide compelling evidence that most spiking in auditory cortex in response to thalamic stimulation occurs during cortical

network activity. Furthermore, this spiking does not appear to follow the spatiotemporal pattern predicted by the canonical microcircuit model. However, each of these electrophysiological techniques has associated limitations, and we used calcium imaging to corroborate these findings and explore the properties of these network events and the cells participating in them further. In particular, the calcium imaging technique allowed us to explore the spatial pattern of spiking probability as a function of cortical layer by simultaneously measuring spiking responses from large numbers of identified cells in layers 2 - 6.

Calcium imaging technique

The calcium imaging technique employed here involves labeling a vertical strip of cortex with several injections of a membrane-permeable fluorescent calcium-sensing dye (OGB-1 AM; Figure 7a) and imaging at low enough power (10X) to capture most of the cortical depth (~80%) in a single field of view (Figure 7B-D). We did not image the most superficial 100 μm corresponding to layer 1, or the deepest 100 - 200 μm corresponding to deep layer 6. Consistent with these slices dwelling primarily in DOWN states, spontaneous spiking activity in cortical cells was rare (not shown). By contrast, afferent stimulation consistently elicited calcium transients in a subset of imaged cells (Figure 7B&C) presumably due to synaptically driven action potentials (Banks et al., 2011) (see below). The laminar profile of spiking activity was obtained by determining the position relative to the pia and white matter of each active cell (Figure 7D). Based on our electrophysiological recordings, we expected that most of these spikes occurred in the context of UP states, but we could not determine this directly because the time resolution of the calcium imaging (at least 30 ms due to the video frame rate and slower still due to the kinetics of OGB-1) is too slow to distinguish monosynaptically-driven spikes from those occurring during UP states. Instead, we recorded extracellularly in layer 5 to determine whether an UP state occurred on

each trial, and used modified ACSF to reduce the likelihood of observing UP states on some trials (see below).

Cells in infragranular layers project to thalamus, and it is possible that electrical stimulation in these slices activated these cells antidromically and triggered the robust spiking activity observed in these layers. Antidromic activation is of particular concern because of previous reports *in vivo* that, at least under anesthesia, cortical network activity can be induced by brief activation of small numbers of layer 5 pyramidal cells (Stroh et al., 2013), or prolonged (3 mins) activation of even single layer 2/3 pyramidal cells (Li et al., 2009). We investigated the incidence of antidromic activation in response to TC stimulation using the ionotropic glutamate receptor antagonists CNQX (10 □M) and APV (40 □M) to block excitatory synaptic transmission. Cells that continued spiking in the presence of CNQX/APV were assumed to be antidromically driven. In 8 experiments, only 3 out of 566 cells (0.5%) of cells that responded to TC stimulation spiked in the presence of CNQX/APV, and all were found in layer 6 (Fig. 7E&F). We also did not encounter antidromically driven cells in any of the patch clamp experiments described above. The low percentage of cells insensitive to CNQX/APV suggests that antidromic activation, and network activity secondary to such activation, was minimal in our experiments.

Although ideally we sought to achieve uniform labeling across the ~800 μm of cortical depth that we targeted for imaging (i.e. layer 2 - superficial layer 6) there was some variability in background labeling density, as measured by raw fluorescence as a function of cortical depth, (Fig. 7G). However, this variability in background did not have a strong effect on cell detection (Figure 7H). We compared background and cell count as a function of cortical depth by normalizing background and cell counts within experiments by their respective maxima and pooling these data across experiments. There was no significant correlation between background and cell count when layers 2/3, 4, and 5 were considered (Figure 7H; slope=0.095, r^2=0.04, p=0.086). The correlation was significant if layer 6 was included,

however the slope was small (slope=0.22, r^2=0.11, p=0.0018) and therefore had minimal impact on cell counts; however we focused our analyses on layers 2/3 through 5.

Next, we verified that a) we could measure the calcium transient due to single action potentials when averaging over a few trials, and b) that the amplitude of the change in fluorescence is linear with the number of action potentials, by simultaneously recording optically and electrically from the same neurons. First, we delivered stimuli directly to cortex in the vicinity of an OGB-1 AM labeled area to evoke robust responses. Next, we obtained an on-cell recording from a randomly selected responding cell in layers 2-5 and simultaneously recorded fluorescence images at 10X and electrophysiological spiking responses to single pulses and brief trains of stimulation. Fluorescence traces on each trial were sorted according to the number of electrically identified spikes on that trial (Fig.8A). Plots of peak ΔF/F versus number of spikes tended to be linear in individual cells but saturated in some cells at higher numbers of spikes (Fig.8B). After normalizing ΔF/F to the fewest spikes fired by a given cell and averaging these normalized values across cells, we find that the calcium-induced change in fluorescence in the population is linear with the number of action potentials fired up to about six spikes (Fig.8C). Cells that fired more than six spikes in response to a train of four stimuli varied in whether they continued to show near-linear increases in fluorescence with increases in spike count or whether they reached a plateau. Electrical stimuli delivered during the calibration experiments were strong, as they were delivered directly to cortex near the recording site, and we very rarely observed cells that fired more than six spikes in response to TC stimulation in patch clamp recordings.

Above, we presented evidence that cells in auditory cortex fire sparsely in response to stimulation of TC afferents, and thus most cells are unlikely to fire in response to every stimulus pulse in a train (Figs. 5 & 6A). To estimate our ability to detect cells that spike with a probability less than one, we simulated fluorescence data based on the calibration results (Fig. 8D). Each simulation consisted of a mixture of *n* trials containing a simulated response (with a peak equal to the peak of the average one-

spike calcium trace for that cell) embedded in Gaussian noise (generated with variance equal to the prestimulus variance for that cell), and 9 – *n* trials of Gaussian noise only, with *n* varied from 0 to 9 (Fig. 8E). For each cell, this process was repeated 1000 times for each value of *n*. Using this procedure we detected a response in about 95% of the simulations that had a one-spike response on every trial of nine, and about 60-70% of simulations that had a one-spike response on four or five trials out of nine (Fig. 8F). These experiments indicate that we can identify cells that spike consistently with a very high probability as well as a majority of those that fire with probability ~0.5 in response to single stimulation pulses. Note that in all of the calcium imaging experiments below, each trial consisted of trains of 4 pulses at 40Hz. Thus, in these experiments, for a cell to fall below our detection limit 50% of the time, it would have to spike in response to less than 1 of 8 afferent stimulation pulses.

Spatial pattern of spiking activity in response to TC stimulation

We investigated the laminar spiking profile in response to activation of thalamic afferents using the calcium imaging technique. In a subset of experiments (n = 5 slices), we simultaneously monitored spiking activity by measuring MUA with multichannel electrodes (an example experiment shown in Fig. 9). In this way, we could compare laminar spiking profiles obtained using the two techniques, both in the absence and presence of evoked UP states, and we could determine the contribution to the calcium responses of early spiking cells. At low stimulus intensities (Fig. 9, *right column*), which either did not evoke UP states or evoked UP states with very long latency, spiking was limited to a small number of trials and a handful of cells located primarily in layers 4 & 5. Modest increases in stimulus intensity elicited UP states and dramatic changes in this spiking profile, with dense spiking observed throughout layers 2-6 (Figure 9, *Left three columns*)). Consistent with the summary data shown in Figure 6D above, the MUA recordings in this example (Fig. 9B) showed that the UP state spiking occurred earliest in layer 5 before spreading to other layers, with supragranular layers typically spiking at longest latency.

Interestingly, in 4 of 5 slices, the threshold for early spiking appeared to be higher than the threshold for UP states, and short latency, well-timed spikes occurred only at the highest intensities and usually in layers 4 & 5 (Fig. 9B). We also note that as stimulus intensity was increased, the spiking profile become relatively invariant, suggesting that above a certain threshold UP state activity saturated. In all cases, there was good correspondence between the laminar spiking profiles obtained using the imaging and electrophysiological techniques (Fig. 9).

We summarize the results of 17 calcium imaging experiments (including the 5 in which multichannel MUA was also recorded) in Figure 10. TC stimulation evoked spiking activity in layers 2 through 6, with peak density in layer 5 (Fig.10A, solid black line). We compared directly the observed pattern of spiking responses observed via calcium imaging to the pattern we observed in on-cell recordings, presented above in Figure 6 (see Methods). This spiking probability was strikingly similar to the cell count profile obtained using calcium imaging after normalizing to the cell count in layer 5 (Fig.10A, gray dotted lines). We performed a statistical analysis of cell counts from the calcium imaging data by fitting a generalized estimated equations (GEE) model using a Poisson distribution with logarithmic link function (see Methods). After normalizing for laminar thickness, layer 5 had a significantly greater density of responding cells than layers 2/3, 4 and 6 (exp ($\beta_{L2/3}$-β_{L5})=.531, 95% CI [0.345 0.818], p=.004; exp (β_{L4}-β_{L5})=.606, 95% CI [0.426 0.862], p=.005; exp (β_{L6}-β_{L5})=.411, 95% CI [0.314 0.536], p<.000001). Other pairwise layer comparisons in control conditions were not significant.

We observed that robust activation of layer 5 was consistent across experiments, whereas activation in the granular and supragranular layers was more variable or perhaps bimodal (Figure 10A). In several experiments, activity was almost entirely absent in L2/3 during UP states recorded in layer 5. To ensure that layer 2/3 cells were healthy (able to spike in response to stimulation) in an experiment where spiking was almost entirely confined to layer 5 (Figure 10B), we also delivered electrical stimuli to cortex in layer 2/3 ~650 um from the recording site (Figure 10C). This stimulation triggered large UP

states that included both layers 2/3 and 5, in contrast to thalamic stimulation. These data suggest that the involvement of supragranular layers in UP states was variable, but not because of the health of the tissue or inadequate labeling. We will return to this issue below.

In those experiments in which we wished to isolate early spike responses from spiking associated with UP states, we suppressed polysynaptic activity and blocked UP states using either high divalent cations ($[Ca^{2+}]$ = 4.0 mM, $[Mg^{2+}]$ = 4.2 mM; n = 13 experiments), which raise spike thresholds and preferentially block polysynaptic activity, or the NMDA receptor antagonist APV (40 μM) (Berry and Pentreath, 1976; Metherate and Cruikshank, 1999; Cruikshank et al., 2002; Rose and Metherate, 2005) (Fig.10D). These procedures left monosynaptic TC synaptic responses relatively unaffected (Fig. 10D, *inset*). We note that a limitation of this method is that the modified ACSF will also raise spike thresholds in cortical cells and thus decrease even monosynaptic spike probability, and that this effect may be cell type-specific. If this is the case then some cell types recorded in modified ACSF may be overrepresented in our sample. However, 290/312 cells observed spiking in the absence of UP states in modified ACSF also spiked in control conditions, indicating that cells observed in modified ACSF were rarely made *more* likely to fire by the modified ACSF, and thus nearly all these cells participated in early spiking activity under control conditions as well. For our experiments it was important to use methods that selectively block evoked UP state activity rather than silencing the cortex, e.g. with muscimol, because we are looking for superthreshold responses that would be blocked by cortical silencing. Below, first we characterize how modified ACSF altered the laminar spiking profile, and then describe the properties of cells targeted for patch clamping under modified versus control ACSF.

TC stimulation in ACSF modified by high divalent cations or APV resulted in less spiking activity than control conditions ($\exp(\beta_{hDiv/APV})$=.102, 95% CI [0.056 0.185], p<.000001), as expected due to the suppression of UP states (Figure 10D, gray line). Although modified ACSF resulted in fewer responding cells in every layer, this effect was not uniform across layers, as is clear in an example experiment

showing responding cells in control (Fig.10E) and modified (high divalent cations, Fig.10F) ACSF. The interaction between layer and modified ACSF was significant (Wald Chi-Square (3)=33.017, p=.00000032). Pairwise interaction comparisons were significant between layers 2/3 and 4 (exp ($\beta_{L2/3*ACSF}$-$\beta_{L4*ACSF}$)=.082, 95% CI [.026 .256], p=.000018), layers 2/3 and 5 (exp ($\beta_{L2/3*ACSF}$-$\beta_{L5*ACSF}$)=.048, 95% CI [.015 .158], p=.0000005), and between layers 2/3 and 6 (exp ($\beta_{L2/3*ACSF}$-$\beta_{L6*ACSF}$)=.053, 95% CI [.014 .203], p=.000018). These interactions indicate that layer 2/3 is more affected by suppression of UP states than are the other layers. Other pairwise comparisons were not significant, but layer 5 was the least affected by suppression of UP states. If layer 5 is primarily driven by layer 2/3, as suggested by the canonical microcircuit, blocking polysynaptic activity would be expected to affect layer 5 more strongly than layer 2/3. These results instead suggest that layer 5 is strongly activated by thalamo-cortical input, independently of the activity of the supragranular and granular layers, as recently shown *in vivo* (Constantinople and Bruno, 2013).

To confirm that cells spiking in modified ACSF were in fact being driven by monosynaptic TC EPSPs, and to identify these early spiking cells' morphology and electrophysiology, we identified specific cells spiking in response to TC stimulation via their fluorescence signals and targeted them for patch clamp recording and subsequent classification. The protocol for these targeted patch experiments was to bathe the slice in modified ACSF, verify the absence of UP states, identify a cell still spiking in the absence of UP states, and obtain a whole-cell recording from that cell. All six cells in layer 5 that were identified via their fluorescence signals as spiking in modified ACSF in the absence of UP states had spikes that were monosynaptically driven by TC stimulation. Three of these cells spiked in response to a single TC stimulus, while the other three spiked in response to stimuli two through four of a 40 Hz train of TC stimuli. Interestingly, none of these targeted, early spiking cells were pyramidal cells. Five cells had morphology and spiking patterns consistent with Martinotti interneurons (Kawaguchi and Kubota, 1996;

1997; 1998;Markram et al., 2004;Wang et al., 2004). The sixth cell had a non-pyramidal, non-spiny, bipolar morphology and a stuttering spiking pattern.

By contrast, we also targeted 7 cells identified via their fluorescence signals as spiking in normal ACSF under control conditions, i.e. in the presence of UP states. All 7 cells were identified as pyramidal cells based on their morphology and firing properties (either regular spiking or burst firing). Only one of these cells fired short latency, well-timed spikes prior to the onset of UP states; the other six cells fired spikes only during UP states. Including cells targeted in modified and normal ACSF and our random whole-cell recordings presented above (Fig. 3D), 9 out of 11 cells that we observed spiking in direct response to monosynaptic EPSPs, outside the context of UP states, were putative interneurons, and 7 of these cells plus two pyramidal cells were located in layer 5. This result is even more striking given the low percentage of cells in neocortex that are GABAergic interneurons (~20%; (Markram et al., 2004;Ascoli et al., 2008)). The cells targeted in the absence of UP states were significantly more likely to be non-pyramidal cells than those targeted in the presence of UP states (Fisher's exact test, p= 0.0047), indicating that there was not simply a greater likelihood of choosing non-pyramidal cells via targeted patching.

Variable activation of layer 2/3 during UP states

The data of Fig.10 suggest that across experiments, the involvement of supragranular layers in UP states is more variable than that of infragranular layers: whereas layer 5 participated strongly in all experiments, layer 2/3 involvement was less consistent. This variability was also manifested on a trial-by-trial basis, even when the stimulus intensity was the same on each trial, both in extracellular electrophysiology (Fig. 11) and calcium imaging (Fig. 12) experiments. In extracellular recordings, we observed two types of UP states in CSDs that differed in their intensity, duration and in their involvement of supragranular layers (Fig. 11A). In the example illustrated, TC responses in granular

layers to a train of four stimuli on trials 1, 3, 4, 6, 7 & 9 first spread to layer 5 and then to supragranular layers as well as layer 6 over the next 200 ms (Fig.11A). By contrast, activity spread to layer 5 and triggered a modest current sink in layer 2 before dying out on trials 2, 5, 8 & 10. These visually distinct responses could also be separated on the basis of the total CSD power during the response window 0<t<300 ms (Fig. 11B). Averaged CSDs of these two types of responses (Fig.11C&D, *top*) showed far larger sinks in supragranular layers for the larger UP states than for the smaller, and simultaneously measured multiunit activity (Fig.11B & C, *bottom*) showed little involvement of layer 2/3 in superthreshold activity on trials with smaller UP states but robust activation on trials with larger UP states. In other CSD experiments (not shown), small increases in stimulus intensity biased the network towards the larger UP states, indicating that involvement of all layers could depend on stimulation being of sufficient strength.

Distinct UP states sizes and associated laminar response patterns were also observed in calcium imaging experiments (Fig.12). In the example illustrated, trials were sorted according to two clearly distinguishable response classes in the local field potential recorded in layer 5 (Fig.12A&B). Calcium traces in individual cells were larger and more cells were active, especially in the superficial layers, on the trials with a "larger" UP state (Figure 6C&D).

Discussion

Thalamically-evoked activity patterns in auditory cortex

We distinguished between two types of spiking responses to thalamic stimulation. In murine auditory cortex, most cells that spike do so during brief network bursts that occurred nearly simultaneously in cells throughout the cortical region; these cells depolarize in response to a barrage of polysynaptic activity and fire occasional spikes during these events. By contrast, only a small number of cells fire action potentials triggered at short latency by monosynaptic TC EPSPs (Fig.3D), even though

short latency, monosynaptic, subthreshold synaptic responses are observed in cells throughout layers 2 – 6. We summarize our results in the circuit diagrams of Figure 13. In this model, monosynaptically driven spiking occurs predominantly in (putative) GABAergic interneurons, including Martinotti and fast spiking cells (Fig. 4), as well as an occasional pyramidal cell. Stimuli of sufficient intensity elicit UP states involving robust spiking activity (Fig. 13B&C). UP state activity occurs primarily in pyramidal cells, and appears with earliest latency in pyramidal cells in layer 5, consistent with previous reports (Chauvette et al., 2010;Wester and Contreras, 2012;Beltramo et al., 2013). In some cases, UP state activity is largely confined to infragranular layers (Fig.13B), where dense interconnectivity between pyramidal cells and depolarized resting potentials allow for sustained network events lasting ~100 msec. Functionally, ascending information during these smaller UP states flows back to subcortical structures and may engage cortico-thalamo-cortical loops, but does not engage direct cortico-cortical hierarchical processing. In other cases, likely only in response to stimuli of sufficient intensity or simultaneous ascending and descending input, UP state activity spreads throughout the column and involves supragranular layers as well (Fig.13C), potentially activating direct cortico-cortical pathways.

Dense spiking in infragranular layers

We observed that short latency and robust spiking in response to thalamic stimulation occurred in layer 5 cells during evoked UP states (Fig.6&10D), and that even in the absence of UP states layer 5 cells could still dominate the spiking responses to TC stimulation. This stands in contrast to the predictions of the canonical microcircuit model, in which the shortest latencies to thalamic stimulation occur in layer 4 spiny stellate cells. Indeed, we would have expected that in the absence of polysynaptic activity (i.e. at low stimulus intensities or in modified ACSF), spiking would have been dominated by cells in layer 4, rather than cells in layer 5, as we observed (Figures 9&10). However, spiny stellate cells are

rare in auditory cortex (Smith and Populin, 2001;Barbour and Callaway, 2008;Sakata and Harris, 2009), and here and elsewhere in cortex pyramidal cells in layers 2-6 with dendrites in thalamo-recipient layers are likely excited directly (Figure 3A-C). These results suggest that layer 5 cells get more direct thalamic input than is appreciated based on afferent terminal density (Gil and Amitai, 1996;Bureau et al., 2006;de Kock et al., 2007). Additionally, cells in layer 5 have more depolarized resting potentials and lower spike thresholds than cells in other layers (see Results) similar to previous results *in vitro* (Huggenberger et al., 2009) and *in vivo* (Manns et al., 2004;Constantinople and Bruno, 2013). A recent study in somatosensory cortex demonstrated direct and early activation of layer 5 cells, independent of granular layer activation (Constantinople and Bruno, 2013). Consistent with these observations, thick-tufted pyramidal cells *in vivo* are the earliest and most likely to be activated by whisker deflection in barrel cortex (de Kock et al., 2007) and most likely to be activated by auditory tones or clicks in auditory cortex (Sakata and Harris, 2009). The purpose of a highly excitable recurrent layer 5 network may be to trigger arousal in response to strong stimuli (Harris and Thiele, 2011), or perhaps to evoke 'packets' of information-carrying activity (Luczak et al., 2013), which have a similar duration to the evoked UP states we observed. If layer 5 cells are both highly responsive to input and directly activated by thalamus, connections from layer 5 to other layers (particularly supragranular layers) may contribute a greater fraction of synaptic current than the number of collateral fibers or response to focal stimulation would suggest. Thus, activation of layer 5 cells by TC input may provide a pathway through which information can ascend the cortical hierarchy, either through UP states and subsequent activation of supragranular cells, or through a cortico-thalamo-cortical circuit (Guillery and Sherman, 2002;Theyel et al., 2010) without active processing in supragranular layers (Constantinople and Bruno, 2013).

Monosynaptic TC activation of non-pyramidal cells

We observed that cells that spiked at short latency to TC stimulation, in the absence of UP states, were most often non-pyramidal, and had firing patterns and morphology consistent with either fast spiking parvalbumin-positive cells (Kawaguchi and Kubota, 1993) (in layers 4 and 5) or low-threshold/burst-spiking somatostatin-positive Martinotti cells (in layer 5) (Kawaguchi, 1993;Kawaguchi and Kubota, 1997;Wang et al., 2004) . The spikes from these latter cells sometimes occurred with a considerable delay after the stimulus (up to 15 ms) and appeared to result from a slow, intrinsic conductance triggered by the initial depolarization similar to that seen with just-threshold current injection.

Preferential activation of fast spiking interneurons by TC afferents has been described previously in somatosensory (Beierlein et al., 2003;Gabernet et al., 2005;Cruikshank et al., 2007) and auditory cortex (Schiff and Reyes, 2012), where these cells are postulated to mediate feedforward inhibition that restricts integration windows and sharpens spike timing. Evidence for short-latency activation of infragranular Martinotti cells is mixed. Several studies have found that these cells, whose axons synapse on the dendrites and apical tufts of pyramidal cells in layers 1, 4 & 5 (Markram et al., 2004;Wang et al., 2004), are only weakly excited by TC afferents compared to fast-spiking interneurons (Gibson et al., 1999;Verbny et al., 2006;Cruikshank et al., 2010). In contrast, others have shown that somatostatin-positive Martinotti cells in layers 2/3 are closer to threshold than regular- and fast-spiking cells at rest (Fanselow et al., 2008) and that layer 5 somatostatin-positive interneurons can mediate feed-forward inhibition (Tan et al., 2008); however, the population sampled in the latter work likely did not include the Martinotti cells specifically, see (Ma et al., 2006). Our results support the notion that both fast spiking and Martinotti cells are directly involved in, and may even dominate, the monosynaptic cortical response to thalamic input. Because many of the early-activated interneurons are located in layer 5,

where evoked UP states are likely to originate (Sanchez-Vives and McCormick, 2000;McCormick et al., 2003;Sakata and Harris, 2009;Chauvette et al., 2010;Wester and Contreras, 2012;Beltramo et al., 2013), these cells may be involved in regulating the onset of evoked UP states.

Although we did not systematically test for the presence of disynaptic (i.e. feedforward) inhibition in every pyramidal cell recorded, of the 33 cells in which we did investigate this we observed short latency inhibitory responses in only 8 cells. This observation is consistent with previous reports in auditory cortex (Hefti and Smith, 2003;Rose and Metherate, 2005;Verbny et al., 2006). A heavy contribution by Martinotti cells to feedforward inhibition in auditory cortex could explain why disynaptic inhibition is not observed more commonly. Because these cells are dendrite-targeting interneurons (Kawaguchi and Kubota, 1997;Markram et al., 2004), these electrotonically-remote inhibitory conductances are unlikely to be well-observed at the soma. This may explain the low percentage of cells with observed disynaptic inhibition relative to the likelihood of putative interneurons to spike in our recordings.

Variable activation of supragranular layers during evoked UP states

Whereas cells in layer 5 were consistently activated during UP states, activation of cells in layer 2/3 was more variable (Figs. 10-12). The paucity of spiking observed in supragranular layers is consistent with previous reports of sparse spiking in layer 2/3 (Barth and Poulet, 2012), and may be a feature of how these cells encode sensory information. It is also possible that once the supragranular network is activated, spiking in layer 2/3 cells is as dense as in layer 5. UP states that involved layer 2/3 were more intense than those that were confined to infragranular layers, and spiking during these larger UP states in supragranular layers was as dense as in infragranular layers (Figs.11&12). In some experiments, we observed that the size of the UP state and the involvement of layer 2/3 depended on stimulus intensity

(not shown), suggesting a model in which the cortical microcircuit gates ascending sensory input: only selected inputs activate layer 2/3 and incorporate into direct cortico-cortical hierarchical processing, whereas 'packets' (Luczak et al., 2013) of spikes occur readily in infragranular layers to provide rapid motor output, and possibly activate cortico-thalamo-cortical loops. This differential involvement of supragranular layers has been observed before in auditory cortex *in vivo*, where spontaneous UP states were shown to only on occasion spread from infra- to supragranular layers (Sakata and Harris, 2009). Probabilistic involvement of layer 2/3 in these network events is consistent with recent observations that layer 2/3 activity occurs as population bursts whose probability depends on stimulus parameters in a nonlinear fashion (Bathellier et al., 2012).

The observation of differential involvement of layers 5 and layer 2/3 in UP states adds to a growing body of evidence that activity in infra- and supragranular layers can be uncoupled and may be linked to different cortical processes. For example, activity in infra- and supragranular layers exhibit different spectral characteristics (Maier et al., 2010), and activity in supragranular layers has been more closely linked to attention and perceptual awareness (He and Raichle, 2009;Buffalo et al., 2011). ‘Avalanches’ in cortical networks have also been observed exclusively in supragranular and not infragranular networks (Beggs and Plenz, 2003;Gireesh and Plenz, 2008;Petermann et al., 2009). These observations are also clearly incompatible with the prediction of the canonical microcircuit that activity in infragranular layers is driven by activity in supragranular layers, and support instead a model of two parallel, interacting networks, as proposed in the original formulation of the model (Douglas et al., 1989;Douglas and Martin, 1991).

Concurrence of electrophysiological and calcium imaging data

Although our calcium imaging technique is less sensitive than those employing two-photon microscopy, our simultaneous on-cell/calcium imaging calibration experiments (Figure 8) demonstrate

that we are able to detect single spikes in cells from all layers. Our main findings using calcium imaging, i.e. that spiking is densest in layer 5 following TC stimulation, that early spiking cells tend to cluster in layers 4 & 5 and are mostly non-pyramidal, and that the participation of layer 2/3 in UP states is variable, were all corroborated with parallel electrophysiological recordings. In addition, we reported calcium responses as the number of responding cells rather than the amplitude of the response in part to avoid bias towards cell populations that are larger, fire bursts of spikes or have lower concentrations of endogenous calcium binding proteins. Thus, the laminar profile of spiking probability following TC stimulation obtained with calcium imaging was nearly identical to that obtained with random on-cell patch experiments (Fig. 10A). In addition, the cells recorded using targeted patch experiments in modified ACSF were mostly interneurons, similar to the cells recorded using random whole-cell patch recordings (Fig. 4). We note that interneurons such as those targeted are smaller than pyramidal cells and likely have high concentrations of calcium buffers (Lee et al., 2000;Aponte et al., 2008), which if anything should make them harder to detect in calcium imaging experiments than pyramidal cells. Although these cells do fire bursts of action potentials, which could make them easier to detect despite their small size, the cells targeted in modified ACSF were not exclusively burst-firing cells, and our calibration experiments showed that cells that fired one spike per trial were easily detected (Fig. 8).We also noted (Fig. 8C) that there is a reduced probability of detecting cells that spike less than once per trial (i.e. <1 spike per four afferent stimulus pulses). Because layer 2/3 cells are reported to fire more sparsely *in vivo* than layer 5 cells (Sakata and Harris, 2009; 2012), we were concerned that these detection limits in our calcium imaging technique may underestimate the participation of L2/3 cells in activity patterns generated by TC stimulation. However, spiking probability in L2/3 estimated via on-cell recordings was consistent with that observed during calcium imaging, though cells in supragranular layers were still observed to fire more sparsely, and at longer latency, than infragranular or granular

cells. The variable involvement of these layer 2/3 cells in evoked UP states observed in calcium imaging experiments was also observed in multichannel electrode recordings (Figure 11C&D).

Functional implications

The data and model presented here present have far-reaching implications for understanding the state-dependence of information processing in auditory cortex. In particular, the observation that supragranular layers may only participate in UP state activity under certain conditions may be relevant to top-down, state-dependent modulation of cortical sensory responses. The low efficacy with which thalamic afferents drive monosynaptic spiking activity in cortex has been noted previously (MacLean et al., 2005), and recent reports emphasize the importance of cortical network activity in responses to sensory stimuli *in vivo* (Bathellier et al., 2012;Hromadka et al., 2013;Luczak et al., 2013). It is clear that extrapolating from the observations presented here to functional interpretations *in vivo* is challenging due to the limitations of the brain slice preparation. In our experiments, the absence of intact cortical networks, the limited influence of subcortical neuromodulators, and the substitution of synchronous fiber bundle stimulation for sensory input all constrain the range of possible cellular and network responses to a subset of those available *in vivo*. In spite of these limitations, however, there are striking similarities between the responses observed here and those observed *in vivo.* For example, UP states in our slices had durations that ranged from ~50 – 200 ms, similar to those reported *in vivo* for UP states (Sakata and Harris, 2009) and 'bumps' (Hromadka et al., 2013) after accounting for temperature differences between preparations. The variable involvement of supragranular layers in UP states that we observed is similar to that reported for spontaneous UP states *in vivo* (Sakata and Harris, 2009), as is the observation of early activation of layer 5 cells (Constantinople and Bruno, 2013). Thus, we suggest that the network activity elicited by repetitive stimulation of TC afferents under control conditions in our

slices is similar to the UP state-associated activity elicited by sensory stimulation *in vivo* (Sakata and Harris, 2009;Luczak et al., 2013). However, in the intact cortico-thalamic network, other afferent inputs and neuromodulators likely bias the network state toward or away from UP state activity and may particularly influence the involvement of the superficial layers.

The stochastic nature of UP states evoked by TC stimulation, for example the variability of their onset latency and duration on successive trials (Fig. 5), as well as their characterization as intracortically-mediated events, raise the question as to whether spikes occurring during UP states are time-locked to the TC stimuli and can carry information about specific temporal features of the TC input train. The observation that most spiking occurs during these intracortically-mediated events is particularly surprising in auditory cortex, given the importance of spike timing in the ascending auditory pathway for sensory coding. Although we observed some evidence for consistent spike timing across trials in the context of UP states (e.g. in the raster plot for the deepest layer 5 cell (Fig. 5B), in which spikes occurring between t=25 and 50 msec on each trial tend to line up vertically, indicating consistent timing on successive trials), in other cells this was not the case. Further experiments aimed specifically at information coding will be better able to quantify spike jitter during UP states and the implications for encoding and decoding.

Conflict of Interest Statement

The authors declare no competing commercial or financial interests.

Acknowledgement

Supported by National Institutes of Health (R01 DC006013 to M. I. Banks and T32 GM007507 to B. M. Krause), and the Department of Anesthesiology, School of Medicine and Public Health, University

of Wisconsin, Madison, WI. The authors thank Sean Grady (Department of Anesthesiology) and Anna Kowalkowski (Department of Neuroscience) for technical support on this project.

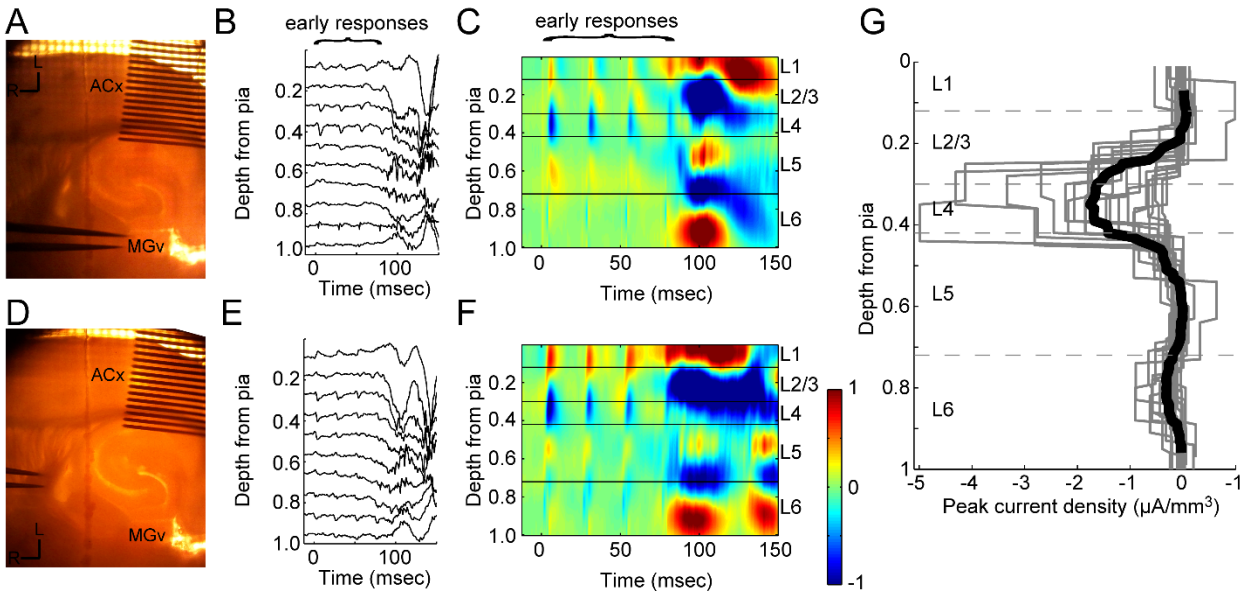

Figure 1. Extracellular responses to stimulation of thalamic afferents. (A) Experiment setup for CSD recordings. A 16-shank electrode is inserted into auditory cortex (100 μm between shanks) and a bipolar stimulating electrode is located in MGv. (B) Example filtered (1-300Hz) LFP from one trial in response to four stimulus pulses at 40 Hz. Stimulus onset at t = 0. (C) CSD for this experiment calculated from an average of 20 trials as in [B] shows the laminar pattern of current sinks (*blue* & *cold colors*) and sources (*red & hot colors)* elicited by stimulation in MGv. Early current sinks are located in layer 4 and deep layer 3 ("early responses"). These early sinks are followed by large current sinks in both infragranular and granular layers which we refer to as UP states (see Fig. 2). The vertical depth axis is normalized to the distance from the pia to white matter, typically around 1 mm for mouse auditory cortex. Color scale is ±1 μA/mm^3. (D-F) Same experiment as in A-C, but with stimulating electrodes placed in the superior thalamic radiation containing thalamo-cortical fibers instead of directly in MGv, as was common in experiments on older animals. Early and late responses were nearly identical between TC fiber stimulation and stimulation in MGv. (G) Peak negative current density in the window 3 < t < 20 ms after the first thalamic stimulus pulse for individual experiments (gray lines) shows the initial monosynaptic

component is located in layer 4 and deep in layer 3 (dark black line: mean across experiments). Dashed lines indicate layer boundaries.

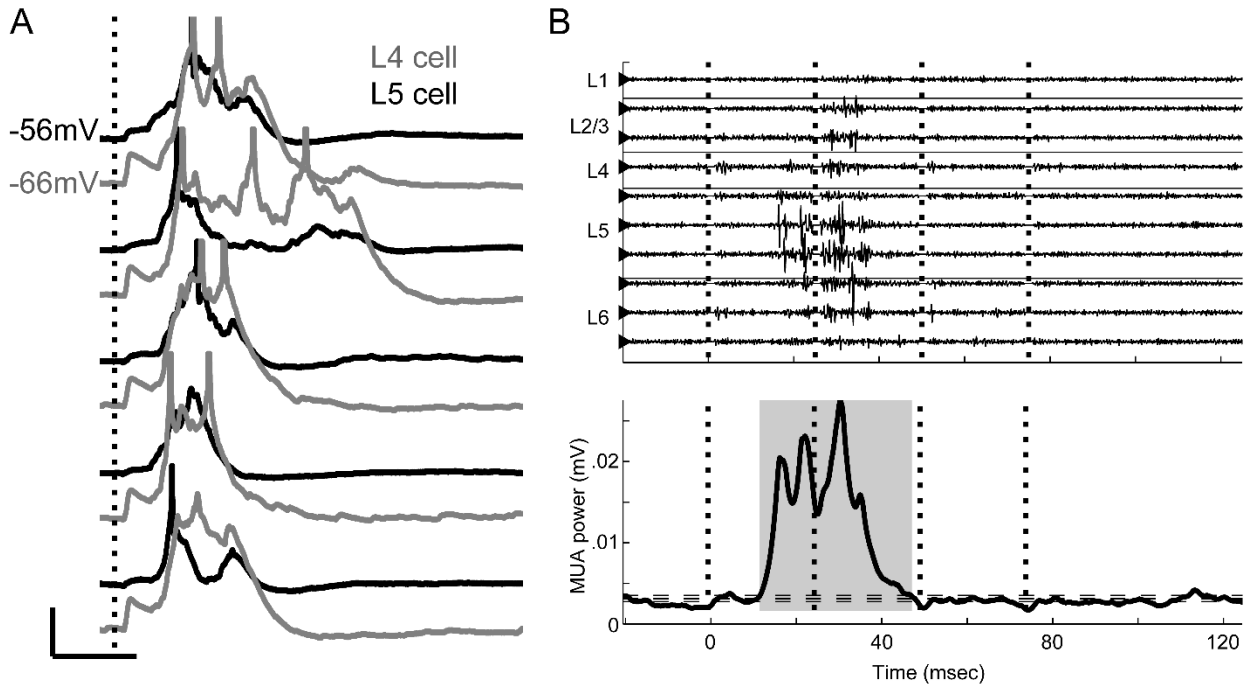

Figure 2. Evoked UP states. (A) Simultaneous whole-cell recordings from a layer 4 cell (gray) and a layer 5 cell (black) on five consecutive trials in response to single stimulation pulse applied to TC afferents (vertical dotted line) show that UP states are network events with variable duration between trials but consistent time course between cells on a given trial. Scale bar: 50 ms, 10 mV. Action potentials are truncated. (B) Multiunit activity (filtered 0.3 – 3kHz) from multichannel recordings similar to Fig. 1 shows the UP state as a burst of high frequency activity occurring on multiple channels, but beginning in layer 5 (*top*). Vertical dotted lines mark stimulus times. The smoothed MUA power in layer 5 is used to detect UP states (shaded gray area, *bottom*) on single trials. Horizontal dashed lines represent the boundaries used to detect UP state onset and offset (see Methods).

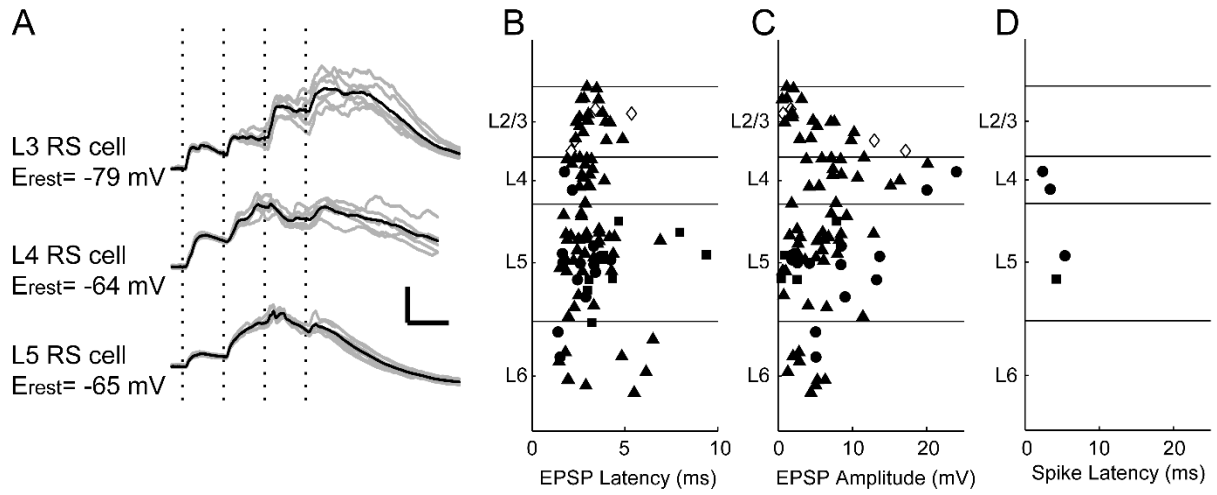

Figure 3. Intracellular responses to TC stimulation. (A) EPSPs evoked by TC stimulation (four 100 µA pulses at 40 Hz, marked with vertical dotted lines) in regular spiking cells of layers 3, 4 and 5. Polysynaptic activity associated with UP states is observed in all three cells after the second stimulus. Gray traces are five consecutive single trials for each cell, black traces are averages. Scale bar: 25 ms, 10 mV. (B) Shortest EPSP latency to TC stimulation (100 µA) was consistent across layers. Symbols represent cell types identified based on spiking patterns to depolarizing current (*filled triangle* = regular spiking, *filled circle* = fast-spike or burst-firing interneurons, *filled square* = intrinsically bursting, *open diamond* = unclassified). (C) EPSP amplitudes plotted with the same conventions and stimulus as in (B). (D) Short latency spikes after a single stimulus pulse were rare. In only four randomly targeted cells were monosynaptic thalamo-cortical inputs superthreshold. Three of these cells were fast-spiking non-pyramidal cells, and one was an intrinsically bursting pyramidal cell (see Figure 4).

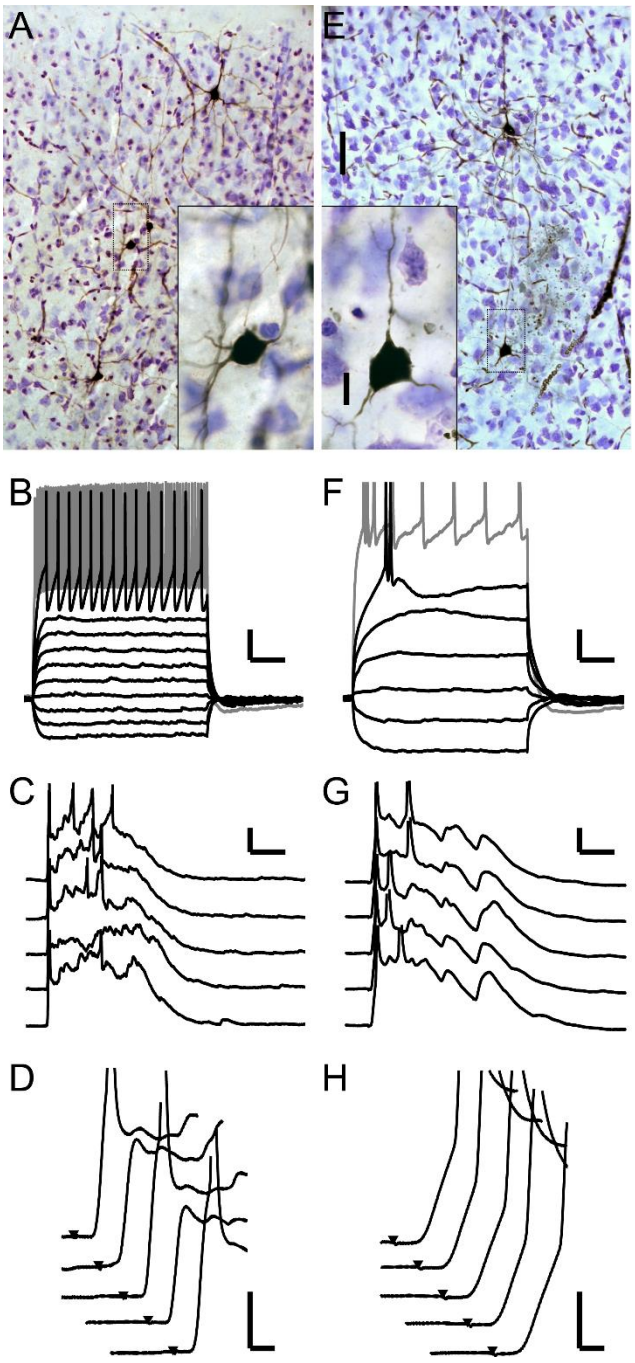

Figure 4. Monosynaptically activated cells. (A-D) One of two monosynaptic spiking interneurons in layer 4. (A) Photomicrograph of this cell along with others recorded in the same slice. The cell is nonpyramidal and aspiny. (B) Polarizing current pulses identify this cell as a fast-spiking cell. (C) This cell fires early, monosynaptically driven spikes as well as later spikes during evoked UP states. Action potentials are truncated. (D) Detailed inspection of the early component of the responses from (C) shows that the spikes occur after a smooth initial depolarization with no evidence of di- or poly-synaptic potentials contributing to the early, monosynaptic spikes. This is also clear on trials two and four where the cell did not fire a spike. (E-H) A monosynaptic spiking pyramidal cell in layer 5. (E) Photomicrograph as in (A). (F) This cell has an intrinsically bursting firing pattern. (G-H) Similar to the cell shown in (A-D) this cell fires early, monosynaptic spikes as well as later spikes during evoked UP states. Scale bars: A, E 50 µm (25X), 10 µm (100X); B, F: 50 ms, 10 mV; C, G: 25 ms, 10 mV; D, H: 2 ms, 10 mV.

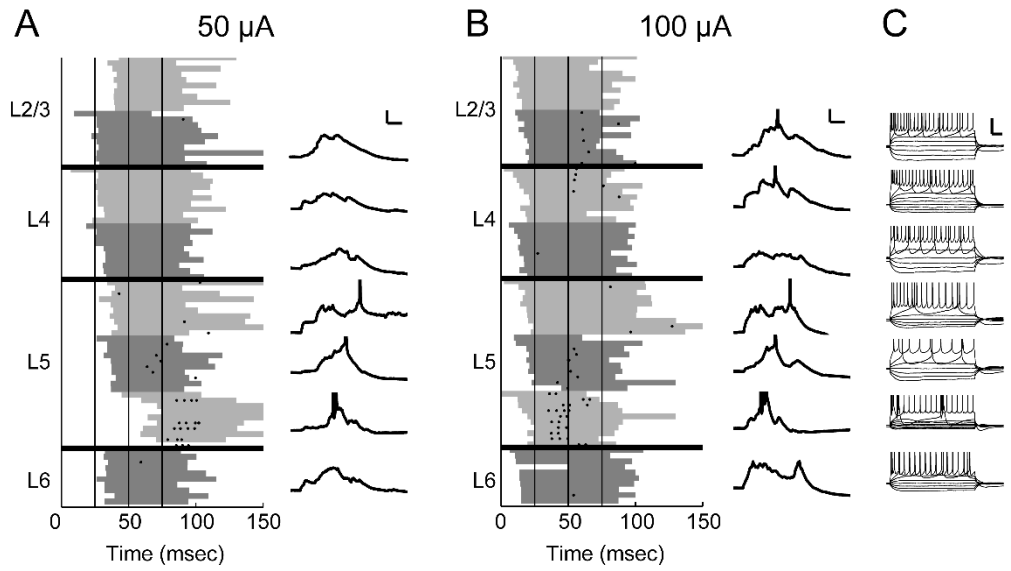

Figure 5. On-cell spiking at moderate and high stimulus intensities. In this example experiment, 8 sequential on-cell recordings were obtained from cells across the cortical laminae. (A) The recorded cells are plotted in order according to their laminar position. A spike raster of ten trials is plotted for each cell (*left*). The shaded gray area delineates UP states detected on the multiunit activity recorded on a low-impedance glass electrode placed in layer 5 for the duration of the experiment. The shade of gray used alternates between light and dark for each cell to better distinguish between cells. Vertical black lines indicate stimulus pulses (4x40Hz). At 50 µA stimulus intensity, UP states are typically evoked after the second stimulus pulse, and on-cell spikes were only detected in the infragranular layers. Whole-cell recordings obtained after the on-cell experiment were available in 7/8 cells (*right*) and confirm that the observed spikes occurred during evoked UP states. Scale bar 25 ms, 10 mV. (B) Conventions as in (A), but at a higher stimulus intensity. At this intensity, UP states are evoked after the first stimulus pulse, and there are some spikes in layers 2/3 and 4 as well as more spikes in cells in layer 5. (C) Polarizing pulses in whole-cell recordings show that 6/7 cells were regular spiking and the deepest layer 5 cell was intrinsically bursting. Scale bar 50 ms, 30 mV.

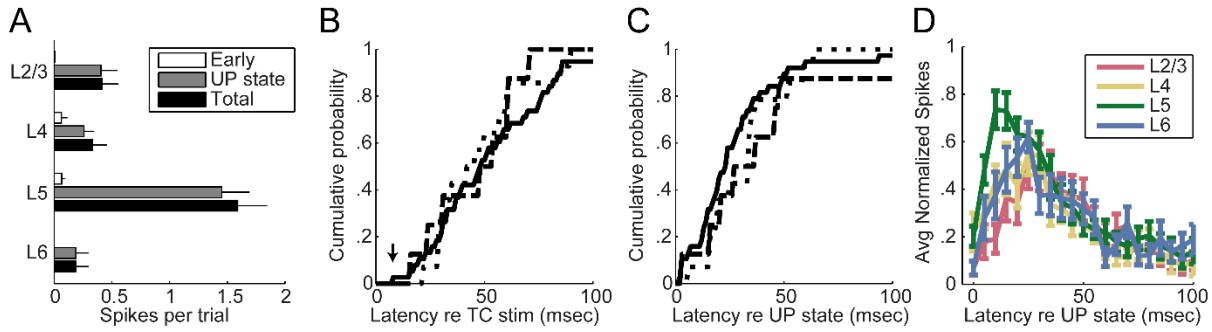

Figure 6. Timing of spiking relative to UP states. (A) Average spikes per trial per cell across all on-cell recordings. Across all on-cell experiments, almost all spikes in all layers were fired during UP states. Error bars represent standard error of the mean. Total spike count includes early and UP state spikes as well as additional spikes that did not fit either category (for example, spikes occurring after an UP state, or spikes occurring at long latency in the absence of a detected UP state). (B) Cumulative mean first-spike latency distributions relative to stimulus onset show no significant differences between layers 2/3, 4, and 5. The mean first spike latency for each cell was determined by averaging the latency to the earliest spike across trials. Layer 6 is omitted from this figure due to the relatively low number of cells recorded in layer 6. (C) Cumulative mean first-spike latency distributions relative to UP state onset similarly show no significant differences between layers. (D) Spike latencies relative to UP states in MUA from multichannel recordings show that layer 5 is active before the other layers during UP states.

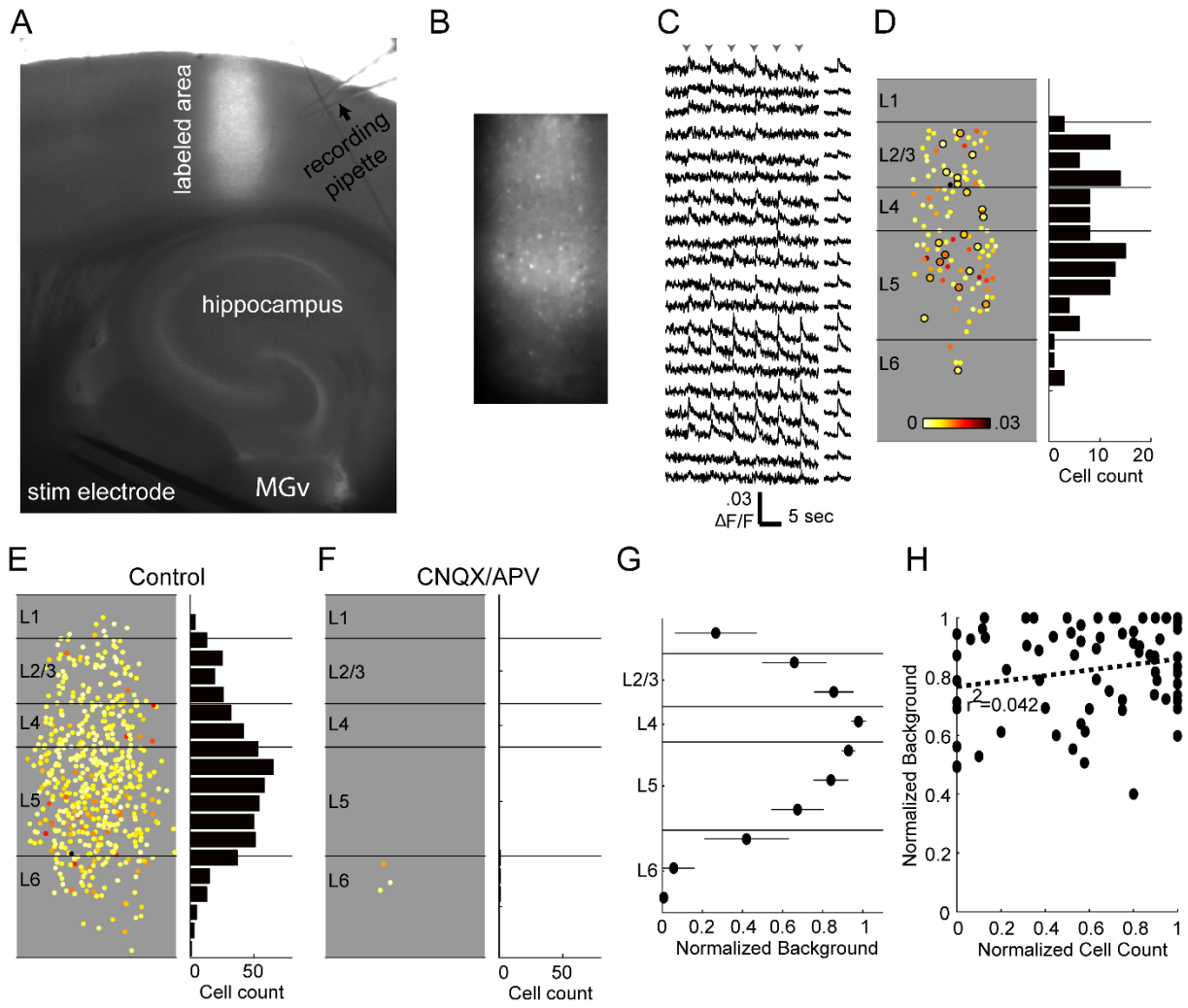

Figure 7. Calcium imaging technique. (A) Low-power combination fluorescence and brightfield micrograph shows OGB-1 dye loaded into a vertical strip of auditory cortex. (B) 10X response image taken by subtracting baseline fluorescence averaged over one second from one second of response to TC stimulation. Single responding cells are clearly seen as bright spots. (C) Sample fluorescence traces from a random selection of cells identified in the labeled region in (B) and sorted by depth (top, superficial; bottom, deep). Traces on the left are from single movies during which six stimuli (arrowheads) were presented five seconds apart and smoothed over 5 frames. Traces on the right are averages across stimulus presentations. Note that here and throughout, the units for fluorescence traces are ΔF/F, ***not*** *%ΔF/F.* (D) *Left,* all responsive cells from the example experiment, plotted according

to their location in the column and average change in fluorescence. Circled cells correspond to those with traces plotted in (C). *Right,* spatial histogram of responding cell counts in 50 μm bins. (E) Cells responding to thalamocortical input in eight separate experiments, plotted on top of each other in normalized depth coordinates. (F) Responses from the same eight experiments in the presence of CNQX/APV. Almost all of the responding cells from (E) are blocked. (G) The background fluorescence signal was averaged within 100 μm depth bins and normalized to the brightest bin as a measure of labeling intensity. Points are plotted as mean ± standard deviation. (H) Normalized background as in (G) versus cell count as in (D) (normalized within experiments to the layer containing the most spikes) for layers 2 - 5. Each point represents the background and cell count in a single 100 μm bin from a single experiment.

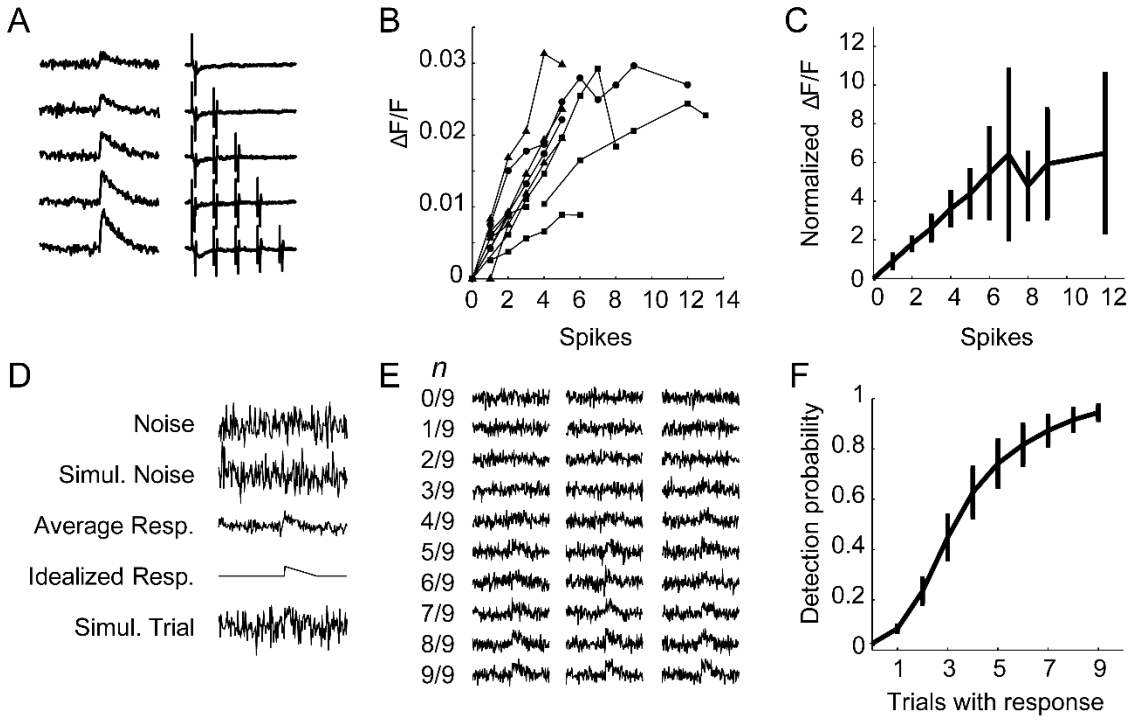

Figure 8. Electrophysiological calibration of calcium signals. (A) In an example calibration recording, averaged calcium traces (left) are sorted by the number of spikes simultaneously detected via on-cell recording (right). (B) Peak calcium transient (ΔF/F) plotted as a function of number of spikes detected using on-cell patch clamp for several cells. Each line represents a single cell, each data point represents the calcium change of the average of all traces in which that number of spikes was observed. Symbols indicate cells from different layers: layer 3 (*triangles*), layer 4 (*circles*), and layer 5 (*squares*). The change in calcium fluorescence is linear with spikes fired up to 6 spikes. (C) Data from (B) are normalized to the fluorescence change observed for the fewest spikes fired for that cell and averaged across cells. Data points are mean ± standard deviation. The normalized ΔF/F is linear up to about six spikes. (D-F) Simulated data was used to estimate the probability of detecting cells that fire less than one spike per trial. (D) The procedure for simulations is shown. For each calibration cell, the variance of the observed fluorescence noise on single trials was used to create Gaussian simulated noise. From the average one-spike response, an idealized response was derived by smoothing the data (5-point moving average) and measuring the peak. A single simulated trial is a simulated noise trial plus this idealized response. (E)

Simulated averaged data consisted of 9 simulated trials, with *n* trials containing noise plus the idealized response and 9 – *n* trials containing only noise. Displayed fractions represent the number of trials containing the idealized response. Three examples of simulated averages are plotted for each trial composition. (F) Probability of detecting a response in the simulations as in (E) as a function of *n*, the number of trials containing a response. Data are plotted as mean ± SEM across calibration cells.

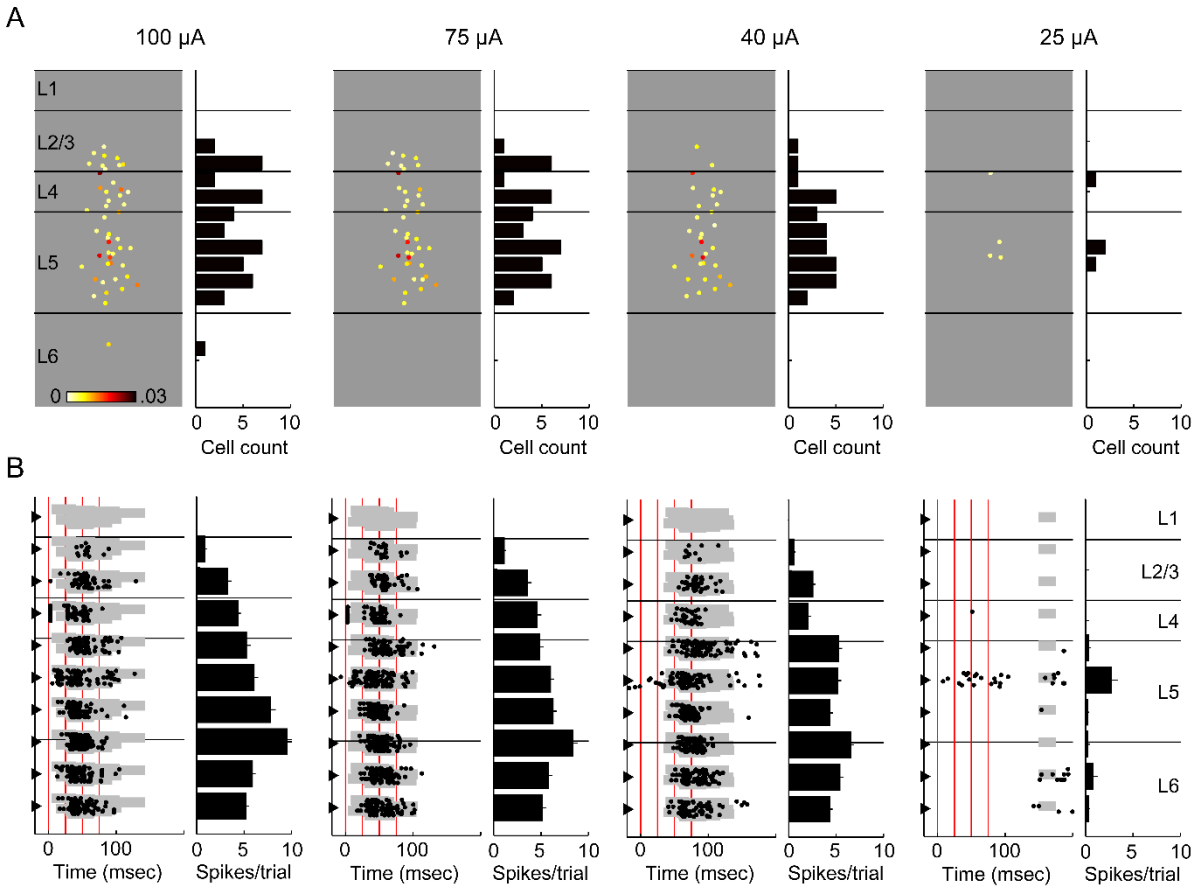

Figure 9. Comparing calcium imaging with simultaneous multichannel recordings. (A) An example experiment at four different stimulus intensities (100-25 µA). At each intensity, responsive cells are plotted at their spatial position (*left*), color-coded to response amplitude. Color scale is 0 to .03 ΔF/F. Lines represent layer boundaries. To the right of each example experiment is a histogram count of the cells in 50 µm depth bins. (B) Simultaneous multichannel, multiunit recordings from the experiment in (A). At each intensity, a spike raster (*left*) from 12 trials is plotted at the depth coordinate of each channel. The gray shaded area indicates detected UP states similar to Fig. 5. Accompanying each raster plot is a depth histogram (*right*) showing the average number of spikes per trial on each channel. Error bars are SEM. Stimulus times are marked by vertical red lines. Note that early spiking activity on the electrode in layer 4 (visible immediately adjacent to the red line indicating stimulus time) is not present at lower stimulus intensities despite robust spiking associated with an evoked UP state. Also, for both

techniques, spiking was very sparse at the lowest stimulus intensity (which did not reliably trigger UP states) and these sparse spikes included activity in layer 5.

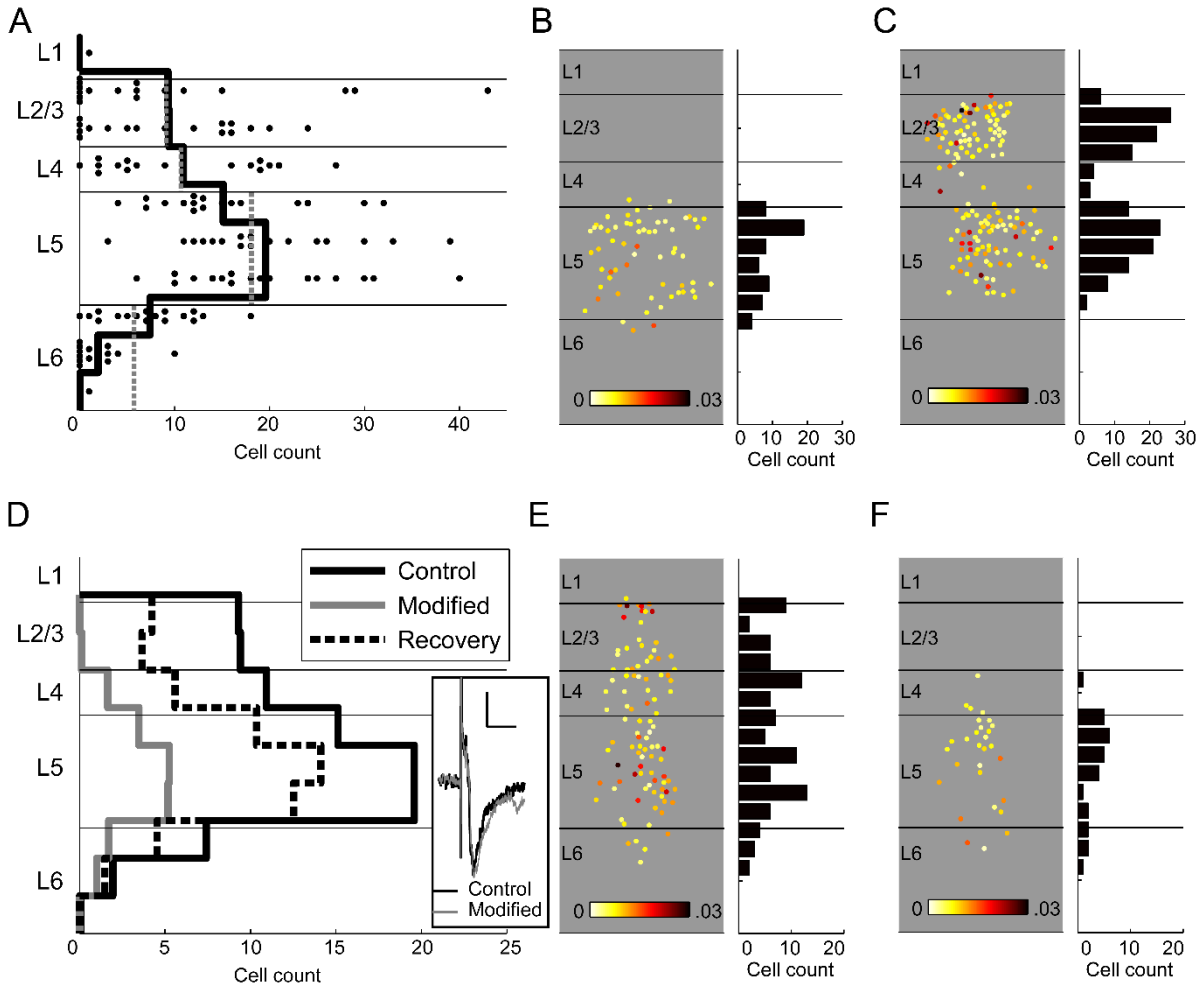

Figure 10. Laminar profile of spiking responses. (A) The number of responding cells detected using calcium imaging is plotted in 100 µm bins (*dots*) as well as the average number of cells per experiment (*solid black line*). In many experiments, there were few if any responding cells in layers 2/3, while every experiment showed robust activity in layer 5. The laminar distribution of cells observed spiking using calcium imaging in control conditions is nearly identical to the expected distribution based on on-cell recordings (*gray dotted lines*). (B) An example experiment in which thalamocortical stimulation primarily activated cells in layer 5, with no activity in layer 2/3. (C) In the same experiment, stimulation of a nearby cortical area triggered robust spiking in the imaged column, including in layers 2/3, demonstrating that the lack of layer 2/3 responses in (B) was not due to poor labeling or health of the superficial layers. (D) Cell counts in control conditions (*solid black lines*; same data as in [A]) show that

layer 5 had a significantly greater density of spiking cells than the other layers. Modified ACSF (*solid grey lines;* modified ACSF contains elevated concentrations of divalent cations or 40 µM APV) strongly reduced spiking across the cortical laminae, and layer 2/3 was more affected than the other layers. Modified ACSF eliminated UP state activity but did not affect the early component of the field potential response (*inset*; scale bar 10 ms, 0.2 mV). Recovery after high divalent cations (*thick dashed lines*) was similar to control cell counts. (E) An example experiment in which spiking cells were seen in all layers in normal ACSF. (F) The same experiment from (E) but with modified, high-divalent ACSF that blocks UP states. Far fewer cells are activated without UP states, and activity in layer 2/3 is completely blocked. Conventions for panels B, C, E, and F are the same as the similar panels in Figs. 7&9.

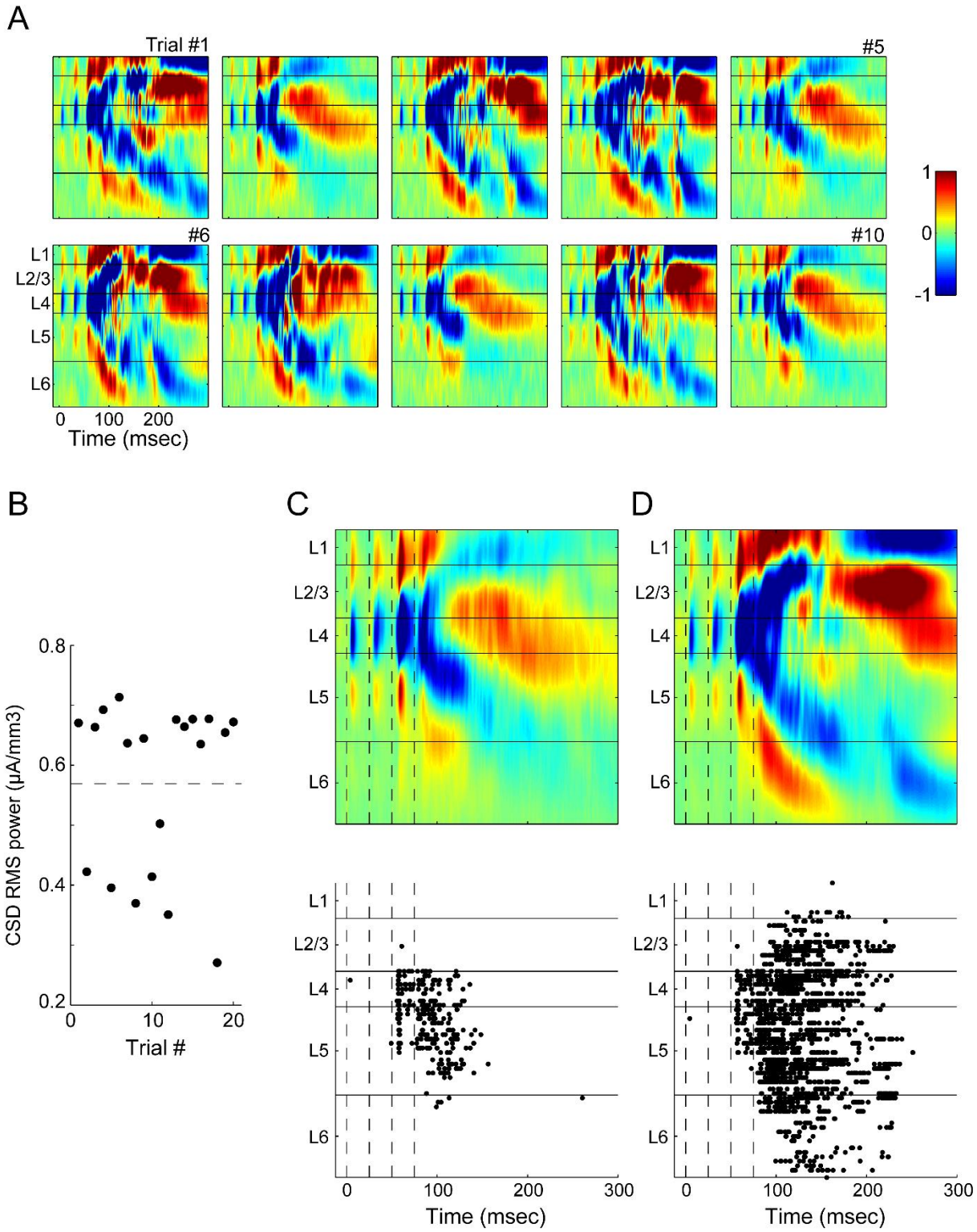

Figure 11. Variable supragranular involvement in UP states in CSD and MUA recordings. (A) Observed UP states varied bimodally in intensity. Each panel is the CSD of a consecutive single trial, and all trials

were at a constant stimulus intensity. Note two classes of responses differing in intensity (e.g., Trial #1 compared to Trial #2). (B) Twenty consecutive trials, including those in A, were separated into small and large UP states based on the root-mean-squared CSD power across channels. Each point represents a single trial, and the horizontal line separates the bimodal distribution of responses. (C&D) CSD responses (*top*) averaged over the small (C) and large (D) UP states from panel B. Multiunit activity (*bottom*) from these same sets of trials was measured on the same electrode array used for CSD recording. Spike data are plotted in raster form, one line for each trial, with trials from different channels separated by a vertical space. On trials for which the CSD showed weak UP states, multiunit spiking activity was observed in layers 4 and 5 but very little in layers 2/3. Trials that showed strong UP states in the CSD showed more multiunit activity in all layers but also involved layer 2/3. Color scale is ±1 $\mu A/mm^3$ for (A, C&D).

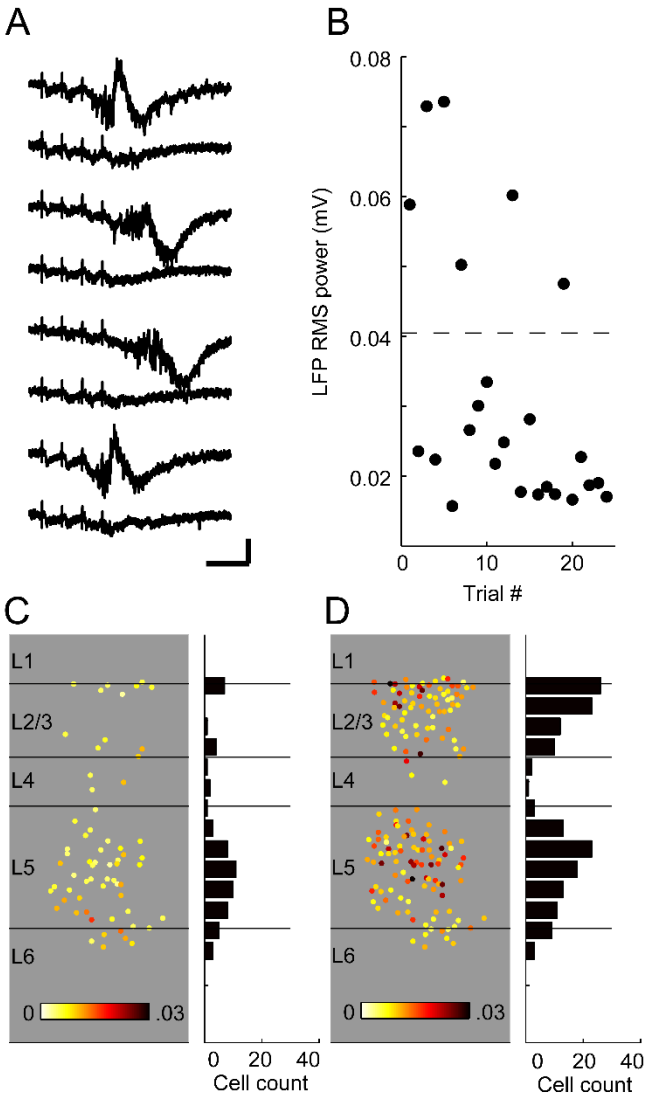

Figure 12. Two classes of UP states in calcium imaging. (A) Shown are LFPs recorded in layer 5 during consecutive trials of a single calcium imaging experiment demonstrating two sizes of UP states (using the same stimulus intensity on all trials). Scale bar: 50 ms, 0.1 mV. (B) Calcium traces were sorted according to the power of the LFP, similarly to the experiment in Fig. 11. Six trials had large UP states, so data from only 6 of the 18 trials (randomly chosen) with small UP states were analyzed. For trials with small UP states (C), most of the responsive cells were found in the infragranular layers. Trials with large UP states (D), were associated with much more robust calcium responses in all layers, with an especially striking change in the superficial layers. Color scale for (C&D) is 0 to .03 ΔF/F.

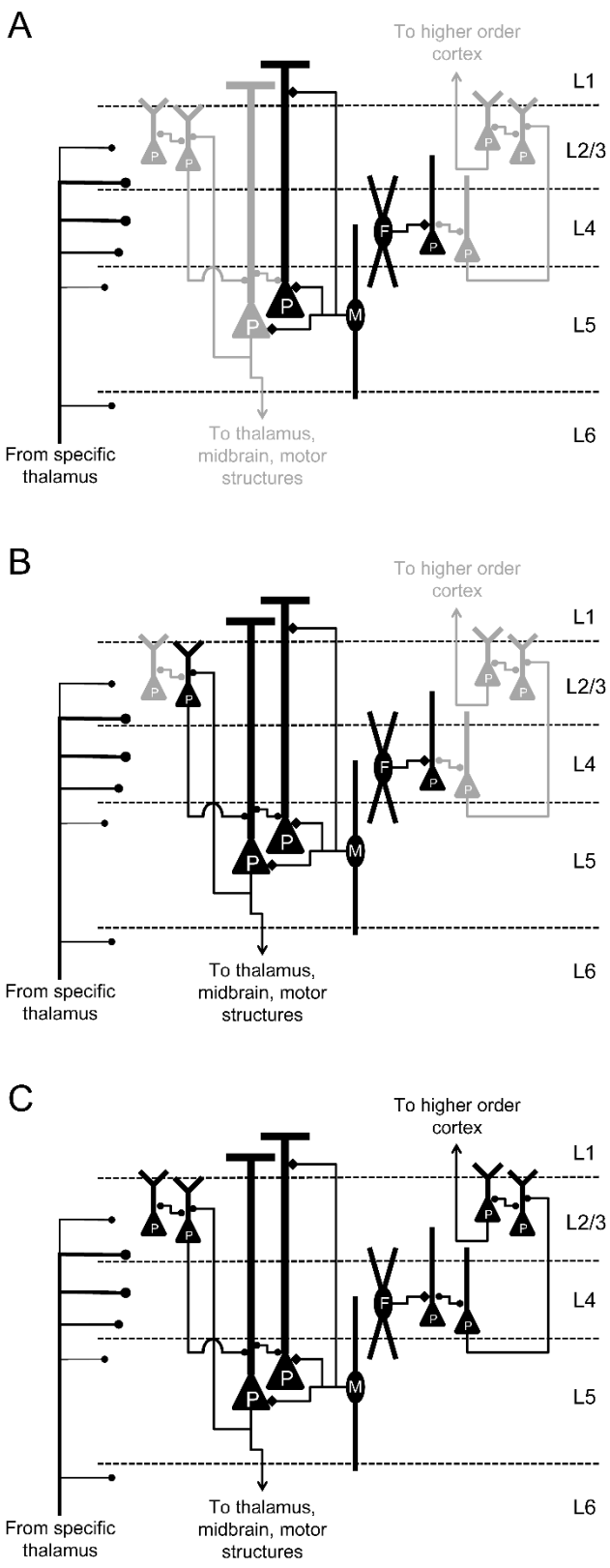

Figure 13. Diversity of activity patterns in response to thalamic stimulation. Circuit diagrams of auditory cortex summarizing key findings from this study and previous reports. Pyramidal cells (triangles) and GABAergic interneurons (ovals; M: Martinotti cells, F: fast-spiking cells) are depicted along with some of their local connections. Active cells are in black, inactive cells are in grey. (A) Thalamic stimulation elicits monosynaptic responses primarily in GABAergic cells and a small number of pyramidal cells in layers 4 and 5. (B) For stimuli of sufficient intensity and after a delay of ~10 - 100 ms, UP state activity emerges in the infragranular network. (C) Strong stimuli trigger UP state activity that spreads to supragranular layers as well.

References

Adams, J.C. (1981). Heavy metal intensification of DAB-based HRP reaction product. *Journal of Histochemistry & Cytochemistry* 29**,** 775.

Aponte, Y., Bischofberger, J., and Jonas, P. (2008). Efficient Ca2+ buffering in fast-spiking basket cells of rat hippocampus. *J.Physiol* 586**,** 2061-2075. doi: jphysiol.2007.147298 [pii];10.1113/jphysiol.2007.147298 [doi].

Ascoli, G.A., Alonso-Nanclares, L., Anderson, S.A., Barrionuevo, G., Benavides-Piccione, R., Burkhalter, A., Buzsaki, G., Cauli, B., Defelipe, J., Fairen, A., Feldmeyer, D., Fishell, G., Fregnac, Y., Freund, T.F., Gardner, D., Gardner, E.P., Goldberg, J.H., Helmstaedter, M., Hestrin, S., Karube, F., Kisvarday, Z.F., Lambolez, B., Lewis, D.A., Marin, O., Markram, H., Munoz, A., Packer, A., Petersen, C.C., Rockland, K.S., Rossier, J., Rudy, B., Somogyi, P., Staiger, J.F., Tamas, G., Thomson, A.M., Toledo-Rodriguez, M., Wang, Y., West, D.C., and Yuste, R. (2008). Petilla terminology: nomenclature of features of GABAergic interneurons of the cerebral cortex. *Nat Rev Neurosci* 9**,** 557-568. doi: 10.1038/nrn2402.

Atencio, C.A., Sharpee, T.O., and Schreiner, C.E. (2009). Hierarchical computation in the canonical auditory cortical circuit. *Proceedings of the National Academy of Sciences* 106**,** 21894-21899.

Banks, M.I., Uhlrich, D.J., Smith, P.H., Krause, B.M., and Manning, K.A. (2011). Descending projections from extrastriate visual cortex modulate responses of cells in primary auditory cortex. *Cereb.Cortex* 21**,** 2620-2638. doi: bhr048 [pii];10.1093/cercor/bhr048 [doi].

Barbour, D.L., and Callaway, E.M. (2008). Excitatory Local Connections of Superficial Neurons in Rat Auditory Cortex. *Journal of Neuroscience* 28**,** 11174-11185.

Barth, A.L., and Poulet, J.F. (2012). Experimental evidence for sparse firing in the neocortex. *Trends Neurosci* 35**,** 345-355. doi: S0166-2236(12)00051-3 [pii];10.1016/j.tins.2012.03.008 [doi].

Bastos, A.M., Usrey, W.M., Adams, R.A., Mangun, G.R., Fries, P., and Friston, K.J. (2012). Canonical microcircuits for predictive coding. *Neuron* 76**,** 695-711. doi: S0896-6273(12)00959-2 [pii];10.1016/j.neuron.2012.10.038 [doi].

Bathellier, B., Ushakova, L., and Rumpel, S. (2012). Discrete neocortical dynamics predict behavioral categorization of sounds. *Neuron* 76**,** 435-449. doi: S0896-6273(12)00657-5 [pii];10.1016/j.neuron.2012.07.008 [doi].

Beggs, J.M., and Plenz, D. (2003). Neuronal avalanches in neocortical circuits. *Journal of Neuroscience* 23**,** 11167-11177.

Beierlein, M., Gibson, J.R., and Connors, B.W. (2003). Two dynamically distinct inhibitory networks in layer 4 of the neocortex. *Journal of Neurophysiology* 90**,** 2987-3000.

Beltramo, R., D'urso, G., Dal Maschio, M., Farisello, P., Bovetti, S., Clovis, Y., Lassi, G., Tucci, V., Tonelli, D.D.P., and Fellin, T. (2013). Layer-specific excitatory circuits differentially control recurrent network dynamics in the neocortex. *Nature Neuroscience* 16**,** 227-234.

Benshalom, G., and White, E.L. (1986). Quantification of thalamocortical synapses with spiny stellate neurons in layer IV of mouse somatosensory cortex. *J Comp Neurol* 253**,** 303-314. doi: 10.1002/cne.902530303.

Berry, M.S., and Pentreath, V.W. (1976). Criteria for distinguishing between monosynaptic and polysynaptic transmission. *Brain Research* 105**,** 1-20.

Binzegger, T., Douglas, R.J., and Martin, K.A. (2004). A quantitative map of the circuit of cat primary visual cortex. *J.Neurosci.* 24**,** 8441-8453. doi: 10.1523/JNEUROSCI.1400-04.2004 [doi];24/39/8441 [pii].

Budd, J.M. (1998). Extrastriate feedback to primary visual cortex in primates: a quantitative analysis of connectivity. *Proc.Biol.Sci.* 265**,** 1037-1044.

Buffalo, E.A., Fries, P., Landman, R., Buschman, T.J., and Desimone, R. (2011). Laminar differences in gamma and alpha coherence in the ventral stream. *Proceedings of the National Academy of Sciences* 108**,** 11262-11267. doi: 10.1073/pnas.1011284108.

Bullier, J., and Henry, G.H. (1979). Laminar distribution of first-order neurons and afferent terminals in cat striate cortex. *Journal of Neurophysiology* 42**,** 1271.

Bureau, I., Saint Paul, F., and Svoboda, K. (2006). Interdigitated Paralemniscal and Lemniscal Pathways in the Mouse Barrel Cortex. *PLoS Biology* 4**,** 2361-2371.

Chang, E.F., Bao, S., Imaizumi, K., Schreiner, C.E., and Merzenich, M.M. (2005). Development of spectral and temporal response selectivity in the auditory cortex. *Proc.Natl.Acad.Sci.U.S.A* 102**,** 16460-16465. doi: 0508239102 [pii];10.1073/pnas.0508239102 [doi].

Chang, E.F., and Merzenich, M.M. (2003). Environmental noise retards auditory cortical development. *Science* 300**,** 498-502. doi: 10.1126/science.1082163 [doi];300/5618/498 [pii].

Chauvette, S., Volgushev, M., and Timofeev, I. (2010). Origin of active states in local neocortical networks during slow sleep oscillation. *Cerebral Cortex* 20**,** 2660-2674.

Christianson, G.B., Sahani, M., and Linden, J.F. (2011). Depth-dependent temporal response properties in core auditory cortex. *J.Neurosci.* 31**,** 12837-12848. doi: 31/36/12837 [pii];10.1523/JNEUROSCI.2863-11.2011 [doi].

Constantinople, C.M., and Bruno, R.M. (2011). Effects and mechanisms of wakefulness on local cortical networks. *Neuron* 69**,** 1061-1068. doi: S0896-6273(11)00162-0 [pii];10.1016/j.neuron.2011.02.040 [doi].

Constantinople, C.M., and Bruno, R.M. (2013). Deep cortical layers are activated directly by thalamus. *Science* 340**,** 1591-1594. doi: 340/6140/1591 [pii];10.1126/science.1236425 [doi].

Creutzfeldt, O.D. (1977). Generality of the functional structure of the neocortex. *Naturwissenschaften* 64**,** 507-517.

Cruikshank, S.J., Lewis, T.J., and Connors, B.W. (2007). Synaptic basis for intense thalamocortical activation of feedforward inhibitory cells in neocortex. *Nat.Neurosci.* 10**,** 462-468.

Cruikshank, S.J., Rose, H.J., and Metherate, R. (2002). Auditory thalamocortical synaptic transmission in vitro. *J.Neurophysiol.* 87**,** 361-384.

Cruikshank, S.J., Urabe, H., Nurmikko, A.V., and Connors, B.W. (2010). Pathway-Specific Feedforward Circuits between Thalamus and Neocortex Revealed by Selective Optical Stimulation of Axons. *Neuron* 65**,** 230-245.

Cunningham, M.O., Pervouchine, D.D., Racca, C., Kopell, N.J., Davies, C.H., Jones, R.S., Traub, R.D., and Whittington, M.A. (2006). Neuronal metabolism governs cortical network response state. *Proc.Natl.Acad.Sci.U.S.A* 103**,** 5597-5601.

Curto, C., Sakata, S., Marguet, S., Itskov, V., and Harris, K.D. (2009). A simple model of cortical dynamics explains variability and state dependence of sensory responses in urethane-anesthetized auditory cortex. *J.Neurosci.* 29**,** 10600-10612. doi: 29/34/10600 [pii];10.1523/JNEUROSCI.2053-09.2009 [doi].

Davis, M.H., and Johnsrude, I.S. (2007). Hearing speech sounds: top-down influences on the interface between audition and speech perception. *Hear.Res.* 229**,** 132-147.

De Kock, C.P., Bruno, R.M., Spors, H., and Sakmann, B. (2007). Layer- and cell-type-specific suprathreshold stimulus representation in rat primary somatosensory cortex. *J.Physiol* 581**,** 139-154. doi: jphysiol.2006.124321 [pii];10.1113/jphysiol.2006.124321 [doi].

Destexhe, A., Hughes, S.W., Rudolph, M., and Crunelli, V. (2007). Are corticothalamic 'up' states fragments of wakefulness? *Trends in Neurosciences* 30**,** 334-342.

Destexhe, A., Rudolph, M., and Pare, D. (2003). The high-conductance state of neocortical neurons in vivo. *Nature Reviews Neuroscience* 4**,** 739-751.

Deweese, M.R., and Zador, A.M. (2006). Non-Gaussian Membrane Potential Dynamics Imply Sparse, Synchronous Activity in Auditory Cortex. *Journal of Neuroscience* 26**,** 12206-12218.

Douglas, R.J., and Martin, K.A. (1991). A functional microcircuit for cat visual cortex. *The Journal of Physiology* 440**,** 735-769.

Douglas, R.J., and Martin, K.A. (2004). Neuronal circuits of the neocortex. *Annu.Rev.Neurosci.* 27**,** 419-451. doi: 10.1146/annurev.neuro.27.070203.144152 [doi].

Douglas, R.J., Martin, K.a.C., and Whitteridge, D. (1989). A canonical microcircuit for neocortex. *Neural Computation* 1**,** 480-488.

Dräger, U.C., and Hubel, D.H. (1978). Studies of visual function and its decay in mice with hereditary retinal degeneration. *The Journal of Comparative Neurology* 180**,** 85-114. doi: 10.1002/cne.901800107.

Fanselow, E.E., Richardson, K.A., and Connors, B.W. (2008). Selective, state-dependent activation of somatostatin-expressing inhibitory interneurons in mouse neocortex. *Journal of Neurophysiology* 100**,** 2640-2652.

Feldmeyer, D., Lübke, J., Silver, R.A., and Sakmann, B. (2002). Synaptic connections between layer 4 spiny neurone-layer 2/3 pyramidal cell pairs in juvenile rat barrel cortex: physiology and anatomy of interlaminar signalling within a cortical column. *The Journal of physiology* 538**,** 803-822.

Freeman, J., and Nicholson, C. (1975). Experimental optimization of current source-density technique for anuran cerebellum. *Journal of Neurophysiology* 38**,** 369-382.

Frick, A., Feldmeyer, D., and Sakmann, B. (2007). Postnatal development of synaptic transmission in local networks of L5A pyramidal neurons in rat somatosensory cortex. *J.Physiol* 585**,** 103-116. doi: jphysiol.2007.141788 [pii];10.1113/jphysiol.2007.141788 [doi].

Fritz, J.B., Elhilali, M., and Shamma, S.A. (2007). Adaptive changes in cortical receptive fields induced by attention to complex sounds. *J Neurophysiol* 98**,** 2337-2346.

Gabernet, L., Jadhav, S.P., Feldman, D.E., Carandini, M., and Scanziani, M. (2005). Somatosensory integration controlled by dynamic thalamocortical feed-forward inhibition. *Neuron* 48**,** 315-327.

Gerstein, G.L., and Kiang, N.Y.S. (1964). Responses of single units in the auditory cortex. *Experimental Neurology* 10**,** 1-18. doi: http://dx.doi.org/10.1016/0014-4886(64)90083-4.

Gibson, J.R., Beierlein, M., and Connors, B.W. (1999). Two networks of electrically coupled inhibitory neurons in neocortex. *Nature* 402**,** 75-79.

Gil, Z., and Amitai, Y. (1996). Properties of convergent thalamocortical and intracortical synaptic potentials in single neurons of neocortex. *Journal of Neuroscience* 16**,** 6567-6578.

Gilbert, C.D. (1983). Microcircuitry of the visual cortex. *Annu.Rev.Neurosci.* 6**,** 217-247. doi: 10.1146/annurev.ne.06.030183.001245 [doi].

Gilbert, C.D., and Wiesel, T.N. (1983). Functional organization of the visual cortex. *Prog.Brain Res.* 58**,** 209-218. doi: S0079-6123(08)60022-9 [pii];10.1016/S0079-6123(08)60022-9 [doi].

Gireesh, E.D., and Plenz, D. (2008). Neuronal avalanches organize as nested theta- and beta/gamma-oscillations during development of cortical layer 2/3. *Proceedings of the National Academy of Sciences* 105**,** 7576-7581. doi: 10.1073/pnas.0800537105.

Goard, M., and Dan, Y. (2009). Basal forebrain activation enhances cortical coding of natural scenes. *Nat Neurosci* 12**,** 1444-1449. doi: nn.2402 [pii];10.1038/nn.2402 [doi].

Goris, R.L., Movshon, J.A., and Simoncelli, E.P. (2014). Partitioning neuronal variability. *Nat Neurosci*. doi: 10.1038/nn.3711.

Guillery, R.W., and Sherman, S.M. (2002). Thalamic relay functions and their role in corticocortical communication: generalizations from the visual system. [Review] [103 refs]. *Neuron* 33**,** 163-175.

Harris, K.D., and Thiele, A. (2011). Cortical state and attention. *Nat.Rev.Neurosci.* 12**,** 509-523. doi: nrn3084 [pii];10.1038/nrn3084 [doi].

He, B.J., and Raichle, M.E. (2009). The fMRI signal, slow cortical potential and consciousness. *Trends in Cognitive Sciences* 13**,** 302-309. doi: http://dx.doi.org/10.1016/j.tics.2009.04.004.

Hefti, B.J., and Smith, P.H. (2003). Distribution and kinetic properties of GABAergic inputs to layer V pyramidal cells in rat auditory cortex. *Jaro.* 4**,** 106-121.

Hirsch, J.A., and Martinez, L.M. (2006). Laminar processing in the visual cortical column. *Curr.Opin.Neurobiol.* 16**,** 377-384.

Hromadka, T., Zador, A.M., and Deweese, M.R. (2013). Up states are rare in awake auditory cortex. *J.Neurophysiol.* 109**,** 1989-1995. doi: jn.00600.2012 [pii];10.1152/jn.00600.2012 [doi].

Huang, C.L., and Winer, J.A. (2000). Auditory thalamocortical projections in the cat: laminar and areal patterns of input. *J Comp Neurol.* 427**,** 302-331.

Hubel, D.H., and Wiesel, T.N. (1963). Shape and arrangement of columns in cat's striate cortex. *J Physiol* 165**,** 559-568.

Huggenberger, S., Vater, M., and Deisz, R.A. (2009). Interlaminar differences of intrinsic properties of pyramidal neurons in the auditory cortex of mice. *Cerebral Cortex* 19**,** 1008-1018.

Johnson, K.R., Erway, L.C., Cook, S.A., Willott, J.F., and Zheng, Q.Y. (1997). A major gene affecting age-related hearing loss in C57BL/6J mice. *Hearing research* 114**,** 83-92.

Kaas, J.H., and Collins, C.E. (2001). The organization of sensory cortex. *Curr.Opin.Neurobiol.* 11**,** 498-504.

Kampa, B.M., Letzkus, J.J., and Stuart, G.J. (2006). Cortical feed-forward networks for binding different streams of sensory information. *Nature neuroscience* 9**,** 1472-1473.

Kawaguchi, Y. (1993). Groupings of nonpyramidal and pyramidal cells with specific physiological and morphological characteristics in rat frontal cortex. *Journal of Neurophysiology* 69**,** 416-431.

Kawaguchi, Y., and Kubota, Y. (1993). Correlation of physiological subgroupings of nonpyramidal cells with parvalbumin and calbinding immunoreactive neurons in layer V of rat frontal cortex. *J Neurophysiol* 70**,** 387-396.

Kawaguchi, Y., and Kubota, Y. (1996). Physiological and morphological identification of somatostatin- or vasoactive intestinal polypeptide-containing cells among GABAergic cell subtypes in rat frontal cortex. *The Journal of Neuroscience* 16**,** 2701-2715.

Kawaguchi, Y., and Kubota, Y. (1997). GABAergic cell subtypes and their synaptic connections in rat frontal cortex. *Cerebral Cortex* 7**,** 476-486.

Kawaguchi, Y., and Kubota, Y. (1998). Neurochemical features and synaptic connections of large physiologically-identified GABAergic cells in the rat frontal cortex. *Neuroscience* 85**,** 677-701.

Kisley, M.A., and Gerstein, G.L. (1999). Trial-to-trial variability and state-dependent modulation of auditory- evoked responses in cortex. *J.Neurosci.* 19**,** 10451-10460.

Lakatos, P., Shah, A.S., Knuth, K.H., Ulbert, I., Karmos, G., and Schroeder, C.E. (2005). An oscillatory hierarchy controlling neuronal excitability and stimulus processing in the auditory cortex. *Journal of Neurophysiology* 94**,** 1904-1911.

Lee, C.C., and Sherman, S.M. (2008). Synaptic Properties of Thalamic and Intracortical Inputs to Layer 4 of the First- and Higher-Order Cortical Areas in the Auditory and Somatosensory Systems. *Journal of Neurophysiology* 100**,** 317-326.

Lee, S.H., Rosenmund, C., Schwaller, B., and Neher, E. (2000). Differences in Ca2+ buffering properties between excitatory and inhibitory hippocampal neurons from the rat. *Journal of Physiology-London* 525**,** 405-418.

Li, C.Y., Poo, M.M., and Dan, Y. (2009). Burst spiking of a single cortical neuron modifies global brain state. *Science* 324**,** 643-646. doi: 10.1126/science.1169957.

Lubke, J., and Feldmeyer, D. (2007). Excitatory signal flow and connectivity in a cortical column: focus on barrel cortex. *Brain Struct.Funct.* 212**,** 3-17.

Lübke, J., Roth, A., Feldmeyer, D., and Sakmann, B. (2003). Morphometric analysis of the columnar innervation domain of neurons connecting layer 4 and layer 2/3 of juvenile rat barrel cortex. *Cerebral Cortex* 13**,** 1051-1063.

Luczak, A., Bartho, P., and Harris, K.D. (2013). Gating of sensory input by spontaneous cortical activity. *J.Neurosci.* 33**,** 1684-1695. doi: 33/4/1684 [pii];10.1523/JNEUROSCI.2928-12.2013 [doi].

Luczak, A., Bartho, P., Marguet, S.L., Buzsaki, G., and Harris, K.D. (2007). Sequential structure of neocortical spontaneous activity in vivo. *Proc.Natl.Acad.Sci.U.S.A* 104**,** 347-352.

Ma, Y., Hu, H., Berrebi, A.S., Mathers, P.H., and Agmon, A. (2006). Distinct subtypes of somatostatin-containing neocortical interneurons revealed in transgenic mice. *Journal of Neuroscience* 26**,** 5069-5082.

Macgregor, D.G., Chesler, M., and Rice, M.E. (2001). HEPES prevents edema in rat brain slices. *Neurosci.Lett.* 303**,** 141-144. doi: S0304394001016901 [pii].

Maclean, J.N., Watson, B.O., Aaron, G.B., and Yuste, R. (2005). Internal dynamics determine the cortical response to thalamic stimulation. *Neuron* 48**,** 811-823. doi: S0896-6273(05)01001-9 [pii];10.1016/j.neuron.2005.09.035 [doi].

Maier, A., Adams, G.K., Aura, C., and Leopold, D.A. (2010). Distinct superficial and deep laminar domains of activity in the visual cortex during rest and stimulation. *Frontiers in Systems Neuroscience* 4. doi: 10.3389/fnsys.2010.00031.

Manns, I.D., Sakmann, B., and Brecht, M. (2004). Sub- and suprathreshold receptive field properties of pyramidal neurones in layers 5A and 5B of rat somatosensory barrel cortex. *Journal of Physiology-London* 556**,** 601-622.

Markram, H., Toledo-Rodriguez, M., Wang, Y., Gupta, A., Silberberg, G., and Wu, C.Z. (2004). Interneurons of the neocortical inhibitory system. *Nature Reviews Neuroscience* 5**,** 793-807.

Maunsell, J.H., and Gibson, J.R. (1992). Visual response latencies in striate cortex of the macaque monkey. *J.Neurophysiol.* 68**,** 1332-1344.

Mccormick, D.A., Shu, Y., Hasenstaub, A., Sanchez-Vives, M., Badoual, M., and Bal, T. (2003). Persistent Cortical Activity: Mechanisms of Generation and Effects on Neuronal Excitability. *Cerebral Cortex* 13**,** 1219-1231.

Metherate, R., and Aramakis, V.B. (1999). Intrinsic electrophysiology of neurons in thalamorecipient layers of developing rat auditory cortex. *Brain Research* Developmental Brain Research. 115**,** 131-144.

Metherate, R., Cox, C.L., and Ashe, J.H. (1992). Cellular bases of neocortical activation: modulation of neural oscillations by the nucleus basalis and endogenous acetylcholine. *J.Neurosci.* 12**,** 4701-4711.

Metherate, R., and Cruikshank, S.J. (1999). Thalamocortical inputs trigger a propagating envelope of gamma-band activity in auditory cortex in vitro. *Experimental Brain Research* 126**,** 160-174.

Mitani, A., and Shimokouchi, M. (1985). Neuronal connections in the primary auditory cortex: an electrophysiological study in the cat. *J.Comp Neurol.* 235**,** 417-429.

Mitzdorf, U. (1985). Current source-density method and application in cat cerebral cortex: investigation of evoked potentials and EEG phenomena. *Physiol Rev.* 65**,** 37-100.

Mountcastle, V.B. (1997). The columnar organization of the neocortex. *Brain* 120 (Pt 4)**,** 701-722.

Mountcastle, V.B., Davies, P.W., and Berman, A.L. (1957). Response properties of neurons of cat's somatic sensory cortex to peripheral stimuli. *J Neurophysiol* 20**,** 374-407.

Oswald, A.M., and Reyes, A.D. (2008). Maturation of intrinsic and synaptic properties of layer 2/3 pyramidal neurons in mouse auditory cortex. *J.Neurophysiol.* 99**,** 2998-3008. doi: 01160.2007 [pii];10.1152/jn.01160.2007 [doi].

Oswald, A.M., and Reyes, A.D. (2011). Development of inhibitory timescales in auditory cortex. *Cereb.Cortex* 21**,** 1351-1361. doi: bhq214 [pii];10.1093/cercor/bhq214 [doi].

Pasley, B.N., Allen, E.A., and Freeman, R.D. (2009). State-dependent variability of neuronal responses to transcranial magnetic stimulation of the visual cortex. *Neuron* 62**,** 291-303. doi: S0896-6273(09)00211-6 [pii];10.1016/j.neuron.2009.03.012 [doi].

Paxinos, G., and Franklin, K.B.J. (2003). *The Mouse Brain in Stereotaxic Coordinates.* San Diego, CA: Academic Press.

Petermann, T., Thiagarajan, T.C., Lebedev, M.A., Nicolelis, M.a.L., Chialvo, D.R., and Plenz, D. (2009). Spontaneous cortical activity in awake monkeys composed of neuronal avalanches. *Proceedings of the National Academy of Sciences* 106**,** 15921-15926. doi: 10.1073/pnas.0904089106.

Peters, A., and Payne, B.R. (1993). Numerical relationships between geniculocortical afferents and pyramidal cell modules in cat primary visual cortex. *Cereb.Cortex* 3**,** 69-78.

Petersen, C.C.H., Hahn, T.T.G., Mehta, M., Grinvald, A., and Sakmann, B. (2003). Interaction of sensory responses with spontaneous depolarization in layer 2/3 barrel cortex. *Proceedings of the National Academy of Sciences of the United States of America* 100**,** 13638-13643.

Pettersen, K.H., Devor, A., Ulbert, I., Dale, A.M., and Einevoll, G.T. (2006). Current-source density estimation based on inversion of electrostatic forward solution: effects of finite extent of neuronal activity and conductivity discontinuities. *J.Neurosci.Methods* 154**,** 116-133. doi: S0165-0270(05)00454-1 [pii];10.1016/j.jneumeth.2005.12.005 [doi].

Reed, J.L., and Kaas, J.H. (2010). Statistical analysis of large-scale neuronal recording data. *Neural Networks* 23**,** 673-684.

Rigas, P., and Castro-Alamancos, M.A. (2007). Thalamocortical Up states: differential effects of intrinsic and extrinsic cortical inputs on persistent activity. *The Journal of Neuroscience* 27**,** 4261-4272.

Rigas, P., and Castro-Alamancos, M.A. (2009). Impact of persistent cortical activity (up states) on intracortical and thalamocortical synaptic inputs. *Journal of Neurophysiology* 102**,** 119-131.

Romand, S., Wang, Y., Toledo-Rodriguez, M., and Markram, H. (2011). Morphological development of thick-tufted layer v pyramidal cells in the rat somatosensory cortex. *Front Neuroanat.* 5**,** 5. doi: 10.3389/fnana.2011.00005 [doi].

Rose, H.J., and Metherate, R. (2005). Auditory thalamocortical transmission is reliable and temporally precise. *Journal of Neurophysiology* 94**,** 2019-2030.

Sakata, S., and Harris, K.D. (2009). Laminar structure of spontaneous and sensory-evoked population activity in auditory cortex. *Neuron* 64**,** 404-418. doi: S0896-6273(09)00720-X [pii];10.1016/j.neuron.2009.09.020 [doi].

Sakata, S., and Harris, K.D. (2012). Laminar-dependent effects of cortical state on auditory cortical spontaneous activity. *Front Neural Circuits.* 6**,** 109. doi: 10.3389/fncir.2012.00109 [doi].

Sanchez-Vives, M.V., and Mccormick, D.A. (2000). Cellular and network mechanisms of rhythmic recurrent activity in neocortex. *Nat.Neurosci.* 3**,** 1027-1034.

Schiff, M.L., and Reyes, A.D. (2012). Characterization of thalamocortical responses of regular-spiking and fast-spiking neurons of the mouse auditory cortex in vitro and in silico. *Journal of Neurophysiology* 107**,** 1476-1488.

Schoonover, C.E., Tapia, J.-C., Schilling, V.C., Wimmer, V., Blazeski, R., Zhang, W., Mason, C.A., and Bruno, R.M. (2014). Comparative Strength and Dendritic Organization of Thalamocortical and

Corticocortical Synapses onto Excitatory Layer 4 Neurons. *The Journal of Neuroscience* 34**,** 6746-6758. doi: 10.1523/jneurosci.0305-14.2014.

Shen, J.X., Xu, Z.M., and Yao, Y.D. (1999). Evidence for columnar organization in the auditory cortex of the mouse. *Hearing Research* 137**,** 174-177.

Shu, Y.S., Hasenstaub, A., Badoual, M., Bal, T., and Mccormick, D.A. (2003). Barrages of synaptic activity control the gain and sensitivity of cortical neurons. *Journal of Neuroscience* 23**,** 10388-10401.

Singer, W. (2013). Cortical dynamics revisited. *Trends in Cognitive Sciences* 17**,** 616-626. doi: http://dx.doi.org/10.1016/j.tics.2013.09.006.

Smith, P.H., and Populin, L.C. (2001). Fundamental differences between the thalamocortical recipient layers of the cat auditory and visual cortices. *J.Comp Neurol.* 436**,** 508-519.

Smith, P.H., Uhlrich, D.J., Manning, K.A., and Banks, M.I. (2012). Thalamocortical projections to rat auditory cortex from the ventral and dorsal divisions of the medial geniculate nucleus. *J.Comp Neurol.* 520**,** 34-51. doi: 10.1002/cne.22682 [doi].

Steriade, M., Mccormick, D.A., and Sejnowski, T.J. (1993). Thalamocortical oscillations in the sleeping and aroused brain. *Science* 262**,** 679-685.

Steriade, M., Timofeev, I., and Grenier, F. (2001). Natural waking and sleep states: A view from inside neocortical neurons. *Journal of Neurophysiology* 85**,** 1969-1985.

Stroh, A., Adelsberger, H., Groh, A., Ruhlmann, C., Fischer, S., Schierloh, A., Deisseroth, K., and Konnerth, A. (2013). Making waves: initiation and propagation of corticothalamic Ca2+ waves in vivo. *Neuron* 77**,** 1136-1150. doi: 10.1016/j.neuron.2013.01.031.

Sugimoto, S., Sakurada, M., Horikawa, J., and Taniguchi, I. (1997). The columnar and layer-specific response properties of neurons in the primary auditory cortex of Mongolian gerbils. *Hearing Research* 112**,** 175-185.

Sun, Y.J., Kim, Y.J., Ibrahim, L.A., Tao, H.W., and Zhang, L.I. (2013). Synaptic mechanisms underlying functional dichotomy between intrinsic-bursting and regular-spiking neurons in auditory cortical layer 5. *J Neurosci* 33**,** 5326-5339. doi: 10.1523/JNEUROSCI.4810-12.2013.

Tan, A.Y., Chen, Y., Scholl, B., Seidemann, E., and Priebe, N.J. (2014). Sensory stimulation shifts visual cortex from synchronous to asynchronous states. *Nature* 509**,** 226-229. doi: 10.1038/nature13159.

Tan, Z., Hu, H., Huang, Z.J., and Agmon, A. (2008). Robust but delayed thalamocortical activation of dendritic-targeting inhibitory interneurons. *Proc.Natl.Acad.Sci.U.S.A* 105**,** 2187-2192. doi: 0710628105 [pii];10.1073/pnas.0710628105 [doi].

Theyel, B.B., Llano, D.A., and Sherman, S.M. (2010). The corticothalamocortical circuit drives higher-order cortex in the mouse. *Nat Neurosci* 13**,** 84-88.

Thomson, A., and Bannister, A. (1998). Postsynaptic pyramidal target selection by descending layer III pyramidal axons: dual intracellular recordings and biocytin filling in slices of rat neocortex. *Neuroscience* 84**,** 669-683.

Thomson, A.M., and Bannister, A.P. (2003). Interlaminar connections in the neocortex. *Cereb.Cortex* 13**,** 5-14.

Thomson, A.M., and Lamy, C. (2007). Functional maps of neocortical local circuitry. *Front Neurosci* 1**,** 19-42. doi: 10.3389/neuro.01.1.1.002.2007 [doi].

Thomson, A.M., West, D.C., Wang, Y., and Bannister, A.P. (2002). Synaptic Connections and Small Circuits Involving Excitatory and Inhibitory Neurons in Layers 2–5 of Adult Rat and Cat Neocortex: Triple Intracellular Recordings and Biocytin Labelling In Vitro. *Cerebral Cortex* 12**,** 936-953. doi: 10.1093/cercor/12.9.936.

Verbny, Y.I., Erdelyi, F., Szabo, G., and Banks, M.I. (2006). Properties of a population of GABAergic cells in murine auditory cortex weakly excited by thalamic stimulation. *J.Neurophysiol.* 96**,** 3194-3208.

Wang, Y., Toledo-Rodriguez, M., Gupta, A., Wu, C., Silberberg, G., Luo, J., and Markram, H. (2004). Anatomical, physiological and molecular properties of Martinotti cells in the somatosensory cortex of the juvenile rat. *J.Physiol* 561**,** 65-90.

Warren, R.M. (1970). Perceptual restoration of missing speech sounds. *Science* 167**,** 392-393.

Watson, B.O., Maclean, J.N., and Yuste, R. (2008). UP states protect ongoing cortical activity from thalamic inputs. *PLoS.One.* 3**,** e3971. doi: 10.1371/journal.pone.0003971 [doi].

Wester, J.C., and Contreras, D. (2012). Columnar interactions determine horizontal propagation of recurrent network activity in neocortex. *J.Neurosci.* 32**,** 5454-5471. doi: 32/16/5454 [pii];10.1523/JNEUROSCI.5006-11.2012 [doi].

White, B., Abbott, L.F., and Fiser, J. (2012). Suppression of cortical neural variability is stimulus- and state-dependent. *J.Neurophysiol.* 108**,** 2383-2392. doi: jn.00723.2011 [pii];10.1152/jn.00723.2011 [doi].

Chapter 4

This Chapter is a draft of a manuscript that will be published in the future.

Inhibitory control of network activity in auditory cortex by somatostatin- and parvalbumin-positive interneurons

Bryan M. Krause, Sean M. Grady, Aeyal Raz, Daniel J. Uhlrich, Matthew I. Banks

Abstract

Inhibitory cells play a substantial, if not dominant, role in regulating network activity and in responses to sensory stimuli. Neocortical inhibitory cells are comprised of diverse subtypes, some of which have been differentiated by their exclusive expression of certain proteins or peptides, as well as morphology, postsynaptic targets, and intrinsic electrophysiological properties. Previous work has shown that different inhibitory interneuron populations participate in UP states to a different degree, and their involvement varies between distinct cortical regions. We found that both PV+ and Sst+ interneurons are active throughout UP states in auditory cortex and fire considerably more spikes on average than pyramidal cells, but that there are subtle differences in the timing of each interneuron type's activity. PV+ cells are biased towards being active earlier in the UP state, whereas Sst+ cells tend to be more active later. PV+ cells also have more precise timing between trials. Additionally, pyramidal cell firing was more coupled to overall population activity than either interneuron subtype. Although activity of both interneuron populations affects levels of population activity, optogenetic inhibition of

PV+ cells additionally reduces UP state onset latency/threshold, whereas optogenetic inhibition of Sst+ cells slightly increases UP state duration.

Introduction

Auditory cortical neurons spike during evoked and spontaneous network bursts *in vivo* and in brain slices (DeWeese and Zador, 2006; Sakata and Harris, 2009; Luczak et al., 2013). These network bursts and similar activity in other areas have been referred to as UP states (Sanchez-Vives and McCormick, 2000; MacLean et al., 2005; Sakata and Harris, 2009), though the terminology is controversial in auditory cortex due to the relative brevity of the events compared to other cortical areas (Hromadka et al., 2013). *In vivo*, spontaneous UP states account for almost all spiking activity during sleep and quiet wakefulness, and can contribute to activity under anesthesia as well (Steriade et al., 1993; Contreras and Steriade, 1995; Steriade et al., 2001; Petersen et al., 2003a). Sensory stimuli during these conditions can also evoke UP states which are similar to spontaneous events (Luczak et al., 2009; Sakata and Harris, 2009; Luczak et al., 2013). *In vitro*, UP states occur spontaneously with physiologically low levels of calcium and magnesium ions (Sanchez-Vives and McCormick, 2000) and in response to electrical stimulation of thalamocortical afferents or white matter (Metherate and Cruikshank, 1999; Shu et al., 2003; Rigas and Castro-Alamancos, 2007; Krause et al., 2014). Direct stimulation of cortex can sometimes also evoke UP states (Raz et al., 2014; Neske et al., 2015), but in other cases may suppress network activity by driving inhibition (Rigas and Castro-Alamancos, 2007).

Excitation and inhibition are relatively balanced during UP states, as in non-pathological cortical activity more generally (Sanchez-Vives and McCormick, 2000; Beggs and Plenz, 2003; Compte et al., 2003; Shu et al., 2003; Wehr and Zador, 2003; Haider et al., 2006; Compte et al., 2009; Sanchez-Vives et al., 2010; Yizhar et al., 2011). Inhibition in cortical networks is mediated by a heterogeneous population of inhibitory interneurons (Markram et al., 2004; Kubota, 2014). Though there may be dozens of distinct

inhibitory cell types, a few classes can be defined by the expression of particular calcium binding proteins, peptides, and receptors (Kawaguchi and Kondo, 2002; Xu et al., 2010; Rudy et al., 2011). Of these, the most-studied types are those expressing either somatostatin (Sst) or parvalbumin (PV). Though distinct from other interneuron types, the Sst+ interneurons are themselves a heterogenous group, varying in spiking pattern, morphology, and post-synaptic connectivity, although they synapse exclusively on the dendrites of their postsynaptic targets (Markram et al., 2004; Kubota, 2014). Sst+ cells inhibit pyramidal cells and other interneuron subtypes (including PV+ cells) but do not typically inhibit other Sst cells (Silberberg and Markram, 2007; Murayama et al., 2009; Pfeffer et al., 2013). The PV class is more well-defined, and consists of fast-spiking cells of basket or chandelier morphology that target somatic and axonal regions, respectively, of post-synaptic cells (Kawaguchi and Kubota, 1998; Kubota et al., 2011). PV+ cells can inhibit each other, but do not typically inhibit other interneuron classes (Pfeffer et al., 2013).

The functional role of different interneuron populations in modulating cortical UP states is not yet clear. Limited blockade of GABAergic transmission increases spontaneous UP state intensity but decreases duration and prolongs the period between UP states; higher levels of GABAergic antagonists result in epileptiform activity (Sanchez-Vives et al., 2010). During spontaneous UP states in cortical slices from young (P12-17) mice, PV cells are active early and decrease firing later in UP states, whereas Sst cells are active later in UP states (Fanselow and Connors, 2010; Neske et al., 2015). The causes of these differences are likely due to differences in short term plasticity at glutamatergic synapses onto interneurons, as excitatory synapses on PV cells tend to show short-term depression whereas synapses on Sst cells show paired-pulse facilitation (Reyes et al., 1998), as well as intrinsic integrative properties.

Sst cells in the superficial layers target nearby pyramidal cells without much organization or specificity (Fino and Yuste, 2011) (but see (Reyes-Puerta et al., 2015)). Together with their facilitating inputs from pyramidal cells (Reyes et al., 1998), this suggests that they control global activity levels and

are likely to be engaged during UP states (but see (Tahvildari et al., 2012)). Based on their preferential inhibition of the distal dendrites, activity in Sst cells is likely to block top-down and modulatory inputs that target those distal dendrites. Consistent with this idea, Sst+ cells in somatosensory cortex are suppressed during active whisking by activation of VIP interneurons, which may enhance top-down inputs to distal dendrites that are normally inhibited by the Sst+ cells (Gentet et al., 2012; Lee et al., 2013b; Pfeffer et al., 2013; Pi et al., 2013; Francavilla et al., 2015). Sst+ cells are also a selective target of cholinergic neuromodulation (Beierlein et al., 2000; Fanselow et al., 2008). In V1, acetylcholine preferentially activates Sst interneurons in superficial layers, which leads to desynchronization of the network (Chen et al., 2015). Cholinergic agonists also suppress synchronous activity in S1 during active whisking (Eggermann et al., 2014), though it is unclear whether this effect is directly mediated by Sst+ interneurons given the previously mentioned suppression of Sst+ cells by VIP+ cells under similar conditions.

PV+ cells are notable for their role in feedforward inhibition, both in hippocampus and neocortex. Because PV+ cells can fire so quickly after an input, they can constrain the firing of excitatory cells to a much narrower window than the relatively slow time course of EPSPs would afford (Pouille and Scanziani, 2001; Wehr and Zador, 2003; Cruikshank et al., 2007). Feed-forward inhibition is strong in auditory cortex and important for precise response timing and stimulus selectivity (Wehr and Zador, 2003; Zhang et al., 2003). However, the role of PV+ cells with respect to persistent network activity is less clear. Gamma oscillations occur during both spontaneous and evoked UP states *in vivo* and *in vitro* (Steriade et al., 1996; Metherate and Cruikshank, 1999; Compte et al., 2008), and likely depend on PV+ cells(Wang and Buzsaki, 1996; Cardin et al., 2009). Gamma oscillations synchronize firing in the network to high precision (Engel and Singer, 2001), and in this way the role of PV+ cells for ongoing and feed-forward stimuli is similar: to refine the timing of spiking in the network. Importantly, despite the strong influence of PV+ cells on their post-synaptic targets, their self-inhibition and structured firing means that

PV+ cells leave windows for target cells to spike even when the average inhibitory conductance over a long time period is high. Postinhibitory rebound resulting from PV+ cell activation can even promote spiking activity and network excitation (Sessolo et al., 2015).

Recent work in somatosensory and entorhinal cortex has shown that different interneuron subtypes participate at different times during cortical UP states, and that there is variation between cortical areas (Fanselow and Connors, 2010; Tahvildari et al., 2012; Neske et al., 2015). Here, we study the participation of Sst and PV cells in UP states in auditory thalamocortical slices and also test the effect of inhibiting each cell population on the activity in the rest of the network. We find that interneurons are the most active cells during UP states, but in temporal patterns that are distinct between the two classes of cells, similar to differences seen in other cortical areas. We observed more activity in Sst+ cells compared to reports from other cortical areas (Tahvildari et al., 2012; Neske et al., 2015), on par with activity in PV+ cells. We find that inactivating either Sst or PV cells increases overall activity during the UP state, but that their effects on UP state latency and duration differ.

Methods

Mice and surgical procedures

All procedures were approved by the University of Wisconsin-Madison Animal Care and Use Committee and conform to American Physiological Society/National Institutes of Health guidelines. To identify specific interneuron types, heterozygous Sst-tdTomato and PV-tdTomato mice were bred from homozygous cre-dependent tdTomato (B6.Cg-*Gt(ROSA)26Sor*$^{tm9(CAG\text{-}tdTomato)Hze}$/J; The Jackson Laboratory) male and Sst-cre (STOCK Sst$^{tm2.1(cre)Zjh}$/J; The Jackson Laboratory) or PV-cre (B6.129P2 - Pvalb$^{tm1(cre)Arbr}$/J; The Jackson Laboratory) female mice. Untargeted patch clamp recordings were also made from B6CBAF1/J mice (F1 hybrid of C57/B6 and CBA/J mice; The Jackson Laboratory). Some of the cre-

expressing animals were used for optogenetic activation/inactivation experiments and were injected with adeno-associated virus expressing cre-dependent halorhodopsin-YFP (AAV5/EF1α-DIO-eNpHR3.0-eYFP, Gene Therapy Center Vector Core, University of North Carolina at Chapel Hill, Chapel Hill, NC) or cre-dependent channelrhodopsin-YFP (AAV5/EF1α-DIO-hChR2(H134R)-eYFP). Injections were performed on 3-5 week old mice of both genders. Animals were anesthetized with isoflurane (1.5-2%) and craniotomized above auditory cortex based on stereotaxic coordinates (Franklin and Paxinos, 2008). A total of 500-1000 nL of virus was injected into 2-3 sites spanning auditory cortex rostral-caudally approximately 500 µm from the lateral pial surface over 20-30 minutes (about 10 minutes per injection site). Injections were performed through a patch pipette broken to a tip diameter of approximately 50 µm and controlled with a Nanoject II (Drummond Scientific Company, Broomall, PA) mounted on a stereotaxic frame. Injected mice recovered for 3-5 weeks prior to preparation of brain slices.

Slice preparation

Auditory thalamocortical slices were prepared using a variation on previously established techniques (Cruikshank et al., 2002; Krause et al., 2014). 4-8 week old *de novo* mice or those recovered from surgery were deeply anesthetized with isoflurane and decapitated. Brains were blocked with three cuts (Figure 1A), each perpendicular to the preceding cut: first, a sagittal cut about 2 mm lateral to the midline, preserving the larger block; second, a 45° rostral-dorsal to caudal-ventral cut, preserving the dorsal/caudal block; and third, a cut 20° off the horizontal-caudal plane, preserving the lateral/caudal block. The resulting block was affixed to a vibrating microtome on the final cut face and sliced into 500 µm sections. Slices at this angle are roughly midway between the coronal-horizontal plane, such that 'caudal' regions of the slice are about equally 'dorsal,' but tilted slightly so that medial regions are ventral to lateral regions. In the adult mouse, this blocking procedure best preserves the ventral medial

geniculate nucleus (MGv) and primary auditory cortex (Au1) in the same slice along with the C-shaped thalamocortical fibers that travel rostal and ventral before arcing caudal on the way to auditory cortex (based on the Allen Mouse Brain Connectivity Atlas, http://connectivity.brain-map.org)(Oh et al., 2014).

During blocking and sectioning, slices were maintained in ice-cold cutting ACSF consisting of (in mM) 111 NaCl, 35 NaHCO3, 20 HEPES, 1.8 KCl, 1.05 CaCl2, 2.8 MgSO4, 1.2 KH2PO4, 10 glucose and bubbled with 95% O_2/5% CO_2. Once cut, slices were immediately placed in cutting ACSF warmed to 34°C, which was allowed to cool to room temperature over at least one hour. For the experiments, slices were moved to regular ACSF consisting of (in mM) 111 NaCl, 35 $NaHCO_3$, 20 HEPES, 1.8 KCl, 2.1 $CaCl_2$, 1.4 $MgSO_4$, 1.2 KH_2PO_4, and 10 glucose and warmed to 30-33°C and bubbled with 95% O_2/5% CO_2.

Electrophysiology and data analysis

Bipolar stimulating electrodes (100KΩ, FHC) were placed into the thalamocortical fiber bundle rostral to hippocampus. Current pulses consisted of a 200 μs biphasic square wave of amplitude 10-100 μA. Responses to thalamocortical stimulation were measured in layer 4 of Au1 at 250 μm increments, using a glass patch pipette filled with ACSF and broken to a resistance of 500-700 kΩ. These layer 4 recordings were used to identify the cortical location with the largest early (<10 ms latency) extracellular responses; further recordings were focused on the vertical strip of cortex ('column') at this location. During data collection, the stimuli were delivered as a train of 4 pulses at 40 Hz, which reliably evokes UP state activity (Krause et al., 2014). The stimulus intensity used for a given experiment was adjusted to give UP states that occurred reliably after pulse 2 and before pulse 4 in the train and likely depended on the integrity of thalamocortical fibers in a given slice.

For single-cell recordings, Sst+ or PV+ interneurons were patched using a combination of fluorescence and differential interference contrast (DIC) microscopy. Light from a mercury arc lamp (X-Cite exacte; Lumen Dynamics, Mississauga, Ontario, Canada) passed through an excitation filter (540-580 nm; Chroma, Bellows Falls, VT) and broad spectrum transmitted light were presented simultaneously to identify labeled cells and surrounding tissue features, respectively, and emission/transmittance (emission filter 593-667 nm; Chroma) captured on a CCD camera (C9100-02, Hamamatsu Corp., Sewickley, PA). A borosilicate micropipette (KG-33, 1.7 mm OD, 1.1 mm ID; King Precision Glass, Claremont, CA), pulled to give open-tip resistance of 3-5 MΩ (P-1000; Sutter Instruments, Novato, CA) filled with intracellular solution (in mM: 140 K-gluconate, 10 NaCl, 10 HEPES, 0.1 EGTA, 2 MgATP, and 0.3% biocytin; pH 7.2), was advanced to contact the targeted cell and a >1GΩ seal made with weak negative pressure. Pyramidal cells were patched similarly, with transmitted light only, and identified based on their visible triangular morphology with apical dendrite under DIC optics. Spikes were recorded in the on-cell configuration in voltage-clamp in response to trains of 4x40 Hz thalamocortical stimuli of varying intensities. After on-cell recording, whole-cell access was established and recordings continued in current-clamp mode. In addition to cre-dependent tdTomato expression and morphological characteristics, cell types were identified by their characteristic responses to current pulses, particularly spiking patterns and rates (i.e., regular-spiking vs. fast spiking). For all recordings, either voltage or current was low-pass filtered at 4 KHz and digitized at 40 KHz.

During all experiments, including during single-cell recordings, extracellular population recordings in layer 5 were used to measure UP state activity. Broken glass pipettes (as above) filled with regular ACSF were inserted into layer 5 slightly deeper than halfway between pia and white matter (and in some experiments also in layers 2/3). Data were low-pass filtered at 4 KHz during collection and digitized at 40 KHz. Stimulus artifacts were blanked by interpolating between points before and after. Extracellular voltage was filtered between 300-5000 Hz, full-wave rectified, and smoothed by

convolution with a Gaussian kernel with unit integral and σ=2 ms to produce a smoothed MUA signal (smMUA), also referred to as "population activity" throughout this paper. A threshold for elevated activity was defined as the geometric mean of all the points greater than the arithmetic mean of the smMUA signal (Sakata and Harris, 2009; Krause et al., 2014). UP state onsets were defined as periods above threshold for at least 80% of points in a 20 ms window, and UP state offsets defined as a decrease below the threshold for 80% of points in a 50 ms window. These criteria reliably identified UP states observed by eye, and did not include early responses to individual stimulus pulses (which are too brief).

To calculate firing rates during UP states, spike trains recorded from single cells via patch clamp were convolved with a Gaussian kernel (σ=2 ms). The segment from UP state onset to offset was resampled at 1001 points on the interval [0 1], with 0 representing the time of UP state onset and 1 representing UP state offset, to allow for comparison between trials and cells. For all other analyses comparing spikes to population activity, the entire smoothed population activity signal was used and determining the onset and offset of UP states was not necessary. To relate the timing of spikes to population activity, the integral of population activity over the interval [0 200 ms] after stimulus onset (this interval contained all recorded spikes) was normalized to 1. For each cell, the average spike timing relative to population was calculated as the average sum of population activity on the interval [0 t_{Spike}].

The spike-triggered population coupling (stPR) was adapted from (Okun et al., 2015). It is calculated as the sum of the element-wise product of a vector representing population activity and a vector representing the smoothed activity of a single cell, normalized to firing rate. The smoothing kernel used for stPR calculation was normalized to its root sum square, such that the pointwise product between the kernel and itself would equal 1. To compare between experiments, the stPR was normalized to the auto-coupling of the population activity with itself, such that a spike train that perfectly followed the population rate would have a value of 1. Similarly, coupling between membrane potential and population activity was calculated by subtracting the resting membrane potential, median

filtered over 3 ms to remove spikes, and calculating the sum of the element-wise product with the population activity.

The spike-time tiling coefficient was adapted from (Cutts and Eglen, 2014) to measure the precision of spike timing in a single cell across trials. Thus, instead of comparing between two simultaneously recorded units as originally described, the measure was computed between all permutations of trials for a given unit. The calculation depends on a free parameter Δt, which defines the window on which spikes are deemed "coincident." Then, two proportions are calculated, P_A which is the proportion of spikes from spike train A that are within Δt of any spike in spike train B, and T_B, the proportion of all time that is within Δt of any spike in spike train B. Then, the STTC is calculated as:

$$STTC = \frac{1}{N(N-1)} \sum_{1 \geq A \geq N} \sum_{B \neq A} \frac{P_A - T_B}{1 - P_A T_B}$$

This measure is high (approaching 1) when all spikes are at the same time as spikes in other trials, and zero for randomly distributed spikes. The STTC was only calculated for cells that fired at least one spike on more than 1/3 of trials.

Statistical comparisons for firing rates, coupling measure, and the tiling coefficient used standard one-way ANOVA when normality was not rejected using a one-way Kolmogorov-Smirnov test, otherwise a Kruskal-Wallis test of analysis of variance by ranks was used. All statistical tests used the MATLAB (Mathworks, Natick, MA) Statistics Toolbox.

Optogenetic inhibition/excitation

Halorhodopsin was activated by passing light from the arc lamp through the microscope objective centered on the cortical region of study (10x) using a filter in the excitation range for

halorhodopsin (540-580 nm). The light was turned on 100 ms before stimulus onset and held on for a total of 500 ms. Light intensity was titrated for each experiment depending on gene expression levels, in the range of 10-50% of total light power. Channelrhodopsin was activated similarly, using a filter near the optimal excitation wavelength (475-505 nm). Light for channelrhodopsin activation was turned on for 2 ms in a train of 4x40 Hz pulses in synchrony with thalamocortical stimulation and used at 10% of total light power. Light-on trials were interleaved with light-off trials. The first 4 trials of either type were discarded because these trials often contained evoked UP states that differed substantially in magnitude and latency from subsequent events.

Linear mixed-effects model

To analyze the effect of optogenetic inactivation of different interneuron populations, we used a form of linear regression called linear mixed-effects modeling (Kristensen and Hansen, 2004; Winter, 2013). This approach differs from standard linear modeling in that it allows for controlling for random effects (often due to repeated measures within subjects), allowing for non-independent samples to be considered in a principled way. We used this method because although more traditional methods (t-tests) showed there were clear effects during individual experiments, these methods cannot be extended to between-experiments results (such as using repeated-measures ANOVA) without enforcing independence by summarizing each experiment with a single value for each condition (such as a mean or median) and therefore losing important information about within-subject variability or consistency.

The experimental design we used consisted of a response variable based on the population activity (integral, peak, UP state latency, or UP state duration), fixed effect of interneuron inactivation (LightOff/Sst+/PV+), and random effect of slice (experiment), with by-condition random slopes for the

effect of slice. In summary, the full model was as follows, with fixed effects as β,random effects as γ, inactivation *i* and slice *j*:

$$Population_{ij} = \beta_0 + \beta_1 (i) + \gamma_{0j} + \gamma_{1j} (i) + \varepsilon_{ij}$$

To determine whether the Inactivation term was significant, we used a likelihood ratio test, comparing the full model to a reduced model containing only random effects:

$$Population_{ij} = \beta_0 + \gamma_{0j} + \gamma_{1j} (i) + \varepsilon_{ij}$$

If the inactivation term significantly improved model likelihood, we further analyze the individual coefficients for Inactivation. If not, we would conclude there was no significant effect of interneuron inactivation in the measure of interest. To test for differential effects on superficial layer activity during UP states, we included measures of population activity recorded in layer 2/3 and added a fixed effect for Layer (L5 or L2/3, *k* in the equations below), interaction between Layer and optogenetic inactivation, and additional random slope for slice that depended on layer.

$$Population_{ijk} = \beta_0 + \beta_1 (i) + \beta_2 (k) + \beta_3 (i,k) + \gamma_{0j} + \gamma_{1j} (i) + \gamma_{2k} (i) + \varepsilon_{ij}$$

To determine whether the interaction between Inactivation and Layer was significant we compared likelihoods for the reduced model below, as above.

$$Population_{ijk} = \beta_0 + \beta_1 (i) + \beta_2 (k) + \gamma_{0j} + \gamma_{1j} (i) + \gamma_{2k} (i) + \varepsilon_{ij}$$

We report likelihood ratio tests using chi-squared values. Residuals were visually inspected to confirm homoscedasticity. For the latency and duration measures, heteroscedasticity was corrected by log-transforming the response variables. The log transformation changes the interpretation of the regression from finding the arithmetic mean of the response variable to the geometric mean, but otherwise the process of analysis is the same. For ease of interpretation, coefficient estimates for these models were exponentiated after fitting to express effects as percent change. For the plots in Figure 6I

and J, these percent values were multiplied by the intercept estimates to express values in the original time units. Coefficients for integral and amplitude measures are reported as mean ± SEM relative to control or each other; coefficients for latency and duration measures are reported with 95% confidence intervals after exponentiation. All data analysis and statistical comparisons used the MATLAB (Mathworks, Natick, MA) Statistics Toolbox and custom MATLAB software.

Results

Identification and properties of Sst-tdTomato and PV-tdTomato cells

Slices expressing tdTomato in Sst+ and PV+ cells showed distinct patterns of labeled cells (Figure 1B&E). Sst-tdTomato slices showed numerous somata in the infragranular layers, sparse labeling in the superficial layers, and a band of fibers in layer 1 (Figure 1B). PV-tdTomato slices showed a nearly complementary labeling pattern with densest expression in the granular layer (Figure 1E). PV-tdTomato expression was also biased towards the region of the slice corresponding to primary auditory cortex (Cruikshank et al., 2001), with weaker expression caudal/dorsally and rostral/ventrally. Electrophysiological properties of targeted interneurons were consistent with previous studies of Sst+ and PV+ cells (Figure 1C, F; Table 1). Sst-tdTomato cells (n=25 from 15 slices) (Figure 1D) had high input resistance, moderately wide action potential widths, showed spike-rate adaptation, and had longer time constants than PV-tdTomato cells (n=29 from 12 slices) (Table 1). Some also fired bursts of action potentials after hyperpolarization. PV-tdTomato cells (Figure 1G) were fast-spiking cells with low input resistance, narrow action potential width, little spike-rate adaptation, and short membrane time constants, and were more homogeneous than Sst-tdTomato cells in their intrinsic properties. Unlabeled regular-spiking and burst-spiking cells (putative pyramidal cells, n=46 from 10 slices) had even wider action potentials, lower maximum firing rates, more spike-rate adapation, and the longest time constants. Overall, input resistances were much higher than in a recent paper studying interneuron

participation in UP states (Neske et al., 2015), but consistent with a prior paper from the same group (Fanselow and Connors, 2010).

A minority of Sst-tdTomato cells had properties similar to classical PV+ cells; these cells could either be truly immunopositive for parvalbumin (and not somatostatin) but expressed somatostatin developmentally and therefore expressed cre-recombinase at some point in their history, leading to tdTomato expression(Hu et al., 2013), or they could represent "FS-like" Sst+ cells that do not express parvalbumin (Ma et al., 2006). However, taken as populations, the laminar distribution and electrophysiological properties of Sst-tdTomato and PV-tdTomato cells were clearly distinct. Both Sst-tdTomato and PV-tdTomato cells also had much higher EPSP slopes in response to thalamocortical stimulation compared to pyramidal cells (slopes were measured instead of amplitudes because of frequent contamination by UP state activity), and latencies were shorter in PV-tdTomato cells.

Spiking of identified inhibitory interneurons and pyramidal cells during UP states

Brief thalamocortical stimulus trains (4x40 Hz, 10-100uA) evoked extracellular potentials in layer 4 consistent with the latency of monosynaptic EPSPs (Cruikshank et al., 2002; Krause et al., 2014; Raz et al., 2014). At moderate to high intensities, thalamocortical stimuli also triggered later network events, as observed previously *in vitro* (Metherate and Cruikshank, 1999; Shu et al., 2003; MacLean et al., 2005; Krause et al., 2014) and with auditory stimuli *in vivo* (Curto et al., 2009; Luczak et al., 2009; Sakata and Harris, 2009; Luczak et al., 2013). We call these events "UP states," consistent with the terminology used by some (Sakata and Harris, 2009; Luczak et al., 2013) but not all groups who study network activity in auditory cortex (Hromadka et al., 2013). Onset, offset, and magnitude of UP states were measured based on high-frequency multiunit activity in layer 5 (Figure 2A; see Methods).

We first investigated the firing properties of interneurons and pyramidal cells. In response to TC stimulation, some Sst-tdTomato and PV-tdTomato interneurons (5/25 and 13/29 respectively) fired early action potentials prior to UP state onset. By contrast, none of the pyramidal cells recorded in these experiments fired early action potentials (0/46), although occasional pyramidal cells that fire prior to UP states have been observed in a prior study (Krause et al., 2014). However, the majority of spikes fired by all three cell types (Sst-tdTomato, PV-tdTomato, and putative pyramidal cells) occurred during UP states (Figure 2B). During UP states, spiking in interneurons was denser and more consistent than in pyramidal cells. Compared to pyramidal cells, both Sst-tdTomato and PV-tdTomato cells fired on more trials (Figure 2C; $H(2)=25.93$, $p<.0001$; Pyr vs. Sst medians 0 vs. 1, $p=.0001$; Pyr vs. PV medians 0 vs. 1, $p=.0001$) and fired more spikes per trial (Figure 2D; $H(2)=33.18$, $p<.0001$; Pyr vs. Sst medians 0 vs. 2.6 $p<.0001$; Pyr vs. PV medians 0 vs. 2.7, $p<.0001$). Thus, although interneurons make up only 10 – 20% of neurons in auditory cortex, their firing activity positions them to exert strong control over thalamically-evoked network activity. There were no significant linear relationships between layer and firing rate or probability (i.e., the Pearson product-moment correlation coefficient was not significant; data not shown) for any of the cell types, nor were there any apparent non-linear relationships.

Firing patterns during UP states varied between cell types (Figure 3A-C). We quantified this by calculating the average firing rate of each cell after normalizing the durations of UP states, then averaging across cells within each cell type (Fig. 3D-E). Plots of raw firing rate (Fig. 3D) illustrate the large difference in firing rates between interneurons and pyramidal cells. By normalizing the firing rates to their peaks, we can compare the time course of activity within each cell type compared to the population activity (Fig. 3E). Though some activity from each population was observed at every stage of the UP state, the time course of activity was distinct for different cell types (Figure 3E). Of the three cell types, PV-tdTomato cells tracked the population activity closest throughout the entire UP state. Pyramidal cells followed the time course of the first half of the UP state population activity, while their

activity deviated negatively from the population activity in the second half of the UP state. Sst-tdTomato cells exhibited the opposite pattern, lagging the population activity early in the UP state and then tracking it more faithfully late in the UP state. To quantify these differences, we computed the average fraction of population activity occurring before each spike for the three cell types (Figure 3F). Although the average spike timing was near the center of mass of the population activity (i.e. population fraction = 0.5) for all three cell populations, activity in Sst-tdTomato cells was shifted to later times and PV-tdTomato cells shifted earlier compared to each other ($F(2,63)=3.93$, $p=.025$; Sst vs. PV $p=.018$). Neither group was significantly different from pyramidal cells. There were no significant linear relationships between layer and average spike timing (i.e., the Pearson product-moment correlation coefficient was not significant; data not shown) for any of the cell types, nor were there any apparent non-linear relationships.

Coupling of population and single-cell firing

Although the analysis of Figure 3D-F indicates the time course of firing, it does not quantify the tendency of cells to fire at times of high population activity. Typically, such tendencies are quantified using a cross-correlation or similar measure, but these measures are firing rate-dependent. Given that we know there are substantial differences in firing rates between different cell types we recorded, we sought an alternative measure: the spike-triggered population coupling (stPC) (Figure 3G). The stPC is an average of population activity at the time of each spike (see Methods, similar to (Okun et al., 2015)), calculated at a range of lags between population and single-cell activity. Cells that fire reliably relative to maximal population activity have high population coupling. Importantly, the population coupling measure is not affected by firing rate differences alone, as observed by removing spikes at random and recalculating the measure (see (Okun et al., 2015); we confirmed this was true with our data, as well;

data not shown). At zero lag (Figure 3H), pyramidal cells had significantly greater population coupling than Sst-tdTomato cells ($H(2)=12.08$, $p=.0024$; Pyr vs. Sst $p=.0018$) and a trend toward greater population coupling than PV-tdTomato cells (Pyr vs. PV $p=.054$). At the peak lag of stPC for each cell (Figure 3I), pyramidal cells had greater population coupling than both interneuron types ($H(2)=19.42$, $p<.0001$; Pyr vs. Sst $p=.0001$, Pyr vs. PV $p=.0016$). The result that pyramidal cells are closely coupled to the population is not surprising, given that the peak population activity also likely represents the peak of excitation during the UP state. The interneuron populations may be less coupled to the population activity because their spikes tended to be more distributed throughout the UP state duration, rather than being concentrated at the peak of the population activity. (e.g., see Figure 3B-C). Because pyramidal cells fired sparsely, and to determine whether this sparse activity was responsible for the differences in population coupling, we computed a similar measure of coupling between the membrane potential and population activity. If no differences in membrane potential coupling were observed, we could conclude that sparse firing was solely the cause of increased population coupling in pyramidal cells. We found that membrane potentials were tightly coupled to population activity in all cell types (Figure 3J), as expected by the nature of UP state activity; the difference between cell populations did not reach the significance threshold ($H(2)=5.49$, $p=.064$), though there was a trend that followed a similar pattern to spike coupling. Therefore, it is likely that differences in the coupling of membrane potential to population activity during the UP state partially contribute to the tight coupling of pyramidal cells to population activity, but that sparse firing in pyramidal cells contributes as well.

There was a significant correlation between cortical depth and spike-population coupling in pyramidal cells both at zero-lag ($R^2=0.26$, $p=.019$) (Figure 3K) and peak lag of the stPC ($R^2=0.25$, $p=.022$) (not shown). Specifically, supragranular pyramidal cells were more tightly coupled to population activity than infragranular cells. There were no significant linear relationships between layer and population coupling for the other cell types or measures.

Although timing relative to population activity may carry important coding information, measures of spike timing or precision more often relate to an external event such as a sensory stimulus, or electrical stimulation in the slice. Spike timing relative to stimulus features is very precise earlier in the auditory hierarchy (Langner, 1992; Krishna and Semple, 2000; Bartlett and Wang, 2007; Wang et al., 2008), and the specializations in auditory cortex for rapid processing of incoming input suggests that timing information is also important in auditory cortex (Rose and Metherate, 2005; Kayser et al., 2010). Although inhibitory cells could also have precise timing relative to peripheral events, our expectation is that precise timing is most important in pyramidal cells (as the output cells of cortex). Many measures have been suggested for quantifying spike timing, but creating a firing-rate independent measure of correlative features such as spike timing across trials is nontrivial (Joris et al., 2006; Cohen and Kohn, 2011; Cutts and Eglen, 2014). We used a variation of the "spike-time tiling coefficient" to quantify the consistency of spike timing within individual cells across trials. The original method was developed to avoid firing-rate influences on measures of synchrony between two separate cells recorded simultaneously (Cutts and Eglen, 2014). We modified this approach to consider spike trains on separate trials from the same cell. Unlike the population-coupling measure, the auto-tiling coefficient measure is primarily affected by timing relative to the thalamocortical stimulus, because this is the only timing guaranteed to be time-locked across trials, whereas the population activity is not necessarily time-locked. We calculated the STTC at a range of coincidence intervals (Figure 4A); the STTC tends to increase as the coincidence interval increases because within a wider window, more spikes are considered coincident. Although there is a lot of variation within cell types, PV-tdTomato cells tended to have higher STTC, particularly at more precise coincidence levels. At 1 ms precision (Figure 4B), PV-tdTomato cells were significantly better timed than Sst-tdTomato cells ($H(2)=9.37$, $p=.0092$; Sst vs. PV $p=.012$), and trended towards being better timed than pyramidal cells (Pyr vs. PV $p=.062$).

There was a significant correlation between depth and STTC at 1 ms precision in pyramidal cells (R^2=0.52, p=.0036) and Sst-tdTomato cells (R^2=0.21, p=.035), but not for PV-tdTomato cells (R^2=0.0005, p=.93) (Figure 4C). For both pyramidal and Sst-tdTomato cells, supragranular cells fired more consistently from trial to trial than infragranular cells. This result is consistent with the relationship between spike timing and population activity for the pyramidal cells, and also consistent with high precision in sparse-firing layer 2/3 pyramidal cells.

Optogenetic inhibition of PV+ and Sst+ cells

Thus far, we have shown that inhibitory interneurons are strongly recruited during UP states and have firing patterns that are distinct from pyramidal cells. However, the functional role of these cells in regulating or shaping UP state activity is unclear. To study the functional role of PV+ or Sst+ interneurons, we injected PV-cre x tdTomato (n=4) and Sst-cre x tdTomato (n=13) mice with AAV carrying cre-dependent halorhodopsin to reduce firing in different interneuron populations (Figure 5). The presence of tdTomato in these animals is not necessary for viral expression but was helpful in identifying potentially virus-expressing cells since their somata are so clearly labeled. We note that although the PV-tdTomato and Sst-tdTomato cell classes may have some limited overlap because of developmental expression of cre-recombinase, the optogenetics experiments may be more selective because they are based on viral injections in adult animals where expression of parvalbumin or somatostatin is more likely to be static.

Viral injection sites were identified by fluorescence of YFP included with halorhodopsin as a fusion protein (Figure 5A, D). To ensure that halorhodopsin expression and activation hyperpolarized interneurons, we recorded whole-cell from tdTomato-positive cells in the vicinity of the injection site (Figure 5B, E). 200 ms pulses of yellow light were delivered through the 10X microscope objective. Even

weak light pulses caused robust hyperpolarization that peaked approximately 40 ms after light onset, and were sustained for the duration of the light (Figure 5C,F).

To test the effect on network activity of inactivating Sst+ and PV+ interneurons, we paired light activation of halorhodopsin with thalamocortical stimuli, and we measured effects on population activity (Figure 6). We found that halorhodopsin-mediated inhibition increased population activity magnitude when expressed in either PV+ or Sst+ interneurons, but there were differences between the two cell types in their effects on UP state latency and duration. Inhibition of Sst+ cells increased population activity relative to baseline (Figure 6A-B). To more clearly compare between light-on and light-off trials, in Figure 6C we plot the integral of the signal in Figure 6A (mean ± SE across trials). Small, early components spaced by 25 ms are early responses to thalamocortical stimuli, but the integral is dominated by the UP state which starts in this example around 80 ms. The light-on and light-off trials are indistinguishable until partway through the UP state when the integral increases at a faster rate in the light-on trials but begins to plateau in the light off trials, around 100-120 ms after the first thalamocortical stimulus. Inhibition of Sst+ cells could also prolong the UP state, evident between 150 and 200 ms in Figure 6B as well as in Figure 6C. Inhibition of PV+ cells also increased population activity relative to baseline, but additionally decreased the latency to UP state onset (Figure 6D-F). We quantified several measures of population activity to compare the effect of halorhodopsin expressed in each population: the integral and peak of population activity, the latency to UP state onset, and the UP state duration. We performed statistical analyses by fitting a linear mixed-effects model to the population activity measures (see Methods), using halorhodopsin inhibition (LightOff/Sst+/PV+) as a fixed effect and slice (i.e., “subject”) as a random effect. This approach allows us to use the reliability of these measures within subjects while drawing population level comparisons.

For the integral of population activity (Figure 6G), the full model was significantly better than the model without the halorhodopsin fixed effect ($\chi^2(2)=15.3$, $p=.00049$). Both Sst+ and PV+

halorhodopsin inhibition significantly increased the integral of population activity (Sst+ vs. control = .169 mV*ms ±.042, p=.000061; PV+ vs. control = .099 mV*ms ± .030, p=.00095), but were not significantly different from each other (p=0.19). Similarly, for the peak amplitude of population activity (Figure 6H) the full model was significantly better than the reduced model ($\chi^2(2)=14.78$, p=.00064). Inhibition of either Sst+ or PV+ cells significantly increased the peak amplitude of population activity (Sst+ vs. control = .00705 mV ± .00222, p=.0016; PV+ vs. control = .0119 mV ± .00244, p=.0000013), but were not significantly different from each other (p=0.11).

For UP state latency and duration measures, the response variables were log-transformed prior to regression; estimated coefficients are reported here in their exponentiated form (see Methods). For the UP state onset latency (Figure 6I), the halorhodopsin effect was significant ($\chi^2(2)=9.28$, p=.0096). Latencies were significantly decreased by halorhodopsin inhibition of either interneuron type (Sst+/control = 96.8%, p=.032, 95% CI [94.0% 99.7%]; PV+/control = 61.5%, p=.00088, 95% CI [46.2% 81.8%]), but much more for PV+ inhibition compared to Sst+ inhibition (PV+/Sst+ = 63.5%, p=.0020, 95% CI [47.7% 84.6%]). Although the onset latency effect of Sst+ inhibition was significant at the level of $\alpha=0.05$, we conclude from the small magnitude of the effect that Sst+ inhibition had little impact on UP state latency whereas PV+ inhibition had a large effect. Because our stimulus protocol is a train of pulses, it is likely that this reduction in latency indicates that UP states are occurring after fewer stimulus pulses, therefore reflecting a reduction in threshold for UP state activation.

Inhibition of interneurons by halorhodopsin also affected UP state duration (Figure 6J; $\chi^2(2)=15.2$, p=.00049), but in opposite directions depending on the type of interneuron inhibited. UP states were slightly longer when Sst+ cells were inactivated (Sst+ vs. control = 107%, p=.013, 95% CI [101% 113%]), whereas UP states were shorter when PV+ cells were inactivated (PV+ vs. control = 79.8%, p=.0000024, 95% CI [72.7% 87.6%]). This effect of producing intense, brief UP states is similar to that observed with moderate concentrations of GABAergic antagonists (Sanchez-Vives et al., 2010).

Effects in supragranular layers of optogenetic inhibition of PV+ and Sst+ cells

UP states can involve partial activation of the column primarily in infragranular layers, or involve the entire column including supragranular layers (Sakata and Harris, 2009; Krause et al., 2014). Given that UP states in the infragranular layers seem to be more robust than in the supragranular layers, we hypothesized that the supragranular layers might be more susceptible to inhibition and therefore more affected by suppression of inhibition. Therefore, we applied the previously described analysis of layer 5 population activity to population activity recorded simultaneously in layer 2/3 (Figure 7).

To incorporate supragranular recordings into our linear mixed effects model, we added an additional factor to our model, recording Layer, including an interaction term between Layer and Inactivation, as well as an additional random slope that depended on Layer and Slice (see Methods). Similar to the approach for Layer 5 data, we evaluated the suitability of the model by comparing to the likelihood of a reduced model, in this case with the interaction term omitted. The structure of the model was specified such that baseline (i.e., the intercept) corresponded to Layer 5 population activity with no light stimulation and model coefficients reflected the effects of inactivating Sst+ or PV+ cells, the effect of recording in layer 2/3 rather than layer 5 in the control, no-light condition, and interaction terms reflecting the difference in layer 2/3 compared to layer 5 measures during inactivation of Sst+ or PV+ cells after accounting for differences between layer 2/3 and layer 5 in the no-light condition. When differences are discussed in the context of interaction terms below, these differences incorporate any necessary adjustment for layer differences in the no-light condition. Therefore, interpretation of the interaction terms requires a consideration of the simple effects (i.e., Layer and Inactivation) as well.

For the integral of multiunit activity, inclusion of the interaction between Layer and Inactivation significantly improved the model ($\chi^2(2)=13.99$, $p=.00092$). Contrary to our expectations, the term for

Layer itself was not significant (L2/3 vs. L5 = 0.0067 mV*ms ± .093, p=.94), meaning that the integral of population activity was the same for layers 2/3 and 5, suggesting that UP state size was the same in infragranular and supragranular layers. The coefficient for Sst-inactivation*Layer was also not significant (L2/3 vs. L5 = -0.021 mV*ms ± 0.027, p=.44), indicating that Sst+ cells had no difference in influence on up states in layer 2/3 compared to layer 5. However, the PV-inactivation*Layer coefficient was significant and positive (L2/3 vs. L5 = 0.20 ± 0.051, p=.000053), indicating that inhibition of PV+ cells had a greater impact on UP state activity in supragranular compared to infragranular layers.

For the peak of population activity, the interaction between Layer and Inactivation was similarly significant ($\chi^2(2)=20.77$, p=.000031). Peak population activity was greater in layer 2/3 than in layer 5, also contrary to expectations (L2/3 vs. L5 = 0.018 mV ± 0.0071, p=0.010). There was not a significant increase during inhibition of Sst+ cells in L2/3 compared to L5 (L2/3 vs. L5 = 0.0038 mV ± 0.0020, p=.054), but a larger and significant increase in L2/3 compared to L5 during inhibition of PV+ cells (L2/3 vs. L5 = 0.016 mV ± 0.0038, p=.000021). Together with the results for the integral, we conclude that inhibition of PV+ cells has a larger effect on the intensity of UP states in layer 2/3 compared to layer 5. PV+ cells are more concentrated in superficial layers and their axons are mostly confined to the layer in which they reside. The difference in effect is likely because PV+ cells exert more inhibitory control over superficial layers compared to Sst+ cells, and are suppressing those layers selectively during UP states.

The interaction between Layer and Inactivation was also significant for the UP state latency measure ($\chi^2(2)=14.23$, p=.00081). UP state latencies were slightly (but not significantly) longer in superficial layers (L2/3 vs. L5 = 108%, p=.15, 95% CI [97.0% 122%]). There was not a significant interaction for Sst+ inhibition by layer (L2/3 vs. L5 = 101%, p=.79, 95% CI [96.8% 104%]), but latencies were significantly reduced with inhibition of PV+ cells in L2/3 compared to L5 (L2/3 vs. L5 = 85.4%, p=.00016, 95% CI [78.7% 92.7%]). These shorter latencies meant that UP states were detected at the same time in L2/3 and L5 when PV+ cells were inactivated.

UP state duration was also significantly affected by the interaction between Layer and Inactivation ($\chi^2(2)=6.48$, p=.039). UP states were briefer in supragranular layers compared to infragranular (L2/3 vs. L5 = 80.5%, p=.00044, 95% CI [71.3% 90.8%]). UP states in L2/3 were significantly shorter than expected during inhibition of Sst+ cells (L2/3 vs. L5 = 92.2%, p=.0096, 95% CI [86.6% 98.0%]). Despite this difference, UP state latencies were similar in layer 2/3 with and without Sst+ inhibition: the interaction term reflects that the increase in duration observed in layer 5 was not observed in layer 2/3. For inhibition of PV+ cells there was no difference from expected durations based on control durations in layer 2/3 and the effects of PV+ inhibiton in layer 5 (L2/3 vs. L5 = 100%, p=.94, 95% CI [89.1% 113%]).

Optogenetic activation of PV+ and Sst+ cells

Experiments in which we inactivated PV+ and Sst+ cells allowed us to evaluate the contributions of those cell populations when activated under the conditions of our experiment. It is also possible that inhibition could be enhanced under other conditions, for example in the case of different network states or with contributions from additional input pathways or neuromodulatory systems. To test the effects of elevated activity of Sst+ or PV+ cells, we selectively activated these interneuron populations using channelrhodopsin. In Figure 8 we show the results of four preliminary experiments (two each of Sst-cre and PV-cre animals injected with cre-dependent channelrhodopsin). Unlike the halorhodopsin experiments in which light was delivered throughout the experiment to inhibit cells uniformly, light activation of channelrhodopsin consisted of brief pulses delivered synchronously with thalamocortical stimulation to avoid overexcitation of channelrhodopsin-positive cells and depolarization block.

In one experiment (Figure 8A-C), activation of Sst+ interneurons increased the latency to UP state onset and greatly reduced UP state amplitude. In a second experiment (Figure 8G-I), activation of

Sst+ interneurons completely blocked the UP state, leaving only early activity immediately after each thalamocortical/light stimulus. In this experiment, early activity was actually increased with paired activation of Sst+ cells and thalamocortical stimulation, which could not be accounted for by subtracting activity triggered by Sst+ cell activation alone (not shown). Pairing thalamocortical input and channelrhodopsin activation is likely to create supralinear interactions by depolarizing the same cells, making it difficult to ascertain this effect in extracellular population recordings.

Similar to the example experiment from Figure 8G-I, channelrhodopsin activation of PV+ interneurons completely blocked UP state activity in both preliminary experiments (Figure 8D-F, J-L). In the latter experiment (Figure 8J-L), the combined thalamocortical/channelrhodopsin activation of PV+ cells caused complex population activity. It is possible that this population activity included some recurrent cortical UP state-like activity but it appeared qualitatively different than other UP states.

We conclude that optogenetic activation of either Sst+ or PV+ cells during thalamocortical input can prevent UP state activity. Although we did not see evidence in halorhodopsin experiments that Sst+ cells were important for regulating UP state onset, the experiment in Figure 8A-C shows that Sst+ cells can affect UP state onset if they are activated outside the context of the thalamocortical afferent pathway.

Interactions between cortico-cortical and thalamocortical inputs

Sst+ cells preferentially target the distal dendrites and apical tufts of pyramidal cells. Therefore, our expectation would be that activation of these cells would suppress the cortico-cortical glutamatergic inputs that synapse onto distal dendrites, particularly in layer 1, and that inhibition of the Sst+ cells would disinhibit the layer 1 cortico-cortical pathway. Others have shown that activation of VIP+ interneurons can suppress Sst+ cells and disinhibit top-down input (Gentet et al., 2012; Lee et al., 2013b;

Pfeffer et al., 2013; Pi et al., 2013). In previous work, we have found that paired stimulation of layer 1 fibers in a neighboring column with thalamocortical fibers (Hentschke et al., 2013) can trigger UP states when stimulus intensities were below threshold for UP states for each fiber pathway alone. This interaction between thalamocortical and layer 1 inputs in the slice gives us a model to test the effects of interneurons on the integration of top-down and bottom-up pathways.

We know that Sst+ cells are active before and during UP states evoked by thalamocortical input (Figure 2), and are therefore positioned to blunt interactions with cortico-cortical inputs. To test the hypothesis that suppression of Sst+ interneurons disinhibits cortico-cortical input, we paired stimulation of thalamocortical and layer 1 afferents with and without simultaneous optogenetic inhibition of Sst+ cells, as well as PV+ cells for comparison. The intended goal was to isolate the contribution of layer 1 inputs under two conditions: first, paired with a thalamocortical stimulus that was just sub-threshold for evoking UP states by itself, and, second, paired with a thalamocortical stimulus that was just sub-threshold for evoking UP states while inhibiting Sst+ (or PV+) cells by activation of halorhodopsin. In both cases, the intensity of the cortico-cortical stimulus would be chosen to be subthreshold for evoking UP states alone. Unfortunately, this paradigm was difficult to implement. The threshold for evoking UP states varied over time, and results were inconsistent, particularly the probability of evoking UP states and latency to UP state onset. Determining whether thalamocortical stimuli remained subthreshold during an extended recording period required more recording time and therefore increased the likelihood that the threshold would shift. We are continuing to refine the experimental design to mitigate these factors and are also searching for alternative ways to evaluate the effect of cortico-cortical inputs with and without inhibition of Sst+ (or PV+) cells.

As a preliminary alternative, in Figure 9 we report on some individual experiments in which we were able to record responses to either thalamocortical stimuli alone that were just suprathreshold for evoking UP states, or to paired thalamocortical and cortico-cortical stimuli that were each just

subthreshold for evoking UP states. We then looked at the effects of halorhodopsin-mediated inhibition of Sst+ cells (Figure 9A-D) or PV+ cells (Figure 9E-F). In one case, inhibition of Sst+ cells had little effect on UP states evoked either by thalamocortical-only (Figure 9A) or paired (Figure 9B) stimuli. In a second case, inhibition of Sst+ cells had the same modest effect on UP states evoked by either thalamocortical-only (Figure 9C) or paired (Figure 9D) stimuli. In one experiment in a halorhodopsin/PV-cre mouse, there was similarly little difference in the effect of inhibition in thalamocortical-only (Figure 9E) versus paired (Figure 9F) responses. For Figure 9A-D and 9F, UP states occurred on 95-100% of trials in both light-on and no-light conditions. In Figure 9E, UP states occurred on 87% of light-on and only 4% of no-light trials. The difference in probabilities likely explains why inhibition of PV+ cells may appear to have less of an effect on paired (Figure 9F) versus thalamocortical-only (Figure 9E), and this difference would probably not have been maintained if the thalamocortical stimulus intensity was chosen slightly higher for Figure 9E.

Based on these preliminary experiments, we do not see evidence that either interneuron type is blocking the effects of cortico-cortical stimuli, although the experiments were not performed in ideal conditions or with ideal experimental design. We are therefore tentative about drawing any strong conclusions from these data and will pursue further experiments to isolate the effect of particular interneuron populations on top-down/cortico-cortical inputs.

Discussion

In this paper we show that, like in other cortical areas (Fanselow and Connors, 2010; Tahvildari et al., 2012; Neske et al., 2015), GABAergic interneurons are highly active during evoked UP states in auditory cortex (Figures 2&3). The strong activation of Sst+ interneurons observed here is similar to previous observations in somatosensory cortex and unlike entorhinal cortex (Tahvildari et al., 2012;

Neske et al., 2015). Optogenetic suppression of PV+ or Sst+ interneurons increases population activity during UP states, and suppressing PV+ interneurons specifically also reduces UP state latency (likely due to a reduced threshold for UP state activation; Figures 6&7). We also observed occasional early activation of PV-tdTomato and Sst-tdTomato cells prior to UP states (Fig. 2), which appears to be common in auditory cortical inhibitory cells but not pyramidal cells (Krause et al., 2014). Early spiking in all cell types, including Sst-tdTomato cells, was likely due to direct thalamocortical input (Tan et al., 2008) because initial EPSP latencies were similar in all cell types (not shown; (Krause et al., 2014)).

UP states in auditory cortex

UP states in auditory cortex are brief (Hromadka et al., 2013) compared to those observed in somatosensory cortex (Petersen et al., 2003a; Neske et al., 2015). To compare our results with the recent results of (Neske et al., 2015), it is important to note that the time scale of the temporal changes described in inhibitory interneuron participation in network activity in that study are longer than the entire UP states observed in our slices. Also, while we observed Sst+ cells participating later than PV+ cells, they were active within a time scale corresponding to the early, intense activity seen by (Neske et al., 2015) in other cell types, but not in Sst+ cells. Therefore, while PV+ cells seem to have a relatively consistent role in UP states across cortical regions, Sst+ cells may be specialized by cortical area. Unlike previous reports in other cortical areas, we found that Sst+ cells were not only more active than pyramidal cells during UP states, but they also fired at roughly the same rates as PV+ cells. Although Sst+ cells are theoretically well-positioned to contribute to termination of UP states due to their facilitating inputs from pyramidal cells and activity late in UP states (Silberberg and Markram, 2007; Melamed et al., 2008; Fanselow and Connors, 2010; Krishnamurthy et al., 2012), inhibition does not appear to be the primary factor in terminating UP states in other cortical areas (Compte et al., 2003; Sanchez-Vives et al.,

2010). This may be different in auditory cortex, where enhanced activity in Sst+ cells during UP states may contribute to the brevity of auditory cortical UP states compared to other areas. Indeed, optogenetic inhibition of Sst+ cells produced longer UP states, whereas optogenetic inhibition of PV+ cells produced shorter UP states. UP state intensity and duration are inversely correlated, as seen in the optogenetic inhibition of PV+ cells here and with GABAergic antagonists previously (Sanchez-Vives et al., 2010). Therefore, we may be underestimating the effect of Sst+ cells on UP state duration if we consider only the approximately 7% increase in duration compared to control (Figure 6). A better comparison would be to slices with PV+ cells suppressed, in which duration differed by 34% with a similar increase in UP state intensity (based on peak and integral measurements).

Spontaneous and evoked UP states

Our experiments also differ from others in that we focused on thalamocortically evoked UP states rather than spontaneous UP states. UP states evoked by sensory stimuli or afferent input are a feature common to several cortical areas (and perhaps cortex in general) (Petersen et al., 2003b; Shu et al., 2003; Sakata and Harris, 2009). Although spontaneous and evoked UP states can be very similar (Luczak et al., 2009), spontaneous UP states likely occur when levels of activity in the network gradually or stochastically reach a minimum threshold for evoking an UP state, whereas extrinsic stimuli that evoke UP states may be at, but could also be significantly above, the minimum threshold for evoking an UP state. Whether spontaneous or evoked, UP states seem to depend on activity in layer 5, but thalamocortical stimuli in auditory cortex directly depolarize cells in all layers (Krause et al., 2014) even if those cells do not participate in the onset of UP state activity. Therefore, evoked UP states may differ from spontaneous events in layers involved, intensity, or duration (Sakata and Harris, 2009; Krause et al., 2014), as well as in the cell types that are recruited. Sensory information could be encoded in this

additional activity and be “read-out” in the context of an UP state that queries the local network to report the status of recent information (Luczak et al., 2013). In the slice, we are limited to a simplified surrogate of bottom-up sensory information via stimulation of thalamocortical afferents, but frequency information or more complex representations could be revealed in the patterns of cells, particularly supragranular pyramidal cells, that participate during evoked network activity depending on stimulus features (Bathellier et al., 2012; Luczak et al., 2013). The generating mechanisms of UP states in the infragranular layers may be separate and parallel to more elaborate information coding by the supragranular cells that project to higher order cortical areas (Sakata and Harris, 2009).

Timing of spikes relative to population activity and afferent input

Pyramidal cells in layer 2/3 are thought to be sparse, informative coders compared to infragranular pyramidal cells (DeWeese et al., 2003; Hromadka et al., 2008; Poulet and Petersen, 2008; Sakata and Harris, 2009; Crochet et al., 2011; Barth and Poulet, 2012). The information carried by action potentials about a stimulus is related to their precision and reliability across trials. Here, we observed that supragranular pyramidal cells were more tightly coupled to population activity than infragranular pyramidal cells, and pyramidal cells were overall more closely coupled to population activity than Sst+ or PV+ interneurons. Supragranular pyramidal cells also fired more consistently timed spikes from trial to trial compared to infragranular pyramidal cells, though not as consistently as PV+ cells. If PV+ cells are important for controlling the timing of pyramidal cell firing (Pouille and Scanziani, 2001; Wehr and Zador, 2003), their precision may set an upper bound on the potential precision of pyramidal cells. Sst+ cells fired less consistently from trial to trial compared to PV+ cells, despite also receiving large EPSPs (Table 1), perhaps due to their slower time constants, lack of inhibition from PV+ cells, or intrinsic conductances that produce bursts of action potentials (Kawaguchi and Kubota, 1996).

Modulation of inhibitory interneuron activity in vivo

Activity in specific populations of inhibitory interneurons can be regulated selectively either by activation of particular circuits or through neuromodulators (Beierlein et al., 2000; Fanselow et al., 2008). VIP+ cells selectively inhibit Sst+ cells and may therefore allow integration of top-down inputs (Lee et al., 2013a; Pi et al., 2013). The robust activity of Sst+ cells during UP states in auditory cortex may mean that top-down information to distal dendrites of pyramidal cells is effectively suppressed during bottom-up thalamocortical transmission unless Sst+-mediated inhibition is itself suppressed. However, in our preliminary experiments we have not been able to selectively modulate the effects of top-down cortico-cortical inputs separately from the effects on the UP state activity as a whole (Figure 9). As noted above, this may reflect a sub-optimal experimental design. However, these results could indicate a fundamentally different role for Sst+ cells in auditory cortex compared to other cortical regions.

Elucidating the roles of specific inhibitory cell populations in regulating network activity in auditory cortex is a critical step in understanding how sensory information is encoded in the activity of these networks and how this process goes awry under pathological conditions. For example, PV+ cell activity may be modulated by hearing loss, which causes a decrease in thalamic drive to fast-spiking (likely PV+) but not to low-threshold spiking interneurons (Takesian et al., 2013). Additionally, aged mice with behavioral signs of tinnitus show enhanced cortical excitability and reduced sensitivity to inhibition (Llano et al., 2012). Tinnitus is thought to be caused by hearing loss and subsequent paradoxical increases in activity in subcortical auditory areas (Auerbach et al., 2014). If PV+ cell activity is important for setting the threshold for evoking UP states, reduced input to PV+ cells could promote recurrent cortical activity at previously subthreshold intensities, perhaps leading to perception of tinnitus. By contrast, upregulation of inhibitory signaling, especially cells such as Sst+ cells whose dendritic targets

align with those of cortical feedback connections, has been proposed to play a role in cognitive and perceptual deficits during post-operative delirium, an acute disorder of consciousness [Sanders et al 2011 REF]. Future experiments utilizing specific animal models for these diseases combined with cre-driver lines for specific interneuron populations will help clarify the mechanisms of these and other conditions.

	RMP (mV)	R_{in} (MΩ)	τ_m (ms)	Spike width (ms)	ISI ratio	EPSP slope (mV/ms)	EPSP Latency (ms)
Pyr	-69.7±11.3	102.0±56.4	11.3±5.9	1.06±0.26	0.32±0.20	1.89±1.38	2.7±0.61
Sst+	-64.0±5.0	175.5±87.9	13.9±9.8	0.66±0.26	0.60±0.26	4.43±8.21	3.3±2.5
PV+	-66.8±11.4	82.0±26.0	4.2±1.3	0.37±0.14	0.86±0.15	15.1±12.5	2.0±0.35

Table 1. Properties of recorded cell types. Values are presented as mean±SD. Spike widths are full-width at half-maximum. ISI ratio is a measure of spike adaptation equal to the ratio of first to last interspike interval for a 400 ms depolarizing current at half-maximal firing rate. RMP did not vary significantly between groups ($F(2,81)=2.14$, $p=.124$). Input resistance was significantly higher in Sst+ cells ($F(2,81)=15.8$, $p<.0001$; Pyr vs. Sst+, $p=.0001$; Pyr vs. PV+, $p=.37$; Sst+ vs. PV+, $p<.0001$). Membrane time constants were significantly shorter in PV+ cells ($F(2,81)=16.4$, $p<.0001$; Pyr vs. Sst+, $p=.30$; Pyr vs. PV+, $p=.0001$; Sst+ vs PV+, $p<.0001$). Spike widths were significantly different between all groups ($F(2,81)=71.0$, $p<.0001$; Pyr vs. Sst+, $p<.0001$; Pyr vs. PV+, $p<.0001$; Sst+ vs PV+, $p=.0002$). Spike adaptation (ISI ratio) was significantly different between all groups ($F(2,81)=55.7$, $p<.0001$; Pyr vs. Sst, $p<.0001$; Pyr vs. PV+, $p<.0001$; Sst+ vs PV+, $p=.0001$). EPSP slopes were greater in PV+ cells ($F(2,56)=13.4$, $p<.0001$; Pyr vs. Sst, $p=.64$; Pyr vs. PV+, $p<.0001$; Sst+ vs PV+, $p=.0012$). EPSP latencies were shorter in PV+ cells than Sst+ cells, but neither significantly different from Pyr+ cells ($F(2,56)=4.53$, $p=.015$; Pyr vs. Sst, $p=.42$; Pyr vs. PV+, $p=.18$; Sst+ vs PV+, $p=.012$).

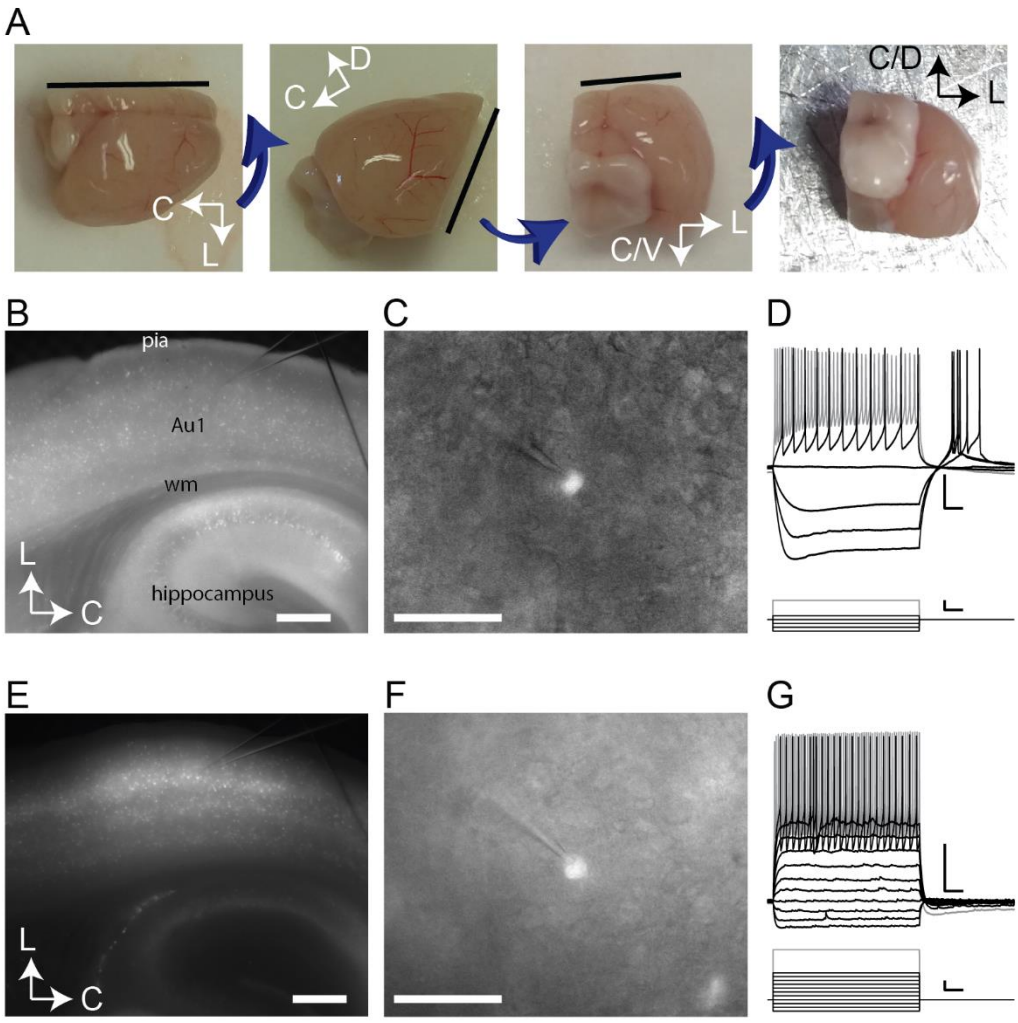

Figure 1. Slicing procedure and targeting of tdTomato-labeled cells. (A) Blocking procedure for cutting thalamocortical slices involves three blocking cuts, from left to right (see methods). Black lines represent planes of section, which were always perpendicular to the previous plane of section (and straight down in the photographs), and arrows between stages represent the rotation necessary to prepare the block for the next cut (which is always onto the face of the previous cut). Directional arrows indicate roughly caudal, lateral, dorsal, and ventral directions (C, L, D, V), including combinations when appropriate. In the final image, the block is oriented with the dorsal/caudal part at the top of the image, and the ventral surface visible at the bottom. Slices were taken parallel to the surface on which the block rests in this final image. (B) Auditory thalamocortical slice from Sst-cre x tdTomato mouse. tdTomato fluorescence

identifies Sst+ cells in neocortex and hippocampus. The highest cell density is observed in the infragranular layers, and a faint band is present in layer 1 likely from Martinotti cell axons. The glass micropipette coming from the upper right is inserted into layer 4 to find the optimal column for thalamocortical input. L & C mark roughly lateral and caudal directions, respectively, although given the complex angle at which the slice is cut, the caudal direction is also dorsal, as is the lateral direction to a lesser extent. Au1: primary auditory cortex, wm: white matter. (C) High-power image combining brightfield and fluorescence imaging to identify and patch a labeled Sst-tdTomato cell. (D) Response of an Sst-tdTomato cell (top) to current steps (bottom). (E) Auditory thalamocortical slice as in B, but prepared from a PV-cre x tdTomato mouse. PV+ cells are most dense in layer 4 and are more dense in primary auditory cortex compared to adjacent regions. Similar to (B), the glass micropipette is inserted into layer 4. (F) Targeted recording of a PV-tdTomato cell. (G) Response of a PV-tdTomato cell (top) to current steps (bottom). Scale bars for (B) and (E) 200 µm, image taken with 2.5X objective; (C) and (F) 25 µm, image taken with 40X objective. For (D) and (G), the scale bar for the current steps is 50 ms, 100 pA and the scale bar for the voltage response is 50 ms, 20 mV.

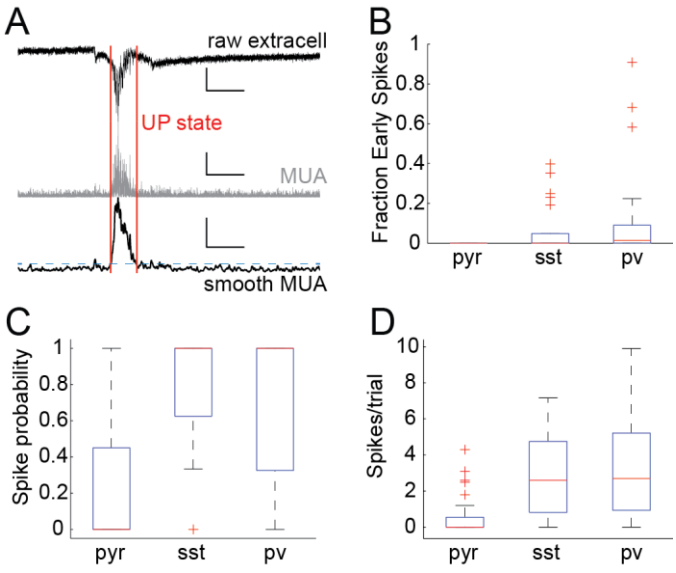

Figure 2. Spiking before and during UP states. (A) Procedure for UP state detection and measuring population activity. The raw extracellular trace (black, top) is filtered between 500-3000 Hz to give the MUA signal (grey, center). The MUA signal is smoothed with a Gaussian kernel to give the smoothed MUA signal (black, bottom). The UP state onset and offset are determined by threshold (blue dashed line) crossings above the geometric mean of the smoothed MUA signal (see Methods). Scale bars are 50 ms and 0.2, 0.05, and 0.02 mV for raw, MUA, and smooth MUA, respectively. (B - C) Distribution of 'early spikes' (B; defined as spikes occurring before UP state onset), spike probability (C; defined as the probability to observe at least one spike on a given trial) and spikes per trial (D) across cell type. Box plots show median (red), interquartile range (blue), range (black), and outliers as red plusses. Early spikes (B) were rare in all cell types, and were not observed at all in pyramidal cells. Most pyramidal cells (pyr) did not spike at all (C), whereas most interneurons (sst and pv) fired at least one spike on every trial. Most pyramidal cells averaged one spike or fewer per trial (D), whereas most interneurons fired more than 2 spikes per trial.

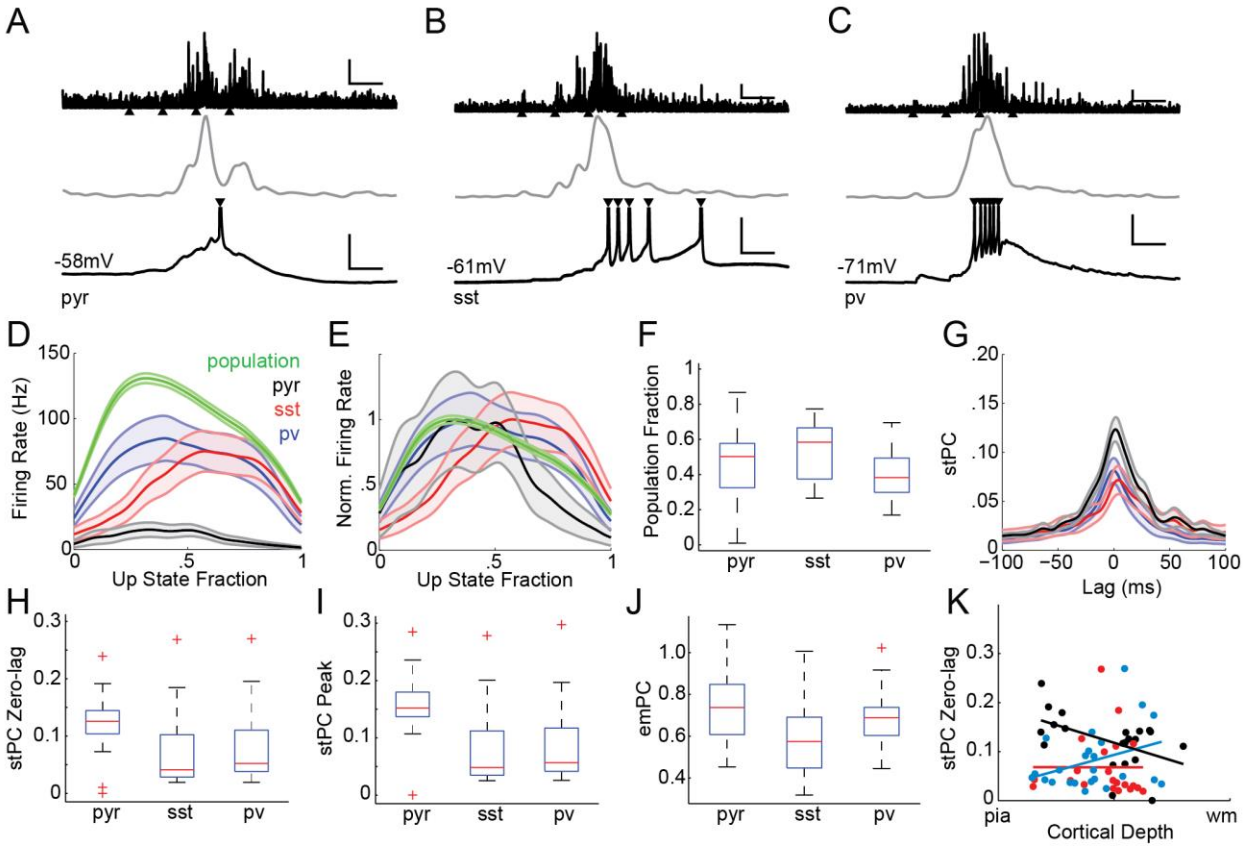

Figure 3. Relationship between single-cell and population activity (A-C) Example MUA (filtered, top; smoothed "population activity", middle) traces from three different slices, along with intracellular recordings (bottom) from a pyramidal, Sst-tdTomato, and PV-tdTomato cell, respectively. Upward-pointing triangles mark the time of thalamocortical afferent stimulus pulses, and downward pointing triangles mark spikes. Spikes are truncated above -20 mV. Values in mV indicate resting membrane potential. Scale bars are 25 ms, 0.03 mV for MUA traces, and 25 ms, 20 mV for intracellular recordings. (D) Firing rate as a function of normalized UP state duration ('UP state fraction') for pyramidal (black), Sst-tdTomato (red), and PV-tdTomato (blue) cells. Population activity (green) is also plotted with arbitrary vertical scale to allow for comparison to other traces. Dark lines indicate means, shaded area is ±SEM. (E) Same data as (D), but each trace is normalized to its own peak. Pyramidal cell firing tended to be shifted earlier, and Sst-tdTomato cells later, than population activity, while PV-tdTomato cells mostly followed the population rate. (F) Mean fraction of population activity occurring before each spike,

displayed as medians across each population of cells. PV-tdTomato cells tended to fire earlier than Sst-tdTomato cells. (G) Spike-triggered population coupling as a function of offset lag. The stPC measures the average population firing at the time of each spike, and is typically maximal near zero because cells fired most of their spikes during UP states. As in other plots, pyramidal cells are in black, Sst-tdTomato in red, PV-tdTomato in blue. Dark lines indicate means, shaded area is ±SEM. (H) The stPC at zero-lag was higher in pyramidal cells than Sst- or PV-tdTomato cells, indicating that pyramidal cells tend to fire when population activity is maximal. (I) Similar to (H), but measured at the peak lag for each cell. (J) Coupling between the membrane potential and population activity followed similar trends to the spike-population coupling as seen in (H) and (I), but the differences between populations were not significant. Overall, membrane potentials were more closely linked to population firing than spikes. (K) Relationship between zero-lag stPC and cortical depth from the surface (pia) to white matter (wm) for pyramidal cells (black), Sst-tdTomato cells (red), and PV-tdTomato cells (blue). Points are individual cells, lines show linear regression. The more superficial pyramidal cells with greater stPC are all in layer 2/3.

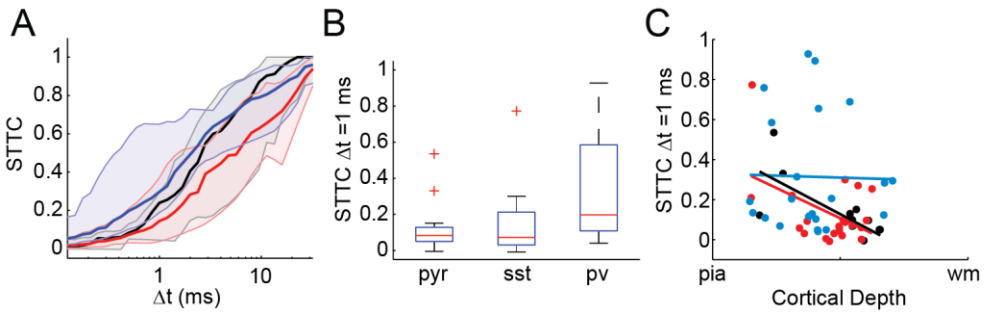

Figure 4. Timing of spikes across trials. (A) The spike-time tiling coefficient measures the precision and reliability of spiking across trials for a given cell. Here, STTC is plotted as a function of the time window (Δt) in which spikes were considered synchronous for pyramidal cells (black), Sst-tdTomato cells (red), and PV-tdTomato cells (blue). Dark lines are medians, and shaded regions indicate the interquartile range. (B) Comparison of STTC between cell populations at Δt = 1 ms. Spiking activity in PV-tdTomato cells was better timed across trials than for pyramidal or Sst-tdTomato cells. (C) Relationship between STTC and cortical depth from the surface (pia) to white matter (wm) for pyramidal cells (black), Sst-tdTomato cells (red), and PV-tdTomato cells (blue). Points are individual cells, lines show linear regression. The more superficial pyramidal cells with greater stPC are in layer 2/3.

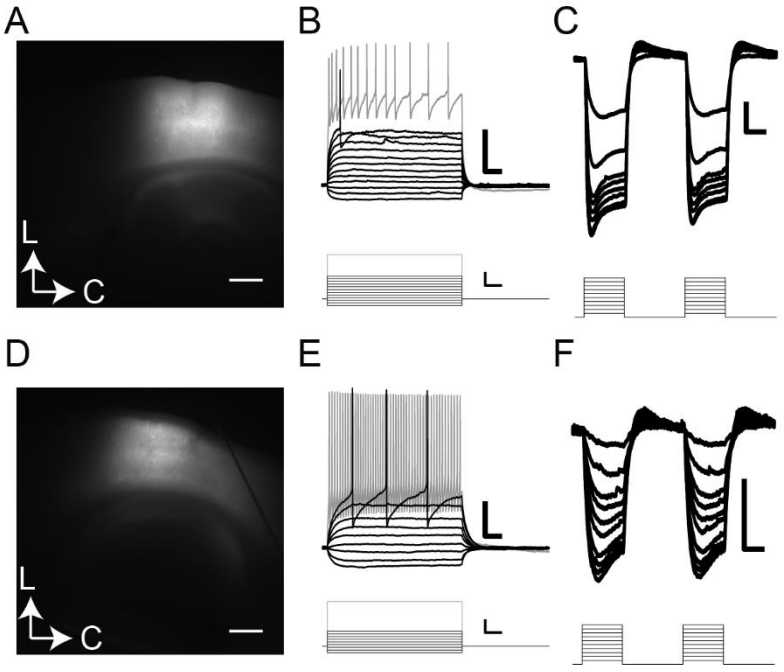

Figure 5. Halorhodopsin-mediated inhibition of specific interneuron types. (A) Slice from an Sst-cre x tdTomato animal injected with a cre-dependent halorhodopsin-YFP fusion protein. Fluorescence pictured is from YFP, showing the injection site in auditory cortex. Scale bar 200 µm, image taken at 2.5X magnification. (B) Voltage responses (top) to current injection (bottom) in a Sst-tdTomato cell in a halorhodopsin-injected slice. Scale bars are 50 ms, 100 pA and 50 ms, 20 mV. (C) Membrane potential (top) in response to light stimulation of halorhodopsin (bottom) in the cell illustrated in B. Light stimulation caused significant hyperpolarization. Light pulses are 200 ms long, with 300 ms apart, and at intensities from 1% to 10% of maximum arc lamp output. Scale bar 100 ms, 10 mV. (D-F) As in (A-C) for PV-cre x tdTomato.

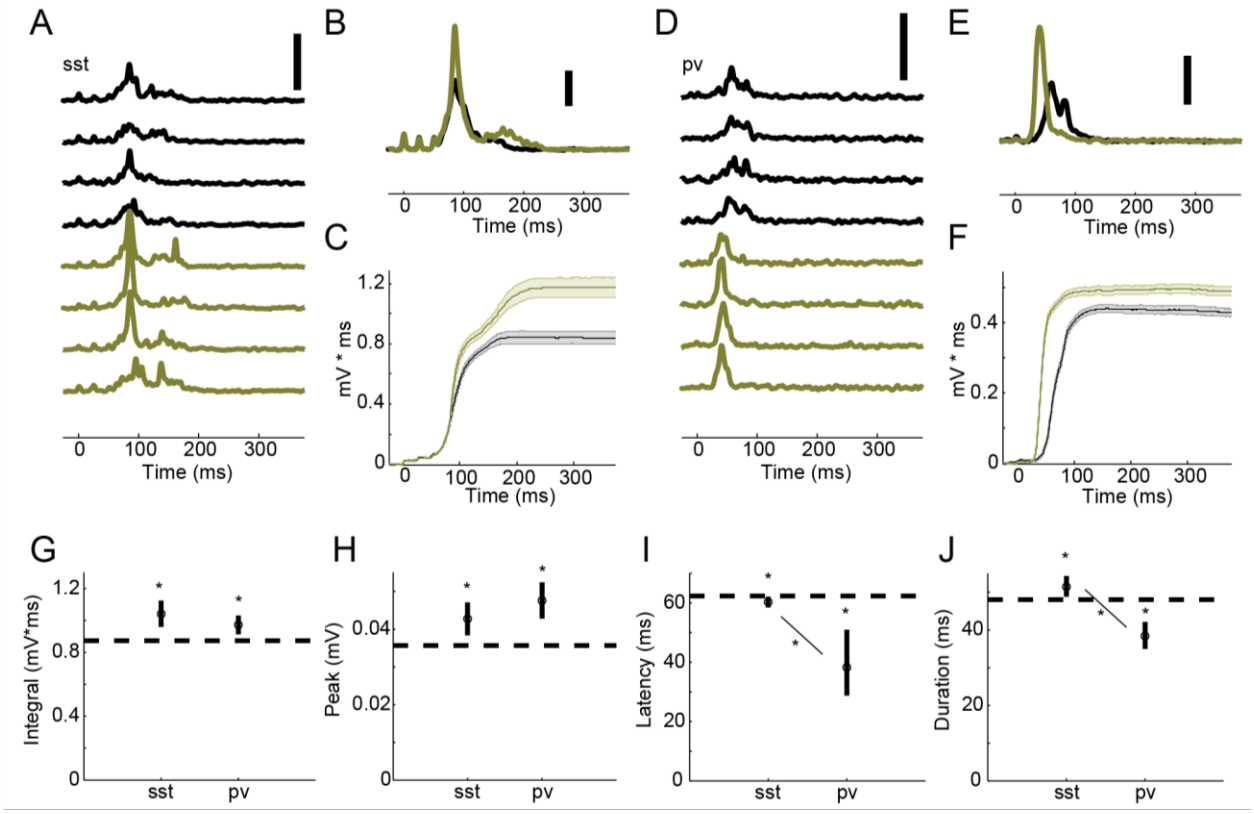

Figure 6. Effects of optogenetic suppression of interneurons during UP states. (A) Consecutive example trials of population activity in a slice from a halorhodopsin-injected Sst-cre with light-off (black) or light-on (yellow, to indicate light for halorhodopsin activation). Light came on 100 ms before activation of thalaocortical afferents (thalamocortical afferents were activated starting at time=0) and lasted a total of 500 ms. Scale bar is 0.05 mV. (B) Average population activity for all light-off and light-on trials from the example experiment in (A). Scale bar is 0.01 mV. (C) Integral of population activity over the duration of the trial for the example experiment in (A-B). Averages for light-off (black) and light-on (yellow) trials are shown as dark lines, and SEM as the shaded area. (D-F) An example experiment for halorhodopsin-injected PV-cre, as in (A-C). (G-J) Parameter estimates (circles) and confidence intervals (vertical error bars) from linear mixed-effects model for four measures of population activity: integral (as seen in C&F), peak (as in the maximum value from B&E, or the maximum slope in C&F), UP state latency (like in Figure 2A), and UP state duration (time between red lines like in Figure 2A). Dashed lines are intercept (light-

off) baseline comparisons. * indicates a significant difference from baseline, connecting lines with * in (I) and (J) indicate significant differences between Sst and PV.

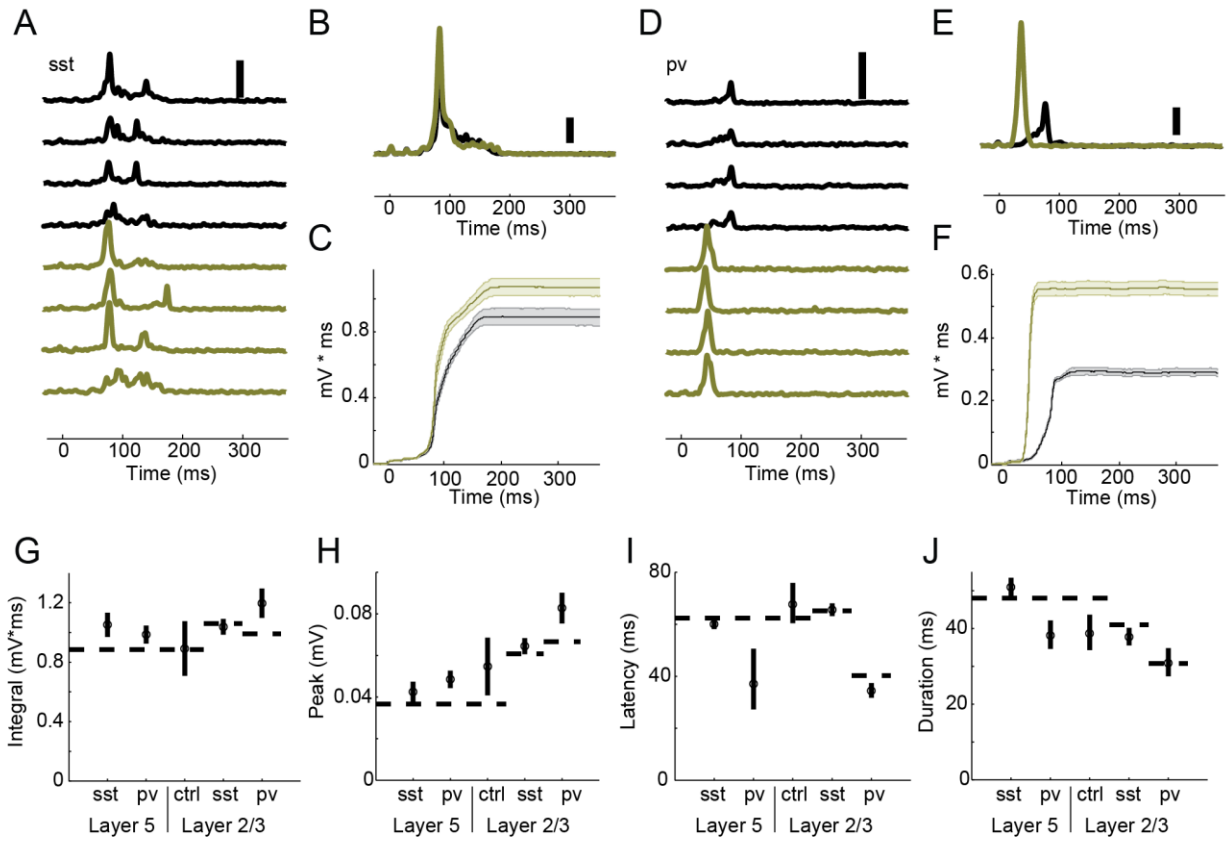

Figure 7. Effects of optogenetic suppression of interneurons on population activity in layers 2/3. (A) Example trials of population activity recorded in layer 2/3 from the same halorhodopsin/Sst-cre slice as Figure 6A-C. Conventions are the same as for Figure 6. (B) Average layer 2/3 population activity for all light-off and light-on trials from example experiment in (A). (C) Integral of population activity, as in Figure 6C. Scale bars are 0.05 mV and 0.01 mV for (A) and (B), respectively. (D-F) Example trials of population activity recorded in layer 2/3 from the same halorhodopsin/PV-cre slice as Figure 6D-F. (G-J) Parameter estimates (circles) and confidence intervals (vertical error bars) from linear mixed-effects model with four population response variables, similar to Figure 6. Note that "layer" refers to recording layer; light was applied across all cortical laminae for all experiments. Layer 5 PV and Sst points indicate the same results in Figure 6 (error bars differ slightly due to inclusion of additional data and inclusion of

additional effects), and their error bars reflect a comparison of the inhibition of that cell type to the no-light control (dashed line). Similarly, the Layer 2/3 control ('ctrl') data point is a comparison between the no-light control recorded in layer 5 and the no-light control recorded in layer 2/3. The layer 2/3 Sst and PV points represent the interaction term for Inhibition*Layer, where Inhibition represents optogenetic inhibition of Sst or PV cells and Layer represents the recording layer. These values are best understood in comparison to the expected values for Sst or PV inhibition in layer 2/3 under the assumption that the inhibition effect is equal to the effect in layer 5. These expected values are plotted as horizontal dashed lines individually for Sst and PV interaction terms, and calculated by the sum of the Sst/PV coefficients (i.e., either the first or second point in each panel) with the difference between layer 2/3 and layer 5 control (i.e., the difference between the dashed line and third point).

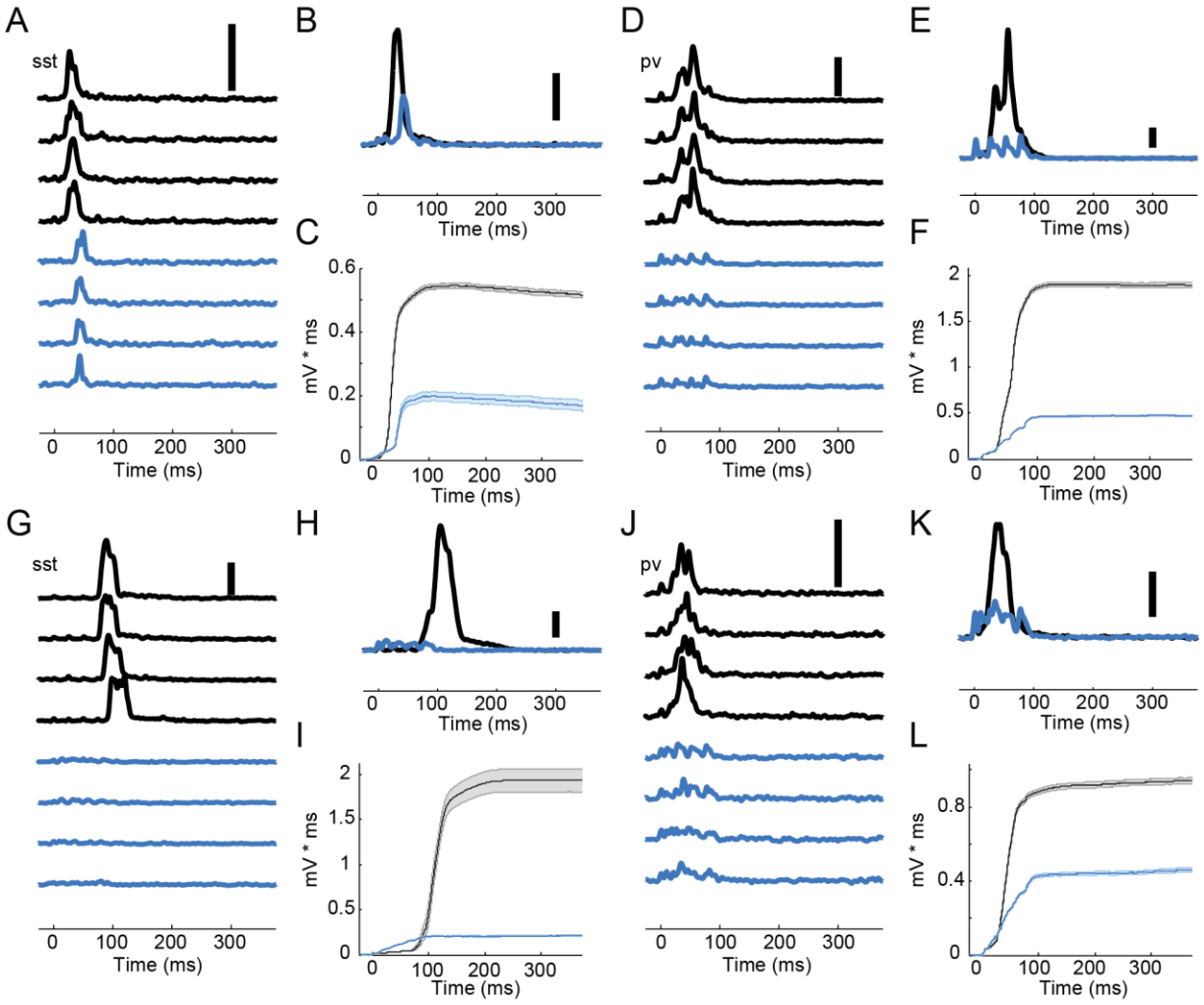

Figure 8. Effects of optogenetic activation of either Sst+ or PV+ interneurons. (A) Example traces, (B) averages, and (C) integral of population activity for a channelrhodopsin/Sst-cre slice. Conventions are the same as for Figures 6 and 7. Light-on trials are in blue to represent blue light for channelrhodopsin activation. Scale bars are 0.05 mV and 0.01 mV for (A) and (B), respectively. (D-F) Similar plots to (A-C) for a channelrhodopsin/PV-cre slice. (G-I) Another experiment from a different channelrhodopsin/Sst-cre slice. (J-L) Another experiment from a different channelrhodopsin/PV-cre slice.

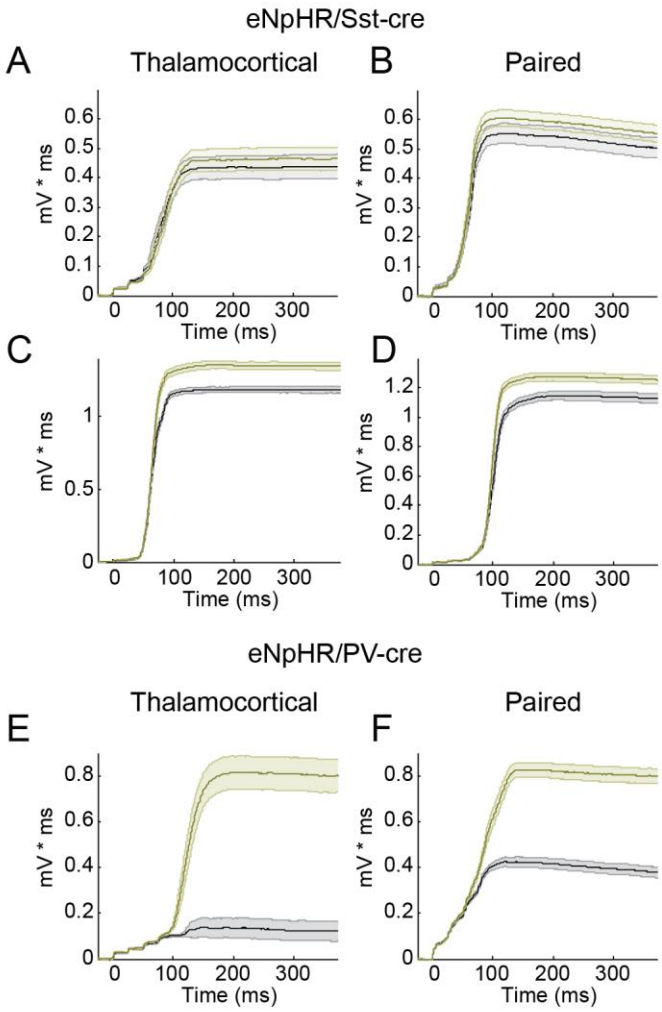

Figure 9. Preliminary experiments pairing thalamocortical and cortico-cortical stimuli with optogenetic suppression of interneurons. (A) Example experiment showing the integral of population activity (as in Figure 6C) in response to thalamocortical stimulation at the minimum intensity for evoking UP states, with (yellow) and without (black) light to inhibit Sst+ interneurons. Lines and shaded region are mean ± SEM. (B) The same slice as in (A), but using a thalamocortical stimulus intensity subthreshold for evoking UP states paired with a cortico-cortical stimulus that is also subthreshold, but which evokes UP states when combined with the subthreshold thalamocortical stimulus. There is little effect of inhibiting Sst+ cells in either (A) or (B). (C-D) Another example similar to (A-B). In this example there is a modest but consistent effect of inhibiting Sst+ cells but this effect does not seem to differ between the thalamocortical-only and paired stimuli. (E-F) Another example, similar to (A-B) and (C-D), but from a PV-cre animal. Similar to (C-D), there is little difference in the effect of inhibiting PV+ cells between thalamocortical-only and paired stimuli, although there was an unintended baseline difference (see text).

References

Auerbach BD, Rodrigues PV, Salvi RJ (2014) Central gain control in tinnitus and hyperacusis. Frontiers in neurology 5.

Barth AL, Poulet JF (2012) Experimental evidence for sparse firing in the neocortex. Trends Neurosci 35:345-355.

Bartlett EL, Wang X (2007) Neural Representations of Temporally Modulated Signals in the Auditory Thalamus of Awake Primates. Journal of Neurophysiology 97:1005-1017.

Bathellier B, Ushakova L, Rumpel S (2012) Discrete neocortical dynamics predict behavioral categorization of sounds. Neuron 76:435-449.

Beggs JM, Plenz D (2003) Neuronal avalanches in neocortical circuits. Journal of Neuroscience 23:11167-11177.

Beierlein M, Gibson JR, Connors BW (2000) A network of electrically coupled interneurons drives synchronized inhibition in neocortex. NatNeurosci 3:904-910.

Cardin JA, Carlén M, Meletis K, Knoblich U, Zhang F, Deisseroth K, Tsai L-H, Moore CI (2009) Driving fast-spiking cells induces gamma rhythm and controls sensory responses. Nature 459:663-667.

Chen N, Sugihara H, Sur M (2015) An acetylcholine-activated microcircuit drives temporal dynamics of cortical activity. Nature neuroscience.

Cohen MR, Kohn A (2011) Measuring and interpreting neuronal correlations. Nature neuroscience 14:811-819.

Compte A, Reig R, Sanchez-Vives MV (2009) Timing excitation and inhibition in the cortical network. In: Coherent Behavior in Neuronal Networks, pp 17-46: Springer.

Compte A, Sanchez-Vives MV, McCormick DA, Wang XJ (2003) Cellular and network mechanisms of slow oscillatory activity (< 1 Hz) and wave propagations in a cortical network model. Journal of Neurophysiology 89:2707-2725.

Compte A, Reig R, Descalzo VF, Harvey MA, Puccini GD, Sanchez-Vives MV (2008) Spontaneous high-frequency (10–80 Hz) oscillations during up states in the cerebral cortex in vitro. The Journal of Neuroscience 28:13828-13844.

Contreras D, Steriade M (1995) Cellular basis of EEG slow rhythms: a study of dynamic corticothalamic relationships. The Journal of Neuroscience 15:604-622.

Crochet S, Poulet JF, Kremer Y, Petersen CC (2011) Synaptic mechanisms underlying sparse coding of active touch. Neuron 69:1160-1175.

Cruikshank SJ, Killackey HP, Metherate R (2001) Parvalbumin and calbindin are differentially distributed within primary and secondary subregions of the mouse auditory forebrain. Neuroscience 105:553-569.

Cruikshank SJ, Rose HJ, Metherate R (2002) Auditory thalamocortical synaptic transmission in vitro. JNeurophysiol 87:361-384.

Cruikshank SJ, Lewis TJ, Connors BW (2007) Synaptic basis for intense thalamocortical activation of feedforward inhibitory cells in neocortex. NatNeurosci 10:462-468.

Curto C, Sakata S, Marguet S, Itskov V, Harris KD (2009) A simple model of cortical dynamics explains variability and state dependence of sensory responses in urethane-anesthetized auditory cortex. JNeurosci 29:10600-10612.

Cutts CS, Eglen SJ (2014) Detecting pairwise correlations in spike trains: an objective comparison of methods and application to the study of retinal waves. The Journal of Neuroscience 34:14288-14303.

DeWeese MR, Zador AM (2006) Non-Gaussian Membrane Potential Dynamics Imply Sparse, Synchronous Activity in Auditory Cortex. Journal of Neuroscience 26:12206-12218.

DeWeese MR, Wehr M, Zador AM (2003) Binary spiking in auditory cortex. Journal of Neuroscience 23:7940-7949.

Eggermann E, Kremer Y, Crochet S, Petersen CC (2014) Cholinergic Signals in Mouse Barrel Cortex during Active Whisker Sensing. Cell reports 9:1654-1660.

Engel AK, Singer W (2001) Temporal binding and the neural correlates of sensory awareness. Trends Cogn Sci 5:16-25.

Fanselow EE, Connors BW (2010) The roles of somatostatin-expressing (GIN) and fast-spiking inhibitory interneurons in UP-DOWN states of mouse neocortex. J Neurophysiol 104:596-606.

Fanselow EE, Richardson KA, Connors BW (2008) Selective, state-dependent activation of somatostatin-expressing inhibitory interneurons in mouse neocortex. J Neurophysiol 100:2640-2652.

Fino E, Yuste R (2011) Dense inhibitory connectivity in neocortex. Neuron 69:1188-1203.

Francavilla R, Luo X, Magnin E, Tyan L, Topolnik L (2015) Coordination of dendritic inhibition through local disinhibitory circuits. Frontiers in synaptic neuroscience 7.

Franklin KBJ, Paxinos G (2008) The Mouse Brain in Stereotaxic Coordinates. Amsterdam: Academic Press.

Gentet LJ, Kremer Y, Taniguchi H, Huang ZJ, Staiger JF, Petersen CC (2012) Unique functional properties of somatostatin-expressing GABAergic neurons in mouse barrel cortex. Nat Neurosci 15:607-612.

Haider B, Duque A, Hasenstaub AR, McCormick DA (2006) Neocortical network activity in vivo is generated through a dynamic balance of excitation and inhibition. The Journal of neuroscience 26:4535-4545.

Hentschke H, Raz A, Krause BM, Grady SM, Banks MI (2013) Effects of isoflurane on cortical UP state activity in brain slices. In: Society for Neuroscience Annual Meeting. San Diego, CA.

Hromadka T, DeWeese MR, Zador AM (2008) Sparse representation of sounds in the unanesthetized auditory cortex. PLoSBiol 6:e16.

Hromadka T, Zador AM, DeWeese MR (2013) Up states are rare in awake auditory cortex. JNeurophysiol 109:1989-1995.

Hu H, Cavendish JZ, Agmon A (2013) Not all that glitters is gold: off-target recombination in the somatostatin–IRES-Cre mouse line labels a subset of fast-spiking interneurons. Frontiers in neural circuits 7.

Joris PX, Louage DH, Cardoen L, van der Heijden M (2006) Correlation index: a new metric to quantify temporal coding. Hear Res 216-217:19-30.

Kawaguchi Y, Kubota Y (1996) Physiological and morphological identification of somatostatin- or vasoactive intestinal polypeptide-containing cells among GABAergic cell subtypes in rat frontal cortex. The Journal of Neuroscience 16:2701-2715.

Kawaguchi Y, Kubota Y (1998) Neurochemical features and synaptic connections of large physiologically-identified GABAergic cells in the rat frontal cortex. Neuroscience 85:677-701.

Kawaguchi Y, Kondo S (2002) Parvalbumin, somatostatin and cholecystokinin as chemical markers for specific GABAergic interneuron types in the rat frontal cortex. Journal of Neurocytology 31:277-287.

Kayser C, Logothetis NK, Panzeri S (2010) Millisecond encoding precision of auditory cortex neurons. ProcNatlAcadSciUSA 107:16976-16981.

Krause BM, Raz A, Uhlrich DJ, Smith PH, Banks MI (2014) Spiking in auditory cortex following thalamic stimulation is dominated by cortical network activity. Frontiers in Systems Neuroscience 8:170.

Krishna BS, Semple MN (2000) Auditory temporal processing: responses to sinusoidally amplitude-modulated tones in the inferior colliculus. Journal of Neurophysiology 84:255-273.

Krishnamurthy P, Silberberg G, Lansner A (2012) A cortical attractor network with Martinotti cells driven by facilitating synapses. PloS one 7:e30752-e30752.

Kristensen M, Hansen T (2004) Statistical analyses of repeated measures in physiological research: a tutorial.

Kubota Y (2014) Untangling GABAergic wiring in the cortical microcircuit. Current opinion in neurobiology 26:7-14.

Kubota Y, Shigematsu N, Karube F, Sekigawa A, Kato S, Yamaguchi N, Hirai Y, Morishima M, Kawaguchi Y (2011) Selective Coexpression of Multiple Chemical Markers Defines Discrete Populations of Neocortical GABAergic Neurons. Cerebral Cortex 21:1803-1817.

Langner G (1992) Periodicity coding in the auditory system. HearRes 60:115-142.

Lee S, Kruglikov I, Huang ZJ, Fishell G, Rudy B (2013a) A disinhibitory circuit mediates motor integration in the somatosensory cortex. Nature neuroscience 16:1662-1670.

Lee S, Kruglikov I, Huang ZJ, Fishell G, Rudy B (2013b) A disinhibitory circuit mediates motor integration in the somatosensory cortex. Nat Neurosci 16:1662-1670.

Llano DA, Turner J, Caspary DM (2012) Diminished cortical inhibition in an aging mouse model of chronic tinnitus. The Journal of Neuroscience 32:16141-16148.

Luczak A, Bartho P, Harris KD (2009) Spontaneous events outline the realm of possible sensory responses in neocortical populations. Neuron 62:413-425.

Luczak A, Bartho P, Harris KD (2013) Gating of sensory input by spontaneous cortical activity. JNeurosci 33:1684-1695.

Ma Y, Hu H, Berrebi AS, Mathers PH, Agmon A (2006) Distinct subtypes of somatostatin-containing neocortical interneurons revealed in transgenic mice. Journal of Neuroscience 26:5069-5082.

MacLean JN, Watson BO, Aaron GB, Yuste R (2005) Internal dynamics determine the cortical response to thalamic stimulation. Neuron 48:811-823.

Markram H, Toledo-Rodriguez M, Wang Y, Gupta A, Silberberg G, Wu CZ (2004) Interneurons of the neocortical inhibitory system. Nature Reviews Neuroscience 5:793-807.

Melamed O, Barak O, Silberberg G, Markram H, Tsodyks M (2008) Slow oscillations in neural networks with facilitating synapses. Journal of computational neuroscience 25:308-316.

Metherate R, Cruikshank SJ (1999) Thalamocortical inputs trigger a propagating envelope of gamma-band activity in auditory cortex in vitro. Experimental Brain Research 126:160-174.

Murayama M, Pérez-Garci E, Nevian T, Bock T, Senn W, Larkum ME (2009) Dendritic encoding of sensory stimuli controlled by deep cortical interneurons. Nature 457:1137-1141.

Neske GT, Patrick SL, Connors BW (2015) Contributions of Diverse Excitatory and Inhibitory Neurons to Recurrent Network Activity in Cerebral Cortex. The Journal of Neuroscience 35:1089-1105.

Oh SW et al. (2014) A mesoscale connectome of the mouse brain. Nature 508:207-214.

Okun M, Steinmetz NA, Cossell L, Iacaruso MF, Ko H, Barthó P, Moore T, Hofer SB, Mrsic-Flogel TD, Carandini M (2015) Diverse coupling of neurons to populations in sensory cortex. Nature 521:511-515.

Petersen CCH, Grinvald A, Sakmann B (2003a) Spatiotemporal dynamics of sensory responses in layer 2/3 of rat barrel cortex measured in vivo by voltage-sensitive dye imaging combined with whole-cell voltage recordings and neuron reconstructions. Journal of Neuroscience 23:1298-1309.

Petersen CCH, Hahn TTG, Mehta M, Grinvald A, Sakmann B (2003b) Interaction of sensory responses with spontaneous depolarization in layer 2/3 barrel cortex. Proceedings of the National Academy of Sciences of the United States of America 100:13638-13643.

Pfeffer CK, Xue M, He M, Huang ZJ, Scanziani M (2013) Inhibition of inhibition in visual cortex: the logic of connections between molecularly distinct interneurons. Nature Neuroscience 16:1068-1076.

Pi HJ, Hangya B, Kvitsiani D, Sanders JI, Huang ZJ, Kepecs A (2013) Cortical interneurons that specialize in disinhibitory control. Nature 503:521-524.

Pouille F, Scanziani M (2001) Enforcement of temporal fidelity in pyramidal cells by somatic feed-forward inhibition. Science 293:1159-1163.

Poulet JF, Petersen CC (2008) Internal brain state regulates membrane potential synchrony in barrel cortex of behaving mice. Nature 454:881-885.

Raz A, Grady SM, Krause BM, Uhlrich DJ, Manning KA, Banks MI (2014) Preferential effect of isoflurane on top-down versus bottom-up pathways in sensory cortex. Frontiers in Systems Neuroscience 8.

Reyes-Puerta V, Kim S, Sun J-J, Imbrosci B, Kilb W, Luhmann HJ (2015) High Stimulus-Related Information in Barrel Cortex Inhibitory Interneurons. PLOS Comput Biol 11:e1004121.

Reyes A, Lujan R, Rozov A, Burnashev N, Somogyi P, Sakmann B (1998) Target-cell-specific facilitation and depression in neocortical circuits. Nature Neuroscience 1:279-285.

Rigas P, Castro-Alamancos MA (2007) Thalamocortical Up states: differential effects of intrinsic and extrinsic cortical inputs on persistent activity. The Journal of Neuroscience 27:4261-4272.

Rose HJ, Metherate R (2005) Auditory thalamocortical transmission is reliable and temporally precise. Journal of Neurophysiology 94:2019-2030.

Rudy B, Fishell G, Lee S, Hjerling-Leffler J (2011) Three groups of interneurons account for nearly 100% of neocortical GABAergic neurons. Developmental neurobiology 71:45-61.

Sakata S, Harris KD (2009) Laminar structure of spontaneous and sensory-evoked population activity in auditory cortex. Neuron 64:404-418.

Sanchez-Vives MV, McCormick DA (2000) Cellular and network mechanisms of rhythmic recurrent activity in neocortex. NatNeurosci 3:1027-1034.

Sanchez-Vives MV, Mattia M, Compte A, Perez-Zabalza M, Winograd M, Descalzo VF, Reig R (2010) Inhibitory modulation of cortical up states. Journal of Neurophysiology 104:1314-1324.

Sessolo M, Marcon I, Bovetti S, Losi G, Cammarota M, Ratto GM, Fellin T, Carmignoto G (2015) Parvalbumin-Positive Inhibitory Interneurons Oppose Propagation But Favor Generation of Focal Epileptiform Activity. The Journal of Neuroscience 35:9544-9557.

Shu YS, Hasenstaub A, McCormick DA (2003) Turning on and off recurrent balanced cortical activity. Nature 423:288-293.

Silberberg G, Markram H (2007) Disynaptic inhibition between neocortical pyramidal cells mediated by Martinotti cells. Neuron 53:735-746.

Steriade M, Nunez A, Amzica F (1993) A Novel Slow (Less-Than-1 Hz) Oscillation of Neocortical Neurons In-Vivo - Depolarizing and Hyperpolarizing Components. Journal of Neuroscience 13:3252-3265.

Steriade M, Amzica F, Contreras D (1996) Synchronization of fast (30-40 Hz) spontaneous cortical rhythms during brain activation. Journal of Neuroscience 16:392-417.

Steriade M, Timofeev I, Grenier F (2001) Natural waking and sleep states: A view from inside neocortical neurons. Journal of Neurophysiology 85:1969-1985.

Tahvildari B, Wölfel M, Duque A, McCormick DA (2012) Selective functional interactions between excitatory and inhibitory cortical neurons and differential contribution to persistent activity of the slow oscillation. The Journal of Neuroscience 32:12165-12179.

Takesian AE, Kotak VC, Sharma N, Sanes DH (2013) Hearing loss differentially affects thalamic drive to two cortical interneuron subtypes. Journal of neurophysiology 110:999-1008.

Tan Z, Hu H, Huang ZJ, Agmon A (2008) Robust but delayed thalamocortical activation of dendritic-targeting inhibitory interneurons. ProcNatlAcadSciUSA 105:2187-2192.

Wang X, Lu T, Bendor D, Bartlett E (2008) Neural coding of temporal information in auditory thalamus and cortex. Neuroscience 157:484-494.

Wang XJ, Buzsaki G (1996) Gamma oscillation by synaptic inhibition in a hippocampal interneuronal network model. Journal of Neuroscience 16:6402-6413.

Wehr M, Zador AM (2003) Balanced inhibition underlies tuning and sharpens spike timing in auditory cortex. Nature 426:442-446.

Winter B (2013) A very basic tutorial for performing linear mixed effects analyses. arXiv preprint arXiv:13085499.

Xu X, Roby KD, Callaway EM (2010) Immunochemical characterization of inhibitory mouse cortical neurons: three chemically distinct classes of inhibitory cells. Journal of Comparative Neurology 518:389-404.

Yizhar O, Fenno LE, Prigge M, Schneider F, Davidson TJ, O/'Shea DJ, Sohal VS, Goshen I, Finkelstein J, Paz JT, Stehfest K, Fudim R, Ramakrishnan C, Huguenard JR, Hegemann P, Deisseroth K (2011) Neocortical excitation/inhibition balance in information processing and social dysfunction. Nature 477:171-178.

Zhang LI, Tan AYY, Schreiner CE, Merzenich MM (2003) Topography and synaptic shaping of direction selectivity in primary auditory cortex. Nature 424:201-205.

Chapter 5

Summary

The previous three chapters of this thesis emphasized the role of intrinsic cortical activity in responses to sensory or thalamocortical input. Chapter 2 showed that in responses to auditory stimuli, variations in evoked activity can be indistinguishable from other mechanisms such as structural changes in circuitry that lead to induced activity or the phase reset of ongoing oscillations. A plausible conclusion is that variable evoked responses reflect a combination of driven bottom-up activity and intracortically generated activity. A similar dominant influence of intracortically generated activity was observed in Chapter 3 in auditory thalamocortical slices. Contrary to the predictions of the canonical microcircuit model, which has substantial support at the level of pairwise and anatomical connectivity (Douglas and Martin, 2004), cortical responses to thalamocortical input are driven by recurrent UP state activity in the infragranular layers which spreads to the supragranular layers. In Chapter 4, the control of this recurrent activity by inhibitory interneurons and the participation of those cells relative to pyramidal cells was studied. At an individual level, inhibitory interneurons participate much more vigorously compared to pyramidal cells, which instead fire sparsely and primarily at the peak of population activity. PV+ cells control the onset of UP states, while Sst+ cells contribute to their termination, and both control overall levels of activity. Cortical UP states seen in slices and *in vivo* may correlate with spatiotemporal patterns of activity that encode stimulus information (Harris, 2005; Bathellier et al., 2012; Luczak et al., 2013). Consideration of cortical network activity (UP states) is necessary to interpret accurately the sensory responses of single cells and information flow.

Future work

The results of the previous chapters of this thesis suggest numerous future approaches for study. Preliminary work towards some of these approaches has already commenced and some of these have already been included in Chapter 4. Here, I will elaborate on this work and also discuss difficulties encountered in early attempts toward these goals.

Calcium imaging to study laminar activity and coding

In vivo, calcium imaging has become a potent tool to study network activity, especially in superficial layers. In brain slices, there is an added advantage in that simultaneous imaging across the cortical laminae is possible without complex multiphoton scanning approaches. Future work with calcium imaging in brain slices is likely to utilize new generations of genetically encoded calcium sensors such as gCaMP6, including from transgenic mice (Chen et al., 2013; Dana et al., 2014). Although Chapter 3 and previous work has shown the importance of activity in layer 5 for producing and propagating network activity (Chauvette et al., 2010; Wester and Contreras, 2012; Beltramo et al., 2013; Stroh et al., 2013; Krause et al., 2014), the sparsely firing superficial layers are more informative about stimulus identity (Sakata and Harris, 2009). We hypothesize that while infragranular cells propagate and maintain UP state activity while carrying rough information about recent stimuli, supragranular cells may encode more detailed stimulus information. To test this hypothesis in the future, we could present different patterns of thalamocortical input and observe participation of cells in different cortical laminae. We predict that cells in infragranular layers will participate consistently whereas different populations of supragranular cells will activate in response to different stimuli. If supragranular cells with different patterns of participation are far apart (i.e., in different columns), calcium imaging may not be necessary, because multichannel electrode recordings could also differentiate supragranular and infragranular

responses; however, calcium imaging will be particularly useful in determining whether neighboring cells also show differential participation.

A remaining challenge is how to deliver stimuli in brain slices that have sufficient diversity to evoke distinct patterns of activity. In young animals, in which the thalamocortical pathway is more easily preserved in a slice, stimulation of different areas in thalamus can produce different foci of activation in layer 4 of auditory cortex (Kaur et al., 2005), similar to what would be expected from acoustic stimuli at different frequencies. Similar techniques may be possible in slices from adult animals using the improved thalamocortical slice preparation described in Chapter 4. Optogenetic methods could also be used by transfecting MGv with channelrhodopsin and delivering focal light pulses either in thalamus or directly in layer 4, however these approaches likely cannot be used in concert with calcium imaging because the wavelengths used to excite the calcium dye will also activate channelrhodopsin.

In addition to these proposed experiments to look at excitatory circuits, I attempted to use calcium imaging methods to study interneuron involvement in UP states as in Chapter 4. As mentioned, optogenetic experiments are contraindicated with calcium imaging, but cre x tdTomato mice could allow for cell type identification in calcium imaging experiments because the excitation wavelengths for tdTomato and the calcium fluorphore OGB-1 do not overlap. Preliminary experiments pairing Sst-cre and PV-cre x tdTomato mice with OGB-1 calcium imaging found that while Sst-tdTomato cells were highly active during UP states, PV-tdTomato cells were not. This result directly conflicted with the result in Chapter 3 that fast-spiking cells were strongly activated by thalamocortical input and were among the only cells to fire early before UP state onset. Further investigation using targeted on-cell patch of PV-cre cells also labeled with OGB-1 found that, indeed, the cells were spiking, but this was not causing substantial calcium transients. Parvalbumin is itself a calcium binding protein, and this and possibly other calcium binding constituents of the PV+ cells compete with OGB-1 for binding free calcium. Even trains of spikes were unable to overcome this intrinsic buffering capacity. Therefore, for this project

calcium imaging methods were abandoned in favor of single-cell patch clamp experiments, and future experiments must account for the fact that PV+ cells will not be represented well in calcium imaging experiments.

Top-down modulation via layer 1 stimulation

Following our previous work that found supralinear interactions between bottom-up (white matter) and top-down (extrastriate visual cortex, V2) inputs to auditory cortex (Banks et al., 2011), we attempted to study the interactions between bottom-up and top-down inputs in the thalamocortical slice. Top-down inputs are of particular interest because of their roles in cognitive processes including priming, context, expectation, and attention (Cauller and Kulics, 1991; Mignard and Malpeli, 1991; Calvert et al., 1997; Tomita et al., 1999; Naya et al., 2001; Fritz et al., 2007) and their impairment when consciousness is lost (Massimini et al., 2005; Alkire, 2008; Ferrarelli et al., 2010; Boly et al., 2011). Although white matter stimulation has been used as a proxy for thalamocortical stimulation in the past in slices, the white matter also contains fibers from many other places including other cortical areas as well as the efferents of the on-beam column, and white matter stimulation can give very different responses compared to thalamocortical stimulation (Cruikshank et al., 2002). Therefore, the thalamocortical slice is a preferred preparation for studying bottom-up input.

Because the thalamocortical slice does not preserve the connections between extrastriate visual cortex and primary auditory cortex, we turned to stimulation of layer 1 as an alternative route to accessing top-down connections. Layer 1 contains the dendrites of pyramidal cells as well as axons from local cortical cells, non-specific thalamic nuclei, and other cortical areas, particularly higher-order cortical areas. I prepared slices in which layer 1 is isolated by making a cut in the slice from layer 2 through the white matter (Cauller and Connors, 1994). Our intention was to study interactions between

bottom-up and top-down pathways by stimulating in layer 1 rostral to the cut, and recording thalamocortical, layer 1, and paired responses caudal to the cut. Unfortunately, even with careful dissection this procedure caused significant damage to the slice, inducing substantial edema, death of superficial layer cells throughout the slice, and changes to evoked UP states. Further, the isolating cut was not even fully successful in preventing antidromic activation due to cells that send axons from the recording region to layer 1 of the stimulating region.

As an alternative, we have transitioned to using cortico-cortical stimulation without ensuring that stimuli are restricted to layer 1 (Raz et al., 2014). These stimuli produced current sinks that were restricted to layer 1 and superficial layer 2, but we cannot exclude activation of other layers as well. Better alternatives for future experiments that emphasize strictly top-down connectively will likely involve optogenetic activation of descending inputs, as in a recent paper in prefrontal cortex (Cruikshank et al., 2012). Paired stimulation of cortico-cortical and thalamocortical input in our slices can sum to produce UP states that would not be produced by either pathway alone (Hentschke et al., 2013) (also seen in Chapter 4). This interaction between pathways is likely also responsible for the supralinear interactions we observed between white matter and V2L stimulation in a previous study (Banks et al., 2011). As suggested in Chapter 4, Sst+ interneurons in particular may regulate integration of top-down inputs in the cortical network due to inhibition of distal dendrites (Kubota, 2014). Anesthetic agents including isoflurane may interfere selectively with top-down connections, either by enhancing inhibition or via presynaptic mechanisms (Raz et al., 2014). In the near future, we intend to test the hypothesis that enhanced effects of inhibition (particularly by Sst+ cells) on distal inputs relative to more proximal inputs cause the differential effect of isoflurane on cortico-cortical over thalamocortical inputs (Raz et al., 2014) by comparing the effects of isoflurane with and without optogenetic inhibition of Sst+ cells.

Effects of matrix/non-specific thalamic inputs

In the experiments in which I stimulated the thalamocortical afferents, I assumed that I was primarily activating the specific ("core") thalamocortical afferents from the ventral medial geniculate nucleus (MGv). This assumption was based on the observation of a robust current sink in layers 3/4 and a weaker sink in layer 6, consistent with the termination patterns of MGv in Au1. However, others working with the auditory thalamocortical slice preparation have also used a slightly different angle to instead capture non-specific ("matrix") thalamic afferents (Cruikshank et al., 2002). These afferents have a different termination pattern and originate in thalamic nuclei that project diffusely to many cortical areas (Jones, 2001). The non-specific afferents seem positioned to regulate cortical network activity such as UP states. In layer 1, non-specific thalamocortical afferents excite both interneurons and pyramidal cells (Cruikshank et al., 2012). Activation of layer 1 interneurons can have both inhibitory (Cruikshank et al., 2012) and disinhibitory (Christophe et al., 2002; Letzkus et al., 2011) effects on pyramidal cells. More generally, non-specific thalamocortical inputs are thought to play a key role in regulating information transmission in cortex and influence arousal and consciousness (Saalmann, 2014). Regulation of UP state activity may be a mechanism through which this regulation occurs.

'Small' versus 'large' UP states

In Chapter 3, UP states were observed that came in at least two varieties: smaller UP states restricted to the infragranular layers, and larger UP states that engaged the entire cortical column (Krause et al., 2014). The distinction between the two may be critical for subsequent information processing. For the small, infragranular-only UP states, information may be communicated to subcortical structures (i.e., thalamus and inferior colliculus) but may not be propagated to higher-order cortical areas and therefore may stay out of conscious perception. If true, the factors that allow for large, full-

column UP states are critical to information processing. In Chapter 4, I compared the effects of Sst+ and PV+ on layer 2/3 population activity compared to layer 5 population activity. Inhibiting PV+ cells had a greater effect on layer 2/3 population activity compared to layer 5, suggesting that the participation during UP states of layers 2/3 is strongly controlled by PV+-mediated inhibition. The strong effect of PV+-mediated inhibition in the supragranular layers is not surprising based the density of PV+ expressing cells in those layers. Additionally, cortico-cortical and (non-lemnsical) thalamocortical inputs to layer 1, as mentioned in the paragraphs above, are also likely candidates for modulating the extent of UP state activity in supragranular layers.

Initiation of evoked UP states

How exactly evoked UP states are triggered in the slice remains a puzzle. It seems that only a small number of excitatory cells can be involved, given that so few excitatory cells are observed spiking before UP state onset (Krause et al., 2014). Spontaneous UP states are known to begin in layer 5 (Chauvette et al., 2010), and it seems likely that evoked UP states also begin in layer 5 via direct thalamocortical input (Agmon and Connors, 1992; Constantinople and Bruno, 2013). Just a few active cells of the right variety may be all that is necessary to begin an UP state (Stroh et al., 2013; Lőrincz et al., 2015). However, activity is also seen in layers 2/3 and 4 at about the same time as and could contribute to UP state onset (Sakata and Harris, 2009; Wester and Contreras, 2012), though our experiments in Chapters 3 and 4 suggest that a lot of this early activity could be in inhibitory interneurons (Krause et al., 2014).

Paradoxically, activation of PV+ interneurons can facilitate seizure production by synchronizing activity in excitatory cells and by postinhibitory rebound (Sessolo et al., 2015), and could have similar influence on UP state initiation. Although either activation or inactivation of interneurons never directly

produced UP states during the experiments of Chapter 4, interneurons could promote UP state initiation when activated by thalamocortical input. In future experiments, we could test the role of interneurons at the time of UP state onset by temporally precise optogenetic inhibition or activation. We could also look more closely at the role of different types of interneurons, including the VIP+ cells that have a significant disinhibitory role (Lee et al., 2013; Pfeffer et al., 2013; Pi et al., 2013).

Archaerhodopsin-mediated optogenetic inhibition

One problem with the optogenetic inactivation experiments of Chapter 4 was that the distribution of interneurons expressing halorhodopsin was not always consistent, and many experiments had to be abandoned because expression was misdirected, either too medial toward the hippocampus or too caudal and beyond the region of auditory cortex receiving thalamocortical input in the slice. When injections were on-target, expression levels varied even when the same volume and concentration of virus was delivered. In the future, using genetic expression of archaerhodopsin instead of viral delivery of halorhodopsin could give more consistent results. Archaerhodopsin is similar to halorhodopsin in that it is a light-driven hyperpolarizing pump, but it pumps protons out of cells rather than pumping chloride ions inward. Generally, transgenic expression of optogenetic constructs has been suboptimal due to low copy number and therefore limited protein expression, whereas viral delivery can lead to expression levels that are several fold higher. However, the new ArchT version of archaerhodopsin has been engineered to give excellent current flow at moderate light intensities (Han et al., 2011). In one preliminary experiment, ArchT activation in PV-cre x ArchT mice had an effect on population activity similar to what was observed with halorhodopsin in Chapter 4. The ionic difference between archaerhodopsin and halorhodopsin is an additional benefit to using ArchT. With extended activation, halorhodopsin can raise intracellular chloride concentrations, and given long enough time

this can shift the reversal potential for chloride sufficiently to cause $GABA_A$-mediated currents to become excitatory (Raimondo et al., 2012). Breeding of PV-cre x ArchT and Sst-cre x ArchT mice is currently in-progress and these experiments will commence shortly.

Anesthetic effects on UP states and the continuum of UP state frequency

Although different anesthetics such as isoflurane, dexmedetomidine, and propofol have distinct molecular targets, they all produce loss of consciousness. Because anesthetic-induced loss of consciousness does not depend on a particular molecular target, commonalities are more likely to be found at a circuit level. Our lab has already published one paper on the effects of isoflurane on activity in auditory thalamocortical slices, focusing on early response components to thalamocortical and corticocortical stimuli (Raz et al., 2014).

Further work on anesthetic actions in slices is likely to focus on UP state activity, including the horizontal propagation and selective effects on thalamocortical versus cortico-cortical evoked UP states (Hentschke et al., 2013). UP states in slices may be an opportunity for studying anesthetic effects specifically on cortical circuits without involving effects on subcortical neuromodulatory systems. Interestingly, even low concentrations of isoflurane have dramatic effects on UP states, blocking them entirely for stimuli that would normally easily evoke UP states (Hentschke et al., 2013). This result is somewhat puzzling if one thinks of activity during the awake, desynchronized state as fundamentally different from activity during the anesthetized/sleeping synchronized state. If anesthetics transition cortex to the synchronized state and UP states are solely a property of the synchronized state, then we would expect anesthetics to increase rather than decrease UP state activity. Alternatively we could think of activity on a continuum from where DOWN states are rare and UP states are common (i.e., the awake/desynchronized state), to where DOWN states are common and UP states less common (i.e., the

synchronized/anesthetized state), to the slice where DOWN states predominate except when stimulated. In this situation, we interpret the effect of isoflurane as shifting the slice even further toward the no-UP state situation to the point that UP states cannot be evoked or sustained. The susceptibility of the slice to anesthetic concentrations much lower than the concentrations that cause loss of consciousness *in vivo* may be because the slice is essentially already in an "anesthetized" state, lacking the presence of neuromodulators that are typically elevated in waking compared to sleeping or anesthetized cortex and also missing substantial long-range and three-dimensional connectivity compared to the whole brain.

Aberrant cortical processing

Abnormal cortical processing underlies diverse conditions, including autism, schizophrenia, tinnitus, and delirium (Gogolla et al., 2009; Uhlhaas and Singer, 2010; Sanders, 2011; Auerbach et al., 2014). The circuit mechanisms of these conditions are only superficially understood. The work in this thesis supports the use of UP states as circuit phenomena with relevance to cortical information processing that can be probed in thalamocortical slices to help understand these and other conditions (Gibson et al., 2008). For example, delirium may be caused by an upregulation of Sst+-mediated inhibition that causes a breakdown in network connectivity (Sanders, 2011), and this impairment could manifest in slices exposed to inflammation by impaired UP state production and integration of top-down with bottom-up inputs. Conversely, auditory cortical hyperexcitability or insensitivity to inhibition after hearing loss may cause the symptoms of tinnitus (Llano et al., 2012; Takesian et al., 2013; Auerbach et al., 2014). In slices taken from animals who have experienced severe hearing loss, we may observe increased spontaneous UP state generation and evoked UP states at lower thresholds and could use this preparation as a model to study cortical mechanisms of tinnitus. Furthermore, in these and other

conditions, network and circuit activity is an important link between molecular and cellular mechanisms and the actual cognitive and symptomatic effects.

References

Agmon A, Connors BW (1992) Correlation between intrinsic firing patterns and thalamocortical synaptic responses of neurons in mouse barrel cortex. Journal of Neuroscience 12:319-329.

Alkire MT (2008) Loss of effective connectivity during general anesthesia. IntAnesthesiolClin 46:55-73.

Auerbach BD, Rodrigues PV, Salvi RJ (2014) Central gain control in tinnitus and hyperacusis. Frontiers in neurology 5.

Banks MI, Uhlrich DJ, Smith PH, Krause BM, Manning KA (2011) Descending projections from extrastriate visual cortex modulate responses of cells in primary auditory cortex. CerebCortex 21:2620-2638.

Bathellier B, Ushakova L, Rumpel S (2012) Discrete neocortical dynamics predict behavioral categorization of sounds. Neuron 76:435-449.

Beltramo R, D'Urso G, Dal Maschio M, Farisello P, Bovetti S, Clovis Y, Lassi G, Tucci V, Tonelli DDP, Fellin T (2013) Layer-specific excitatory circuits differentially control recurrent network dynamics in the neocortex. Nature Neuroscience 16:227-234.

Boly M, Garrido MI, Gosseries O, Bruno MA, Boveroux P, Schnakers C, Massimini M, Litvak V, Laureys S, Friston K (2011) Preserved feedforward but impaired top-down processes in the vegetative state. Science 332:858-862.

Calvert GA, Bullmore ET, Brammer MJ, Campbell R, Williams SC, McGuire PK, Woodruff PW, Iversen SD, David AS (1997) Activation of auditory cortex during silent lipreading. Science 276:593-596.

Cauller LJ, Kulics AT (1991) The neural basis of the behaviorally relevant component of the somatosensory-evoked potential in SI cortex of awake monkey evidence that backward cortical projections signal conscious touch sensation. ExpBrain Res 84:607-619.

Cauller LJ, Connors BW (1994) Synaptic physiology of horizontal afferents to layer I in slices of rat SI neocortex. Journal of Neuroscience 14:751-762.

Chauvette S, Volgushev M, Timofeev I (2010) Origin of active states in local neocortical networks during slow sleep oscillation. Cerebral Cortex 20:2660-2674.

Chen T-W, Wardill TJ, Sun Y, Pulver SR, Renninger SL, Baohan A, Schreiter ER, Kerr RA, Orger MB, Jayaraman V, Looger LL, Svoboda K, Kim DS (2013) Ultrasensitive fluorescent proteins for imaging neuronal activity. Nature 499:295-300.

Christophe E, Roebuck A, Staiger JF, Lavery DJ, Charpak S, Audinat E (2002) Two types of nicotinic receptors mediate an excitation of neocortical layer I interneurons. Journal of Neurophysiology 88:1318-1327.

Constantinople CM, Bruno RM (2013) Deep cortical layers are activated directly by thalamus. Science 340:1591-1594.

Cruikshank SJ, Rose HJ, Metherate R (2002) Auditory thalamocortical synaptic transmission in vitro. JNeurophysiol 87:361-384.

Cruikshank SJ, Ahmed OJ, Stevens TR, Patrick SL, Gonzalez AN, Elmaleh M, Connors BW (2012) Thalamic Control of Layer 1 Circuits in Prefrontal Cortex. The Journal of Neuroscience 32:17813-17823.

Dana H, Chen T-W, Hu A, Shields BC, Guo C, Looger LL, Kim DS, Svoboda K (2014) Thy1-GCaMP6 transgenic mice for neuronal population imaging in vivo.

Douglas RJ, Martin KA (2004) Neuronal circuits of the neocortex. AnnuRevNeurosci 27:419-451.

Ferrarelli F, Massimini M, Sarasso S, Casali A, Riedner BA, Angelini G, Tononi G, Pearce RA (2010) Breakdown in cortical effective connectivity during midazolam-induced loss of consciousness. ProcNatlAcadSciUSA 107:2681-2686.

Fritz JB, Elhilali M, Shamma SA (2007) Adaptive changes in cortical receptive fields induced by attention to complex sounds. J Neurophysiol 98:2337-2346.

Gibson JR, Bartley AF, Hays SA, Huber KM (2008) Imbalance of neocortical excitation and inhibition and altered UP states reflect network hyperexcitability in the mouse model of fragile X syndrome. Journal of neurophysiology 100:2615-2626.

Gogolla N, LeBlanc JJ, Quast KB, Südhof TC, Fagiolini M, Hensch TK (2009) Common circuit defect of excitatory-inhibitory balance in mouse models of autism. Journal of neurodevelopmental disorders 1:172-181.

Han X, Chow BY, Zhou H, Klapoetke NC, Chuong A, Rajimehr R, Yang A, Baratta MV, Winkle J, Desimone R, Boyden ES (2011) A High-Light Sensitivity Optical Neural Silencer: Development and Application to Optogenetic Control of Non-Human Primate Cortex. Frontiers in Systems Neuroscience 5:18.

Harris KD (2005) Neural signatures of cell assembly organization. Nature Reviews Neuroscience 6:399-407.

Hentschke H, Raz A, Krause BM, Grady SM, Banks MI (2013) Effects of isoflurane on cortical UP state activity in brain slices. In: Society for Neuroscience Annual Meeting. San Diego, CA.

Jones EG (2001) The thalamic matrix and thalamocortical synchrony. Trends in neurosciences 24:595-601.

Kaur S, Rose HJ, Lazar R, Liang K, Metherate R (2005) Spectral integration in primary auditory cortex: Laminar processing of afferent input, in vivo and in vitro. Neuroscience 134:1033-1045.

Krause BM, Raz A, Uhlrich DJ, Smith PH, Banks MI (2014) Spiking in auditory cortex following thalamic stimulation is dominated by cortical network activity. Frontiers in Systems Neuroscience 8:170.

Kubota Y (2014) Untangling GABAergic wiring in the cortical microcircuit. Current opinion in neurobiology 26:7-14.

Lee S, Kruglikov I, Huang ZJ, Fishell G, Rudy B (2013) A disinhibitory circuit mediates motor integration in the somatosensory cortex. Nat Neurosci 16:1662-1670.

Letzkus JJ, Wolff SB, Meyer EM, Tovote P, Courtin J, Herry C, Lüthi A (2011) A disinhibitory microcircuit for associative fear learning in the auditory cortex. Nature 480:331-335.

Llano DA, Turner J, Caspary DM (2012) Diminished cortical inhibition in an aging mouse model of chronic tinnitus. The Journal of Neuroscience 32:16141-16148.

Lőrincz ML, Gunner D, Bao Y, Connelly WM, Isaac JT, Hughes SW, Crunelli V (2015) A Distinct Class of Slow (~ 0.2–2 Hz) Intrinsically Bursting Layer 5 Pyramidal Neurons Determines UP/DOWN State Dynamics in the Neocortex. The Journal of Neuroscience 35:5442-5458.

Luczak A, Bartho P, Harris KD (2013) Gating of sensory input by spontaneous cortical activity. JNeurosci 33:1684-1695.

Massimini M, Ferrarelli F, Huber R, Esser SK, Singh H, Tononi G (2005) Breakdown of cortical effective connectivity during sleep. Science 309:2228-2232.

Mignard M, Malpeli JG (1991) Paths of information flow through visual cortex. Science 251:1249-1251.

Naya Y, Yoshida M, Miyashita Y (2001) Backward spreading of memory-retrieval signal in the primate temporal cortex. Science 291:661-664.

Pfeffer CK, Xue M, He M, Huang ZJ, Scanziani M (2013) Inhibition of inhibition in visual cortex: the logic of connections between molecularly distinct interneurons. Nature Neuroscience 16:1068-1076.

Pi HJ, Hangya B, Kvitsiani D, Sanders JI, Huang ZJ, Kepecs A (2013) Cortical interneurons that specialize in disinhibitory control. Nature 503:521-524.

Raimondo JV, Kay L, Ellender TJ, Akerman CJ (2012) Optogenetic silencing strategies differ in their effects on inhibitory synaptic transmission. Nat Neurosci 15:1102-1104.

Raz A, Grady SM, Krause BM, Uhlrich DJ, Manning KA, Banks MI (2014) Preferential effect of isoflurane on top-down versus bottom-up pathways in sensory cortex. Frontiers in Systems Neuroscience 8.

Saalmann YB (2014) Intralaminar and medial thalamic influence on cortical synchrony, information transmission and cognition. Front Syst Neurosci 8:83.

Sakata S, Harris KD (2009) Laminar structure of spontaneous and sensory-evoked population activity in auditory cortex. Neuron 64:404-418.

Sanders RD (2011) Hypothesis for the pathophysiology of delirium: role of baseline brain network connectivity and changes in inhibitory tone. Med Hypotheses 77:140-143.

Sessolo M, Marcon I, Bovetti S, Losi G, Cammarota M, Ratto GM, Fellin T, Carmignoto G (2015) Parvalbumin-Positive Inhibitory Interneurons Oppose Propagation But Favor Generation of Focal Epileptiform Activity. The Journal of Neuroscience 35:9544-9557.

Stroh A, Adelsberger H, Groh A, Ruhlmann C, Fischer S, Schierloh A, Deisseroth K, Konnerth A (2013) Making waves: initiation and propagation of corticothalamic Ca2+ waves in vivo. Neuron 77:1136-1150.

Takesian AE, Kotak VC, Sharma N, Sanes DH (2013) Hearing loss differentially affects thalamic drive to two cortical interneuron subtypes. Journal of neurophysiology 110:999-1008.

Tomita H, Ohbayashi M, Nakahara K, Hasegawa I, Miyashita Y (1999) Top-down signal from prefrontal cortex in executive control of memory retrieval. Nature 401:699-703.

Uhlhaas PJ, Singer W (2010) Abnormal neural oscillations and synchrony in schizophrenia. Nature reviews neuroscience 11:100-113.

Wester JC, Contreras D (2012) Columnar interactions determine horizontal propagation of recurrent network activity in neocortex. JNeurosci 32:5454-5471.